Development of molecular diagnostic and microfluidic methods based on molecular transport and reactions

By

Lindsay Pearl Schneider

B.S., Worcester Polytechnic Institute, 2017

A dissertation submitted in partial fulfilment of the requirements for the degree of Doctor of Philosophy in Biomedical Engineering at Brown University

PROVIDENCE, RHODE ISLAND

February 2022

This dissertation by Lindsay Pearl Schneider is accepted in its present form by the Biomedical Engineering program, a joint program in the Division of Biology and Medicine and the School of Engineering as satisfying the dissertation requirement for the degree of Doctor of Philosophy.

Date	Anubhav Tripathi, Ph.D., Advisor

Recommended to the Graduate Council

Date	Vicki Colvin, Ph.D., Reader
Date	Geralyn Messerlian, Ph.D., Reader
Date	Gary Wessel, Ph.D., Reader
Date	Michelle Fraser, Ph.D., Reader

Approved by the Graduate Council

Date	Andrew Campbell, Ph.D., Dean of the Graduate School

ABSTRACT

Molecular diagnostic testing provides critical information to patients that can lead to earlier detection and disease prevention, specific treatment options, and personalized medicine. The workflow for this type of testing begins with initial sample collection followed by target analyte extraction and purification from the original sample, then amplifying the analyte to a level where detection can be performed. This complex workflow can be laborious, time consuming, and expensive which is why many molecular diagnostic tests have turned to microfluidic technologies to improve all steps. In this thesis, we utilize experimental, computational, and theoretical approaches to characterize molecular transport and reactions. Moreover, we will use microfluidic geometries to develop and improve molecular diagnostic tests. In particular, we will present the design and use of microfluidic devices for nucleic acid extraction and purification using a combination of solid phase extraction on magnetic beads and electrokinetic purification within a microfluidic channel. We show the effect of magnetic beads, free DNA, and sample contaminant transport within this system and how that can change amplification, detection, and even DNA sequencing results. Additionally, this thesis further investigates methods for improved amplification and detection through exploring fundamental components of these steps. We show the development of a new method using targeted nucleic acid sequence to size-based separation analysis as well as the process for creating a model to be used for predicting false-positive results when using loop mediated isothermal amplification through understanding molecular interactions. Overall, the work described in this thesis aims to reduce false-positive diagnosis errors, increase sample purity, and reduce human errors all within the context of molecular diagnostics. The impact of this thesis work includes reducing costs, reagent volumes, and hands on work time using microfluidics, all while improving or maintaining the sensitivity and specificity of these tests particularly through the use of method designs and translatability for automation. Ultimately, through investigating the fundamentals underlying molecular diagnostics we have developed translatable technology useful to a variety of applications.

CURRICULUM VITAE

Lindsay Pearl Schneider

EDUCATION

Ph.D. in Biomedical Engineering September 2017 – December 2021
Brown University, Providence, RI
Development of molecular diagnostic and microfluidic methods based on molecular transport and reactions
Thesis advisor: Anubhav Tripathi, Ph.D.

B.S. in Biomedical Engineering September 2013 – May 2017
Worcester Polytechnic Institute, Worcester, MA
Graduated with Distinction

PUBLICATIONS

JOURNAL PUBLICATIONS

9. **Schneider, L.,** Tripathi, A., *Sequence to size-based separation using microfluidic electrophoresis for targeted DNA analysis*. Under Review.

8. **Schneider, L.,** Usherwood, T., Tripathi, A., *A Microfluidic Platform for High-Purity Cell Free DNA Extraction from Plasma for Non-Invasive Prenatal Testing.* Under Review.

7. **Schneider, L.,** Naranbat, D., Kantor, R., Beckwith, C., Bazerman, L., Gillani, F., Sahu, S., Rapoza, K., Sam, S., Novitsky, V., Shin, J., Hipolito, E., Diaz, I., Carnevale, D., Tripathi, A., *DirectDetect SARS-CoV-2 Direct Real-time RT-PCR Study using Patient Samples*. Under Review.

6. **Schneider, L.,** Tripathi, A., *Progress and Challenges in Laboratory-Based Diagnostic and Screening Approaches for Aneuploidy Detection during Pregnancy*. **SLAS TECHNOLOGY: Translating Life Sciences Innovation**, 24726303211021787, 2021.

5. **Schneider, L.,** Fraser, M., Tripathi, A., *Integrated Magento-Electrophoresis Microfluidic Chip Purification on Library Preparation Device for Preimplantation Genetic Testing for Aneuploidy Detection.* **RSC Advances,** 11, 14459-14474, 2021.

4. **Schneider, L.,** Cui, F., Tripathi, A., *Isolation of target DNA using synergistic magnetic bead transport and electrokinetic flow*. **Biomicrofluidics,** 15(2), 024104, 2021.

3. Deraney, R., **Schneider, L.,** Tripathi, A., *Synergistic use of electroosmotic flow and magnetic forces for nucleic acid extraction*. **Analyst,** 145(6), 2412-2419, 2020.

2. Timmermann, M., Lukat, N., **Schneider, L.,** Shields, C., Lopez, G.P., Selhuber-Unkel, C., *Migration of microparticle-containing amoebae through constricted environments*. **ACS Biomaterials Science & Engineering**, 6(2), 889-897, 2019.

1. **Schneider, L.,** Blakely, H., Tripathi, A., *Mathematical Model to Reduce Loop Mediated Isothermal Amplification (LAMP) False-Positive Diagnosis*, **Electrophoresis**, 40(20), 2706-2717, 2019.

CONFERENCE PROCEEDINGS

2. Schneider, L., Usherwood, T., Tripathi, A., *An electrokinetic microfluidic platform for solid-phase cell free DNA extraction from plasma for non-invasive prenatal testing (NIPT)*, 2021. Miniaturized Systems for Chemistry and Life Sciences Conference Proceedings.

1. Schneider, L., Cui, F., Brodsky, A., Fraser, M., Toloue, M., Tripathi, A., *A Fully Automated Instrument for Preimplantation Genetic Testing (PGT-A) Library Preparation*, **Reproductive BioMedicine Online**, 39, e35, 2019. Conference Proceedings.

RESEARCH EXPERIENCE

Graduate Researcher September 2017- December 2021
Center for Biomedical Engineering, School of Engineering
Brown University, Providence, RI
Advisor: Professor Anubhav Tripathi
Development of molecular diagnostic and microfluidic methods based on molecular transport and reactions

- Developed a mathematical model to identify non-specific DNA amplification for Loop Mediated Isothermal Amplification (LAMP) to reduce false positive diagnosis.
- Used computational modeling analysis to optimize an automated, microfluidic device for Next Generation Sequencing (NGS) library preparation for preimplantation genetic testing for aneuploidy (PGT-A).
- Evaluated clinical samples for COVID-19 using novel SARS-CoV-2 diagnostic test that reduced hands-on time and the number of reagents needed for sample preparation prior to virus detection.
- Developed microfluidic and microbiology-based techniques for cell free fetal DNA extraction and analysis from plasma during non-invasive prenatal testing (NIPT).
- Understood the biochemistry, molecular, and engineering concepts underlying LAMP, NGS, and PGT-A.
- Created collaborations within the biotechnology industry (Ultivue, PerkinElmer).

SKILLS : Nucleic Acid Extraction and Sample Preparation, Quantitative Polymerase Chain Reaction (qPCR), COMSOL Multiphysics Modeling Software, Next Generation Sequencing Library Preparation, Agilent Bioanalyzer 2100, NanoDrop, Microfluidic Design, Rheometer, Flow Cytometry, SolidWorks, Adobe Illustrator, Python, LabView, SI Programmer, MATLAB, R, ImageJ, Microfluidic Master Mold Fabrication, PDMS soft lithography.

Research and Development Engineer March 2020 – June 2021
Ximedica, Providence, RI

- Contributed technical advice and work for different projects as a part time consultant.
- Created and presented two 1-hour presentations titled *The Basics of Sample Preparation* to the company.

Pfizer Intern June - August 2017
Pfizer, Groton, CT

- Worked in the Solid Dose Manufacturing Group and gained experience working for a large company.
- Assisted in protocol organization, archive management, and machine training with the Ackley Laser Drill.

DAAD RISE Intern, University of Kiel, Kiel, Germany June - August 2016
Institute of Materials Science, Biocompatible Nanomaterials
University of Kiel, Kiel, Germany
Advisor: Professor Christine Selhuber-Unkel and Michael Timmermann, Ph.D.

- Worked with a Ph.D. student designing and conducting experiments feeding Acanthamoeba Cells various particles to measure their movement through a constricted microenvironment made by PDMS pillars.
- Utilized cell culturing, light microscopy, and fluorescent microscopy techniques.
- Completed the internship for 10 weeks in Germany while learning the German language and culture.
- Supported by Deutscher Akademischer Austauschdienst (DAAD) through a RISE (Research Internships in Science and Engineering) Fellowship (Kiel_EN_1579).

Fiber Optics Engineering Intern June - August 2015
Legrand, Inc., New London, CT

- Worked in the Fiber Optics department of the Ortronics branch of Legrand, Inc.
- Was responsible for using SolidWorks 2014 software to create and edit parts, assemblies and drawings when requested by fellow colleagues.
- Gained knowledge of fiber optic cables, storage units, and Legrand Data Communications Products.
- Provided design suggestions for development of a new Data Communications Cabinet product.

TEACHING EXPERIENCE

Research Mentor, Brown University October 2017 – December 2021

- Mentored three Brown University Undergraduate Students and one Master's summer student from KTH Royal Institute of Technology in Sweden.
- Taught and performed experiments one-on-one with students, discussed results and scientific insight, and collaborated on scientific writing for future publications.

Supplemental Teaching Assistant, Brown University September 2017- May 2021

- Biomaterials: Fall 2017 and Fall 2018.
- Biomedical Engineering Design and Innovation: Fall 2019, 2020 and Spring 2020, 2021.
- Held office hours, graded assignments and exams, and worked with students to explain classroom materials.

Teaching Assistant, Brown University January – April 2021

- C5 MTL2000 Effective Leadership: Theory and Practice course in Brown's Master of Science in Technology and Leadership
- Grade homework and other assignments, providing feedback on content and writing.
- Organized and helped to facilitate Zoom sessions for the 37 professionals taking the course.

Summer @ Brown Teaching Assistant, Brown University August 2019

- Engineering Biomedical Systems
- Worked with high school aged students facilitating activities during the course.

CONFERENCE PRESENTATIONS

POSTER PRESENTATIONS

9. Schneider, L., Usherwood, T., Tripathi, A., An electrokinetic microfluidic platform for solid-phase cell free DNA extraction from plasma for non-invasive prenatal testing (NIPT), *Miniaturized Systems for Chemistry and Life Sciences (μTAS) 2021*, October 2021.

8. Schneider, L., Tripathi, A., Size-Based Chromosome Tags for Aneuploidy Detection Using Cell Free Fetal DNA for Non-Invasive Prenatal Testing, *Biomedical Engineering Society 2020 Virtual Annual Meeting*, October 2020.

7. Schneider, L., Fraser, M., Tripathi, A., An Engineering Approach to Next Generation Sequencing Library Preparation for Preimplantation Genetic Testing, *Biomedical Engineering Society 2020 Virtual Annual Meeting*, October 2020.

6. Schneider, L., Brodsky, A., Feder, J., Fraser, M., Tripathi, A., An Engineering Approach to Next Generation Sequencing Library Preparation for Preimplantation Genetic Testing, *Beyond a Million Genomes: From Discovery to Precision Health, Keystone Symposia*, Breckenridge, CO, January 2020.

5. Schneider, L., Cui, F., Brodsky, A., Feder, J., Snider, A., Fraser, M., Warren, K., Toloue, M., Tripathi, A., A fully automated instrument for preimplantation genetic testing (PGT-A) library preparation, *WiSTEM, Womxn in STEM Symposium*, Brown University, Providence, RI, October 2019.

4. Schneider, L., Cui, F., Brodsky, A., Feder, J., Snider, A., Fraser, M., Warren, K., Toloue, M., Tripathi, A., A fully automated instrument for preimplantation genetic testing (PGT-A) library preparation, *18th International Conference on Preimplantation Genetics (PGDIS)*, Geneva, Switzerland, April 2019.

3. Schneider, L., Blakely, H., Tripathi, A., DNA Size Analysis of Loop Mediated Isothermal Amplification (LAMP) Using Gel Electrophoresis Followed by RNase H and S1 Nuclease Digestions, *Young Scholar's Conference*, Brown University, Providence, RI, October 2018.

2. Schneider, L., Blakely, H., Tripathi, A., DNA Size Analysis of Loop Mediated Isothermal Amplification (LAMP) Using Gel Electrophoresis Followed by RNase H and S1 Nuclease Digestions, *3rd Bioengineering and Translational Medicine Conference (AIChE Community)*, Boston, MA, September 2018.

1. Schneider, L., Czamara, A., McLoughlin, A., McNamara, K., A Fastening Device for Rotator Cuff Repair. *43rd Annual Northeast Bioengineering Conference*, New Jersey Institute of Technology, Newark, NJ, March 2017.

ORAL PRESENTATIONS

1. Schneider, L., A fully automated instrument for preimplantation genetic testing (PGT-A) library preparation, 2019, *18th International Conference on Preimplantation Genetics (PGDIS)*, Geneva, Switzerland, April 2019.

PROFESSIONAL ACTIVITIES AND SERVICE

Brown University

Writing Associate, Brown University November 2018 - December 2020

- Worked one-on-one with undergraduate, graduate, faculty, and staff writers in the Brown University Writing Center for one-hour sessions.

- Organized writing sessions to collaboratively review the piece of writing with the writer, discussing organization, clarity, strength of argument, grammar, and more.

Sheridan Center Teaching Certificate Program, Brown University September - December 2020
- Participated in Teaching Modules covering critical reflection and inclusive pedagogy; rhetorical practice and classroom communication; learning design; and student engagement.
- Presented in mini-teaching sessions where I received feedback on my lesson and provided feedback to fellow students.

Invited Speakers Committee, Biomedical Engineering and Biotechnology Board (BMEB) March 2020 - December 2021
- Facilitated student nominations and voting on student-invited speakers for Center of Biomedical Engineering Seminar series every year.
- Coordinated student meeting or student lunches with every seminar speaker to increase student interaction with speakers.

Social Chair, Graduate Biomedical Engineering Society, Brown University May 2018 - May 2019
- Organized social events for Graduate Biomedical Engineering students.
- Planned activities for incoming and present students during Biomedical Engineering orientation to help welcome new students and build comradery within the program.

PROFESSIONAL DEVELOPMENT

- Womxn in STEM Symposium, Brown University, October 2019
- COMSOL Multiphysics Intensive Training, Montreal, Canada, August 2019
- Young Scholar's Conference: Communicating Your Science, Brown University, October 2018
- Introduction to Microfluidics Course, Brandeis University, Waltham, MA, June 2018

AFFILIATIONS

Society for Biological Engineering (An AIChE Technological Community) August 2018 – Present
Biomedical Engineering Society (BMES) September 2018 – Present
Phi Sigma Sigma Fraternity, Gamma Iota, WPI, alumni sister May 2017 - Present
Phi Sigma Sigma Fraternity, Gamma Iota, WPI, active sister November 2013 – May 2017
Scholarship Chair (2014-2015), Risk Manager (2016), Bursar (2016-2017)
Rho Lambda Greek Honors Society November 2016
Order of Omega Greek Honors Society November 2015

ACKNOWLEDGEMENTS

There are many people who need to be thanked for not only making this thesis possible, but for their positivity and support throughout my graduate school journey. To begin, I would like to thank my advisor, Dr. Anubhav Tripathi, for without him, none of this would have been possible. Dr. Tripathi has provided endless support and enthusiasm for me as a researcher and a person since the time he met me for coffee at WPI before making my decision to attend Brown University and join his research group, until this very moment. He has taught me endless lessons from how to attack research problems, when to ask an expert for help, and that you can never have too many control experiments. I credit my appreciation for modeling and fundamental science to him, as well as my excitement for women's health research, this journey would not have been the same without him.

In addition to the advising a received from Dr. Tripathi, I would also like to thank my thesis committee members, Dr. Vicki Colvin, Dr. Geralyn Messerlian, Dr. Gary Wessel, and Dr. Michelle Fraser. I appreciate the time and effort they dedicated to contributing to the direction of my thesis work and their support and suggestions were helpful every step of the way.

The next people I would like to thank for their support along this graduate school journey are my lab mates. I have noted this since the day I joined the lab in 2017, Dr. Tripathi knows how to recruit a collaborative, caring, intelligent, compatible, and all-around fun group of people to work together. From the more senior students in the lab who I had the privilege of following (Frank, Rachel, Christina, and Adam), to the more junior students who I had the privilege of growing with (Kiara, Cel, Duuluu, Ramisa, and Adriana). To every one of these Ph.D. students, along with the post-doc, Master's, and Undergraduate students I was fortunate to overlap with in my time at Brown, I want to say thank you. It takes a special group of people to consistently provide help, guidance, and support no matter the challenges and I know that I would not have grown as much as a researcher or person without the comradery in the lab.

Next, I wanted to provide a special thank you to Dr. Kareen Coulombe for taking the time to meet with me and provide unwavering support and guidance before and throughout my Ph.D. journey. I appreciate her

taking so much time and energy to help me grow and navigate graduate school. Additionally, I would also like to acknowledge people in and out of the Center for Biomedical Engineering who made the experience in graduate school much more streamlined thanks to their hard work and impressive organization. Carolyn Sherman, for always being so timely in placing orders and answering all of my questions, even when they were repetitive, as well as sending a witty email that always made me laugh. John Lee, for always taking the time to receive packages with great care and help me when I needed to ship something, I hope people in my lab continue to return carts in a timely fashion. Jess Bello and Melodie Vincenty, thank you for all of the work and dedication to organizing retreats, orientations, and everything in between, these events have made the graduate school experience very special.

Additionally, I wanted to thank my friends in and outside of the BME program, I always felt I had someone to share my good and bad days with who would know exactly how I was feeling or exactly how to cheer me up. I feel very fortunate to have had their support along the way and they provided a necessary amount of work-life balance, which I was constantly striving for.

Lastly, I wanted to thank my family, both Schneider and Opsahl, for being there every step of the way. For the Opsahl family who always asked for updates and exciting news, I want to thank you for all of the support. To my parents, Phil and Donna, and sisters, Nicole and Paige, who saw my love for biomedical engineering from the start, thank you for still being excited for me and sharing in my good and bad days, I was so lucky they were only a phone call or a short drive away. Or, in the craziest turn of events, right down the hall as I had the privilege of sharing a condo with my mom for 3.5 years of graduate school, I could not have asked for a better support system.

To conclude, the last person I would like to acknowledge and thank repeatedly is my lifelong best friend and boyfriend, Adam Opsahl. Thank you for being my rock throughout this whole process, I could not have imagined the experience without him, and I thank him for his patience, kindness, support, and excitement. He has encouraged me every step of the way and I am beyond lucky to share this journey with him.

CONTENTS

LIST OF FIGURES

LIST OF TABLES

LIST OF SUPPLEMENTAL INFORMATION (SI) FIGURES

LIST OF SUPPLEMENTAL INFORMATION (SI) TABLES

CHAPTER 1

Background

1.1 Motivation

Molecular diagnostic tools provide critical, patient specific, information for an abundance of clinically relevant applications. These tests are essential as they lead to more informed medical decisions, lower costs with early detection and prevention, and personalized medicine. There are a large number of molecular diagnostic tests which are utilized depending on the sample type available, necessary sensitivity and specificity, target analyte, and application. Additionally, molecular screening tests are also common and provide clinically relevant information which can then be confirmed with a follow up diagnostic test if needed as screening methods have a detection rate lower than diagnostic tests and a higher false positive rate[1]. Some examples of molecular diagnostic or screening tests that can be performed using different input sample types include prenatal testing, HIV, and glucose using a blood sample; coronavirus disease 2019 (COVID-19), flu, and respiratory syncytial virus (RSV) using a nasal swab; and urinary tract infection, kidney disease, and diabetes using a urine sample.

While this testing provides lifesaving information, the importance was further emphasized as COVID-19 disease, caused by severe acute respiratory syndrome coronavirus 2 (SARS-CoV-2), led to a global pandemic infecting hundreds of millions of people worldwide beginning in 2019. This public health emergency caused a surge in demand for reliable and robust molecular detection methods as an important factor in disease prevention and control[2]. Within one year of the pandemic outbreak, hundreds of nucleic acid based tests were developed to aid in the timely diagnosis of this disease, highlighting the importance of this field of research[2]. While molecular diagnostic tests have been developed at rapid speeds, especially as it pertains to the global pandemic, there remains a fundamental technical challenge associated with these types of tests which is a major focus of this thesis work: rapid molecular diagnostics in microscale geometries alter time scales of biochemical reactions and binding, as well as molecular and electric

transport which must be understood to ensure sensitive and specific testing outcomes. Overall, these reduced volumes can increase the speed and throughput of specific tests, while maintaining accurate results.

1.2 Molecular Diagnostics Overview

Regardless of sample type or application, molecular diagnostic tests follow a similar workflow which can be broken down into five major steps: sample collection, extraction, purification, amplification, and detection. To better understand this workflow Figure 1.1 provides a visual explanation for how this process works for the application of non-invasive prenatal testing (NIPT)[3]. To begin, sample collection consists of a maternal blood draw, then, plasma is separated from the whole blood sample and cell free DNA (cfDNA) is extracted from the plasma. Figure 1.1 shows a magnetic bead-based extraction procedure which is also utilized to purify the target analyte for the third step in the molecular diagnostic workflow[4]. Lastly, amplification and detection are performed to analyze the cfDNA sample, in this example that is done using Next Generation Sequence (NGS). This provides one case for how the molecular diagnostic workflow is applied to a specific application and while it is broken down into five simple steps, there are many scientific challenges associate with each part. Table 1.1 outlines a number of the scientific challenges considered while developing molecular diagnostic technologies correlated with each highlighted step.

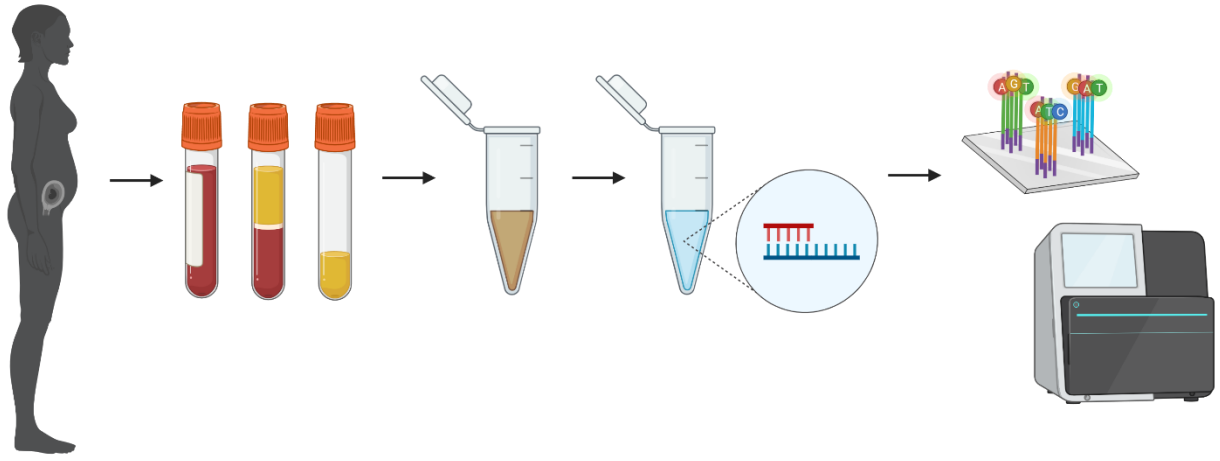

Figure 1.1: Example of molecular diagnostics workflow for the application of NIPT. Sample collection from a female is performed using a blood draw, followed by plasma separation and cfDNA extraction and purification using a bead-based method. Lastly, the amplification and detection steps are performed using a sequencing platform for this example. Created with BioRender.com

Table 1.1: Scientific challenges associated with different steps of the molecular diagnostics workflow.

Molecular Diagnostics Step	Scientific Challenges
Sample collection	• Complex sample retrieval • Intricate biochemical makeup • Sample volume and size • Sample stability/time sensitivity
Extraction	• Small, dilute analyte • Added inhibitors of downstream reactions • Reaction kinetics (i.e., binding) • Liquid viscosity and analyte diffusion
Purification	• Reducing inhibitor carryover • Analyte adsorption • Non-specific capture of off target analytes
Amplification	• Non-specific amplification • Reaction kinetics (i.e., temperature) • Primer specificity and sensitivity
Detection	• Fluorophore crosstalk • Reaction kinetics (i.e., fluorophores binding) • Need for specialized equipment • Analyte concentration • Sample behavior
Overall	• Cost • Time of protocol • Laborious • Access to laboratory

1.3 Microfluidic Technologies for Molecular Diagnostic Applications

As the molecular diagnostics workflow has many scientific challenges, there are numerous solutions to continuously improve different components of these tests. One strategy that has helped to increase the speed, portability, throughput, and automation of molecular diagnostic tests, while reducing associated costs, is utilizing microfluidic technologies[5-7]. Microfluidic devices contain microchannels allowing for the movement and manipulation of small liquids[6]. Applications for microfluidic devices include pathogen tracking, food-based microorganism detection, and infectious disease diagnostics[5,6]. More specifically, microfluidic devices can be used at each stage in the molecular diagnostics workflow to address at least one scientific challenge. Sample collection can be performed using a variety of methods depending on the sample type and microfluidic devices may be particularly advantageous for sample types where low volumes are available for testing, such as in bone marrow aspiration or cerebrospinal fluid[8]. Additionally,

the sample preparation steps of the workflow, extraction and purification, can be performed using microfluidic technologies[8,9]. These process may incorporate microfluidic-based lysis methods using techniques like electro-lysis, laser lysis, or mechanical lysis to aid in sample extraction[9]. As well as magnetic bead-based nucleic acid purification where techniques such as oil interfaces on a microfluidic chip can increase sample purity[10,11]. Lastly, sample amplification can be performed on a microfluidic device in applications such as droplet PCR where single molecules can be analyzed[12], and detection can be performed using capillary electrophoresis[13]. In addition to performing individual steps of this workflow on a microfluidic device, there are applications of integrated microfluidic technologies that perform all steps from sample collection to analyte detection in one microfluidic system. One example of this is using paper-based microfluidic devices which can collect and pretreat samples followed by signal amplification or transduction and signal output either in an instrument-free system or device-assisted setup[14].

1.4 Nucleic acid extraction and purification

While there are many target analytes relevant to molecular diagnostic testing, applications involving nucleic acids will be expanded upon further with a focus on microfluidic-based extraction and purification of nucleic acids. In general, extraction methods can be grouped into liquid phase extraction and solid phase extraction. Liquid phase extraction or isolation uses an electric field or chemical reagent to capture and separate nucleic acids[15]. The chemical reagent approach often uses the phenol chloroform extraction method where hydroxybenzene-chloroform-isoamyl alcohol (PCI) is used as an organic phase so that when it is mixed with a lysate, proteins are denatured, transferred to the organic phase, and charged DNA remains in the aqueous phase[15]. While chemical-based liquid phase extraction has many applications, it can be detrimental to downstream processes in molecular diagnostics if reagents are not fully removed[15]. Next, liquid phase extraction can also be performed using an electric field and techniques such as electrophoresis[16,17] and dielectrophoresis[18,19] for nucleic acid isolation. Micro free flow electrophoresis is one microfluidic method that works by applying an electric field perpendicular to the pressure driven flow in a channel and is advantageous since new liquid sample can be continuously introduced into the device, for continuous analyte separation and collection[16]. Moreover, dielectrophoresis incorporates particle

movement by a trapping force in a non-uniform electric field when the particles and medium they are suspended in have different polarizabilities[19]. Dielectrophoresis is suitable for DNA isolation due to the need for small sample volumes and single DNA molecule resolution[19].

Solid phase extraction of nucleic acids is, however, the primary method used for extraction and purification as, compared to liquid phase extraction, it is faster, less labor intensive, and results in higher yield and purity of the nucleic acid targets[20]. This extraction method works by nucleic acids adsorbing to a solid surface where they are able to bind and release under specific conditions[20]. A common solid surface used for nucleic acid purification is silica in the form of a membrane, often a spin-column, or the coating of magnetic beads[7,15,20]. Moreover, solid phase reversible immobilization (SPRI) is a technique which binds nucleic acids of an appropriate size to the surface of carboxy-coated magnetic particles in high poly(ethylene glycol) (PEG) and salt concentrations[21]. Once bound to the magnetic particle the nucleic acids can be washed before the bead solution is then rehydrate in a polar solvent to create a purified sample[7,21]. When the magnetic particles are suspended during the washing steps, chaotropic agents, such as ethanol, are used for washing as the nucleic acids will not desorb from the particles under these conditions. This is important since microfluidic devices can be filled with reagents used for washing while nucleic acid-bound magnetic beads are moved through channels for purification in a stationary microfluidic setup[10]. Stationary microfluidic chips can also incorporate an immiscible phase such as air or oil to further purify nucleic acids bound to magnetic beads[10].

Another strategy that has been used is to combine microfluidic chip-based solid phase extraction with an electric field for improved enrichment of a target sample and increased separation of unwanted impurities[22]. Key electrokinetic phenomena that can be incorporated into a microfluidic chip design include electrophoresis and electroosmotic flow (EOF), especially in the context of improving DNA purification during solid phase extraction on a microfluidic chip. While stationary microfluidics can be used to transport DNA-bound magnetic beads throughout a microfluidic channel, coupling that movement with an electric field can drive flow, move analytes, and separate ionic species away from the target being purified[23]. As buffer is added to a microchannel, an electric double layer (EDL) spontaneously forms at the interface

between a solid, in this case the channel walls, and an electrolyte[23,24]. This electrolyte contains counter-ions to the surface charge which condense onto the surface, reducing the surface charge density[23]. Importantly, additional counterions will remain solubilized or diffuse within the channel and the thickness of the diffuse layer is known as the Debye length, determined by the balance of electromigration to the surface and diffusion from the surface[23]. The Debye length is a function of ion density[24]. When the EDL is present in a channel and an external electric field is applied, EOF will be generated[24]. This EOF creates bulk motion of the liquid in the channel due to ion drag of diffuse counterions caused by the tangential electric field[23,24]. While EOF is occurring, electrophoresis is also taking place as this is the observable drift velocity of all mobile ions in the channel, also induced by the external electric field[23].

Figure 1.2 highlights the importance of EOF and electrophoresis in the context of DNA based nucleic acid extraction and purification in a microchannel. As there are many options for microfluidic device materials and fabrication, the polymeric material, polydimethylsiloxane (PDMS) is one of the most popular due to its low fabrication cost, inert and non-toxic properties, optical transparency, and high thermal stability[5]. Soft lithography techniques are used to create microfluidic designs out of PDMS using a micro-fabricated master template which can be plasma treated and bonded to a glass slide to make an enclosed fluidic environment[5]. This is important because under the conditions of the near-neutral wash buffers used during DNA extraction and purification, the glass slide has a negative surface charge which attracts free positive ions forming an EDL, as demonstrated in Figure 1.2[25]. Thus, when an external electric field is applied, bulk liquid movement in the channel will move towards the negative electrode via EOF. However, due to the nature of the sample analyte and the negative charge of DNA, electrophoresis will move the free DNA in the microchannel towards the positive electrode when the external electric field is applied. It is, therefore, critical to understand the opposition of these electrokinetic phenomena in the microchannel in order to increase the purity of DNA extraction and purification when combining magnetic bead-based solid phase extraction and electrokinetic purification.

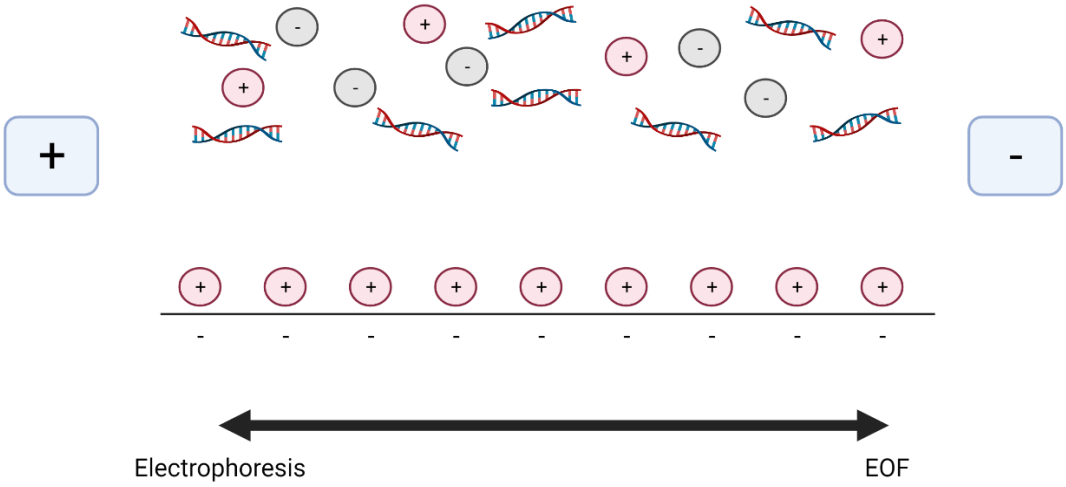

Figure 1.2: Opposing electrophoresis vs electroosmosis in microfluidic channel due to negatively charged surface and free-floating, negatively charged DNA. Created with BioRender.com

1.5 Nucleic acid amplification and detection

Following nucleic acid extraction and purification in molecular diagnostic applications, the target analyte is often at too low of a concentration for any detection without more processing[26]. In the case of nucleic acids, the best way to increase the signal of the analyte within the solution is to amplify the target. There are a variety of methods that can be used for this amplification but, in general, they are divided into two categories, isothermal and non-isothermal amplification methods. Non-isothermal amplification methods require precise heating and repeated heating cycles which translates to the need for specialized equipment capable of these specifications[26,27]. Isothermal amplification methods, however, are advantageous as they can be performed at one temperature because instead of using heating cycles for DNA strand separation, specific enzymes with strand displacement capabilities are used instead[27]. Lastly, another key step in the molecular diagnostics workflow that can work in conjunction with nucleic acid amplification is detection. Depending on the testing needs and capabilities, separate or combined amplification and detection can be used[27]. Separating the amplification and detection steps can be allow for analytical sensitivity and specificity to be assessed during both steps as they occur at different times and often using different equipment[27]. Conversely, when the two steps are combined, real-time quantification of the amplified product is possible which can potentially decrease the time needed to analyze the sample target because the

steps occur simultaneously[27]. Overall, there are many considerations for designing robust nucleic acid amplification and detection methods, including the template being amplified, operating temperature, procedure simplicity, ability to multiplex, input sample contamination, sensitivity, specificity, assay timing, and the amplification product produced[27].

1.5.1 Non-isothermal Amplification and Detection Techniques

The most common non-isothermal amplification technique and the standard technique for many clinical diagnosis applications is polymerase chain reaction (PCR). This method is divided into three steps: denaturation to separate double stranded DNA into single stranded DNA using a high temperature; annealing where custom primers hybridize to a complementary sequence on the denatured single stranded DNA; and extension using Taq DNA polymerase to create a new strand of DNA from the annealed primer complementary to the single stranded DNA[26]. These three steps are performed at two or three different temperatures requiring repeated heating and cooling to create an exponential amount of the target DNA. Additionally, PCR is conducive to target RNA as well using reverse transcriptase to produce complementary DNA (cDNA) which can then be amplified using PCR, known as RT-PCR[26].

As for the detection of PCR products, both endpoint and real-time analysis are possible. Endpoint analysis of PCR products can be conducted using gel or capillary electrophoresis where the migration time of the PCR product in the system is used to calculate the size, in base pairs, and in cases the concentration, compared to known sizes and concentrations of nucleic acids[28]. Droplet digital PCR can also be used for endpoint analysis and absolute quantification of DNA copy numbers[29]. This method includes loading samples and reagents into an oil droplet generator to make droplets, performing PCR through temperature cycling, then analyzing the droplets to quantify the absolute number of positive reactions, correlating to the DNA copy number in the sample[29]. Droplet digital PCR is unique in that it provides absolute quantification rather than a comparison to a known concentration of DNA which can increase the accuracy in quantifying a DNA sample[29].

Real-time analysis can be performed using real-time quantitative PCR (qPCR) where the amount of PCR products increase across additional temperature cycles. This increase in PCR products is quantified using

fluorescence and first increases exponentially, then linearly, then plateaus as the reaction is exhausted[30]. Fluorescence-based detector molecules can quantify DNA using probe sequences that fluoresce upon hydrolysis or hybridization, fluorescent hairpins, or intercalating dyes[30]. Two common methods used during real-time qPCR are TaqMan probes which fluoresce upon hydrolysis and SYBR Green, which is an intercalating dye, attaching to the backbone of double stranded DNA[30]. Overall, PCR, and its variations, have been used extensively in applications ranging from infectious disease detection[31,32], cancer screening[33-35], mRNA expression analysis[36,37], and sequencing[38,39] and continues to be the gold standard in the field of molecular diagnostics.

1.5.2 Isothermal Amplification and Detection Techniques

Isothermal amplification techniques are beneficial as they produce rapid target amplification at a single temperature which can reduce equipment complexity compared to PCR-based methods[40]. Example isothermal amplification techniques include loop mediated isothermal amplification (LAMP), rolling circle amplification (RCA), nucleic acid sequence-based amplification (NASBA), and strand displacement amplification (SDA). To expand upon some of the techniques, LAMP utilizes 4-6 primers to amplify a few copies of DNA to 10^9 copies in less than one hour[41]. Through strand displacement DNA synthesis primers are able to hybridize to the target DNA and lead to the production of a single stranded loop where additional primers can hybridize and create stem and loop DNA products with multiple inverted repeats of the target[41]. LAMP has been used for applications such as influenza[42], microbial pathogens in food[43], mRNA detection[44], and, more recently RT-LAMP has been used for COVID-19 detection[45,46].

Another isothermal amplification technique to highlight is RCA which uses strand displacing polymerase and one primer to generate long, single stranded DNA or RNA based on a circular template[47]. This isothermal amplification method can be performed in solutions or on solid supports including cells or be used in the construction of DNA nanostructures[47]. RCA is extremely versatile as it can be used for different nucleic acid targets as well as DNA methylation analysis[48], single nucleotide polymorphisms (SNPs)[49], small molecules[50], and protein detection[47,51].

Similarly, to PCR, these isothermal amplification techniques can be detected using endpoint or real-time analysis. Gel and capillary electrophoresis[26] as well as digital LAMP[52] are options for endpoint analysis. Additionally, colorimetric assays have been used to analyze positive vs negative isothermal reactions for LAMP and RCA[42,43,47] as well as turbidity detection[26] and intercalating dyes for LAMP[27]. Finally, real-time quantification and analysis can be utilized for these isothermal amplification methods[53,54].

1.6 Clinical Application of Molecular-based testing

1.6.1 Aneuploidy detection using molecular diagnostics and screening

When reviewing the capabilities of molecular diagnostic technologies there are endless applicable applications. However, one clinically relevant application to note is aneuploidy detection. Aneuploidy is an abnormal number of chromosomes, either too few or too many, and can lead to pregnancy failures when it occurs in embryos[55]. Out of all clinically recognized pregnancies, approximately 10-15% end in spontaneous abortions and of these, chromosomal abnormalities account for up to 50-60% of the causes with trisomy and polyploidy making up a large part of that percentage[56]. Moreover, it is important to note that chromosome abnormalities during pregnancy are associated with increased maternal age among other factors and the most common aneuploidies involve chromosomes X, Y, 13, 18, and 21[55]. Aneuploidy detection is unique in that there is a range of clinical samples that can be used for molecular testing, as well as different timepoints throughout pregnancy when a sample can be collected for analysis.

1.6.1.1 Preimplantation Genetic Testing for Aneuploidy

One aneuploidy detection test used during in vitro fertilization is preimplantation genetic testing for aneuploidy (PGT-A). This is a diagnostic method which uses a trophectoderm (TE) biopsy sample from a blastocyst-stage embryo prior to implantation[57]. This cell population is then analyzed using techniques such as array comparative genomic hybridization (aCGH) or NGS for aneuploidy analysis[57]. Following this analysis, the goal is to transfer a euploid, standard chromosome count, embryo for pregnancy. Technical challenges associated with this diagnostic method include the limited amount of extracted sample and mosaic embryos which contain both euploid and aneuploid cells and can affect the sample analysis and the success of the pregnancy[57].

1.6.1.2 Non-Invasive Prenatal Testing

Another form of aneuploidy detection is NIPT which can be used as a screening method during pregnancy. NIPT is defined as the analysis of cell free fetal DNA (cffDNA) that is extracted from maternal plasma but originates from placental apoptosis[58]. Previously, fetal aneuploidies have been diagnosed using amniocentesis during the second trimester of pregnancy for women of advanced maternal age or chorionic villous sampling (CVS) for high-risk individuals recognized by screening using fetal nuchal translucency (NT) and serum biochemistry[59]. Although these two methods are able to diagnose fetal aneuploidy, they include invasive procedures which are associated with the risk of miscarriage in 0.1-0.5% of cases[60]. Following cffDNA extraction during NIPT, aneuploidy analysis can be performed using PCR , NGS, or another method[61]. If this screening tests results in a positive outcome, invasive diagnostic testing would be necessary to confirm these results[62]. Technical challenges associated with this screening test include the low concentration of extracted sample and the fetal fraction of the cfDNA, or the percentage of cfDNA of fetal origin[63].

1.6.2 COVID-19 detection using molecular diagnostics

Another important application of molecular diagnostic tests that has been of particular importance is for COVID-19 detection. While there are many platforms for testing for COVID-19, including antibody and antigen testing, molecular-based tests have been advantageous for early disease diagnosis compared to these other forms of tests[64]. Molecular-based tests include real time qPCR, LAMP, and more, and investigate the presence of the viral RNA in a patient sample[64]. Conversely, antibody tests look for SARS-CoV-2 specific antibodies, such as IgM and IgG, and antigen tests show if a person is currently infected based on the presence of proteins, such as the spike protein found on the surface of the SARS-CoV-2 virus, in the sample[65].

1.7 Summary and Research Overview

This thesis focuses on fundamental approaches to developing and improving molecular diagnostics through reducing false-positive diagnosis errors, increasing sample purity for downstream reactions, and reducing human errors that may be affected by precise and accurate reagent handling and time management. Figure

1.3 provides a visual overview of this thesis work and organization for how each chapter is aligned with the focus of this thesis.

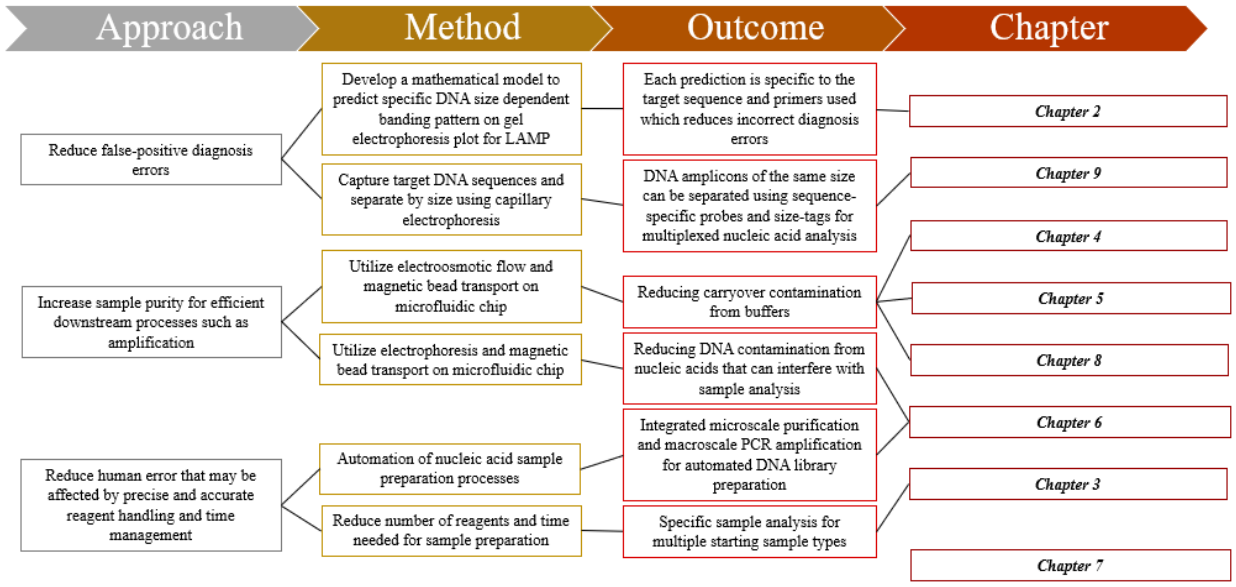

Figure 1.3: Outline of thesis work based on key approaches to developing and improving molecular diagnostics.

Chapter 2 describes the development of a new way to understand isothermal amplification. This chapter investigates the molecular reaction occurring during LAMP and the resulting, differently sized DNA structures which are identified by a banding pattern on gel electrophoresis plots. While LAMP is a specific amplification technique, it requires complex primer design and amplification which can lead to false-positive results, especially when only interpreting the presence of any banding pattern on gel electrophoresis plots. To address this limitation, we developed a mathematical model derived from the various components of a LAMP structure to predict the full LAMP structure size in base pairs. This model can be implemented by users to make predictions for specific, DNA size dependent banding patterns on their gel electrophoresis plots and each prediction is specific to the target sequence and primers used and therefore reduces incorrect diagnosis errors through identifying true-positive and false-positive results.

Chapter 3 evaluates a new way to perform COVID-19 detection using real patient samples. This involves testing the DirectDetect diagnostic method for COVID-19 which is advantageous as it does not require viral transport medium or viral RNA extraction prior to nucleic acid amplification and detection. For this work

we tested dry and wet patient sample swabs for SARS-CoV-2 and found the method worked well for multiple different starting sample types (dry nasal swabs in no transport medium, treated wet nasal swabs in transport medium with RNA extraction, and untreated wet nasal swabs in transport medium without RNA extraction). The limit of detection for SARS-CoV-2 was 12.5 copies/reaction and the positive agreement between swab types and a clinical laboratory test were 91.7% for dry swabs, 83.3% for treated wet swabs, and 87.5% for untreated wet swabs.

Chapter 4 begins our work in developing a fundamental understanding of magnetic bead transport under electrokinetic flow in a microfluidic chip. This study evaluates the removal of buffer contaminants during nucleic acid sample preparation that can inhibit downstream processes, such as amplification. The designed microfluidic chip combined selective adsorption of target DNA onto magnetic beads with subsequent transport of beads through a microchannel undergoing an antiparallel EOF to isolate DNA into a clean, inhibitor-free solution. Results showed the carryover volume of unwanted sample contaminants was reduced to 0.22 ± 0.03% and there was a 15% increase in DNA extraction yield for the microfluidic chip with the voltage applied vs without.

Chapter 5 continues to study magnetic bead transport under electrokinetic flow, now focusing on the removal of carryover DNA during NGS library preparation. This is important as the carryover of small DNA created during library preparation, known as adapter dimers, can interfere with sequencing results. The same combination of magnetic bead transport and EOF as Chapter 4 was utilized but with a different microfluidic chip design. Automated magnetic bead transport on the microfluidic chip resulted in 84% of beads transferring under 800 V vs 81% using manual transfer. Additionally, higher voltages showed better removal of adapter dimers as EOF increases and the percent adapter dimer was comparable to the manual conditions at 150 V applied across the microfluidic chip.

Chapter 6 extends our investigation into magnetic bead transport under electrokinetic flow and adds the development of an automated platform for NGS library preparation for PGT-A as a sequencing application. The goal of the automated platform was to integrate automated microscale purification and macroscale PCR amplification to replace manual DNA library preparation and magnetic bead-based cleanup steps. Reagent

mixing and thermoelectric cooler-based capillary heating and cooling was modeled to better understand the system and electrophoresis was integrated with magnetic bead transport on a microfluidic chip to remove primer and adapter dimers. The result of this work showed DNA libraries conducive to sequencing as >4 ng/μL of library was produced with sample loss or evaporation contributing to concentration difference between on-device and manual preparations. Additionally, sequencing results showed that the percent of mapped reads and PG-find quality scores were not statistically significantly different between library preparation methods.

Chapter 7 describes progress and challenges in laboratory-based diagnostic and screening approaches for aneuploidy detection during pregnancy in the form of a review article. This work investigates molecular and engineering-based approaches for detecting and study aneuploidy as well as challenges and considerations for the field of aneuploidy detection during pregnancy to provide parents with critical information about their unborn child

Chapter 8 shows the investigation of cfDNA transport and purification in a microfluidic channel for NIPT as increasing the yield and purity of cfDNA is important since inefficiencies can dramatically affect the sensitivity and specificity of the test. False positives may occur during NIPT as the total amount of cfDNA found in plasma ranges from around 1.8 ng/mL to 22 ng/mL and the fetal fraction is around 13.4% of the sample. Solid phase extraction and microfluidic chip purification were coupled with EOF to increase the purity of the extracted sample and used to maximize the workflow's simplicity and potential for automation. This work optimized existing cfDNA isolation kit buffers and volumes to adapt to microfluidic chip for the washing procedure. Results found the optimized condition for the highest purity sample without sacrificing yield was Wash 1 only on-chip with 300V applied and an average yield of 68.19%, which is as good or better than other commercial kits.

Chapter 9 explains the development of a method for target DNA analysis that transform different sequences of the same size into different sizes followed by separation using capillary electrophoresis. Sequence specific probes and size-based tags are hybridized to target DNA prior to universal amplification and capillary electrophoresis separation for the analysis of the presence of the DNA target in the sample. The

robustness of this method was evaluated using target DNA dilutions in genomic or fragmented DNA as well as target DNA extraction from plasma before method analysis. Results showed this method could work for as little as 0.003 ng of target DNA and multiplexing and separation of six different sizes.

Chapter 10 provides concluding thoughts and future perspectives on each of the project areas of this thesis. This includes a summary of the work presented, limitations of that work, and future research directions from this thesis.

CHAPTER 2

Mathematical model to reduce loop mediated isothermal amplification (LAMP) false-positive diagnosis

---

Chapter 2 has been published as an original research article.

Schneider, L., Blakely, H., Tripathi, A., *Mathematical Model to Reduce Loop Mediated Isothermal Amplification (LAMP) False-Positive Diagnosis*, **Electrophoresis**, 40(20), 2706-271, 2019.

2.1 Abstract

Loop mediated isothermal amplification (LAMP) is a nucleic acid amplification technique performed under isothermal conditions. The output of this amplification technique includes multiple different sizes of DNA structures which are identified by a banding pattern on gel electrophoresis plots. Although this is a specific amplification technique, the complexity of the primer design and amplification still lead to the issue of obtaining false-positive results, especially when a positive reading is determined solely by whether there is any banding pattern in the gel electrophoresis plot. Here, we first performed extensive LAMP experiments and evaluated the DNA structures using microchip electrophoresis. We then developed a mathematical model derived from the various components that make up an entire LAMP structure to predict the full LAMP structure size in base pairs. This model can be implemented by users to make predictions for specific, DNA size dependent, banding patterns on their gel electrophoresis plots. Each prediction is specific to the target sequence and primers used and therefore reduces incorrect diagnosis errors through identifying true-positive and false-positive results. This model was accurately tested with multiple primer sets in house and was also translatable to different DNA and RNA types in previously published literature. The mathematical model can ultimately be used to reduce false-positive LAMP diagnosis errors for applications ranging from tuberculosis diagnostics to E. coli to numerous other infectious diseases.

2.2 Introduction

Nucleic acid sequences are an invaluable tool in diagnosing diseases and understanding an individual's genetic makeup. There are a variety of DNA amplification techniques used to increase the quantity of target DNA fragments for diagnostics. One commonly used method of DNA amplification is polymerase chain reaction (PCR). This technique works by using three different temperatures to amplify the DNA[66]. Due to the restrictions that the temperature cycling needed to run PCR places on equipment and experimental setup, there has been an emphasis on developing DNA amplification techniques that can be performed at one temperature, or isothermally. Isothermal techniques of note are loop mediated isothermal amplification (LAMP), rolling circle amplification (RCA), and nucleic acid sequence-based amplification (NASBA). RCA works with a single stranded, circular DNA template and strand displacing DNA polymerase[67]. The DNA polymerase performs strand-displacing synthesis on the single stranded DNA and 'rolls' out a copy of the circular DNA under isothermal conditions[67,68]. NASBA is also executed under isothermal conditions but is a transcription-based amplification procedure that copies single stranded RNA or DNA sequences[67,69]. Two RNA primers and three enzymes are used, and the procedure includes both an initiation phase and an amplification phase to create the final amplification product[67]. Although these methods perform well under isothermal conditions, the focus for this mathematical model analysis is LAMP.

LAMP was discovered in 2000 by Notomi *et al.* and uses four to six primers to target six to eight primer binding sites within the target DNA[41]. The primers include forward and backward inner primers (FIP and BIP), outer primers (F3 and B3), and loop primers. A detailed schematic of the LAMP process is outlined in Fig.2.1. The LAMP process begins with a double stranded DNA template (Step 1). Next, the *Bst* DNA polymerase enzyme used in this reaction causes strand displacement by the FIP primer hybridizing F2 to the primer binding site at F2c (Step 2)[41]. The inner primers are made up of two parts, one with the sense (5' to 3') and one with the antisense (3' to 5') strand complementary to the template DNA[41]. Strand displacing DNA polymerase separates the double stranded DNA and create a new copy of the template DNA starting from the inner primer[41]. Hybridization of the outer primer (F3) to its respective primer binding site (F3c) then creates another new copy of the template while displacing the single-stranded DNA created from the

inner primer (Step 3)[41]. Nucleotides are added to the F3 3' end which releases the single strand of DNA including the FIP primer and the F1 and F1c sites are bound together using hydrogen bonds, creating a self-hybridizing, single-stranded loop (Step 4). This is then used as a template to repeat this process on the opposite end of the DNA structure with new, corresponding backward inner and outer primers, culminating in the production of a dumbbell structure (Steps 5-7)[41].

Next, LAMP cycling begins with extension from the 3' end of the dumbbell structure, creating the first 'stem and loop' structure (Step 8). A new FIP primer binds to the F2c primer binding site (Step 9) and a new strand of DNA makes a copy of the stem and loop structure which creates a new loop between B1c and B1 primer binding sites (Step 10). Lastly, nucleotides are added to the 3' end of DNA structure again which releases the newly created strand of DNA which will fold into a dumbbell structure and new stem and loop LAMP structure is also created which has and additional target sequence from the previous structure (Step 11). The newly created stem and loop DNA structure is used as another template for LAMP cycling using one inner primer at a time, either the forward or backward inner primer[41]. The overall result of LAMP can make 10^9 copies of the target DNA when starting from a few copies within under an hour[41]. This efficient amplification is a major advantage of LAMP, as well as its ability to produce these DNA copies all under isothermal conditions.

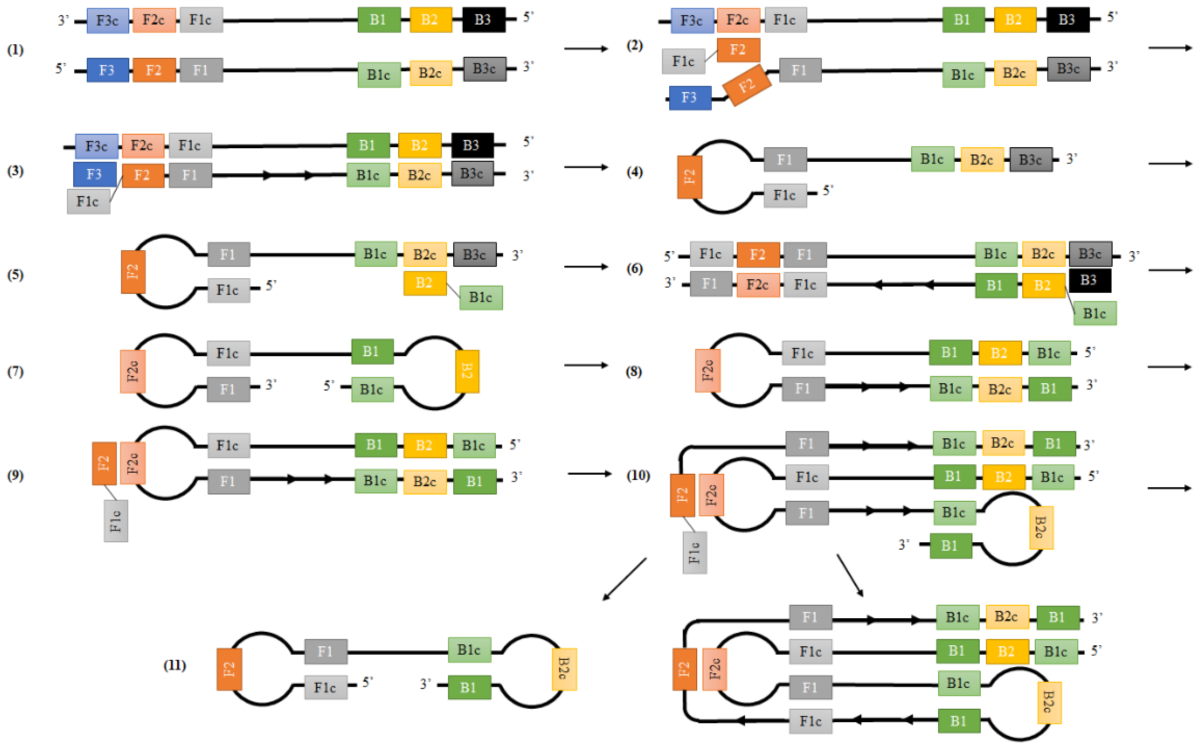

Figure 2.1: LAMP Dumbbell Formation (Steps 1-7) and LAMP Cycling (Steps 8-11) schematic using FIP binding sites (F1 and F2), F3 binding site, BIP binding sites (B1 and B2), and B3 binding site. All complement sequences are noted with a ‘c’ following the primer binding site name.

Currently, LAMP has been widely used for infectious disease diagnostic applications where the researcher’s main objective is to correctly identify positive and negative LAMP reactions to identify a specific disease[70-72]. A positive LAMP reaction indicates that the target DNA sequence, representing a disease or other diagnosis such as human influenza viruses H1 or H3[73], has been amplified, and therefore identified in that sample. A negative LAMP reaction indicates that the sample does not contain that target sequence since it has not been identified and amplified in the reaction, therefore leading to a negative reaction and a negative diagnosis. Here, the focus is on better understanding the DNA structures that are created through this amplification technique since, unlike PCR, DNA copies created through LAMP are dissimilar in size. This investigation is done using mathematical modeling to predict the size of different DNA structures produced through LAMP using gel or microchip electrophoresis.

Mathematical modeling for LAMP has been used once previously to quantify the LAMP amplification process[74]. This model uses the concentration versus time curves of LAMP experiments to determine the time-to-positive (T_p) of LAMP samples which is considered equivalent to the threshold cycling time in PCR reactions[74]. Here, an alternative approach to better understanding the amplification process is provided. This new mathematical model makes it possible to instead predict the banding pattern associated with positive LAMP samples during gel electrophoresis. A major benefit of this model is that it creates a user-friendly prediction method for positive LAMP samples which allows for false-positive reactions to be more easily identified and increases researchers' understanding on different DNA products in the reaction. The developed mathematical model fills a gap in the research on LAMP as a simple, easy to use tool that quickly recognizes false-positive LAMP reactions. Since the stem and loop structures created through LAMP are complex in nature, creating this simple tool can be relatively difficult[75]. In conventional PCR, researchers can predict the output DNA sizes of their amplified product in a true-positive reaction based on the location of the forward and reverse primers on the template DNA. The complexity of the LAMP process does not allow for that same predictive method. However, this mathematical model is a new tool that allows researchers to make those same predictions for the sizes of the different amplified products produced through a true-positive LAMP reaction based on the target and primer sizes. Similar to recognizing true-positive reactions on gel electrophoresis plots for PCR, this model allows researchers to quickly recognize true-positive and false-positive amplification for LAMP because they will know what the correct banding patter should be. Thus, if the gel electrophoresis plot shows an alternative banding pattern, the researchers can identify the sample as a false-positive which can help to reduce the likelihood of an incorrect diagnosis. Current methods to reduce the chance of false-positive LAMP reactions include optimizing LAMP reactions using multiple runs and techniques to find true positive results[76,77] or using more intricate methods such as molecular beacons that only fluoresce when bound to target DNA or restriction enzyme digestions[41,73,78]. Overall, this mathematical model helps to create a predictive method for researchers to implement into their LAMP experimental design that is of no extra cost to them, uses information already gathered during LAMP primer design, and reduces the likelihood of false-positive identifications.

2.3 Materials and Method

2.3.1 Template DNA

The LAMP analysis conducted in this study used M13mp18 (GenBank Accession #: X02513) as the template DNA. This is a double stranded phage vector that originated from bacteriophage M13 and was purchased from New England Biolabs (Ipswich, MA). It is covalently closed circular DNA that contains 13 different restriction sites.

2.3.2 Primer Design

The two sets of LAMP Primers (Table 2.1) used in this study were designed from M13mp18 template DNA (New England Biolabs, Ipswich, MA). The EIKEN Primer Explorer version 5 software was used to generate the sequences for each forward inner primer (FIP), forward outer primer (F3), backward inner primer (BIP), and backward outer primer (B3). The target positions of the primers are illustrated in Fig. 2.2. All primers were then synthesized by Integrated DNA Technologies (Coralville, IA). Forward and backward loop primers were not originally used in this study to keep the LAMP procedure as simple as possible for this modeling application. Forward loop and backward loop primers were created and tested when evaluating the robustness of the model.

Table 2.1: LAMP primers designed to be used with M13mp18 template DNA.

Primer Name	Length	Sequence (5'-3')
FIP-1 (F1c + F2)	40-mer	GCTATTACGCCAGCTGGCGAAGGAAAACCCTGGCGTTACC
BIP-1 (B1c + B2)	38-mer	CACCGATCGCCCTTCCCAACGCCGGAAACCAGGCAAAG
FIP-2 (F1c + F2)	41-mer	ACAACATACGAGCCGGAAGCAAGTTAGCTCACTCATTAGGC
BIP-2 (B1c + B2)	42-mer	ACACAGGAAACAGCTATGACCACAGGTCGACTCTAGAGGATC
F3-1	20-mer	CGTCGTTTTACAACGTCGTG
B3-1	18-mer	GCACTCCAGCCAGCTTTC
F3-2	19-mer	GCGCAACGCAATTAATGTG
B3-2	18-mer	GTAAAACGACGGCCAGTG
Forward loop	18-mer	GCGAAAGGGGGATGTGCT
Backward loop	18-mer	AGTTGCGCAGCCTGAATG

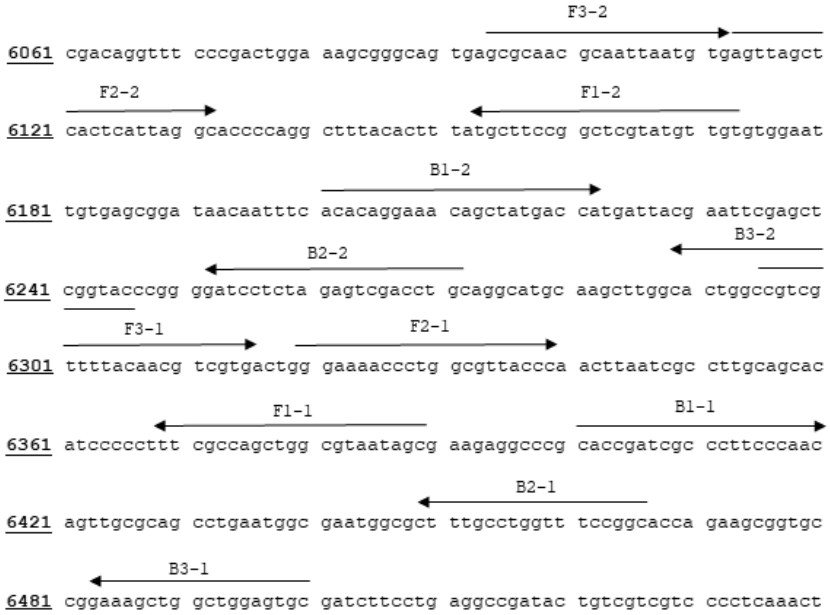

Figure 2.2: Schematic of LAMP primer sites within the M13mp18 template DNA.

2.3.3 LAMP Reaction Conditions

The LAMP reaction was conducted in a total volume of 25 µL and followed WarmStart® LAMP Kit (DNA & RNA) specifications (New England Biolabs, Ipswich, MA). The reaction mixture included 12.5 µL of NEB WarmStart LAMP 2X Master Mix which contains a combination of the enzymes *Bst* 2.0 WarmStart DNA Polymerase, WarmStart RTx Reverse Transcriptase, dNTPs, and $MgSO_4$. These enzymes were contained within an Isothermal Amplification Buffer optimized for LAMP and RT-LAMP reactions according to the manufacturer. The exact concentration of these enzymes was not specified by NEB. The mixture also contained the following primers: 1.6 µM of FIP and BIP, and 0.2 µM of F3 and B3. Lastly, 9 µL of nuclease free water and 100 ng (1.28×10^{10} copies) of the M13mp18 target DNA was added to each LAMP reaction. Samples were heated to 67°C for 30 minutes, followed by a 5-minute *Bst* 2.0 WarmStart DNA Polymerase inactivation step at 95°C.

2.3.4 Gel Electrophoresis Assessment of the LAMP Product

Following every LAMP reaction, 1 µL of each sample was run through the Agilent Bioanalyzer 2100 machine with the Agilent DNA 1000 Kit and DNA Chip for On-Chip-Electrophoresis (Agilent Technologies, Santa Clara, CA). According to the Agilent DNA 1000 Kit Guide, the sensitivity of the kit

is ± 5 base pairs (bps) with samples between 25 and 100 bps, ± 5% between 100 and 500 bps, and ± 10% between 500 and 1000 bps. The output of the Agilent Bioanalyzer 2100 is a gel electrophoresis plot, an electropherogram plot, and the concentration (ng/μL) and molarity (nmol/L) associated with each band or peak. The individual DNA sample concentrations at each band or peak were added together to find the overall concentration produced in the reaction.

2.3.5 Optimization of LAMP Assay

Optimizing the LAMP procedure with the first set of LAMP primers (FIP-1, BIP-1, F3-1, B3-1) was required prior to LAMP product analysis. Optimization criteria included: creating a large amount of total LAMP product (~30-50ng/μL or more), creating a distinct banding pattern – represented by the lowest number of peaks on the electropherogram, and running the experiment in the least amount of time. The criteria were chosen to produce an abundant amount of DNA product with an easily identifiable banding pattern in an efficient amount of time. The variables tested during the optimization process were: adding a LAMP enzyme (*Bst* 2.0) inactivation temperature step, temperature, time, and temperature of LAMP enzyme inactivation step.

2.3.6 Development of Mathematical Model for Base Pair Size Analysis of LAMP Structures

The DNA analysis tool used in this study was the Agilent Bioanalyzer 2100. This machine was essential for the novel evaluation and interpretation of LAMP products under varying conditions because it could give precise readouts for DNA structure. The Agilent Bioanalyzer 2100 device clearly demonstrated that the LAMP experiments led to distinct and relatively consistent products – within ~10 bps – based on the DNA target sequence being used. Conventional gel electrophoresis does not provide specific base pair size outputs for each reaction, which is why this microchip electrophoresis machine was used in this study. The Bioanalyzer data also showed varying amounts of noise most likely caused by incomplete LAMP structures depending on the length of time and the temperature the test was run at. The most important analysis to note from the Bioanalyzer is the base pair sizes associated with the largest peaks on the electropherogram plots as these were the most common product sizes and the values used to create this mathematical model.

As previously noted, the main aim of this study was to provide users with a simple tool that can quickly recognize false-positive LAMP reactions. This was approached was through developing a mathematical model to easily create predictions for the sizes of different LAMP structures before performing any experiments. Thus, these predictions can be used to identify true-positive and false-positive LAMP reactions using gel electrophoresis banding pattern analysis.

The overall process of creating this model involved transforming the qualitative LAMP structure into a quantitative LAMP structure size. The first step of the model development was to identify how many times different primer binding sequences (F1, F2, F3, B1, B2, B3) appeared in the final LAMP product. This was important so that the size (bp) of each of these sequences could be multiplied by the number of times they appear in the final structure resulting in the overall structure size. Fig. 2.1 shows that regardless of the number of target sequences, the final LAMP product will contain the same four primer binding sites: F1, F2, B1, and B2. Additionally, the sequences between F1 and F2 (known as F_{space}), and B1 and B2 (known as B_{space}) will be in every final structure. Lastly, every LAMP structure will contain a specified amount of target sequences. The number of times each of these seven components appear in a LAMP structure is important when predicting the overall size. Therefore, different LAMP structures were evaluated to count the number of times each of these parts are found. Fig. 2.1 was used for analyzing the Stem and Loop x1 and Stem and Loop x2 structures, and additional LAMP schematics by Notomi *et al.*[41] were used for structures up to Stem and Loop x7 which contains 7 target sequences. Table 2.2 breaks down this quantitative analysis to show a population count for how many times each primer binding site, F_{space}, B_{space}, and target appears in each structure. These counts are consistent between any LAMP structure, no matter the diagnostic application. As amplification occurs, each cycle adds one target sequence and one primer binding site – either FIP (F1 and F2) or BIP (B1 and B2), depending on the structure that was amplified. Due to the self-hybridizing loop that appears in the stem and loop structures, the addition of new primer binding sites during each amplification cycle can be complex to understand, therefore making Table 2.2 helpful in determining how many times each primer binding site appears for any given structure.

Table 2.2: Quantitative analysis of the number of times six components of the LAMP structure appear in relation to the number of target sequences.

Structure	Target	B2	B_{space}	B1	F1	F_{space}	F2
Stem and Loop x1	1	1	1	1	2	1	1
Stem and Loop x2	2	2	2	3	2	1	1
Stem and Loop x3	3	2	2	3	4	2	2
Stem and Loop x4	4	3	3	5	4	2	2
Stem and Loop x5	5	3	3	5	6	3	3
Stem and Loop x6	6	4	4	7	6	3	3
Stem and Loop x7	7	4	4	7	8	4	4

Upon detailed analysis, Table 2.2 identifies a pattern when comparing the number of times different primer binding sites and spaces appear in the LAMP structure to the number of target sequences. This pattern was essential in the development of the mathematical model. Also, since each amplification cycle adds either a FIP or BIP primer the model was split into two parts to account for this. It was also assumed that the loop of the stem and loop structure always included B2 – part of the BIP primer – for developing this model. Therefore, an odd number of targets will end with the FIP primer represented by one equation, and an even number of targets will end with the BIP primer represented by a second equation. Each component of the final two equations were individually derived through relating the number of times a primer binding site appeared in a structure versus a target site. Equation 2.1 and Equation 2.2 demonstrate how to relate the primer binding site B2 to the target for odd and even numbers of targets, respectively.

Equation 2.1: Number of B2 Sequences in a LAMP Structure with an odd Target Number (x);

$$B2\ Sequences = \left(x - \left(\frac{x-1}{2}\right)\right) \qquad (2.1)$$

As an example, in a LAMP structure that has 3 target sequences, Equation 2.1 multiplies out to 2 when x = 3. This indicates that there are two B2 sequences in this structure and is confirmed again by Table 2.2. This equation will give the correct number of B2 sequences in all structures with an odd number of targets.

This equation derivation is repeated for B2 sequences when there is an even number of target sequences.

Equation 2.2: Number of B2 Sequences in a LAMP Structure with an even Target Number (x):

$$B2\ Sequences = \left(x - \left(\frac{x}{2} - 1\right)\right) \quad (2.2)$$

This equation is tested using an example LAMP structure with 4 target sequences (x=4). According to Equation 2.2, the structure will have three B2 sequences which corresponds with the value in Table 2.2. This evaluation is repeated for each of the six components of the LAMP structure (in Table 2.2) to relate the number of times they are repeated to the number of times the target sequence is present.

To convert the number of times each primer binding site appears in the equation to how many base pairs this will add to the overall structure, each of the values calculated in Equation 2.1, Equation 2.2, and subsequent derivations, were multiplied by the respective size (bp) of the primer binding site. This information is easily and immediately available to the user when creating specific LAMP primers. Using Fig. 2.2 for example, this shows the location of different primer binding sites in the target sequence so that each component of the LAMP structure can be identified, and the number of base pairs contained in that component can be counted. Then, in the final equations that calculate the overall structure sizes (bp) in this model, each of the individual primer binding site sizes will be inputted to the respective variable. One assumption made in this model is that the loops created in stem and loop structures are considered base pairs in this size estimation although they are single stranded nucleotides. Ultimately, following individual derivation for each component of the LAMP structure, two master equations are outputted: one that predicts the LAMP structure size (bp) with an odd number of target sequences (Equation 2.4) and one that predicts the LAMP structure size (bp) with an even number of target sequences (Equation 2.5). A breakdown of how to interpret these equations is first presented in Equation 2.3.

$$\begin{aligned} &LAMP\ Structure\ Size\ (bp) \\ &\quad = (B2\ sequence\ size + B_{space}\ sequence\ size)(Number\ of\ times\ B2\ and\ B_{space}\ appear\ in\ the\ structure) \\ &\quad + (B1\ sequence\ size)(Number\ of\ times\ B1\ appears\ in\ the\ structure) \\ &\quad + (Target\ sequence\ size)\ (Number\ of\ times\ the\ Target\ appears\ in\ the\ structure) \\ &\quad + (F1\ sequence\ size)(Number\ of\ times\ F1\ appears\ in\ the\ structure) \\ &\quad + (F2\ sequence\ size + F_{space}\ sequence\ size)(Number\ of\ times\ F1\ and\ F_{space}\ appear\ in\ the\ structure) \end{aligned} \quad (2.3)$$

Equation 2.4: LAMP Structure Size when there are an Odd Number of Target Sequences in Structure:

$$Structure\ Size\ (bp) = \left(B2 + \left(B_{space}\right)\right)\left(x - \left(\frac{x-1}{2}\right)\right) + (B1)(x) + Target\ (x) + (F1)(x+1) + \left(F2 + \left(F_{space}\right)\right)\left(x - \left(\frac{x-1}{2}\right)\right)$$

(2.4)

Equation 2.5: LAMP Structure Size when there are an Even Number of Target Sequences in Structure:

$$Structure\ Size\ (bp) = \left(B2 + \left(B_{space}\right)\right)\left(x - \left(\frac{x}{2} - 1\right)\right) + (B1)(x+1) + Target\ (x) + (F1)(x) + (F2 + \left(F_{space}\right))(x - \frac{x}{2})$$

(2.5)

After deriving the LAMP structure size analysis model, it was tested using the optimized LAMP primer mix. Then it was verified by testing the robustness of the model through varying the concentration of input DNA, adding loop primers to the LAMP primer mix, creating a new set of LAMP primers, and testing against different types of DNA and RNA LAMP reactions recorded in the literature.

2.4 Results and Discussion

2.4.1 Optimal LAMP Assay

Results of optimization testing showed that running the experiment at 67°C created the largest amount of product (Fig. 2.3A). This optimized temperature can be explained by the melting temperature (T_m) of the FIP and BIP primers. At 70°C and 72.2°C, respectively, the temperature at which they anneal for amplification will be around 5°C below the T_m. Therefore, the range for the annealing temperature is between 65°C and 67.2°C, which includes the optimized temperature[79]. The time optimization testing showed that the Bioanalyzer was able to analyze the amount of LAMP product produced after running the reaction for 30 minutes (Fig. 2.3B). A reason for this is that at 30 minutes, the amount of amplified DNA was now above the threshold of what the Bioanalyzer machine could recognize. Additionally, adding the heat inactivation step for the *Bst* enzyme at 95°C for 5 minutes helped to stop the reaction and, most likely, reduce the amount of secondary DNA structures which were interfering with the most prominent LAMP products during the control experiments. This heat inactivation step is not required for LAMP experiments but was important in this application to ensure the reaction was completely stopped after 30 minutes. The control procedure used as a comparison to the optimized assay was obtained from the WarmStart® LAMP Kit (DNA & RNA) specifications (New England Biolabs, Ipswich, MA). Fig. 2.3C shows the difference in

the total concentration of product produced between the control and final assays where an unpaired T-test indicated a statistically significant difference in these results. This is the optimal LAMP assay for our application because there is a statistically significant larger amount of total DNA produced compared to the control, there are fewer distinct peaks based on base pair size as compared to the control (data not shown), and it was run in the shortest amount of time possible to still produce a substantial amount of amplified DNA. An electropherogram of the typical result of this LAMP reaction using the first set of primers (FIP-1, BIP-1, F3-1, B3-1) is seen in Fig. 2.3D.

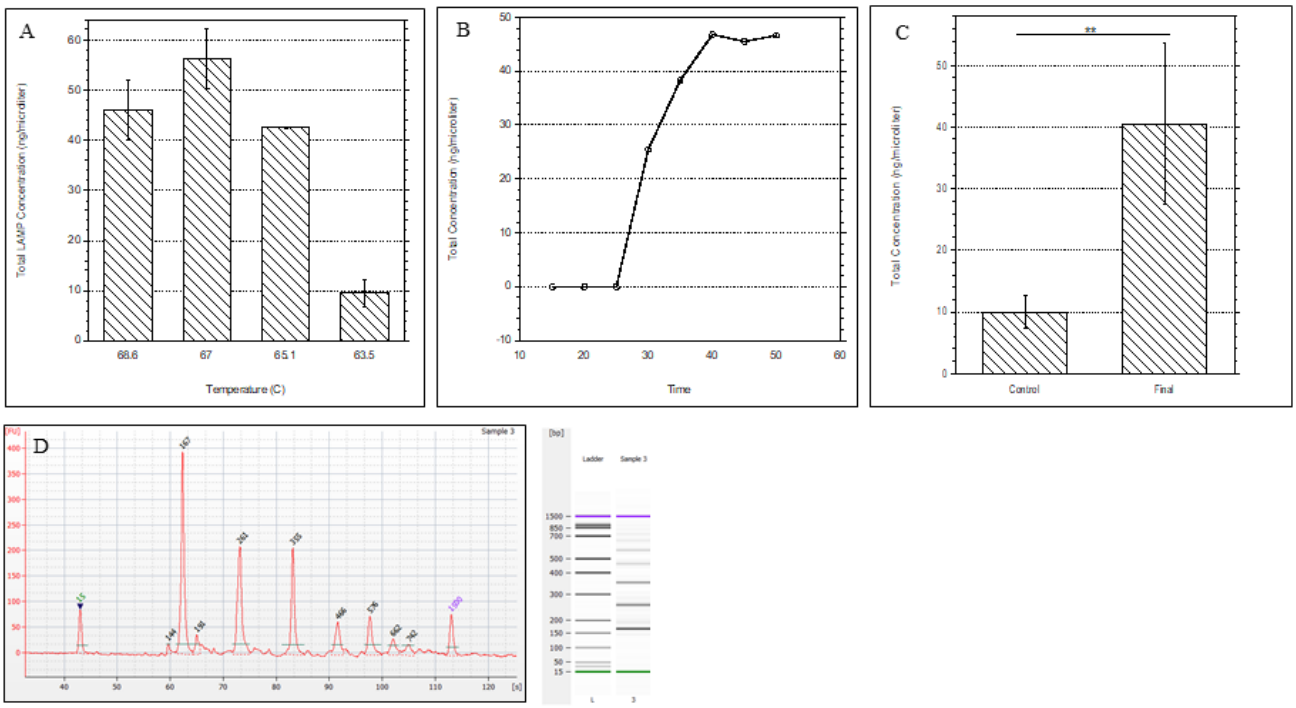

Figure 2.3: LAMP experimental results. (**A**) Comparison of LAMP Assay at different temperatures under same buffer conditions. (**B**) Comparison of LAMP Assay at different times under same buffer conditions. (**C**) Comparison of total amplified DNA under control conditions (65°C for 30 minutes) vs final optimized assay (67°C for 30 minutes, 95°C for 5 minutes). (**D**) Electropherogram of final optimized assay.

2.4.2 Robustness Testing of the True-Positive Banding Pattern Prediction Mathematical Model

Following the derivation of this model, different conditions were tested to evaluate how robust the model was at predicting the sizes of different LAMP structures. The first condition tested was the optimized set of LAMP primers containing only FIP, BIP, F3, and B3 primers in the primer mix and 100 ng of input DNA. Next, the concentration of input DNA was varied using the same set of primers. The concentrations

tested were 50 ng, 200 ng, and 400 ng of input DNA. Following this test, another test was run with a new LAMP primer mix using the first set of LAMP primers plus forward loop and backward loop primers. Then, an additional set of FIP, BIP, F3, and B3 LAMP primers were created to test the model. Lastly, the model was applied to LAMP testing found in the literature to test it against different types of DNA and RNA.

The predicted shape values under each of these conditions were compared to the average base pair sizes of the largest peaks (highest DNA concentration) from the electropherograms of the LAMP experiments. Based on the sensitivity of the Agilent Bioanalyzer 2100 machine, the accepted error rate is ±5% when the bp sizes are in the range of 100 and 500 bp or ±10% when the bp size is between 500 and 1000 bp. An acceptable error range was then established for each predicted size value to assess the accuracy of the mathematical model to evaluate how the experimental data compared with the model's predictions.

2.4.2.1 Testing on Optimized Set of LAMP Primers

Once the mathematical model was established, the next step was to test this model on the optimized LAMP assay. This process began with identifying the size and location of each primer and the number of nucleotides between them within the M13mp18 template DNA for the first primer set (Fig. 2.2 and Table 2.1). This information was readily available in the software used for LAMP primer design, so this did not create an extra evaluation step to use this model. Table 2.3 provides the given variable and corresponding base pair size for this first primer set and the outcome predicted DNA structure sizes exported from the mathematical model are listed under 'Predicted Size (bp)' in Table 2.4. When comparing the difference between the predicted size and the average structure size, 100% of the bp differences fell within this accepted range for each structure. The predicted vs actual structures sizes were also graphed and, using an unpaired T-test, it was determined that six of the seven structures sizes did not have a statistically significant difference between the predicted and actual sizes, which is expected (Fig. 2.4A). Although, one structure did show a statistically significant difference between the predicted and actual values, seven out of the seven compared structures had a difference that was less than that of the sensitivity of the Bioanalyzer, which indicated the success of the predictions (Fig. 2.4A). Fig. 2.4B shows an electropherogram of the optimized LAMP experiments and qualitatively presents what DNA structure is represented by each peak.

Table 2.3: Variable inputs for mathematical model using LAMP Primer Set 1 and LAMP Primer Set 2.

Variable	Base Pair Size Inputs for LAMP Primer Set 1	Base Pair Size Inputs for LAMP Primer Set 2
F2	19	20
F_{space}	30	20
F1c	21	21
Target	11	27
B1c	20	22
B_{space}	28	29
B2	18	20

Table 2.4: Predicted LAMP Structure Size vs Real LAMP Structure Size for optimized set of LAMP primers (Primer Set 1). n = 5

Structure	Predicted Size (bp)	Average Structure Size (bp)	Difference (bp)
Stem and Loop, x=1	168	172	4
Stem and Loop x2, x=2	265	263	2
Stem and Loop x3, x=3	367	354	13
Stem and Loop x4, x=4	464	461	3
Stem and Loop x5, x=5	566	572	6
Stem and Loop x6, x=6	663	666	3
Stem and Loop x7, x=7	765	768	3

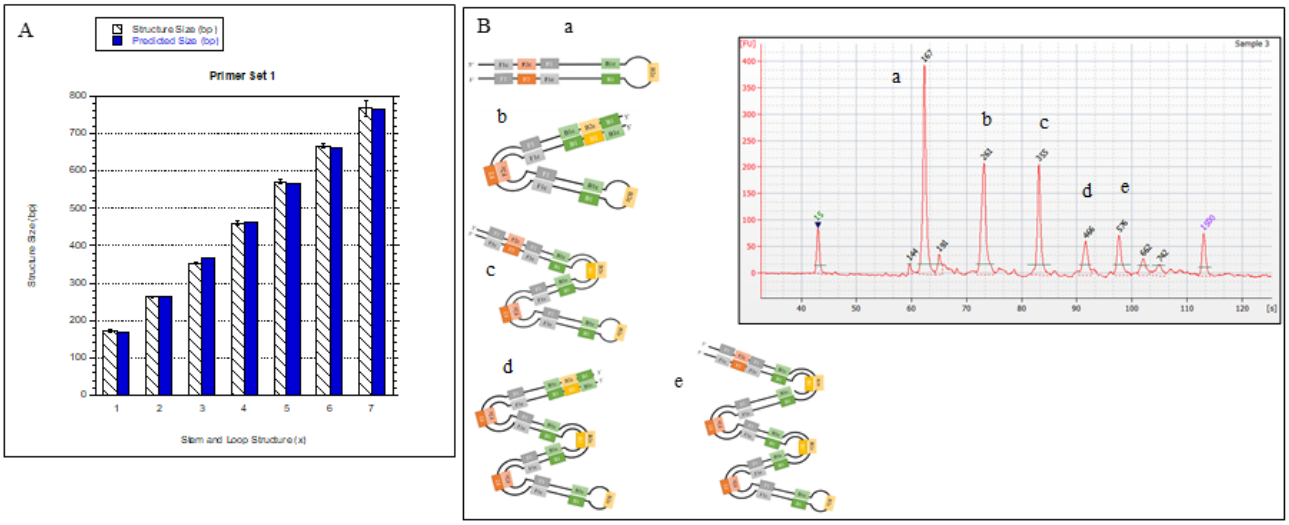

Figure 2.4: (A) Graphical comparison between the predicted and experimentally determined structure size and for every stem and loop structure size using the first set of LAMP primers. (B) Electropherogram of final LAMP Assay with corresponding structure sizes. Predicted peak sizes were (a) 168, (b) 265, (c) 367, (d) 464, (e) 566 which fall within 5% of the peak sizes produced by this assay. Each stem and loop structure produced has inverted repeats of the target sequence found between the forward and backward primer sections.

2.4.2.2 Effect of varying starting DNA concentrations

The original concentration of DNA used for the optimized set of LAMP primers experiments was 100 ng. The input DNA concentration was varied during the robustness testing. The different concentrations were 50 ng (6.39×10^9 copies), 200 ng (2.56×10^{10} copies), and 400 ng (5.11×10^{10} copies). Copy number values are calculated based on the assumption that the average base pair weight is 650 Daltons. The same information from Table 2.3 for the first primer set and Predicted Sizes from Table 2.4 were used to assess the results of these experiments. In each of the three concentration groups, it was found that the Stem and Loop x3 structure fell outside of the sensitivity of the Bioanalyzer with an average peak size of 345 bp for 50 ng, 344 bp for 200 ng, and 341 bp for 400 ng of input DNA where the predicted size is 367 bp with a sensitivity range of 18.35 bp. The Stem and Loop x3 structure was also the only structure in the optimized LAMP primers testing to show a statistically significant difference between the predicted and actual values. One reason this specific structure may results in product sizes further from the predicted value is due to incomplete elongation of a new LAMP structure. This could be caused by annealing between alternatively inverted repeats in the same strand of DNA which would explain why the results show a slightly smaller size for this structure.

Additionally, with a starting concentration of 400 ng, the average structure size also fell outside of the range of the Bioanalyzer sensitivity at 438 bp where the predicted size is 464 bp which may also be explained by the same principles used for the Stem and Loop x3 structure. Overall, it is hypothesized that concentration does not affect the validity of this model since each of these concentrations had a similar result with Stem and Loop x3, although a starting concentration of 400 ng did produce an additional structure size outside of the sensitivity of the Bioanalyzer. One way to test how these specific structures fell outside of the respective predicted ranges would be to increase the experiment time to confirm all structure elongation has occurred.

2.4.2.3 Effect of including loop primers in the LAMP primer mix

The original LAMP primer design did not include loop primers so that the LAMP amplification could be kept as simple as possible for the predictive model development. But, to test the robustness of the model,

researchers were interested in investigating the effect of adding these loop primers to the primer mix. The new loop primer mix used primers at a final concentration of 1.6 μM of FIP-1 and BIP-1, 0.2 μM of F3-1 and B3-1, and 0.4 μM of forward loop and backward loop primers (Table 2.1). The same predicted sizes from Table 2.4 were also used in this testing analysis. The result of adding the loop primers showed that 100% of the LAMP structures still fell within the range of the Bioanalyzer sensitivity, results are presented in Table 2.5. The only significant difference when using the loop primer mix was that each of these reactions also showed a peak on the electropherograms around 75 bp which is hypothesized to be caused by a primer dimer formation, caused by primers binding to themselves and amplifying. One reason why a primer dimer may be found when using the loop primer mix is because there is now a larger concentration of LAMP primers starting in the reaction, therefore it is possible that some may bind to each other, rather than existing LAMP structures.

Table 2.5: Predicted LAMP Structure Size vs Real LAMP Structure Size for loop primer mix testing. n = 4

Structure	Predicted Size (bp)	Average Structure Size (bp)	Difference (bp)
Stem and Loop, x=1	168	169	1
Stem and Loop x2, x=2	265	261	4
Stem and Loop x3, x=3	367	355	12
Stem and Loop x4, x=4	464	466	2
Stem and Loop x5, x=5	566	577	11
Stem and Loop x6, x=6	663	668	5
Stem and Loop x7, x=7	765	749	16

2.4.2.4 Testing on New Set of LAMP Primers

To further confirm the validity of this mathematical model, a new set of LAMP primers were designed and tested (FIP-2, BIP-2, F3-2, B3-2, Table 2.1) while keeping all other testing conditions the same as the optimized LAMP primers testing. Using the length of the primers and their location in the M13mp18 DNA sequence (Fig. 2.2), each variable of the mathematical model was identified (Table 2.3, Primer Set 2) and predicted sizes were outputted (Table 2.6). Although this LAMP procedure was not optimized for this new primer set, the mathematical model still showed a 100% prediction accuracy when compared to the experimentally gathered structure sizes, still accounting for the same sensitivity of the Bioanalyzer machine. An example electropherogram of this data is presented in Fig. 2.5A and a graphical comparison of the

predict and experimentally determined structure sizes is provided in Fig. 2.5B. Using these primers, only one of the structures showed no statistical significance for the difference between the predicted and actual value using an unpaired T-test. This variation is to be expected though, because the experiment was not optimized for these primers and therefore the difference in the mean base pair sizes of the structures may be further apart than if the experiment was optimized. The model still does prove to be robust though because seven out of the seven structures tested did have a difference in size that was less than the sensitivity of the Bioanalyzer, which is how the success of this model is determined.

Table 2.6: Predicted LAMP Structure Size vs Real LAMP Structure Size for LAMP Primer Set 2. n = 5

Structure	Predicted Size (bp)	Average Structure Size (bp)	Difference (bp)
Stem and Loop, x=1	180	189	9
Stem and Loop x2, x=2	300	290	10
Stem and Loop x3, x=3	409	407	2
Stem and Loop x4, x=4	529	544	15
Stem and Loop x5, x=5	638	660	22
Stem and Loop x6, x=6	758	784	26

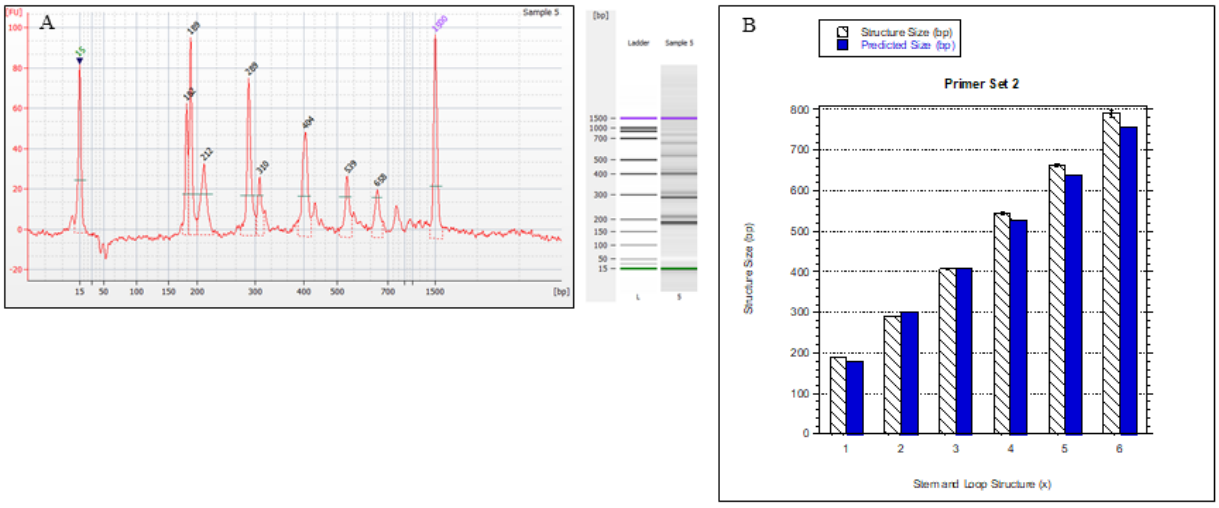

Figure 2.5: (A) Electropherogram of final LAMP Assay with Primer Set 2. (B) Graphical comparison between the predicted and experimentally determined structure size and for every stem and loop structure size.

2.4.2.5 Testing with LAMP experiments found in the literature

Following successful mathematical predictions using two different sets of LAMP primers and M13mp18 template DNA, this model was compared to LAMP data presented in current literature. Table 2.7 shows

the results of this analysis. The given studies were chosen because they included a figure that showed the location of the LAMP primers in the DNA sequence used. This provided the input values for the mathematical model to make the size predictions. Additionally, there was a gel electrophoresis plot to compare the mathematically derived predictions to so that there could be an evaluation regarding whether the model worked or not. A benefit of using the Agilent Bioanalyzer 2100 for this study is that exact base pair values were exported for every peak, for every LAMP sample. In other literature on LAMP, most studies are not analyzed using an Agilent Bioanalyzer 2100, but with standard gel electrophoresis, therefore experimental values are written as an approximation if not otherwise specified by the author of that study. Even LAMP experiments analyzed with a Bioanalyzer did not provide exact sizes for the banding pattern. Overall, it was determined that the predicted sizes outputted from the mathematical model fall within the same accepted error range used in the previous testing. Therefore, this data shows that the developed mathematical model is translatable to many different diseases, to RT-LAMP, and to different gel electrophoresis materials.

Table 2.7: Result of mathematical modeling predictions for currently published LAMP experiments.

Reference	DNA type	Gel Type	Predicted Sizes (bp)	Structure Sizes (bp)
Notomi[41]	M13mp18	2% agarose gel and followed by SYBR Green I stain	x= 1: 261 x= 2: 422 x = 3: 584 x= 4: 745 x= 5: 907 x=6: 1068	x= 1: ~270 x= 2: ~440 x = 3: ~600 x= 4: ~800 (Fig. 3A, Lane 4)[41]
Iwamoto[71]	Genomic DNA from Mycobacterium tuberculosis	3% agarose gel and followed by ethidium bromide stain	x= 1: 157 x= 2: 249 x = 3: 342 x= 4: 434 x= 5: 527 x=6: 619	x= 1: ~150 x= 2: ~250 x = 3: ~350 x= 4: ~450 (Fig. 2, Lane 1)[71]
Iwamoto[71]	Genomic DNA from Mycobacterium avium ATCC 25291	3% agarose gel and followed by ethidium bromide stain	x= 1: 174 x= 2: 273 x = 3: 375 x= 4: 474 x= 5: 576 x=6: 675	x= 1: ~165 x= 2: ~285 x = 3: ~390 x= 4: ~490 (Fig. 2, Lane 6)[71]
Iwamoto[71]	Genomic DNA from Mycobacterium	3% agarose gel and followed by ethidium bromide stain	x= 1: 180 x= 2: 300 x = 3: 411 x= 4: 531	x= 1: ~180 x= 2: ~275 x = 3: ~395 x= 4: ~500

	intracellular ATCC 13950		x= 5: 642 x=6: 762	(Fig. 2, Lane 11)[71]
Thai[80]	Severe Acute Respiratory Syndrome Coronavirus (SARS-CoV)	3% agarose gel and followed by ethidium bromide stain	x= 1: 168 x= 2: 277 x = 3: 364 x= 4: 473 x= 5: 560 x=6: 669	x=1: ~175 x=2: ~280 x=3: ~380 x=4: ~490 (Fig. 2, Lane 2)[80]
Dukes[81]	RT-LAMP of Foot and Mouth Disease Virus Strain O UKG 35/2001	Agarose gel with Picogreen®	x= 1: 154 x= 2: 252 x = 3: 340 x= 4: 438 x= 5: 526 x=6: 624	x= 1: ~150 x= 2: ~240 x = 3: ~350 x= 4: ~450 (Fig. 3, Lane 1)[81]
Han[82]	*Plasmodium* genus	3% agarose gel and followed by ethidium bromide stain	x= 1: 162 x= 2: 255 x = 3: 348 x= 4: 441 x= 5: 534 x=6: 627	x= 1: ~155 x= 2: ~250 x = 3: ~340 x= 4: ~430 (Fig. 3, Lane 1)[82]
Han[82]	*P. falciparum*	3% agarose gel and followed by ethidium bromide stain	x= 1: 165 x= 2: 275 x = 3: 374 x= 4: 484 x= 5: 583 x=6: 693	x= 1: ~ 160 x= 2: ~ 270 x = 3: ~ 370 x= 4: ~ 480 (Fig. 3, Lane 3)[82]
Han[82]	*P. vivax*	3% agarose gel and followed by ethidium bromide stain	x= 1: 165 x= 2: 269 x = 3: 364 x= 4: 468 x= 5: 563 x=6: 667	x= 1: ~ 160 x= 2: ~ 260 x = 3: ~ 350 x= 4: ~ 450 (Fig. 3, Lane 5)[82]
Han[82]	*P. malariae*	3% agarose gel and followed by ethidium bromide stain	x= 1: 195 x= 2: 307 x = 3: 422 x= 4: 534 x= 5: 649 x=6: 761	x= 1: ~ 200 x= 2: ~ 310 x = 3: ~ 420 x= 4: ~ 530 (Fig. 3, Lane 7)[82]
Han[82]	*P. ovale*	3% agarose gel and followed by ethidium bromide stain	x= 1: 183 x= 2: 304 x = 3: 404 x= 4: 525 x= 5: 625 x=6: 746	x= 1: ~ 175 x= 2: ~ 290 x = 3: ~ 390 x= 4: ~ 510 (Fig. 3, Lane 9)[82]

2.4.3 LAMP Theoretical Analysis

Following the true-positive banding pattern prediction mathematical modeling, LAMP structures were also evaluated using the thermodynamic modeling software, MFold. Mfold is used to predict the folding and

hybridization of single stranded nucleic acids[83]. This was an important analytical tool because it was able to validate that the LAMP structures predicted from the DNA sequences in the mathematical model were also the most thermodynamically likely DNA structures. Input settings for the modeling software were a folding temperature at 67℃ and a Mg^{2+} concentration of 8mM based on the composition of the LAMP WarmStart Mix being used in this reaction. From this technology the most likely structure was determined by the minimum ΔG ($kcal.mole^{-1}$) or Gibbs free energy. ΔG is the amount of energy capable of doing work during a reaction where temperature and pressure are constant[84]. If ΔG is a negative number, it releases free energy and the reaction is exergonic, and if the ΔG is positive it gains free energy and is an endergonic reaction[84]. Equation 2.6 is used in the calculations for the thermodynamics of folding. Where ΔH is the change in enthalpy, T is temperature, and ΔS is the change in entropy.

$$\Delta G = \Delta H - T\Delta S \qquad (2.6)$$

Equation 2.7 provides the DNA folding thermodynamics for the stem and loop structure while Equation 2.8 repeats this analysis for Stem and Loop x2, both provided by the MFold software.

$$\Delta G = \Delta H - T\Delta S = -78.30 \frac{kcal}{mol} at\ 67℃ \qquad (2.7)$$

$$\Delta G = \Delta H - T\Delta S = -153.44 \frac{kcal}{mol} at\ 67℃ \qquad (2.8)$$

For both of these calculations the standard errors for this thermodynamic folding were roughly ± 5% for ΔG, ±10% for ΔH, ± 11% for ΔS, 2-4 ℃ for melting temperature (T).

A significant finding with MFold technology was that the stem and loop structures predicted (Fig. 2.6), were also the only possible structures created under these conditions according to this software under the 2-state model, further validating this developed mathematical modeling tool. The simple 2-state model means that the nucleic acid sequence is either folded in the configuration shown, or entirely single stranded[83]. According to Zuker, to test the 2-state model, the sequences can be refolded, using MFold, near the respective predicted T_m values, and if the new T_m is 'significantly' larger than the original, this would

imply that the molecule can be refolded into another geometry at a larger T_m[83]. To test whether these structures could be refolded into another geometry, the stem and loop and stem and loop x2 sequences were rerun using MFold under the same conditions other than a new temperature setting at 95°C. The T_m values of the stem and loop and stem and loop x2 structures during the first test were 95.2°C and 97.8°C, respectively. These temperatures were near to the final heating temperature used experimentally, 95°C, so this temperature was selected for the new testing. The software results showed that both structures maintained the same thermodynamic folding with only a slight change in T_m. The stem and loop structure now had a ΔG of -3.19 kcal/mol at 95°C and a T_m of 96.2°C. The stem and loop x2 structure had a ΔG of -4.22 kcal/mol at 97.8°C and a T_m of 96.2°C. Due to the complexities of the LAMP structures and size constraints from the MFold modeling software, these were the only structures tested. However, this theoretical analysis strongly indicates that the predicted structures using DNA base pair size analysis are consistent with what is most likely to happen thermodynamically during single stranded nucleic acid folding and hybridization.

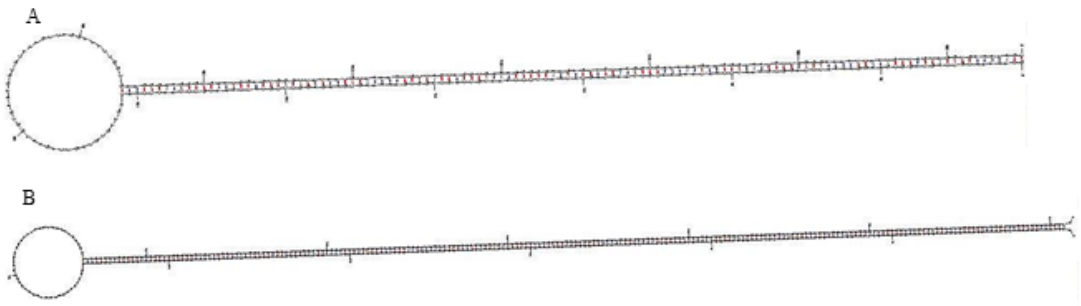

Figure 2.6: Output structures from MFold Modeling (A) Stem and Loop, (B) Stem and Loop x2.

2.5. Concluding Remarks

In summary, the model presented here correctly predicted the DNA structure sizes for various LAMP protocols from experimental data and primary literature examples. As LAMP has found a strong niche in diagnostic applications, it is essential that it is used accurately, and false-positive diagnosis is avoided. This mathematical model can be used as a tool to easily validate positive diagnostic results using any set of LAMP primers because the correct banding pattern on a gel electrophoresis plot can now be predicted.

Additionally, this model provides scientists with a stronger understanding of the various DNA structures being produced in their LAMP experiment. This model was validated using two sets of LAMP primers with 100% of the average DNA base pair sizes appearing within an accepted error margin of the LAMP predictions according to the sensitivity of the Agilent Bioanalyzer 2100 device. The model was also tested using different DNA concentrations, using loop primers, and using previously published literature of LAMP experiments with a similar level of accuracy. This model helps to fill a gap in the current LAMP research and provides an easy-to-use tool to efficiently and accurately identify a true-positive LAMP reaction which can reduce false-positive diagnosis.

2.6 Acknowledgement

We would like to thank PerkinElmer and the Brown University Graduate School Fellowship for providing funding for this exclusively research project.

The authors have declared no conflict of interest.

CHAPTER 3

DirectDetect SARS-CoV-2 direct real-time RT-PCR study using patient samples

---

Chapter 3 has been submitted as an original research article.

Naranbat, D.[1¶], **Schneider, L.[1¶]**, Kantor, R.[2,3], Beckwith, C.G.[2,3], Bazerman, L.[3], Gillani, F.[2,3], Sahu, S.[3], Rapoza, K.[3], Sam, S.[2,3], Novitsky, V.[2,3], Shin, J.[3], Hipolito, E.[4], Diaz, I.[4], Carnevale, D.[4], Tripathi, A.[1*]. ¶Co-first authors

[1]Center for Biomedical Engineering, School of Engineering, Brown University, Providence, RI, USA
[2] Division of Infectious Diseases, Brown University Alpert Medical School, Providence, RI, USA
[3] The Miriam Hospital, Providence, RI, USA
[4] Rhode Island Hospital, Providence, RI, USA

¶ DN and LS are co-first authors and contributed equally to this work. Author order was decided alphabetically.

3.1 Abstract

COVID-19 is an infectious disease that caused a global pandemic impacting people worldwide. As disease detection and vaccine rollout continue to progress, there is still a need for efficient diagnostic tools to satisfy continued testing needs. This preliminary study evaluated a novel SARS-CoV-2 diagnostic test called DirectDetect SARS-CoV-2 Direct Real-time RT-PCR based on limited sample size of 24 respiratory samples from 13 SARS-CoV-2 positive patients. The test is advantageous compared to others on the market since it does not require viral transport medium or viral RNA extraction prior to nucleic acid amplification and detection. This capability transforms the hours-long sample preparation time into a minutes-long procedure while also eliminating the need for many costly reagents which may be difficult to obtain during the surge in nucleic acid-based testing during the pandemic. The results show a positive agreement of 91.7%, 83.3%, and 87.5% between dry sample swabs, treated samples, and untreated samples tested using the DirectDetect SARS-CoV-2 Direct Real-time RT-PCR compared to the test used in the clinical laboratory, respectively. The findings indicate that DirectDetect can be used for multiple different sample types while reducing the number of reagents and time needed for diagnosis, overall, contributing to the current need for COVID-19 testing.

3.2 Introduction

In 2019, a novel strain of coronavirus known as severe acute respiratory syndrome coronavirus 2 (SARS-CoV-2) caused a global pandemic outbreak of coronavirus disease (COVID-19)[85]. Since the first reporting of the virus, it has spread throughout the world to millions of people, causing hundreds of thousands of deaths with increased morbidity and mortality in older patients or those with coexisting health conditions[85,86]. As of May 2021, the basic reproduction number of SARS-CoV-2 was 4.08, meaning that on average every infected person passes the virus on to four additional people[87]. Moreover, the containment of the virus has been complicated by the existence of asymptomatic carriers, or the people with no symptoms of the virus[88,89]. It has been noted that the viral load in asymptomatic patients is similar to symptomatic patients indicating the ability for these people to transmit the virus[89]. While asymptomatic patients may later develop symptoms, this group of people demonstrates the importance of widespread testing for SARS-CoV-2 as part of the public health response[89].

The commonly used procedure for detection of SARS-CoV-2 is outlined in Fig 3.1 which begins with a nasopharyngeal (NP), oropharyngeal (OP), or nasal swab to collect a sample from the upper respiratory tract[90]. After collection, the swab is placed directly into a viral (universal) transport medium where it can then be transported from the testing site to the clinical laboratory[90]. Once the sample is in a clinical laboratory of an appropriate safety level, nucleic acid extraction is performed to remove the viral RNA from the rest of the virus material prior to analysis by transferring the sample into lysis buffer. The lysis buffer often contains a guanidinium-based inactivating agent and nondenaturing detergent to inactivate SARS-CoV-2 if it is present in the sample[90]. Following the sample preparation, nucleic acid amplification and detection is performed to assess whether the sample contains SARS-CoV-2.

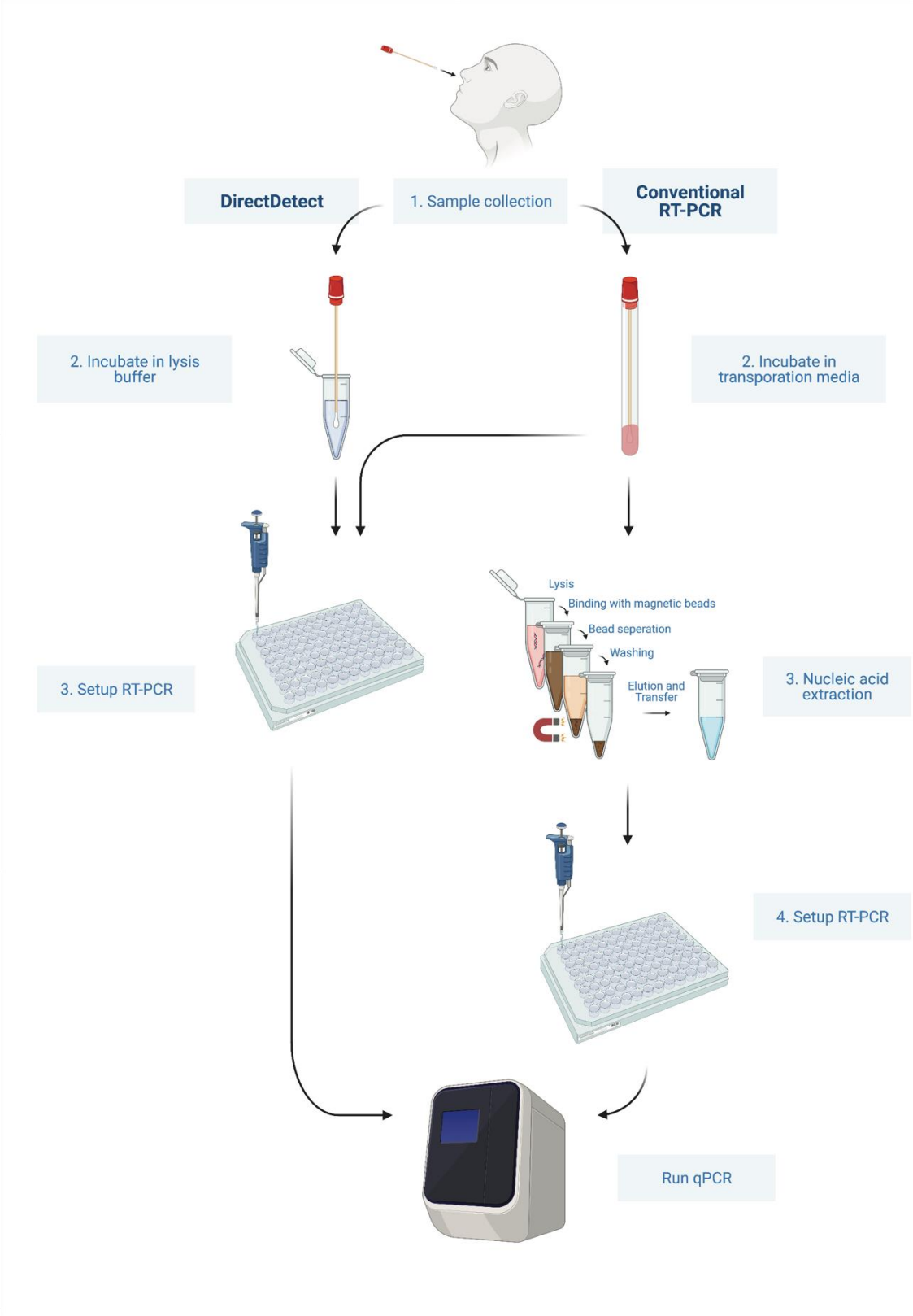

Figure 3.1: Detection of SARS-CoV-2 by the commonly used manual RT-PCR procedure vs. DirectDetect procedure.

The most commonly used amplification and detection method is real-time reverse transcriptase polymerase chain reaction (RT-PCR), but other methods such as loop mediated isothermal amplification (LAMP) have also been used for SARS-CoV-2 diagnostic testing[46,90,91]. Additionally, antibody-based testing can be performed using immunoassays, such as lateral flow assays, to detect antigens like the SARS-CoV-2 virus, or antibodies like IgM and IgG against COVID-19[90,92,93]. Sequencing methods such as next generation sequencing and metagenomic next generation sequencing are also molecular-based techniques that are utilized to determine SARS-CoV-2 mutations as opposed to the use for diagnostic purposes[90,94,95]. While each of these methods can specifically identify and diagnose patients with COVID-19, real-time RT-PCR remains the worldwide gold standard for testing patients suspected of SARS-CoV-2 infection given its high sensitivity and specificity[96]. Even patients with a low viral load in their upper respiratory tract after recovering from symptoms can still test positive for SARS-CoV-2 detection using real-time RT-PCR[97]. However, the availability of currently authorized real-time RT-PCR assays for SARS-CoV-2 diagnostic testing is still limited as large-scale application of testing efforts are continuously hindered by worldwide supply chain issues and a shortage of human resources for fast and efficient testing. Hence, our efforts have been centered around expediating and improving the current real-time RT-PCR testing procedure.

This study presents and analyzes a new COVID-19 diagnostic test called DirectDetect SARS-CoV-2 Direct Real-time RT-PCR (PerkinElmer, Waltham, MA, USA). Currently, this kit is commercially available for detection of SARS-CoV-2, using real-time RT-PCR, from environmental surfaces. The aim of this study, however, is to provide a preliminary evaluation regarding the effectiveness of the DirectDetect assay for the successful detection of SARS-CoV-2 in patient sample swabs. The goal of this work is to remove the bottleneck of RNA extraction step, which has been exacerbated by worldwide shortages in RNA-extraction kits[98], and to reduce the processing time of the test, decreasing the turnaround time for diagnosis. As shown in Fig 3.1, this test removes the need for viral transport medium as well as reagents and equipment needed for viral RNA extraction from samples. This test begins with a swab collected from patients that is then used for direct detection with little sample processing, lyses, and amplification set up for RT-PCR.

Since the outbreak of COVID-19, there have been several detection tests developed across the world for screening and diagnostic purposes. Of those tests, there are some that also use methods that avoid nucleic acid extraction and only a select number have received Emergency Use Authorization (EUA) from the U.S. Food and Drug Administration (FDA), some of which are outlined in Table 3.1. The FDA utilizes EUA tests to authorize unapproved medical products to be used in an emergency to diagnose, treat, or prevent serious or life-threatening diseases or conditions.

Table 3.1: Comparison of Selected Individual EUAs for Molecular Diagnostic Tests for SARS-CoV-2 to DirectDetect (not approved as an EUA test) that do not use nucleic acid extraction.

Company	**Assay Name**	**Specimen Used**	**Gene Targets**	**Amplification**	**Transportation Media Needed**
Bioeksen R&D Technologies Ltd.	Bio-Speedy Direct RT-qPCR SARS-CoV-2	NP or OP swab	ORF1ab gene Internal control detects RNase P gene	Real-time RT-PCR	Yes
Yale School of Public Health, Department of Epidemiology of Microbial Diseases	Saliva Direct	Saliva	N gene using CDC-validated primer/probe sets Internal human *Ribonuclease P* (RP) control	Real-time RT-PCR	No
DiaSorin Molecular LLC	Simplexa COVID-19 Direct assay	NP, nasal swab (NS), nasal wash/aspirate (NW), or bronchoalveolar lavage (BAL)	S gene ORF1ab gene Internal Control RNA	Real-time-RT-PCR	Yes
Quidel Corporation	Lyra Direct SARS-CoV-2 Assay	Nasal, NP, or OP	Non-structured polyprotein (pp1ab) Process Control (PRC)	Real-time-RT-PCR	Yes
Fluidigm Corporation	Advanta Dx SARS-CoV-2 RT-PCR Assay	Saliva	N gene, RNase P internal control	Real-time-RT-PCR	No
PerkinElmer	DirectDetect™ (not approved as an EUA test)	NP, OP, or nasal swab	N gene ORF1ab gene Internal Control (bacteriophage MS2)	Real-time-RT-PCR	No

Like currently available EUA approved diagnostic tests, DirectDetect is designed to amplify the target genes: nucleocapsid (N) gene and open reading frame 1ab (ORF1ab) gene. With the emerging number of genetic variants of SARS-CoV-2, DirectDetect's dual target assay amplifies two different regions of the viral genome simultaneously where the N gene is recommended as a screening assay and the ORF1ab gene is recommended as a confirmatory assays[99,100].

Out of more than 200 EUA approved diagnostic assays, only a fraction (Table 3.1) utilized similar extraction-free detection methods placing the DirectDetect SARS-CoV-2 Direct Real-time RT-PCR test in a selective category that offers many advantages based on reduced reagent needs compared to other assays. While some other testing methods are also capable of multiplexing to target multiple genes simultaneously, like Simplexa COVID-19 Direct assay capable of detecting S gene and ORF1ab gene with an internal control, DirectDetect is also unprecedented in that it can detect SARS-CoV-2 using dry swabs (nasal swab collected from patients without transportation media) without the need for nucleic acid extraction. All other diagnostic tests that use NP, OP, or nasal sample swabs mentioned in Table 3.1 require some form of transportation reagent for valid detection of SARS-CoV-2 from patients.

The goal of DirectDetect is to contribute significantly to the global COVID-19 screening efforts and to simplify the process of diagnosing patients by reducing the number of procedural steps and reagents needed for successful detection. With the rapid shift of decentralizing diagnostic infrastructures, that is allowing patients to self-test or self-collect specimen for testing, DirectDetect could be a valuable addition to the testing armamentarium. The DirectDetect kit can be utilized by patients for easier self-collection processes using only a cotton swab for nasal specimen collection without the need for monitoring reagent contamination. The work presented analyzed the capabilities of this detection method using real patient samples.

3.3 Materials and Methods

3.3.1 Patient Selection and Sampling

Approval for patient selection and sampling was granted by The Miriam Hospital IRB (protocol 208820). Patients were enrolled in a separate study that collected multiple longitudinal specimens (NP, OP, saliva,

and nasal specimens) from patients admitted to the hospital with COVID-19, all of whom had a positive test for SARS-CoV-2 performed in the hospital clinical laboratory using a commercial kit with nucleic acid purification step. GeneXpert System test, Xpert Xpress, for SARS-CoV-2, Flu A/B, and RSV (Cepheid, Sunnyvale, CA, USA) was used for samples 1-4, 6 and Genmark Eplex Respiratory Panel 2 (GenMark Diagnostics, Carlsbad, CA, USA) was used for samples 5, 7-24. These tests have a similar workflow as the Fig 3.1 manual RT-PCR procedure but with an automated process. For this study, two nasal samples were collected from each patient: one swab was collected in a dry tube and the other in viral transport medium. There were total of 13 patients enrolled in this study and 24 samples retrieved. Additional metrics regarding when the patient samples were collected, how they were stored, and when they were tested can be found in Table SI 3.1.

3.3.2 DirectDetect Sample Preparation for SARS-CoV-2

Although DirectDetect™ SARS-CoV-2 Real-time RT-PCR for Environmental Surfaces (PerkinElmer, Waltham, MA, USA) was designed to be used with dry swabs samples collected from environmental surfaces that were not placed in transport medium, to test the robustness of this assay, dry patient samples swabs and patient samples collected in transport medium were both tested. The samples placed in transport medium were tested under two different conditions. In the first condition, a sample of the transport medium was added directly to the RT-PCR assay which is referred to as an untreated wet swab. In the second condition, the sample underwent RNA extraction from the transport medium before the sample was ready for RT-PCR, referred to as a treated wet swab. This resulted in three different sample preparations for analysis using DirectDetect: dry swab, treated wet swab, untreated wet swab.

Following nasal swab specimen collection, the swab was placed in a clean, dry collection tube according to manufacturers' instructions (Fig 3.2) or transport medium. The dry samples are stable at room temperature for up to 24 hours between collection and testing or 72 hours when stored between 2°C and 8°C. The dry patient sample swabs were also prepared for RT-PCR using the manufacturer's instructions for environmental surfaces. For the treated sample swabs undergoing RNA extraction before RT-PCR, the chemagic™ Viral DNA/RNA 300 Kit (PerkinElmer, Waltham, MA, USA) was used for the extraction of

SARS-CoV-2 viral RNA. Standard operating procedures provided by the manufacturer was followed and the purified RNA was extracted into a purified suspension and placed into a clean tube for further processing with DirectDetect.

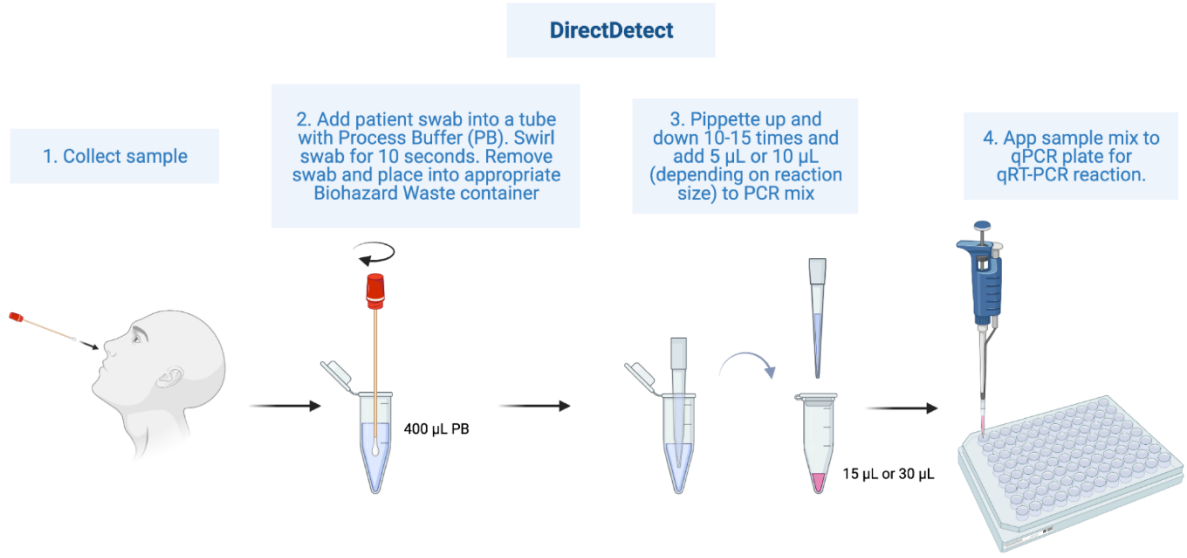

Figure 3.2: DirectDetect SARS-CoV-2 Direct Real-time RT-PCR sample preparation workflow.

3.3.3 Real-time reverse transcriptase (RT) polymerase chain reaction

The real-time RT-PCR used in this assay targeted the N and ORF1ab genes of SARS-CoV-2. TaqMan probes were used to generate target-specific signals to identify the two genetic regions where the N gene was labeled with FAM and the ORF1ab gene with ROX fluorescent dyes. To evaluate the assay in real time, an RNA internal control (IC, bacteriophage MS2) was also used in every sample and was labeled fluorescently with HEX fluorescent dye. Lastly, deoxyuridine triphosphate (dUTP) and uracil-DNA glycosylase (UNG) were also incorporated into this RT-PCR assay as a method to reduce carryover and false positive results caused by contamination of reagents or samples[101].

Table 3.2 outlines the reagents and volumes used to prepare the samples for RT-PCR. To begin, nCoV Reagent A, nCoV Reagent B, nCoV Enzyme Mix, nCoV Reagent D, nCoV IC, and nuclease free water were all combined, vortexed, and spun down in a 200 µL tube (USA Scientific, Ocala, FL, USA). Next, 2.5

μL or 5 μL, depending on the RT-PCR machine being used, of patient sample, nCoV Direct Positive Control, or nCoV Negative Control were added to the previously combined reagents. A 5-fold dilution of the Positive Control was performed using TE buffer before it was added to the reagent mix. All tubes were vortexed and centrifuged for 5 minutes at 350 x g. Following this step, the samples were pipetted from the reagent tube to a Bio-Rad Hard-Shell 96-Well or 384-Well PCR Plate (Hercules, CA, USA). The Bio-Rad CFX96 Touch Real-Time PCR Detection System or Bio-Rad CFX384 Touch Real-Time PCR Detection System (Bio-Rad Laboratories, Hercules, CA, USA) was used for RT-PCR in this study.

Table 3.2: DirectDetect Kit Components and reagent volumes per sample.

Component Name	**Volume (384-well)**	**Main Ingredients**
nCoV Reagent A	3.75 μL	Buffers, dNTPs, Mg^{2+}
nCoV Reagent B	0.75 μL	TE buffer, primers, probes
nCoV Enzyme Mix	0.5 μL	Taq DNA polymerase, Reverse Transcriptase, RNAse inhibitor, UNG
nCoV Reagent D	0.5 μL	PCR enhancer for DirectDetection
nCoV IC	5 μL	TE buffer, bacteriophage MS2
Nuclease Free Water	2 μL	
Sample		
Patient Sample	2.5 μL	
nCoV Direct Positive Control	2.5 μL	SARS-CoV-2 synthetic RNA oligos encapsulated in recombinant virus
nCoV Negative Control	2.5 μL	TE buffer

3.3.4 Testing and Statistical Analysis

Following real-time RT-PCR the internal control (IC) signals were first analyzed. Table 3.3 outlines how the samples were evaluated following successful negative and positive control evaluation. All patient samples were run using DirectDetect at least three times and the Ct value presented are the average of these three trials. The limit of detection for DirectDetect was also tested using the AccuPlex™ SARS-CoV-2 Reference Material Kit (Seracare Life Sciences Inc, Milford, MA, USA) before patient sample testing. Twelve trials were run for six different amounts of input RNA reference material (25, 12.5, 6.25, 3.13, 1.56,

0.78 copies per reaction) for this assay. Considering the results have a continuous response (dependent variable) and are described in terms of multiple levels or categories (dry swab, treated wet swab, untreated wet swab), a t-test (parametric) or Wilcoxon test (non-parametric) was performed for statistical analysis of the real time RT-PCR data.

Table 3.3: Patient sample evaluation for SARS-CoV-2 using DirectDetect Real-Time RT-PCR based on the Ct value of each fluorophore corresponding with a different gene during RT-PCR.

Internal Control (HEX fluorophore)	N gene (FAM fluorophore), ORF1ab gene (ROX fluorophore)	Result Interpretation
Ct ≤ 40	Both targets undetected or Ct >42	SARS-CoV-2 not detected
Ct value detected	Both targets Ct ≤ 42	SARS-CoV-2 detected
Ct value detected	One target Ct ≤ 42	SARS-CoV-2 detected
Ct > 40 or undetected	Both targets undetected or Ct >42	Invalid test, retest sample

3.4 Results

3.4.1 DirectDetect limit of detection (LoD)

The DirectDetect SARS-CoV-2 Direct Real-time RT-PCR assay was first tested using the AccuPlex™ SARS-CoV-2 Reference Material Kit (Seracare Life Sciences Inc, Milford, MA, USA) to analyze the limit of detection for this assay. This material is non-infectious, has a real viral protein coat, and includes target regions in the ORF1a, RdRp, E, and N regions. The concentration of the reference material used is 10,000 copies/mL thus the limit of detection was tested with 25, 12.5, 6.25, 3.13, 1.56, or 0.78 total copies in the RT-PCR assay of a 15 µL reaction. Table 3.4 presents the results for this study where the LoD at which 100% of samples detected was 12.5 copies/reaction. The percent of positive sample detection decreased as the copies of viral RNA per reaction decreased, however, 2/12 N gene sequences and 8/12 ORF1ab gene sequences were still identified at 1.56 copies per reaction. Per the requirements of the DirectDetect assay, only one of the N or ORF1ab genes need to be identified to consider SARS-CoV-2 as detected, therefore at 1.56 copies per reaction 8/12 samples are confirmed positive, in this case.

Table 3.4: Limit of Detection results for DirectDetect using AccuPlex™ SARS-CoV-2 Reference Material Kit, n = 12 for each group.

Sample Input Volume (µL)	Concentration of Viral RNA (cp/µL)	Amount of Viral RNA per reaction (cp/reaction)	Number Tested	SARS-CoV-2: N gene (FAM)			SARS-CoV-2: ORF1ab gene (ROX)			Internal Control (HEX		
				Positive	Ct (avg)	SD	Positive	Ct (avg)	SD	Positive	Ct (avg)	Sd
2.5	10	25	12	12 (100%)	37.68	0.89	12 (100%)	35.48	0.56	12 (100%)	30.52	0.34
2.5	5	12.5	12	10 (83.3%)	37.66	0.94	12 (100%)	35.28	0.74	12 (100%)	30.09	0.30
2.5	2.5	6.25	12	10 (83.3%)	38.60	0.89	11 (91.7%)	36.12	0.92	12 (100%)	29.99	0.35
2.5	1.25	3.13	12	5 (41.7%)	38.89	0.63	10 (83.3%)	36.98	0.65	12 (100%)	29.84	0.30
2.5	0.625	1.56	12	2 (16.7%)	38.87	1.35	8 (66.7%)	38.21	0.64	12 (100%)	29.82	0.25
2.5	0.3125	0.78	12	0 (0.0%)	-	-	3 (25.0%)	38.77	0.06	12 (100%)	30.10	0.43

3.4.2 SARS-CoV-2 detection using DirectDetect in patient samples

Overall, most patient samples were kept at 4°C and tested within 72 hours of being procured unless there was an invalid test caused by the IC being undetected, in which case the sample was retested as soon as possible. On average the patient samples for this study were first tested 2.25 days following sample procurement, but the number of days ranged from zero to 7 due to delays in testing in some cases (Table SI 3.1). The expected result showed a Ct (threshold cycle) value of ≤40 for all samples including negative and positive controls. This proved that the nucleic acid amplification was successful since the IC is included in every sample so it should always be amplified. The negative control would show no signal (Undetermined or Ct >42) for both the N gene (FAM) and ORF1ab gene (ROX), where the positive control needed to show amplification for the two genes. Once the controls were analyzed the patient samples could be interpreted for SARS-CoV-2 detection. An overview of the results for the patient sample testing for different sample types and genes is provided in Fig 3.3 where the Ct value for each result is plotted. From the total of 24 dry swab samples tested, 22 samples tested positive for SARS-CoV-2 and 2 tested negative for SARS-CoV-2 (Table SI 3.2). For patient samples tested with RNA extraction (treated wet swab), 20 samples tested positive and 4 tested negative (Table SI 3.3). Lastly, for patient samples in transport medium tested without RNA extraction (untreated wet swab), 21 samples tested positive and 3 tested negative (Table SI 3.4). The Ct values of the positive and negative controls for the respective samples included in that RT-PCR analysis can be found in Table SI 3.5. All controls needed to pass the metrics defined by this protocol for the test results to be considered for analysis.

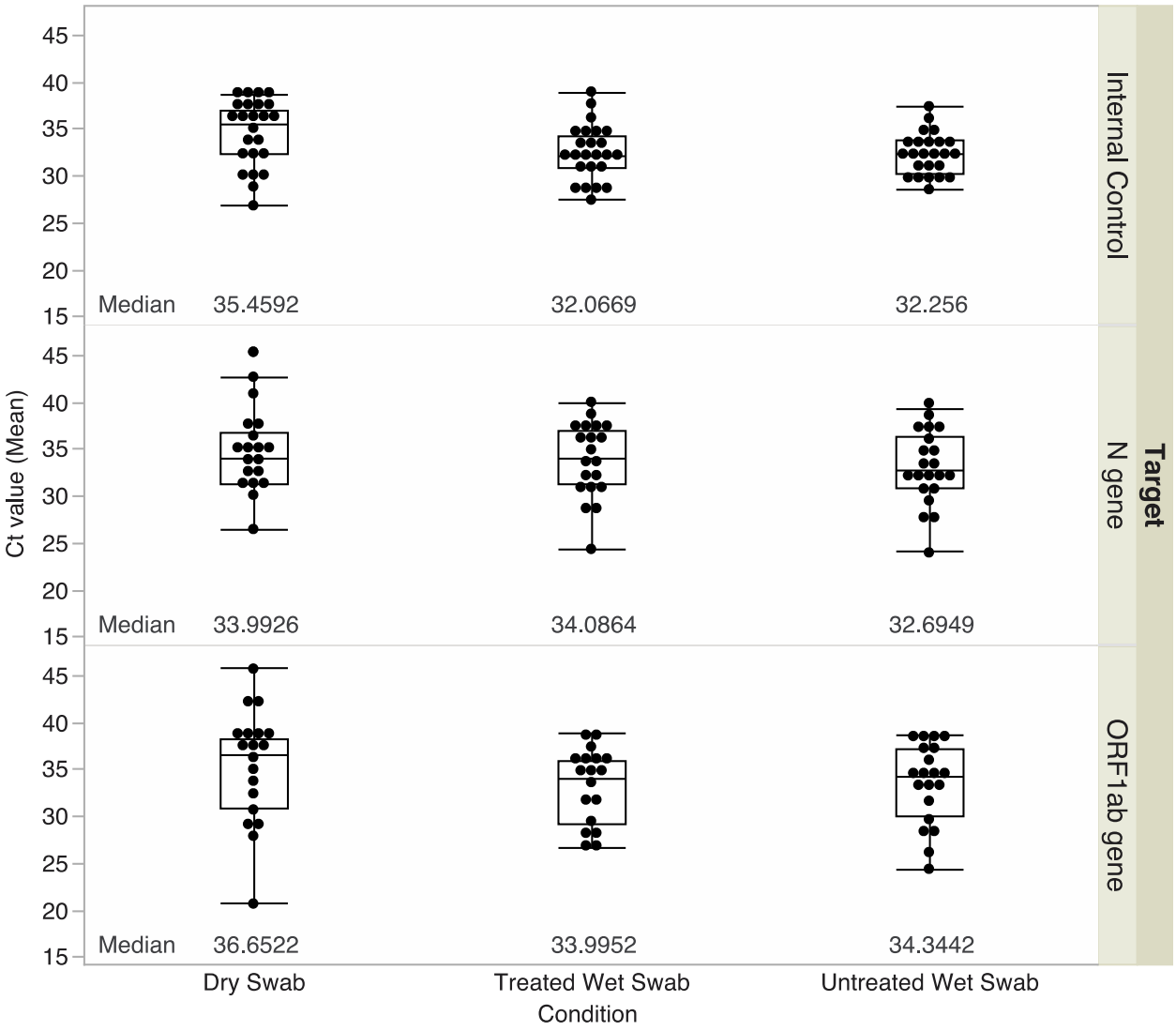

Figure 3.3: Overview of Ct value (mean) for different genes vs. conditions/sample type with reported median. Each error bar is constructed using ± Target.

The DirectDetect assay was tested on a total of 24 patient samples from 13 individuals and tested under three different conditions. Fig 3.4 shows a comparison in Ct values between different nasal swabs in dry and wet conditions tested for different fluorophores. The median Ct values for N gene were 33.99, 34.09, and 32.70 for dry swab, treated wet swab, and untreated wet swab conditions, respectively. The median Ct values for ORF1ab gene were 36.65, 34.00, and 34.34 for dry swab, treated wet swab, and untreated wet swab conditions, respectively. Lastly, the median Ct values for the IC were 35.46, 32.07, 32.26 for dry swab, treated wet swab, and untreated wet swab conditions, respectively.

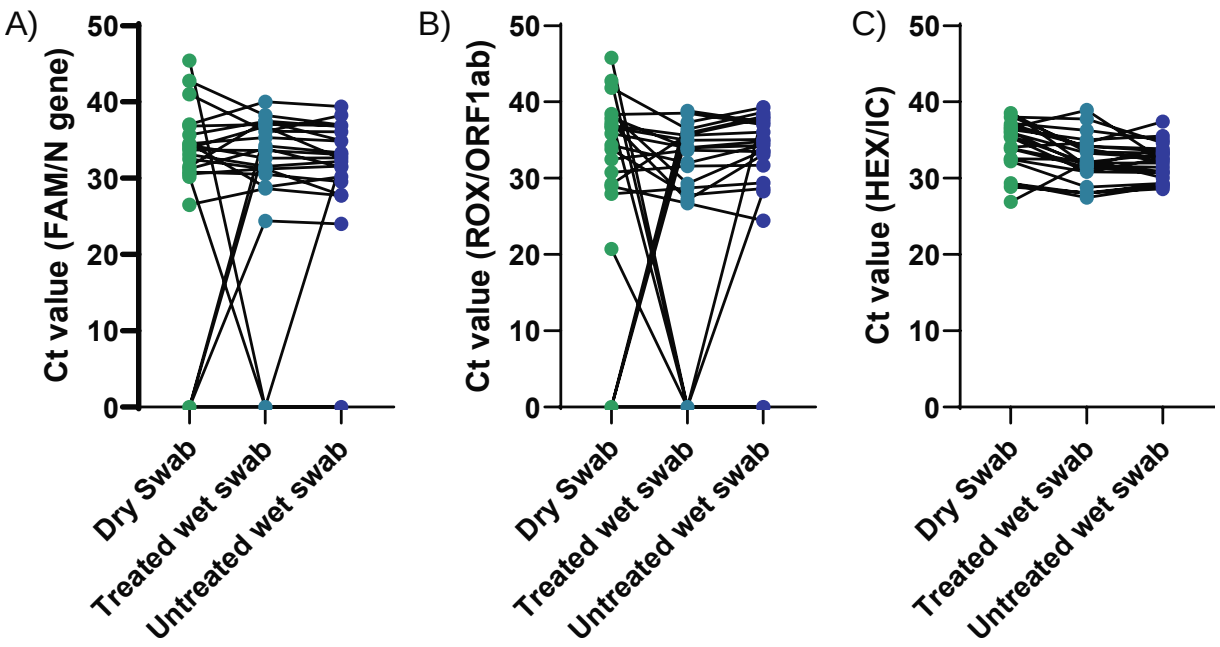

Figure 3.4: Ct value for different genes vs. sample type per individual patient, (a) Comparison for N gene detected by FAM fluorophore, (b) Comparison for ORf1ab gene detected by ROX fluorophore, (c) Comparison for IC detected by HEX fluorophore.

When examining the Ct values for different genes from different starting samples, it is clear there are variations between the conditions tested (Fig 3.4). However, there were no statistically significant differences in Ct values for the two target genes between dry swab and treated wet swab samples, with the difference in medians of 0.09 and 2.66 Ct values for N gene (FAM) and ORF1ab gene (ROX), respectively (Wilcoxon; N: p=0.92, ORF1ab: p=0.17). This confirms that some variation does exist between sample types of dry swab and treated wet swab samples, but dry swab samples are a valuable alternative to treated wet swabs. Similarly, there were no statistically significant differences found in Ct values for the N and ORF1ab target genes between dry swab and untreated wet swab samples, with the difference in medians of 1.30 and 2.05 Ct values for N gene (FAM) and ORF1ab gene (ROX), respectively (Wilcoxon; N: p=0.49, ORF1ab: p=0.32). This also confirms that while there are some variations between dry swab and untreated wet swabs, untreated viral transportation media can still be used as an input sample for successful testing which bypasses the extraction step. There was however a statistically significant difference for the IC (HEX) between dry swab and treated wet swab conditions with the difference in medians of 3.39 Ct values (Wilcoxon; p=0.025). Similarly, there was also a statistically significant difference for the IC (HEX)

between dry swabs and untreated swabs with the difference in medians of 3.20 Ct values (Wilcoxon; p=0.013). Lastly, no statistically significant differences were found in Ct values for the three target genes between treated wet swab and untreated wet swab samples, with the difference in medians of 1.39, 0.61, and 0.19values for N gene (FAM), ORF1ab gene (ROX), and IC (HEX) respectively (Wilcoxon; N: p=0.46, ORF1ab: p=0.80, IC: p=0.88), again suggesting that treated wet swabs and untreated wet swabs are equally capable of detecting SARS-CoV-2 in testing. This information is expanded upon in Figures SI 3.1-3.3.

The different starting samples were further compared by evaluating the positive agreement in SARS-CoV-2 detection between the groups which is seen in Table 3.5. The concordance between SARS-CoV-2 detection using dry swabs and treated wet swabs was 95.0%, dry swabs and untreated wet swabs was 95.2%, and treated wet swabs and untreated wet swabs was 95.2%. Additionally, the positive agreement between each sample condition and the clinical test which confirmed the original COVID-19 diagnosis was also calculated. The clinical diagnosis reported 24/24 samples tested positive, therefore, the overall concordance between the testing conditions and the clinical test was 91.7% for dry swab samples, 83.3% for treated samples, and 87.5% for untreated samples.

Table 3.5: Evaluation of positive and negative agreement for overall SARS-CoV-2 detection using DirectDetect and different starting sample types.

		Treated wet swab	
		Positive	Negative
Dry swab	Positive	19	3
	Negative	1	1
Total		20	4
Positive agreement = 95.0%			
Negative agreement = 75.0%			
		Untreated wet swab	
		Positive	Negative
Dry swab	Positive	20	2
	Negative	1	1
Total		21	3
Positive agreement = 95.2%			
Negative agreement = 66.7%			

		Untreated wet swab	
		Positive	Negative
Treated wet swab	Positive	20	0
	Negative	1	3
Total		21	3
Positive agreement = 95.2%			
Negative agreement = 100%			

3.5 Discussion

Based on limit of detection and patient sample testing, DirectDetect has been shown to be a simple real-time RT-PCR technique for detecting SARS-CoV-2. Overall, this work shows the capabilities of DirectDetect as it was further tested using multiple variations of biospecimen starting samples which include dry nasal swabs, transportation media suspended nasal swabs, and RNA purified samples from nasal swabs. Successful viral detection from these different specimen shows the flexibility and adaptability of DirectDetect. The ability to detect SARS-CoV-2 from a dry or non-purified sample can allow for simpler sample preparation and processing protocols compared to the conventional real-time RT-PCR testing by removing the nucleic acid extraction step. This can allow for high-throughput testing for patients suffering from COVID-19 without the need for an expensive nasal swab stabilizing viral transport medium or nucleic acid extraction kit while also reducing the real-time RT-PCR reagents used per sample reaction. However, a distinct limitation of this study has been the low number of accessible patient samples. Therefore, the presented findings here show the preliminary results of effectively detecting SARS-CoV-2 using DirectDetect on the limited number of patient samples.

Findings from this study show that the median Ct value for all testing conditions and genes are relatively consistent over the 24 patient samples tested (Fig 3.3). This value ranged from 32.07 for the treated wet swab IC to 36.65 for the ORF1ab gene dry swab, however there were no trends identified between a condition or gene and the Ct values. One consistency throughout the data was that there were variations in Ct values between conditions tested however (Fig 3.4). It was possible to have a sample detected for one condition and not the others but the only statistically significant differences in Ct values identified in this study were within the IC gene tested between the dry swab and treated or untreated wet swabs. This could

have been caused by different sample conditions and differences in sample preparation procedures but does not impact the results of the target testing since the amplification is successfully detected within the IC in all cases.

The positive agreement between testing conditions was also analyzed in this study. The percent of samples that tested positive between both sample swab preparation types show that although there was variation in the Ct values, for the true COVID-19 detection among different conditions, there was still a positive agreement of 95% or more (Table 3.5). In addition to evaluating the positive agreement between samples tested with DirectDetect, it was also critical to understand the positive agreement with the original clinical diagnosis. When performing this analysis, it was found that the positive agreement for the dry sample swab was the highest indicating that it worked the best out of the three conditions tested.

While the results suggest that DirectDetect can identify SARS-CoV-2 in nasal swabs, there was still less than 100% positive agreement between DirectDetect, and the commercially available real-time RT-PCR kit used for the initial diagnosis. It is hypothesized one reason for this discrepancy is due to the delay between sample procurement and sample testing where SARS-CoV-2 viral RNA could have degraded. In addition to delays between procurement and testing, many of the samples were collected days after the original positive test using the commercial assay, up to 13 days (Table SI 3.1). This delay could lead to a decrease in the viral load within the patient as they recovered from COVID-19 and therefore affect the positive agreement between DirectDetect and the original clinical assay as well. In a typical clinical patient nasal sample swab, the average RNA load is 6.76×10^5 copies per whole swab until five days after the symptom onset[102]. In this study, this hypothesis was tested as Samples 12, 13, and 14 were cases of the same patient retested again every day for 3 days after the initial testing to see if there was change in viral load. The Ct value for a patient changed from one visit to the next, indicating a change in the viral load of the patient by the 3rd test. A larger Ct value indicates a smaller viral load as it will take more PCR cycles for the fluorescence to reach the threshold and a Ct value of 0 means that SARS-CoV-2 was no longer detected in that sample.

Additionally, beyond comparing DirectDetect to the commercial assay original diagnosis, one more hypothesis for the difference in positive agreement between testing conditions (dry, treated, untreated) in this study is that two different samples were collected and used for each sample, a dry nasal swab and a transport medium suspended nasal swab. It is likely that virus attachment to the cotton swabs contact area may have been bypassed, potentially leading to false-negative results in cases[103].

As SARS-CoV-2 spread rapidly and the global pandemic worsened, a surge in development and authorization of molecular diagnostic tests presented a challenge in comparing testing performances[104]. The exuberant number of methods being developed by independent researchers was causing many unstandardized comparisons. However, as the emergency use of diagnostics for SARS-CoV-2 was deemed essential, the FDA granted emergency use authorizations for tests and specified the requirement for reference material to establish an absolute limit of detection for each method to evaluate performance and directly compare assays[104]. A similar limit of detection methods was used in this study for evaluating the sensitivity of DirectDetect by testing a known quantity of inactivated virus to assess viral detection in samples. The observed test limit of detection for DirectDetect is 1667 copies/mL (25 copies/reaction) for both the N and ORF1ab target genes to be detected in 100% of samples or 832 copies/mL (12.5 copies/reaction) for 100% of samples to test positive for SARS-CoV-2 using DirectDetect according to the manufacturer's instructions, testing positive for at least one of the target genes. These metrics are comparable to or better than most of the other FDA EUA authorized SARS-CoV-2 PCR test kits with nucleic acid extraction methods (180 – 600,0000 units/mL)[105]. While the PerkinElmer New Coronavirus Nucleic Acid Detection Kit (PerkinElmer, Inc., Waltham, MA, USA) and Viracor SARS-CoV-2 assay (Viracor Eurofins Clinical Diagnostics, Lee's Summit, MO, USA) have an LOD of 180 units/mL, these kits use swabs in transport medium while DirectDetect does not require that reagent but has still shown it is capable of detection within that range. Overall, DirectDetect is one of the few SARS-CoV-2 PCR tests capable of diagnosis without the need for transport medium of which there are currently only four EUA kits which use dry NP or nasal swabs. The LOD for these kits range from 60000 to 540000 units/mL, showing DirectDetect is more sensitive than these other assays. Compared to other diagnostic kits using no nucleic

acid extraction, mentioned in Table 3.1, DirectDetect had limit of detection that is as sensitive as 4 of the 5 tests and is approximately three hundred times more sensitive than Lyra Direct SARS-CoV-2 Assay (540000 units/mL)[105,106]. DirectDetect, like many other PCR tests, has performed substantially better than any antigen-based tests[105].

Furthermore, these results show that the DirectDetect kit can contribute significantly to the global COVID-19 screening efforts and simplify the process of diagnosing patients. Reducing the number of procedural steps and reagents used for proper detection of SARS-CoV-2 among patients is an area of improvement many testing kits have focused on and DirectDetect was able to achieve. Additionally, DirectDetect has the potential to be further implemented in decentralized diagnostic efforts by providing patients the option to self-collect testing specimen for rapid and reliable monitoring since only a cotton swab for nasal specimen retrieval is required with no need for monitoring reagents contamination. Lastly, the DirectDetect assay can be further modified to target other gene sites and monitor other nucleic based pathogens, or variants of SARS-CoV-2.

3.6 Conclusion

Overall, the goal of this work was to evaluate the DirectDetect SARS-CoV-2 Direct Real-time RT-PCR test. Limit of Detection testing for DirectDetect indicated that the test was comparable to or better than other COVID-19 detection assays approved for EUA by the FDA, especially other tests using dry swabs. Additionally, this study indicates that DirectDetect can be used for multiple different sample types. Although the goal of the assay is to use dry sample swabs for detection of SARS-CoV-2 without the need for RNA extraction materials and reagents, this work showed that DirectDetect can be adapted and successful using a sample of the transport medium directly to the RT-PCR assay (untreated wet swab) or a sample that undergoes RNA extraction from the transport medium before RT-PCR (treated wet swab) as well. Thus, this procedure can successfully identify SARS-CoV-2 using minutes-long or hours-long sample preparation techniques or further implemented for decentralized diagnostic efforts. In the future it is possible this sample preparation can be adapted for other infectious diseases or variants of SARS-CoV-2

and be an easy to implement test due to the reduced amounts of reagents, materials, and time needed between sample procurement and analysis.

3.7 Acknowledgements

The authors would like to acknowledge financial and technical support from PerkinElmer including Yanhong Tong. In addition, specimen collection was supported by Gilead Sciences, Inc. and facilitated with support from the Providence/Boston Center for AIDS Research (P30AI042853). Neither entity had input on the research. Lastly, the authors would like to acknowledge funding received from the Brown University COVID-19 Research Seed Fund.

3.8 Supporting Information

Table SI 3.1: Additional information collected regarding patient samples.

Sample Number	Patient	Commercial Assay used for initial testing	Days elapsed since positive test	Date Procured	Storage Condition	Sample Prep Date	Sample Run Date *Rerun Date
1	1	Cepheid GenXpert	8	3/4/2021	-80°C	3/10/2021	3/10/2021 *3/17/2021
2	2	Cepheid GenXpert	2	3/4/2021	-80°C	3/10/2021	3/10/2021 *3/17/2021
3	2	Cepheid GenXpert	6	3/8/2021	-80°C (Wet Swab)/ 4°C (Dry Swab)	3/10/2021	3/10/2021 *3/17/2021
4	3	Cepheid GenXpert	4	3/10/2021	4°C	3/11/2021	3/11/2021 *3/17/2021
5	4	Genmark RPP2	1	3/11/2021	4°C	3/12/2021	3/12/2021 *3/17/2021
6	1	Cepheid GenXpert	0	3/24/2021	4°C	3/25/2021	3/25/2021 *5/14/2021
7	5	Genmark RPP2	1	3/29/2021	4°C	3/30/2021	3/30/2021
8	5	Genmark RPP2	2	3/30/2021	4°C	3/30/2021	3/30/2021
9	6	Genmark RPP2	1	4/1/2021	4°C	4/2/2021	4/3/2021
10	6	Genmark RPP2	2	4/2/2021	4°C	4/2/2021	4/3/2021
11	7	Genmark RPP2	5	4/6/2021	4°C	4/6/2021	4/6/2021 *5/14/2021
12	8	Genmark RPP2	1	4/6/2021	4°C	4/8/2021	4/8/2021
13	8	Genmark RPP2	2	4/7/2021	4°C	4/8/2021	4/8/2021
14	8	Genmark RPP2	4	4/9/2021	-80°C	4/15/2021	4/15/2021 *5/14/2021

15	9	Genmark RPP2	1	4/21/2021	4°C	4/21/2021	4/21/2021 *5/14/2021
16	9	Genmark RPP2	2	4/22/2021	4°C	4/25/2021	4/25/2021 *5/14/2021
17	9	Genmark RPP2	6	4/26/2021	4°C	4/26/2021	4/27/2021 *5/14/2021
18	10	Genmark RPP2	1	5/11/2021	4°C	5/12/2021	5/12/2021
19	11	Genmark RPP2	13	5/14/2021	-80°C	5/17/2021	5/19/2021
20	12	Genmark RPP2	1	5/19/2021	4°C	5/19/2021	5/19/2021
21	12	Genmark RPP2	2	5/20/2021	4°C	5/21/2021	5/21/2021
22	13	Genmark RPP2	1	5/25/2021	4°C	5/25/2021	5/25/2021
23	13	Genmark RPP2	2	5/26/2021	-80°C	6/2/2021	6/2/2021
24	13	Genmark RPP2	3	5/27/2021	-80°C	6/2/2021	6/2/2021 *6/30/2021

Table SI 3.2: DirectDetect Patient Results using dry swab sample. (* Indicates data is from sample rerun since original test was invalid).

Sample Number	**N gene (FAM) Ct value**	**ORF1ab gene (ROX) Ct value**	**Internal Control (HEX) Ct value**	**Dry Swab - Detected with DirectDetect**
1	Undetected*	Undetected*	28.90079*	No
2	26.51923*	27.95477*	32.24657*	Yes
3	Undetected*	Undetected*	29.36429*	No
4	34.36715*	35.83848*	28.94511*	Yes
5	32.50903*	34.35093*	29.30486*	Yes
6	Undetected*	28.92124*	38.55001*	Yes
7	33.08366	38.4553	37.09523	Yes
8	34.52932	37.25306	34.10142	Yes
9	36.84412	Undetected	36.80375	Yes
10	34.51917	36.90813	36.39590	Yes
11	Undetected*	29.22471*	33.84360*	Yes
12	35.67146	36.65216	38.03538	Yes
13	37.08298	37.86197	37.24099	Yes
14	30.17625*	Undetected*	32.48642*	Yes
15	42.77917*	20.7180033*	35.40308*	Yes
16	Undetected*	45.80533*	33.94396*	Yes
17	45.44475*	42.77814*	36.1019267*	Yes
18	30.5675067	33.8312767	35.9925933	Yes
19	33.71185	37.96575	35.51534	Yes

20	30.82887	30.76629	38.15157	Yes
21	31.28569	32.48432	32.58117	Yes
22	33.99263	38.33963	36.54755	Yes
23	41.00391	41.86322	38.68647	Yes
24	31.55807*	Undetected*	26.88523*	Yes

Table SI 3.3: DirectDetect Patient Results using sample swab in transport medium with RNA extraction (treated wet swab). (* Indicates data is from sample rerun since original test was invalid).

Sample Number	N gene (FAM) Ct value	ORF1ab gene (ROX) Ct value	Internal Control (HEX) Ct value	Treated Wet Swab - Detected with DirectDetect
1	Undetected*	Undetected*	28.12407*	No
2	28.64784*	28.74585*	28.84022*	Yes
3	36.13314*	37.31631*	27.49562*	Yes
4	32.66185*	34.00058*	28.08429*	Yes
5	31.23936*	32.03415*	28.02078*	Yes
6	24.3917*	26.72727*	33.45329*	Yes
7	31.55878	29.25571	34.20317	Yes
8	28.86748	27.12957	34.62884	Yes
9	37.06548	35.89296	34.20245	Yes
10	35.36672	35.59005	35.04639	Yes
11	34.28188*	35.74202*	31.44656*	Yes
12	37.48373	34.97814	37.77041	Yes
13	40.02308	Undetected	36.27925	Yes
14	Undetected*	Undetected*	30.84713*	No
15	38.26182*	Undetected*	30.81472*	Yes
16	Undetected*	Undetected*	31.92116*	No
17	Undetected*	Undetected*	31.65484*	No
18	31.26749	27.80778	33.31288	Yes
19	33.63711	33.98974	32.04151	Yes
20	30.51895	31.60588	33.86419	Yes
21	33.89098	33.68595	32.45449	Yes
22	36.81067	38.57762	38.91866	Yes
23	36.1685	36.42425	31.60518	Yes
24	37.53848	38.83624	32.09238	Yes

Table SI 3.4: DirectDetect Patient Results using sample swab in transport medium without RNA extraction (untreated wet swab). (* Indicates data is from sample rerun since original test was invalid).

Sample Number	N gene (FAM) Ct value	ORF1ab gene (ROX) Ct value	Internal Control (HEX) Ct value	Untreated Wet Swab - Detected with DirectDetect
1	Undetected*	Undetected*	29.18035*	No
2	27.7403*	29.38749*	29.30328*	Yes
3	38.25466*	39.32669*	28.96561*	Yes
4	32.69494*	34.8265*	28.60919*	Yes
5	31.59595*	34.3794*	29.20468*	Yes
6	24.01851*	24.43084*	33.32258*	Yes
7	32.2366	33.60831	33.55182	Yes
8	30.24998	33.09664	37.42244	Yes
9	36.90089	38.09871	33.86185	Yes
10	34.85323	36.07289	35.52707	Yes
11	33.36448*	37.85662*	30.69342*	Yes

12	34.95653	35.12045	34.65843	Yes
13	39.40505	38.53343	35.0155	Yes
14	32.17112*	Undetected*	30.74884*	Yes
15	36.98141*	28.25951*	32.66469*	Yes
16	Undetected*	Undetected*	30.87712*	No
17	Undetected*	Undetected*	33.92664*	No
18	27.82464	28.66593	32.6913367	Yes
19	33.09333	34.30895	32.01034	Yes
20	29.57417	31.70079	32.12281	Yes
21	31.43844	33.49482	30.06356	Yes
22	32.56502	37.0065	32.38924	Yes
23	36.08482	38.62675	31.45827	Yes
24	36.75215	37.40799	33.13808	Yes

Table SI 3.5: Ct values of positive and negative controls for each RT-PCR run.

Sample Numbers included in RT-PCR run	**Positive Control**			**Negative Control**			**Controls Passed or Failed**
	N gene (FAM)	**ORF1ab gene (ROX)**	**Internal Control (HEX)**	**N gene (FAM)**	**ORF1ab gene (ROX)**	**Internal Control (HEX)**	
1-5	36.64032	36.75011	28.51095	N/A	N/A	28.41399	Pass
6-8	38.31679	35.95525	33.20374	N/A	N/A	32.15562	Pass
9-10	37.00116	36.53321	34.48649	N/A	N/A	34.16089	Pass
11	39.6225	36.12985	36.37756	N/A	N/A	34.92038	Pass
12-13	37.21064	35.69948	36.06466	N/A	N/A	35.60047	Pass
14	38.98471	36.79374	35.96389	N/A	N/A	34.76218	Pass
15	36.82667	37.58769	33.83064	N/A	N/A	33.25749	Pass
16	34.85418	34.28343	35.1033	N/A	N/A	35.23047	Pass
17	36.7979	35.02124	34.94556	N/A	N/A	34.48281	Pass
18	37.5995	36.37551	29.70862	N/A	N/A	29.61867	Pass
Rerun 6, 11, 14-17	35.52098	34.52856	30.544	N/A	N/A	30.24515	Pass
19-20	38.60495	36.8258233	32.3945433	N/A	N/A	31.67165	Pass
21	35.07178	34.32331	30.97024	N/A	N/A	30.90972	Pass
22	36.00344	35.5048233	30.81376	N/A	N/A	30.3694567	Pass
23-24	36.771527	35.946257	31.275307	N/A	N/A	30.654113	Pass

Oneway Analysis of N gene (FAM) Ct By Condition

Oneway Anova

Summary of Fit

Rsquare	0.024763
Adj Rsquare	-0.00946
Root Mean Square Error	4.107138
Mean of Response	33.75077
Observations (or Sum Wgts)	60

Analysis of Variance

Source	DF	Sum of Squares	Mean Square	F Ratio	Prob > F
Condition	2	24.41393	12.2070	0.7237	0.4894
Error	57	961.50923	16.8686		
C. Total	59	985.92316			

Means for Oneway Anova

Level	Number	Mean	Std Error	Lower 95%	Upper 95%
Dry Swab	19	34.5513	0.94224	32.664	36.438
Treated Wet Swab	20	33.7908	0.91838	31.952	35.630
Untreated Wet Swab	21	32.9884	0.89625	31.194	34.783

Std Error uses a pooled estimate of error variance

Nonparametric Comparisons For Each Pair Using Wilcoxon Method

q*	Alpha
1.95996	0.05

Level	- Level	Score Mean Difference	Std Err Dif	Z	p-Value	Hodges-Lehmann	Lower CL	Upper CL	Difference Plot
Treated Wet Swab	Dry Swab	-0.35921	3.652685	-0.098342	0.9217	-0.04744	-3.12779	2.605287	
Untreated Wet Swab	Dry Swab	-2.50627	3.701475	-0.677099	0.4983	-1.01691	-3.75079	1.565657	
Untreated Wet Swab	Treated Wet Swab	-2.78214	3.742771	-0.743338	0.4573	-0.91247	-3.49907	1.534553	

Figure SI 3.1: One-way analysis of N gene (FAM) Ct value by condition.

Oneway Analysis of ORF1ab gene (ROX) Ct By Condition

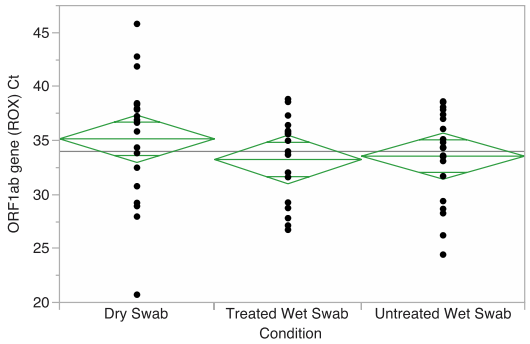

Oneway Anova

Summary of Fit

Rsquare	0.031454
Adj Rsquare	-0.00442
Root Mean Square Error	4.759794
Mean of Response	33.9897
Observations (or Sum Wgts)	57

Analysis of Variance

Source	DF	Sum of Squares	Mean Square	F Ratio	Prob > F
Condition	2	39.7309	19.8655	0.8768	0.4219
Error	54	1223.4047	22.6556		
C. Total	56	1263.1356			

Means for Oneway Anova

Level	Number	Mean	Std Error	Lower 95%	Upper 95%
Dry Swab	19	35.1565	1.0920	32.967	37.346
Treated Wet Swab	18	33.2411	1.1219	30.992	35.490
Untreated Wet Swab	20	33.5550	1.0643	31.421	35.689

Std Error uses a pooled estimate of error variance

Nonparametric Comparisons For Each Pair Using Wilcoxon Method

q*	Alpha
1.95996	0.05

Level	- Level	Score Mean Difference	Std Err Dif	Z	p-Value	Hodges-Lehmann	Lower CL	Upper CL	Difference Plot
Untreated Wet Swab	Treated Wet Swab	0.89722	3.610556	0.24850	0.8037	0.35484	-2.24720	3.005912	
Untreated Wet Swab	Dry Swab	-3.64342	3.652685	-0.99746	0.3185	-1.63434	-4.76533	1.204463	
Treated Wet Swab	Dry Swab	-4.92251	3.560327	-1.38260	0.1668	-2.08396	-5.46183	1.146867	

Figure SI 3.2: One-way analysis of ORF1ab gene (ROX) Ct value by condition.

Oneway Analysis of Internal Control Ct By Condition

Oneway Anova

Summary of Fit

Rsquare	0.098545
Adj Rsquare	0.072416
Root Mean Square Error	2.980125
Mean of Response	32.93962
Observations (or Sum Wgts)	72

Analysis of Variance

Source	DF	Sum of Squares	Mean Square	F Ratio	Prob > F
Condition	2	66.99000	33.4950	3.7715	0.0279*
Error	69	612.79917	8.8811		
C. Total	71	679.78917			

Means for Oneway Anova

Level	Number	Mean	Std Error	Lower 95%	Upper 95%
Dry Swab	24	34.2968	0.60832	33.083	35.510
Treated Wet Swab	24	32.3801	0.60832	31.167	33.594
Untreated Wet Swab	24	32.1420	0.60832	30.928	33.356

Std Error uses a pooled estimate of error variance

Nonparametric Comparisons For Each Pair Using Wilcoxon Method

q*	Alpha
1.95996	0.05

Level	- Level	Score Mean Difference	Std Err Dif	Z	p-Value	Hodges-Lehmann	Lower CL	Upper CL	Difference Plot
Untreated Wet Swab	Treated Wet Swab	-0.6250	4.041452	-0.15465	0.8771	-0.12600	-1.85760	1.32390	
Treated Wet Swab	Dry Swab	-9.0417	4.041452	-2.23723	0.0253*	-2.19402	-4.34926	-0.35669	
Untreated Wet Swab	Dry Swab	-10.0417	4.041452	-2.48467	0.0130*	-2.80167	-4.42473	-0.47608	

Figure SI 3.3: One-way analysis of Internal Control (HEX) Ct value by condition.

CHAPTER 4

Synergistic use of electroosmotic flow and magnetic forces for nucleic acid extraction

---

Chapter 4 has been published as an original research article.

Deraney, R. N., **Schneider, L.**, Tripathi, A., *Synergistic use of electroosmotic flow and magnetic forces for nucleic acid extraction*, **Analyst**, 145(6), 2412-2419, 2020.

4.1 Abstract

Nucleic acid sample preparation is essential for biological sample-based diagnostics. It is crucial that diagnostic tests be both specific and sensitive as to provide the most accurate diagnosis possible. Inefficient sample preparation can hinder the specificity and sensitivity of these tests since carryover contaminants can inhibit downstream processes, such as amplification. Microfluidic devices have been used previously to extract nucleic acids from a biological sample due to lower reagent volumes and ease of use. A novel microfluidic chip has been designed for nucleic acid sample preparation which combines electroosmotic flow and magnetic bead-based extraction to isolate DNA from a plasma sample. A steady electric field was incorporated into the microfluidic chip design, which when combined with a glass clover slip and a voltage differential, creates electroosmotic flow. With the goal of isolating nucleic acids into a clean, inhibitor free solution, the electroosmotic flow is the driving force and separation mechanism purifying the DNA sample captured on magnetic beads in the microfluidic chip system. Carryover volume, or the volume of unwanted sample contaminants that accompany the nucleic acids into the final elution buffer, was minimized to 0.22± 0.03%. In combination with magnetic bead based nucleic acid extraction techniques, a 15% increase in DNA extraction yield is reported for the microfluidic chip with the voltage applied versus without. Although the literature on nucleic acid separation in microfluidic chips is abundant, this is the first to combine microfluidic chip design, magnetic bead-based isolation and electroosmotic flow.

4.2 Introduction

Sample preparation is the critical first step in any biological sample analysis. In order to use the information stored at a molecular level, the target nucleic acids must be extracted from a complex sample into a clean, purified solution prior to any amplification or other downstream applications. Nucleic acid extraction into a purified sample ensures that further amplification, such as quantitative polymerase chain reaction (qPCR), can be performed accurately and produce a sensitive and specific diagnosis[107]. Examples of tests that require sample preparation would be identification of bacterial DNA[108] for diagnosis or measuring viral RNA to determine viral load[109]. There are currently multiple techniques used to separate biomolecules from a sample, including organic aqueous liquid extraction, affinity columns, dielectrophoresis, chromatography and functionalized beads[110]. These methods follow the same basic steps for separation: lysis and binding, washing, extraction and purification[111]. Magnetic bead-based separation is a popular functionalized bead method for nucleic acid separation, isolation or extraction[112]. This technique utilizes silica coated beads, which often contain a magnetic iron oxide core[113]. In the presence of a chaotropic agent, nucleic acids adsorb to silica through a combination of intermolecular electrostatic forces, dehydration and intermolecular hydrogen bonding[114]. Magnetic forces can be applied to control the location of the beads and to ultimately immerse them in elution buffer, where the nucleic acids will unbind from the beads. The beads can then be removed and the extracted nucleic acids are ideally concentrated in an inhibitor free solution, ready for down-stream processing[107].

Multiple systems have been developed to improve the use of magnetic bead-based separation, often by incorporating the use of microfluidic devices. Whether the goal is increasing extraction efficiency, reducing carryover volumes, eliminating wash steps or minimizing run time, microfluidics can be used. Microfluidics can also reduce sample sizes and reagent consumption which can be helpful when there is a limited amount of starting nucleic acid sample. Additionally, these devices are also often translational to use in automated systems[113]. In addition to magnetic bead-based separation on the microfluidic scale, electric field induced capture of DNA is another method used to isolate DNA from a sample. Researchers have successfully used microelectrodes and dielectrophoresis to concentrate DNA[115], and there are multiple reports of collecting

the concentrated DNA in microtips[116-118] as well as within microchip systems[119,120]. These techniques are advantageous for DNA extraction for their high speed, efficiency and throughput as well as their low sample and reagent consumption[119].

Magnetic bead and electric field separation techniques both present unique ways for isolating and purifying nucleic acids from a biological sample. Therefore, this research presents a design that combines these physical techniques in a microfluidic chip that can move nucleic acids from a sample well into a clean, inhibitor free elution well creating a purified sample. Commercially available magnetic beads used for nucleic acid capture were used to collect the sample of interest and move through the microfluidic chip – via a magnet – in parallel with an electric field. In this system, a steady electric field is used to induce electroosmotic flow as a separation mechanism which works to minimize the amount of amplification inhibitors carried over to the elution buffer during the extraction process in the microchip. The microfluidic chip used is fabricated by bonding polydimethylsiloxane (PDMS) to a glass cover slide where the glass cover slide has a negative zeta potential[121]. As electroosmotic flow velocity is related directly to zeta potential[122],this negative charge will create an electric double layer when the microchip separation channel is filled, in this case, with isopropanol. Isopropanol is able to create this electric double layer because of its small dielectric constant which means it will not shield any positive or negative charges in solution, in turn allowing this electric double layer to form. Since the glass cover slide has a negative charge, this surface charge is then one of two parallel charged layers in the microchip. The second parallel charged layer is the positively charged ions attracted to the negatively charged surface area of the glass cover slip via coulomb force[123]. When an electric field is applied via electrodes incorporated into the chip design, the net positive charge of the electric double layer will move towards the negative electrode and create a bulk flow[123]. The chip configuration moves this electroosmotic flow in the direction of the sample input well which is in the opposite direction of the nucleic acid bound bead movement. This is designed to minimize the carryover volume of amplification inhibitors while extracting nucleic acids of interest that are bound to the magnetic beads. These forces are illustrated in Figure 4.1. While electroosmotic flow has been used previously in

microfluidics[124], this design is the first to combine magnetic bead isolation and electroosmotic flow within a microfluidic chip for nucleic acid extraction.

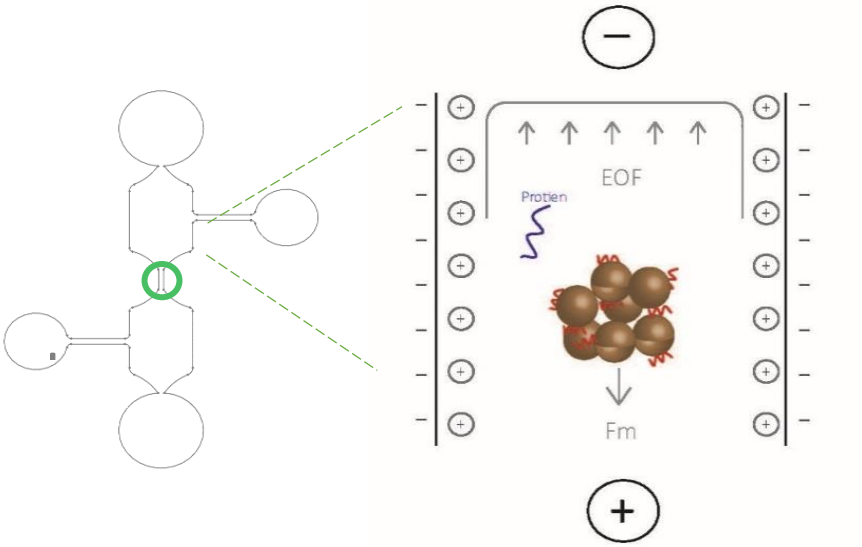

Figure 4.1: Forces at play in the microfluidic chip. The electroosmotic flow moves in the opposite direction of the applied magnetic force.

4.3 Methods

4.3.1 Microfluidic chip design and fabrication:

The device consists of a sample input well, an elution well and a separation channel. This channel has two wider segments symmetric across a thin section connecting the two. Various widths of this thin section were tested in this study. The dimensions used were 0.12mm, 0.15mm, 0.18mm and 0.21mm, labeled channel width A-D, respectively. The height of the channels was kept constant at 180µm throughout the study. Additionally, the chip was designed with two electrode wells which each connect to one of the two wider segments of the channel. The electrode wells were placed in the design to create a steady electric field across the thin section of the channel when a voltage source (Matsusada Precision Inc, Japan) is applied. A chip diagram is shown in Figure 4.2, and an accompanying photograph can be found in SI Figure 4.1. The chip was designed to maximize the electroosmotic flow through the channels while still allowing for the magnetic beads to pass from one well to the other under magnetic forces, creating an optimal nucleic acid extraction and purification device. SolidWorks (2018, Waltham, Massachusetts) was used to create the

chip design and an SU8-Si mold was ordered from FlowJem (Toronto, ON, Canada), becoming the mold for the microfluidic chip.

The device fabrication is composed of a microscope slide bonded to solid PDMS chip, fabricated via soft lithography techniques. PDMS precursor and curing agent (Dow Corning, Midland, MI) were mixed in a 10:1 mass ratio, degassed for 1 hour to remove air bubbles and used to fill the designed SU-8 structure mold. The PDMS then cured for 1 hour at 70˚C. The solid polymer was then removed with the patterned molded into the PDMS. Hole punches were used to create the sample, elution and electrode wells with their locations specified by the patterned mold. Finally, the PDMS was bonded to a microscope slide after both the molded PDMS chip and the microscope slide were treated with a plasma wand. The chip was finally incubated at 70˚C for an additional 30 minutes to enhance bonding.

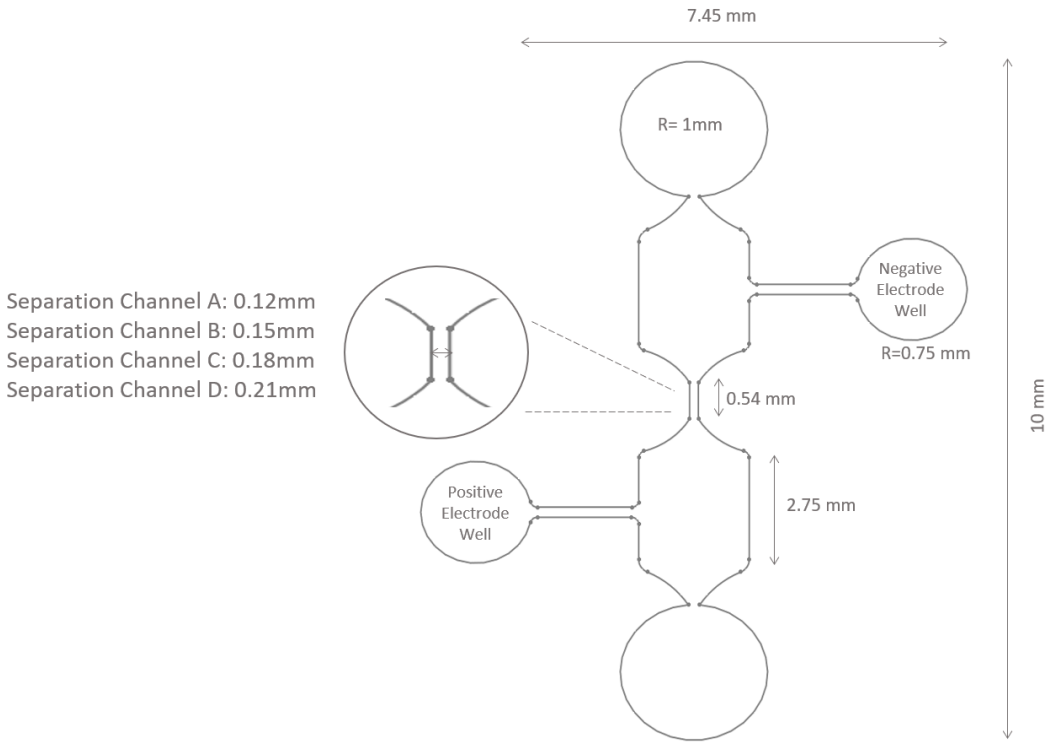

Figure 4.2: Chip Design Channel Widths A-D (0.12-0.21mm) are provided along with other chip dimensions.

4.3.2 Microfluidic Chip Numerical Simulations

Each microfluidic chip used was designed with one of four different center channel widths that allowed for a more thorough investigation into how this dimension can affect electroosmotic flow, and thus, unwanted

sample contaminants in the microfluidic chip. In addition to an experimental design, theoretical modeling was conducted to better understand the effect of this center channel dimension on the electroosmotic flow. A 2D SolidWorks drawing of the microfluidic chip was imported into COMSOL Multiphysics® Modeling Software 5.4 where Electric Currents and Laminar Flow were modeled. These physics modules solved for the electric potential, velocity, and pressure. A stationary study was utilized for computational modeling for each of the four channel widths: 0.12mm, 0.15mm, 0.18mm and 0.21mm (A-D).

4.3.3 PCR Inhibitors Investigation

Before any carryover experiments could be performed on the microfluidic device it was important to measure inhibition of amplification during sample analysis off the microfluidic chip. Various amounts of plasma, isopropanol or lysis binding solution, all which can inhibit PCR and are included in our protocol, were used with the amplification starting sample of HPV with 1.2x 10^7copies HPV / µL. The percent inhibitor is based off 4µL total with 1µL diluted HPV making up the 5µL starting sample. Inhibitor samples less than 100% are diluted in 1X TE buffer (IDTE Coralville, Iowa). The lysis binding solution used in these experiments is from the MagMax Viral RNA isolation kit, and the exact composition is proprietary. However, chaotropic salts such as guanidine hydrochloride or guanidinium thiocyanate are typically used as part of a lysis step[107].

4.3.4 Quantification of Green Fluorescing Protein for carryover measurements:

Carryover measurements were performed on the microfluidic chip using green fluorescing protein (GFP, Sigma Aldrich, St. Louis, MO) diluted in 1X TE buffer (IDTE, Coralville, Iowa) for a final stock concentration of 400ng/µL. Then, 5µL of GFP stock was combined in 5µL bead mix where the bead mix was 1:1, MagMAX beads: lysis binding enhancer solution, (Magmax Viral RNA Isolation Kit Thermofisher Scientific, Waltham, MA) to create the 10µL starting sample. The magnetic beads are approximately 450nm[125]. Each sample was vortexed for 1 minute to allow for equal distribution of GFP throughout the sample.

To perform an extraction run on the microfluidic chip, 30µL of 100% isopropanol (Sigma Aldrich, St. Louis, MO) was added to fill the separation channel though the positive electrode well. Then, the negative

and positive electrodes are placed in their respective wells and the voltage was set and turned on. After 30 seconds, 10µL of sample was added to the sample well quickly followed by adding 10µL elution buffer (MagMAX kit) to the elution well. Then, with the electric field still on, the magnet was dragged by hand under the chip from the sample well towards the elution well, which moved the beads, and any nucleic acids bound to them, into the elution well. The ongoing electric field allowed for electroosmotic flow in the opposite direction of the bead movement, to minimize the carryover volume. The beads were collected and the amount of GFP in the final elution buffer was measured. The Nanodrop 3300 fluorospectrometer (Thermoscientific, Waltham, MA) machine was used to quantify the GFP carried over from the sample well to the elution well. UV light (365nm excitation) was used for the GFP excitation. The emission wavelength was measured at 509nm and the machine output is relative fluorescing units (RFU). A calibration curve ($R^2 = 0.997$) of GFP concentration vs RFU was created and used as the standard for the results. The carryover volume in this microfluidic chip was measured using the four different separation channel widths (0.12mm – 0.21mm) at four different voltages (-300V, 0V, 150V and 300V). When the voltage is at -300V that indicates that the positive and negative electrode placements have been exchanged and electroosmotic flow is now moving in the direction of the elution buffer well as opposed to the sample input well on the microfluidic chip. In this study, the final GFP concentration in the elution well was measured for each separation channel and divided this by the starting GFP concentration to determine the percent GFP carried over.

4.3.5 DNA Sample

Human Papillomavirus-18 (HPV-18) purified plasmid DNA was purchased from American Type Culture Collection (ATCC Manassas, VA) at an insert size of 7.857 kb (7857 base pair). This was spiked into AcroMetrix EDTA Plasma (Thermofisher Scientific, Waltham, MA) to create a positive DNA sample.

4.3.6 DNA Extraction Protocol

A DNA sample (HPV) totaling 10µL was added to 120µL of AcroMetrix EDTA Plasma (Thermofisher Scientific, Waltham MA), creating a spiked sample for testing. Next, 200µL of lysis buffer solution (MagMAX Viral RNA Isolation Kit, Thermofisher Scientific, Waltham, MA) was combined with 2µL

carrier RNA (MagMAX kit) and then added to the sample for lysis. This reaction was done in an Eppendorf tube, which was then heated for 10 minutes at 70˚C. After the heating step, 250µL of ethanol (Pharmco-Aaper, Brookfield, CT, USA) was added to aid in nucleic acid precipitation. Finally, 50µL of bead mix (1:1, MagMAX beads: lysis binding enhancer solution) was added to the lysed sample. This solution was slowly mixed by vortex for 5 minutes, allowing for the exposed nucleic acids to bind to the beads. Finally, using a magnet (D82-N52 K&J Magnetics, Pipersville, PA) the nucleic acid bound beads were collects at the bottom of the Eppendorf tube and all but 100µL of the supernatant was discarded. The remaining 100µL which contains all of the nucleic acid bound beads was aliquoted into 10, 10µL samples.

The same nucleic acid extraction microfluidic chip protocol described previously was now performed. Lysed samples, 10µL, were added into the microfluidic chip after the electrodes were in place and the voltage was turned out. The nucleic acid bound beads were moved from the sample well into the elution well, by dragging a magnet from one well to another at a speed of approximately 1mm/second. Previous studies[10] in our microchip system report this as the optimal speed to move beads through a microfluidic channel in a cluster formation. Cluster movement is visible by eye so the end user is able to observe movement and adjust magnet speed accordingly. If beads are moved too quickly, bead loss, and therefore DNA loss, will negatively impact purification results. Once the magnetic beads were in the elution well, the solution and magnetic beads, 10µL, were removed from the microfluidic chip and incubated at 70°C for 10 minutes to allow for nucleic acid desorption. The beads were removed, and the supernatant now contained the extracted nucleic acids.

Based on preliminary results, channel B (0.15 mm) was used for the nucleic acid extraction testing as it provided a noticeable electroosmotic flow while being able to move the magnetic beads through the channel in an efficient amount of time. The voltage and direction of the electric flow was varied to measure DNA extraction at 300V, 0V, and -300V and four extractions were performed per study condition. Additionally, a commercially available kit (Invitrogen PureLink Viral RNA/DNA Mini Kit, Thermofisher Scientific, Waltham, MA) was used as a positive control.

4.3.7 Quantification of HPV-18 plasmid extraction

Quantitative PCR was performed on all extracted HPV DNA in this study. Rotor Gene SYBR Green PCR kit (Qiagen, Valencia, CA) was used with a PikoReal 24 Real-Time PCR instrument (ThermoScientific, Waltham, MA). Primers, forward (CGAACCACAACGTCACACAA) and reverse (ACGGACACACAAAGGACAGG) were designed in house and used at a final concentration of 1pmol. Cycling conditions can be found in the supplemental information. Nuclease free water was run as a no template control (NTC). A calibration curve (Figure 4.3) of log copy number of HPV in sample vs ct ($4.47x10^8$ – 44.7 copies) was created and used as the standard for the results. 5µL of eluted nucleic acid was used per 25 µL PCR reaction volume.

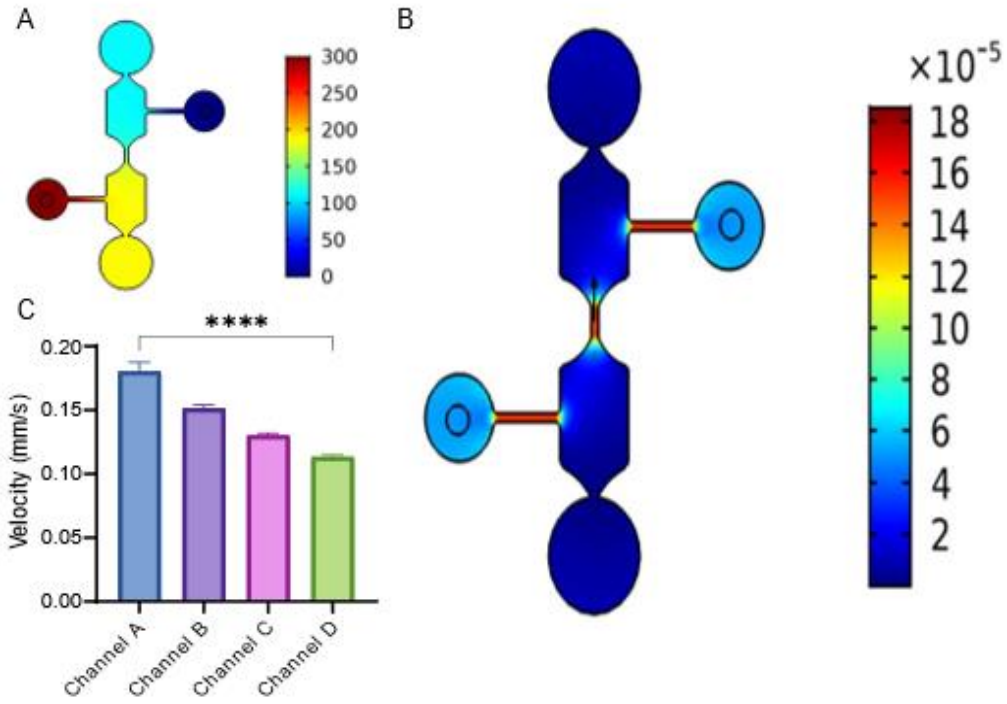

Figure 4.3: (A) Electric potential (V) surface plot for Channel B. (B) Velocity magnitude (m/s) surface plot and current density arrows for Channel B. (C) Velocity magnitude (mm/s) within center channel (A-D).

4.4 Results

The goal of the microfluidic chip is to extract and purify the genomic DNA bound to the magnetic beads using magnetic forces to move the beads through the microfluidic channel coupled with the application of

an electric field to induce electroosmotic flow. The electroosmotic flow within each of the four channel designs (A-D) (Figure 4.2) was modeled using COMSOL Multiphysics® Modeling Software 5.4 to better understand the effect the channel dimension has on the electroosmotic flow. In experimental testing isopropanol is used as the separation buffer, filling the channels of the microfluidic chip before any samples are added. Therefore, the properties of isopropanol were utilized as the basis for the material used in this modeling including the relative permittivity (17.9), density (785 kg/m^3), and dynamic viscosity (2.381 mPa*S) provided by various manufacturing sources. In addition to isopropanol, the buffers in the bead mix and DNA aggregate play a role in the electroosmotic flow that takes place in the cleanup when the electric field is applied. Thus, the known parameters of this bead mix and DNA aggregate were also taken into consideration to finalize the properties that were used for this modeling, especially when determining the electrical conductivity in the microfluidic chip. Since these material properties were not exact values mirroring the experimental system, modeling was performed for all four microfluidic chip center channel versions (A-D). Then, each of these simulations were compared to investigate the effect channel width has on the electroosmotic flow modeling since it was the only parameter changed between the simulations.

The electroosmotic flow profile of the liquid in the channel was modeled in the microfluidic chip based on the Helmhotz-Smoluchowski (HS) slip velocity boundary condition which approximates the motion of the electric double layer in the microchannel flow[126]. The HS relation provides the electroosmotic velocity (u) at the edge of the electric double layer in a straight microchannel in terms of the electric field. The HS equation is provided in Equation 4.1, where ε, ψ_0, E, and μ are the electric permittivity of the fluid, wall zeta potential, electric field, and viscosity of the fluid, respectively.

$$u = -\frac{\varepsilon \psi_0 E}{\mu} \qquad (4.1)$$

The magnetic beads that are used to move the DNA through the microfluidic chip were not included in this modeling since the goal is to show the electroosmotic flow of the liquid in the channel that will contain free DNA and PCR inhibitors not captured by the magnetic beads. In the COMSOL Multiphysics® Modeling Software 5.4 used for the computational modeling, the HS relation was presented as the “Electroosmotic

Velocity" Wall boundary condition for Laminar Flow with the zeta potential of the glass cover slide (-0.035V) and relative permittivity (17.9) as the input variables. This wall condition was applied to the entire channel excluding the four wells. The zeta potential of the PDMS was not included in the 2D simulations because the negatively charged glass slide was being modeled since it was predominantly responsible for inducing electroosmotic flow based on the buffer used. The Electric Potential used in the modeling was 300V applied to the electrode well closest to the elution well and 0V applied to the electrode well closest to the sample well. Figure 4.3A shows the electric potential (V) in microfluidic chip B as an example of the simulation result, this surface plot was consistent for all channel widths. The velocity output from the COMSOL simulations represent the results of the HS slip velocity which are indicative of the electroosmotic flow in each microfluidic chip iteration (A-D). Figure 4.3B shows the velocity magnitude (m/s) surface profile for channel B with the current density arrows showing the direction of the velocity moving from the 300V well to the 0V well. Lastly, Figure 4.3C shows the average velocity, representing the electroosmotic flow, in the center channel of the microfluidic chip which was taken from the Velocity plots on COMSOL. An ordinary one-way ANOVA test was performed to compare the different velocities and a statistically significant difference in velocity was found ($p<0.0001$). This COMSOL modeling demonstrates the center channel width has a statistically significant effect on electroosmotic flow in the microfluidic chip.

Experimental testing into PCR inhibitors from the microfluidic chip was also essential since it showed how PCR becomes less efficient, i.e. amplifies less HPV DNA, when the amount of inhibitors in the final sample is increased, therefore validating the need for an efficient purification technique. Plasma isopropanol and lysis binding solution all show less HPV amplification with increase of percent inhibitors in the solution. Plasma has the greatest effect on HPV DNA yield while isopropanol has the smallest effect (Figure 4.4) where there was still 89% PCR efficiency with 10% isopropanol in the PCR reaction, but less than 1% PCR efficiency for the same proportion of plasma or lysis binding solution in the PCR reaction.

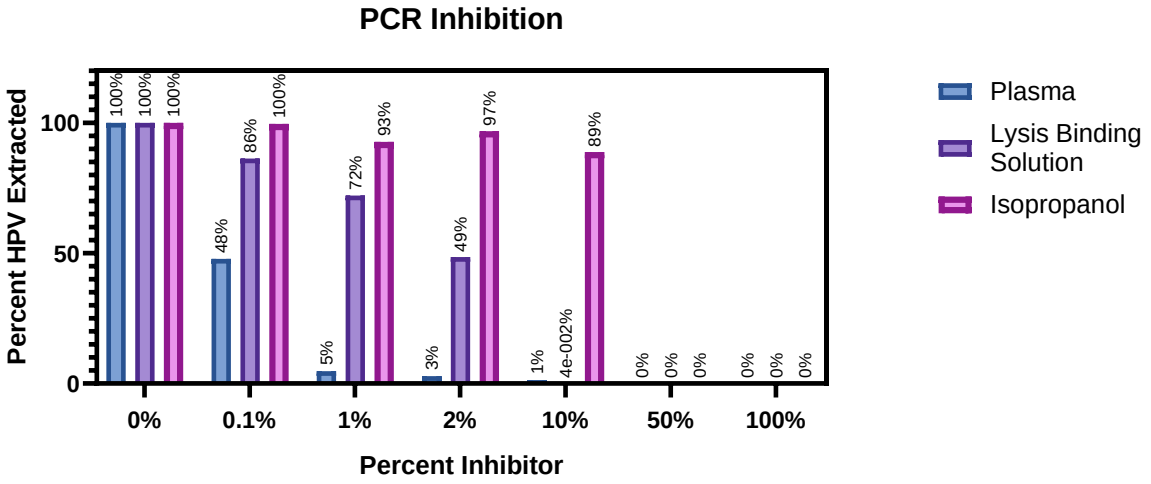

Figure 4.4: Efficiency of PCR with varied percent of inhibitor in sample.

The carryover volume analysis, based on the GFP carryover in the microfluidic chip, was less than 17% for all test conditions, (Figure 4.5). For channels A-C (0.12 mm, 0.15 mm, 0.18 mm), there was a statistically significant difference between the -300V condition carryover and the 300V condition carryover ($p<0.05$). For channel D (0.21 mm) there was no significant difference between any of the voltage test condition's carryover. Additionally, when looking at the 300V test condition, there is less carryover at smaller channel widths (0.12 mm and 0.15 mm).

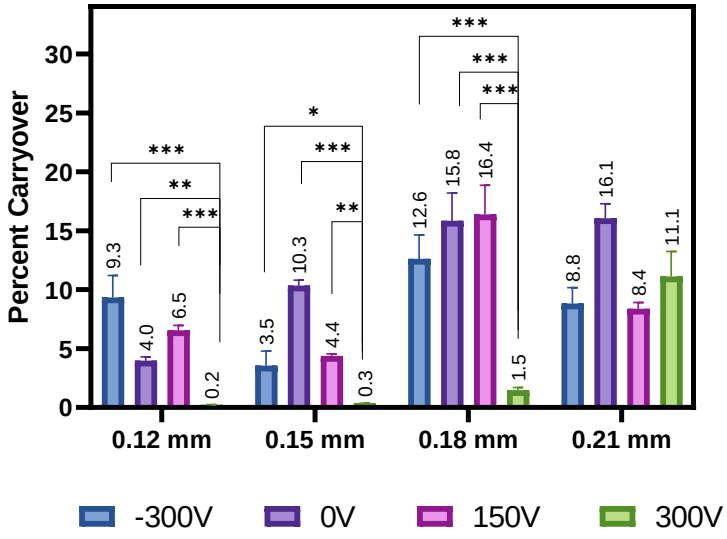

Figure 4.5: Percent carryover volume (GFP) for each chip dimension at varying voltages. (∗ = P<0.05, ∗∗ = P <0.005 and ∗∗∗ = P <0.001)

This GFP carryover study showed that channel B (0.15 mm) can minimize inhibitor carryover better than the larger channels (0.18 mm and 0.21 mm) based on the electroosmotic flow cleanup results. Additionally, although channel A (0.12 mm) also showed significant minimization of inhibitor carryover, this channel width proved to be too narrow for the magnetic beads to efficiently move through the chip. Channel B provided more efficient magnetic bead movement and therefore was selected for the DNA extraction experiments.

The DNA extraction experiments showed the average ct value for HPV DNA extraction for the kit control was 12.33 ± 1.37 where the average experimental ct results for -300V, 0V and 300V in channel B were 22.25 ± 2.94, 21.73 ± 7.74 and 15.04 ± 2.03, respectively. Using the calibration curve shown in SI Figure 4.1, the amount of HPV extracted at each voltage was calculated and results are shown in Figure 4.6. The kit control extracted an average of 7.7 x 10^6 copies HPV. The -300V runs averaged, 6216 copies HPV while the 0V averaged extracted 9049 copies HPV. Finally, the 300V extracted an average of 1.1 x 10^6 copies HPV. The 300V results are statistically different than the -300V runs and the 0V runs.

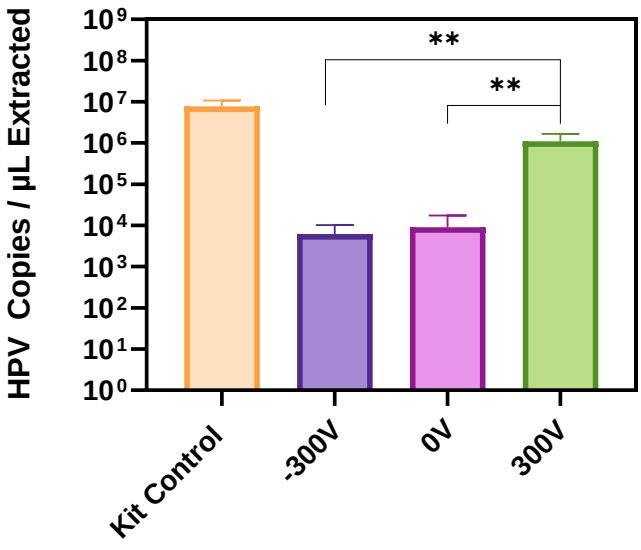

Figure 4.6: Number of HPV copies extracted at various voltages. Results shown are from channel B.

4.5 Discussion

COMSOL Multiphysics® Modeling Software 5.4 results show that the velocity induced by the electroosmotic flow is affected by the width of the center channel of the microfluidic chip. Experiments and modeling verify that when this channel in the microfluidic chip was too wide (channel D, 0.21mm), 300V was not able to induce a large enough electroosmotic flow to minimize carryover volume within this channel. It is hypothesized that a larger electric potential can induce electroosmotic flow to contain inhibitors in the sample well, which is measured by the velocity in the center channel. Thus, the electric potential (V) was varied within the COMSOL simulations for channel D to test this hypothesis. The aim of varying the electric potential was to study whether there was a voltage that would cause the velocity in the center channel to have no statistically significant difference from the original modeling for channels A-C at 300V, respectively. This would then show that changing the electric potential applied to this microfluidic chip could increase the electroosmotic flow enough to overcome the PCR inhibitor carryover based on COMSOL simulations and experimental data. Results (Figure 4.7) show no statistically significant differences in velocities between channels A-C and channel D at 475V, 400V, and 340V, respectively. Therefore, this analysis shows that changing the electric potential applied to this microfluidic chip can also affect the electroosmotic flow in addition to changing the center channel width.

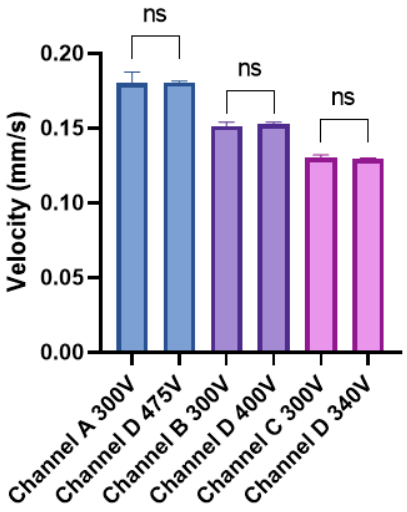

Figure 4.7: Velocity magnitude (mm/s) within center channel (A-C) at 300V comparison to the velocity magnitude (mm/s) within the center channel D at various voltages.

Experimental data using GFP showed the carryover volume was significantly lowered in the microfluidic chip at the 300V testing condition for channels A-C compared to all other test conditions. This shows that this voltage is large enough to induce electroosmotic flow that is strong enough to keep GFP, which represent PCR inhibitors, in the sample well and minimize their carryover into the elution well. Lower voltages reported here (0V and 150V) are not sufficient at inducing electroosmotic flow in this system and the trend between voltage and carryover volume is not linear. This data suggests a threshold voltage must be reached before a reduction in carryover volume can be observed. These results support the hypothesis that moving magnetic beads in the opposite direction of voltage induced electroosmotic flow can reduce the carryover volume because when the direction of the electroosmotic flow and bead motion are the same (-300V), there is a statistically significant difference in the amount of carryover (Figure 4.5). This protocol is beneficial when compared to traditional methods because it has minimal end user steps and creates a stable, effective interface within the chip which minimizes carryover to levels which are comparable to or less than other microfluidic chips used for nucleic acid extraction[11]. The results of the GFP carryover volume study also showed no statistically significant difference between the -300V, 0V and 150V testing conditions for channels A-C and all testing conditions with separation channel D (width at 0.21mm). Under the 300V condition, less than 2% carryover of GFP in channels A-C was observed. Compared to the percent inhibition and PCR efficiency experiments (Figure 4.4), this carryover volume is minimal and will not significantly reduce PCR efficiency.

Finally, experimental results showed that DNA can be extracted from a spiked plasma sample using the microchip and electroosmotic flow system and result in a DNA sample pure enough to be efficiently amplified. Since PCR was shown to be less efficient when inhibitors are present in the amplified solution, which aligns with other sources in the literature[127], it was hypothesized that the 300V condition would provide the least amount of these inhibitors and therefore the most efficient PCR. The ct values for the control kit and 300V testing condition are not significantly different (t-test, $p= 0.13$) showing the microfluidic chip channel B (0.15 mm) can extract DNA from a starting sample as efficient as the kit control. Conversely, the 300V versus the -300V ct values are significantly different in channel B (t-test,

p=0.025) showing the direction of the applied voltage, and thus the electroosmotic flow, makes a statistically significant difference in the success of the DNA extraction and purification. Overall, with the presence of an electroosmotic flow from 300V, the microchip channels A-C can be used to prevent carryover volume and extract quality DNA that is ready for amplification based on COMSOL modeling and GFP and DNA extraction experiments.

4.6 Conclusion

Electroosmotic flow can be used in combination with magnetic bead-based separation in a microfluidic system for the extraction of DNA. When the electrodes are arranged so the electroosmotic flow is in the opposite direction of the magnetic bead movement (150V, 300V), the resulting force of the electroosmotic flow minimizes PCR inhibitors from leaving the sample well and moving through the microfluidic chip towards the elution buffer well. However, when the electroosmotic flow is reversed, (-300V) inhibitors are carried into the elution buffer, negatively impacting the success of the PCR amplification. Inhibitor free elution is crucial for specific and sensitive diagnostic tests since DNA PCR works more efficiently when inhibitors are removed. For optimal results in this microfluidic chip, the separation channel width must be less than or equal to 0.18 mm and the voltage should be above 300V.

4.7 Supplemental Information

Figure SI 4.1: A photograph of the microchip used in this study. A) Shows microchip at an angle to display channels while B) has electrodes set for run.

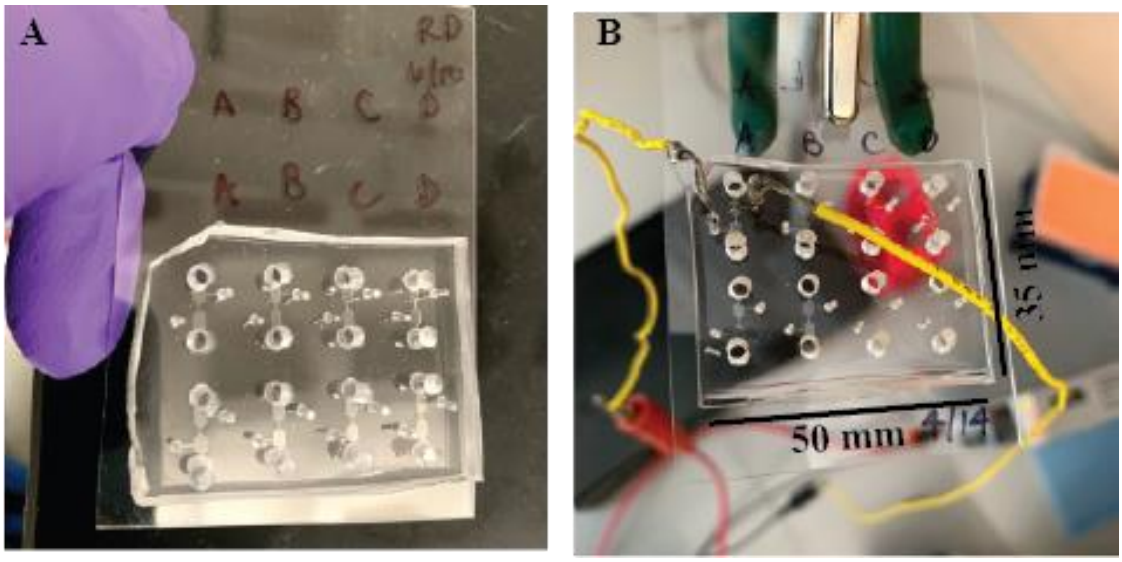

Figure SI 4.2: Calibration curve used for HPV concentration versus PCR ct value.

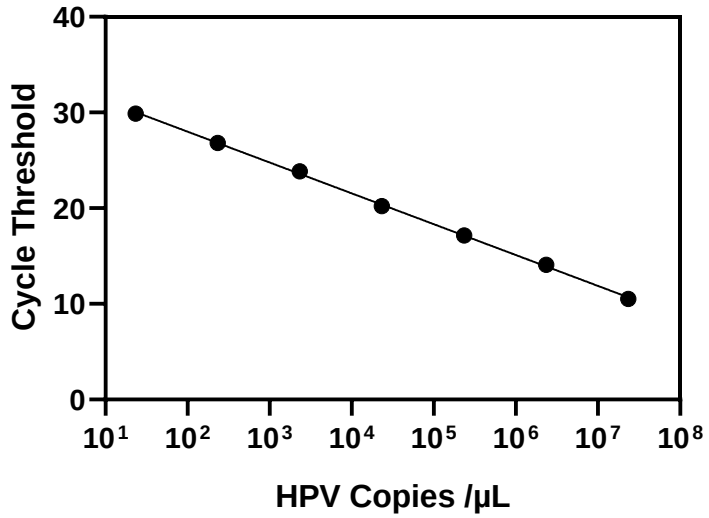

Table SI 4.1: PCR Cycling Conditions

95°C	5 minutes	
95°C	5 seconds	Cycle 40x
54°C	10 seconds	
72°C	30 seconds	

CHAPTER 5

Isolation of target DNA using synergistic magnetic bead transport and electrokinetic flow

---

Chapter 5 has been published as an original research article.

Schneider, L., Cui, F., Tripathi, A., *Isolation of target DNA using synergistic magnetic bead transport and electrokinetic flow*, **Biomicrofluidics**, 15(2), 024104, 2021.

5.1 Abstract

The advent and dissemination of next-generation sequencing (NGS) technologies such as Illumina's sequencing platforms has brought forth vast reductions in the cost, time, and technical difficulty associated with DNA and RNA sequencing. Despite this trend, the workflow required to generate nucleic acid libraries for sequencing remains time-consuming and laborious. The following research proposes a method for simplifying and streamlining this process by replacing the manual wash steps of the common magnetic bead-based cleanup with a novel microfluidic method by integrating magnetic separation and electrokinetic purification (MSEP). Requiring no pumps, pipette mixing, vortexing, or centrifugation, MSEP relies on selective adsorption of target DNA onto the magnetic beads with subsequent transport of beads through a microchannel undergoing an antiparallel electroosmotic flow. The synergetic flow conditions were optimized using a simple electrohydrodynamic flow model. This work demonstrates that MSEP is as effective in eliminating adapter-dimers from the post-ligation library mix as the manual method, while also greatly reducing the hands-on time and amount of pipetting required. Although MSEP has been applied specifically towards NGS library preparation at this time, it has the potential to be adapted and employed for any bead-based separation scheme, namely solid phase extraction, sequence-specific hybridization, and immunoprecipitation on a microscale.

Keywords: Sample preparation, Next generation sequencing, Purification, Microfluidics, Electroosmosis

5.2 Introduction

Next generation sequencing (NGS) has transformed the biomedical landscape and ushered in a new age of discovery in genomics. In the domain of human medicine alone, NGS has had a significant impact in areas such as prenatal screening[128], rare disorder diagnosis[129], cancer research[130] and many others. The capability to sequence millions of individual DNA fragments simultaneously and align the reads back to a reference genome has led to massive reductions in the cost, labor, and hours that would have been required with capillary sequencing[131]. While the first human genome was sequenced for roughly $300 million, today it can be done for around $1000[132,133]. With sequencers such as Illumina's iSeq and Oxford Nanopore's MinION available on the market, sequencing has become cheaper and more accessible than ever before. Unfortunately, while sequencing has made huge strides in reducing the requisite cost, time, and workload, sample preparation for sequencing has lagged behind in its progress. For applications requiring less data, such as microbial whole genome sequencing or RNA-seq, the majority of the total cost to sequence is contributed by sample preparation—a critical upstream process that can ultimately determine the success or failure of a sequencing run[134]. In addition to accounting for a large portion of the total cost of sequencing, sample preparation can be complex and time-consuming; often requiring nucleic acid extraction from a genomic sample followed by a series of enzymatic reactions and intermediate purification steps. These consequently require a significant amount of pipetting, centrifugation, or magnetic bead handling, all of which are nontrivial to automate. To alleviate these limitation for sample preparation, there is a need for new technologies that can help automate the workflow, thereby reducing the number of steps and total procedural time, as well as sources of human error[135].

For the case of whole genome sequencing, sample preparation begins with the extraction of genomic DNA followed by fragmentation. Fragmentation can be done enzymatically, mechanically using nebulization or sonication, or other methods[136].To ensure high library complexity, it is important to obtain a large yield from the DNA extraction and to select a fragmentation method that does not introduce bias[136]. Following fragmentation, the DNA fragments are ligated to barcoded adapters that will eventually enable hybridization to the flow cell and cluster generation during sequencing. To achieve proper ligation, the ends

of the fragments are blunted, adenylated, and 5' phosphorylated to enable subsequent ligation and amplification[137]. This reaction may also generate unwanted byproducts, known as adapter-dimers, in which the barcoded adapters are ligated to one another rather than to the DNA fragments. Adapter-dimers can be problematic in that they will readily hybridize and amplify on the flow cell, thereby taking the place of a DNA fragment from the original starting sample and ultimately provide useless sequencing data. A post-ligation purification is thus typically performed often using solid phase reversible immobilization (SPRI), a method that uses magnetic beads to size-select DNA by selectively precipitating larger DNA fragments onto the surfaces of the magnetic beads in a high-salt, high-polyethylene glycol solution[138]. This process involves DNA precipitation onto magnetic beads followed by multiple washes using a chaotropic salt or an alcohol-based solutions which can rinse away unwanted particles from the buffer while the DNA remains precipitated[114]. Lastly, the magnetic beads are resuspended in a water-based solution, such as an Elution Buffer, Resuspension Buffer, or simply nuclease free water or Tris EDTA (TE) buffer before moving to the next steps in the library preparation. This purification protocol, however, remains manual and time-consuming, requiring many large volume washes with pipette mixing.

To combat these limitations, many different microfluidic strategies have been developed to simplify the purification procedure by reducing the time, volume, and pipette handling steps compared to conventional methods[134,139-143]. For example, Kim et al. employed pressure-driven flow in a microfluidic chip to wash the magnetic bead suspensions[134]. While beneficial in some areas compared to manual purification, this method was designed to require an external pressure controller and the secure connection of many pneumatic lines, which ultimately complicates its implementation as a widely-used, microfluidic-based purification strategy[134]. Conversely, other technologies have sought to replace pressure-driven flow, and the associated complexities of those systems, with magnetic bead translocation within a microfluidic chip from one part of the chip to another. This methodology is beneficial because it forgoes the use of a pump, instead employing simple permanent magnet motion to move the magnetic beads. Using this technique, separation between the magnetic beads and the contaminating solution can be affected by physical distance[144-147]. While facile to operate, this method requires very long channels to ensure adequate separation to reduce

the influence of diffusion of the same contaminates that should be purified out of the DNA libraries[144-147]. Alternatively, magnetic bead separation on microfluidic chips has also been achieved by pulling the magnetic beads out of the contaminating solution and through an immiscible phase barrier such as oil[10,109,148-150]. Though oil-water interfaces provide an effective means of separating aqueous volumes, they are nontrivial to set up correctly, requiring fine-tuning of the interfacial energies between the various phases to achieve reproducible magnetic bead transport and purification.

With the goal of providing a purification method that can be simple yet easily conducive to automation, this work instead introduces a novel technique for magnetic bead-based purification assays called magnetic separation with electrokinetic purification, or MSEP. This method relies on (1) the transport of a magnetic bead suspension with adsorbed DNA library from a contaminated well into one containing purified buffer by way of a connecting channel, actuated by automated linear permanent magnet motion; and (2) the simultaneous application of an electric field along the connecting channel so as to induce electrokinetically-driven migration of non-adsorbed contaminants in the opposing direction of magnetic bead translocation. The latter feature serves to effectively remove contaminants such as adapter-dimers that have been hydrodynamically dragged into the connecting channel with the magnetic beads. MSEP has been applied toward the purification procedures typical in an NGS library preparation workflow and demonstrate its efficacy through the library preparation and sequencing of the E. coli genome.

5.3 Materials and methods

5.3.1 Device fabrication

MSEP devices were fabricated using polydimethylsiloxane (PDMS) soft lithography. A 10:1 mixture of Sylgard 184 elastomer base and curing agent was mixed then placed in a vacuum chamber for one hour to dissolve any air bubbles. Next, the mixture was transferred onto a mold made from SU-8 (FlowJEM, Toronto, ON, Canada) and allowed to cure at 70°C for 90 minutes. After curing, the PDMS was removed from the mold and circular wells were punched out using 3.5 mm, 1.2 mm, and 0.75 mm-diameter hole punches according to the respective well size. The PDMS was then bonded to a glass microscope slide following plasma treatment with a high frequency generator. Lastly, the microfluidic chip was returned to

the oven set to 70°C for 30 minutes, then kept at room temperature for at least 24 hours before use to ensure uniform chip-to-chip zeta potential. Further information on the MSEP device fabrication and uniformity is provided in the Supplementary Material.

The microfluidic chip was used in conjunction with automated magnetic bead translocation which was performed using a neodymium bar magnet (K&J Magnetics, Pipersville, PA, USA) that was mounted to the arm of a small hobby servo motor which controlled whether the magnet was in contact with the microfluidic chip or not. The MSEP chip was placed on a linear screw-drive stage (IGUS, East Providence, RI, USA), which allowed the chip to move with respect to the stationary magnet. A stepper motor was used to drive the linear stage (Applied Motion Products, Watsonville, CA, USA), and a Si Programmer script (Applied Motion Products Watsonville, CA, USA) was used to program the stepper, while a Python script was used to activate the servo and switch the electrode power supply on and off.

5.3.2 MSEP protocol for SPRI

SPRI magnetic bead-based purification is used within a library preparation workflow after ligating barcoded adapters to DNA library fragments in order to selectively capture and isolate the ligated fragments, while smaller DNAs such as adapter-dimers (~120 bp) are washed away. The SPRI protocol which was used as a control to compare the microfluidic chip to, outlined in Fig. 5.1a, consists of an initial DNA capture onto the suspended magnetic beads, followed by a magnetic bead pull-down and aspiration of the supernatant. The magnetic beads are then pipette mixed with a large volume of alcohol-based solution and pulled down again; the supernatant is then aspirated, and the wash is repeated. Finally, a resuspension buffer is mixed in to elute the captured DNA from the magnetic beads. Conversely, purification by MSEP is achieved through the steps outlined in Fig. 5.1b. Each microfluidic separator has a depth of 150 μm and consists of four wells: the sample input well (S), the resuspension well (R), the filling well (F) and the electrode well (E). First, 30 μL of separation buffer, composed of 70% isopropyl alcohol, is loaded into well F. Due to the low contact angle between alcohol and PDMS, the separation buffer passively fills the channels of the device, including the small-diameter E well, without filling the larger-diameter S and R wells. The separation buffer is able to completely fill the E well to the top of the microfluidic chip. If the separation buffer does not fill

the E well it is possible to create an air bubble as the electrode is placed into the well which can interfere with the electric field being applied. Once wells E and F are filled with separation buffer, platinum electrodes connected to a high-voltage power supply are then placed into those wells. Following the electrode placement, the DNA-SPRI bead mixture is loaded into well S and an equal volume (typically 20 μL) of resuspension buffer (10 mM Tris-HCl, pH. 8.0) is loaded into well R. The purification process on the microfluidic chip then proceeds with the bar magnet engaging so that it is adjacent to the microfluidic chip and the DNA-adsorbed magnetic beads in well S are pulled down to the bottom of the well via the magnetic forces. Next, by way of the automated linear motion of the linear screw drive stage, the magnet moves in the direction of well R so that the beads exit well S and move through the channel of the microfluidic chip. Simultaneously, a potential difference of V0 is applied across wells E and F such that a cathodic electroosmotic flow (EOF) is generated that is antiparallel to the velocity of the beads (outlined in Figure 5.1b, step iv.). This disparity in relative velocity is greatest in the field focusing channel, where the 120- μm width results in concentrated electric field and thus a greater electroosmotic velocity. Separation between the library-carrying magnetic beads and the adapter-dimers in solution, which are hydrodynamically dragged along with the bead suspension, is therefore achieved by creating a bulk EOF that washes the beads as they are pulled in the opposite direction. Once the beads are pulled into well R, the DNA can resuspend for 2 minutes before aspiration.

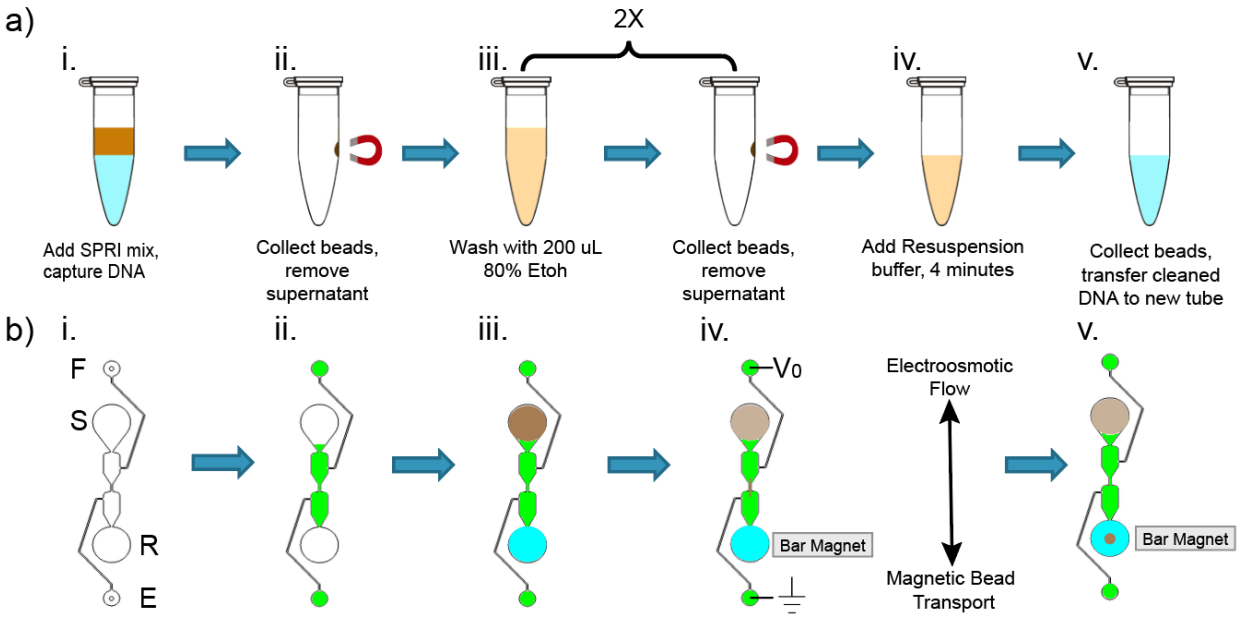

Figure 5.1: Purification workflow of magnetic bead suspensions. (a) Manual purification requires repeated rounds of washing, pipetting, and magnetic bead pull-downs. (b) i. MSEP is performed on a microfluidic device consisting of a filling well F, sample well S, electrode well E, and resuspension well R; ii. Separation buffer (green) is loaded into well F and fills the channel via capillary action; iii. Bead mix (brown) is loaded into well S and resuspension buffer (blue) is loaded into well R; iv. A potential difference is applied between wells F and E and a bar magnet transports the beads (brown) from well S to well R providing the opposing directions of the electroosmotic flow and magnetic bead transport; v. DNA library resuspends by desorbing from the magnetic beads in well R and is aspirated out of the microfluidic chip.

5.3.3 Library construction and quantification

Illumina MiSeq-compatible DNA libraries were constructed with the NEXTFLEX Rapid DNA-Seq library prep kit (Bioo Scientific, Austin, TX, USA) following the manufacturer's instructions. DNA pseudo-library and pseudo-adapter-dimer, used in assessing MSEP performance, were generated by using polymerase chain reaction (PCR). A 480-bp amplicon was used for the pseudo-library and a 123-bp amplicon was used for the pseudo-adapter-dimer and both amplicons were made by amplifying regions of the pUC19 cloning vector (New England Biolabs, Ipswich, MA, USA). These fragment sizes were chosen to model typical library and adapter-dimer lengths. The pseudo-library was produced using the forward primer sequence 5' - CTG TCA TGC CAT CCG TAA GAT - 3' and reverse primer sequence 5' - GCG CGG TAT CCC GTA TT - 3', while the pseudo-adapter-dimer required the forward primer sequence 5' - CTG TCA TGC CAT CCG TAA GAT - 3' and reverse primer sequence 5' - GCG CGG TAT CCCGTA TT - 3'. All primers were purchased from Integrated DNA Technologies (Coralville, IA, USA).

The total DNA yield produced by MSEP was assessed using the Quant-iT Picogreen dsDNA Assay (Invitrogen, Carlsbad, CA, USA) following the manufacturer's instructions and fluorometrically quantified in an EnVision Multilabel Reader (PerkinElmer, Waltham, MA, USA). The carryover concentration of 123-mer pseudo-adapter-dimer was calculated by qPCR using a Luna Universal qPCR Master Mix (New England Biolabs, Ipswich, MA, USA), the aforementioned pseudo-adapter-dimer primers, and the PikoReal Real-Time PCR System (Thermo Fisher Scientific, Waltham, MA, USA). Melt curve analysis was performed after every qPCR run to rule out off-target amplification. DNA library quality was assessed by Agilent Bioanalyzer 2100 and the Agilent High Sensitivity DNA Kit (Agilent Technologies, Santa Clara, CA, USA).

5.3.4 Electrokinetic modeling and numerical simulations

Electrokinetic transport modeling was performed using COMSOL Multiphysics. Three-dimensional CAD models were designed in SolidWorks (Dassault Systémes, Vélizy-Villacoublay, France) and imported into COMSOL as the Geometry for the simulations. The Electric Currents, Laminar Flow, and Transport of Diluted Species modules were used to solve for the electric field; electroosmotic flow; and the convection, diffusion, and electrophoresis of charged species, respectively. Solutions for velocity and pressure, electric potential, and concentration were discretized using P1+P1, quadratic, and linear elements, respectively. A stationary study step was first executed to compute the electric potential, velocity, and pressure, utilizing the conjugate gradient method for the potential computation and the generalized minimal residual method (GMRES) for the latter two. Upon convergence to a relative tolerance of 10^{-3}, a backward differentiation formula time stepper and GMRES was used to solve for the evolution of the concentration field.

The Nernst-Planck equation for a steady electric field $\nabla\phi$,

$$\frac{\partial c_i}{\partial t} = \nabla \cdot \left[D_i \nabla - \mathbf{u} + \frac{D_i z_i e}{k_B T} \nabla\phi \right] c_i + R_i \tag{5.1}$$

can be used to model the advective, diffusive, and electrophoretic flux of a charged species, c_i, in a velocity field, $\mathbf{u}$. The electrophoretic term can be rewritten as the product of the electrophoretic mobility, μ_{EP}, and the electric field, where,

$$\mu_{EP} = -\frac{D_i z_i e}{k_B T} \tag{5.2}$$

An electrophoretic drift velocity can then be defined as,

$$\mathbf{u}_{EP} = \mu_{EP} \nabla \phi \tag{5.3}$$

In addition to electrophoresis, microfluidic channels (including PDMS-glass devices) typically exhibit the phenomenon of EOF when a potential gradient is applied along the length of the channel[151]. EOF results in a plug flow of velocity, $\mathbf{u}_{EOF} = \mu_{EOF} \nabla \phi$, in which the electroosmotic mobility,

$$\mu_{EOF} = \frac{\varepsilon \zeta}{\eta} \tag{5.4}$$

is given by the electrical permittivity, ε, the substrate zeta potential, ζ, and the dynamic viscosity, η. Assuming no other hydrodynamic flow or reactions, Eq 5.5 can be rewritten as,

$$\frac{\partial c_i}{\partial t} = \nabla \cdot [D_i \nabla - (\mu_{EOF} + \mu_{EP}) \nabla \phi] c_i \tag{5.5}$$

Additionally, the drift velocity of a charged particle is the sum of electroosmotic and electrophoretic contributions, such that,

$$\mathbf{u}_{d,i} = \left(\frac{\varepsilon \zeta}{\eta} - \frac{D_i z_i e}{k_B T}\right) \nabla \phi \tag{5.6}$$

5.4 Results

5.4.1 Evaluation of automated magnetic bead transport within microfluidic chip

The magnetic beads were transported from well S to well R in the MSEP microfluidic chip using the automated linear motion of the screw-drive stage with respect to a stationary permanent bar magnet. Successful well-to-well magnetic bead transfer was accomplished by transporting the magnetic beads in

the configuration of thin stream of particles rather than as a single large aggregate, which often led to the magnetic beads becoming stuck at narrow portions of the separator channel (i.e., at the field focusing channel in the center of the chip and at the opening of well S). The thin stream configuration was attained by utilizing a pulsatile motion for the linear stage which involved momentarily bringing the magnet toward well S and then retreating towards well R to not allow for time for the magnetic beads to aggregate together. This strategy led to magnetic bead transfer that was as effective as manually manipulating the magnet. Transport efficiency, or the proportion of magnetic beads to reach well R, was assessed by particle counting with a hemocytometer (Fig. 5.2) with both manual and automated methods producing efficiencies of 81% and 78% at zero applied voltage, respectively. With an applied voltage of 800V, transfer efficiency for the automated method dropped to 73%, however when the motion script was extended from 1 minute to 2 minutes duration, efficiency rose to 84%.

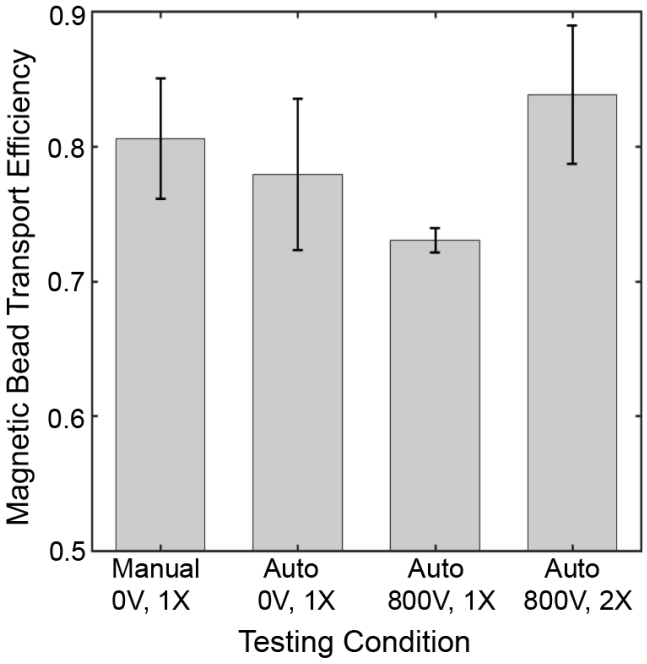

Figure 5.2: The proportion of magnetic beads to successfully translocate from well S to well R was quantified. 'Manual' and 'Auto' denote manual and automated magnet motion, respectively. 1-minute (1X) or 2-minute (2X) magnet motion protocols were performed at either 0V or 800V.

5.4.2 Electrokinetic modeling, numerical simulations, and measurements

Based on the electrokinetic modeling presented in Eq 5.1-5.6, an important result of Eq 5.6 is that for negatively charged particles and surface zeta potentials, the electrophoretic and electroosmotic velocities oppose one another, which will inhibit the advective transport of anionic contaminants away from the magnetic beads. This opposition of electrokinetic phenomenon occurs in the current MSEP system with negatively charged DNA moving by electrophoresis in one direction and a negative zeta potential of the glass surface of the chip controlling EOF in the opposite direction. But it is important to consider that SPRI purifications require the use of an alcohol-based solution as the wash buffer to prevent premature elution of DNA from the magnetic beads. Nucleic acids have low solubility in alcoholic solutions due to alcohol's lower dielectric constant, which allows the positive counterions in solution and the negative phosphate backbone of DNA to precipitate and thus results in a 90% reduction in the DNA charge[152]. It was therefore determined that this would therefore shrink μ_{EP} by 90% in the MSEP system and EOF would dominate the DNA transport.

To test this, MSEP was performed using DNA of 480 base pairs (bp) in size that was stained with Picogreen and mixed with magnetic beads in a non-binding solution. The MSEP separator was then filled with separation buffer (70% isopropyl alcohol, 1 mM SDS) and the stained DNA was added. The magnetic beads were then pulled into the channel, bringing along the DNA in the mixture, and then pulled back into well S with the goal of leaving behind the stained DNA to study under the electric field. An electric field was then applied while the MSEP separator was imaged via widefield fluorescence microscopy at one frame per second. Fig. 5.3a shows a cathodic DNA velocity that can be visualized by the moving front of the fluorescent zone, suggesting that the DNA is being swept along by the EOF, concordant with the theory that EOF would occur in the MSEP separator under these conditions.

A COMSOL Multiphysics simulation was used to replicate the above conditions and assess whether a similar outcome would be achieved. Using a 3D CAD model of the microfluidic separator, the same voltage condition was applied, and a spatial distribution of solute was initialized to mimic that of the experiment. The solute was given a charge number of -96, or 10% that of the expected full charge of 480-mer DNA, as

well as a diffusivity of 5.75×10^{-12} m^2s^{-1} [153]. To model the EOF, a slip velocity at the walls was prescribed such that,

$$\mathbf{u} = \mathbf{u}_w - (\mathbf{u}_w \cdot \hat{n})\hat{n} \quad | \quad \mathbf{u}_w = \frac{\varepsilon_r \varepsilon_0 \zeta}{\eta} \tag{5.7}$$

The dynamic viscosity was set to $\eta = 1 \times 10^{-3}$ Pa·s, and a relative permittivity, $\varepsilon_r = 35$, was applied[154]. The zeta potential was approximated, ζ = -100 mV, given the addition of 1 mM SDS in the separation buffer[155]. Using these parameters, the numerical model was able to generate a time-dependent solution that matched closely with the observed EOF speed (Fig. 5.3b).

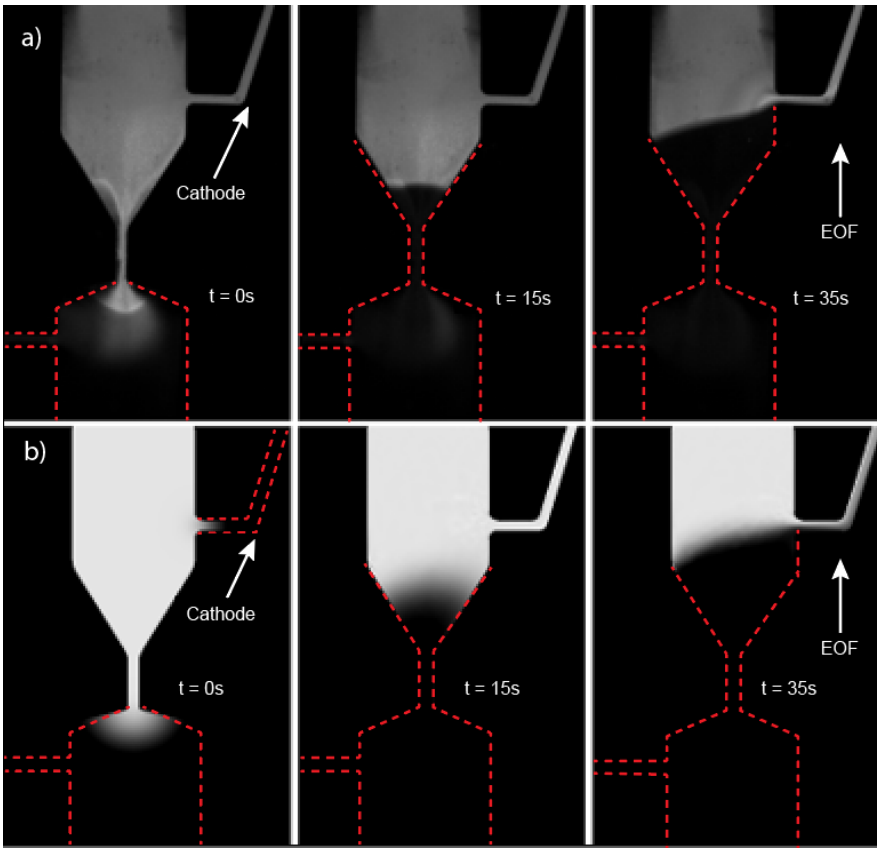

Figure 5.3: Electrokinetic transport via EOF (labeled) in MSEP device. (a) Fluorescent images of DNA-picogreen (light colored) transport in separator with 1000V applied. Separation buffer = 70% isopropyl alcohol, 1 mM SDS. (b) Numerical solutions at identical times display similar speed and direction of migrating solute (white) front.

5.4.3 Yield and purity performance of MSEP Device

Anticipating a cathodic EOF to dominate the advection of dissolved anionic contaminants, the polarity of the electrodes was set such that the EOF velocity would oppose that of the translocated magnetic beads. The effect of this can be visualized in Fig. 5.4 in which MSEP is performed on a fluorescein-magnetic bead mixture where the magnetic beads are mixed with fluorescein dye. Fluorescein dye is negatively charged and was selected to mimic the movement of the non-binding DNA contaminants in the microfluidic chip with and without the electric field. In this experiment, the fluorescein-magnetic bead mixture was added to well S of the microfluidic chip (shown in Figure 5.1b) and a bar magnet was again placed below well R to move the magnetic beads while the dispersed dye was imaged using a fluorescence microscope. In one channel when no voltage is applied, the fluorescein is transported along with the magnetic beads through the channel (Fig. 5.4a). Long range hydrodynamic interactions between the magnetic beads and the surrounding fluid result in the dragging of nearby contaminants, leading to this carryover. However, in a second channel when the voltage is applied, the fluorescein is effectively swept away by the EOF towards the cathode, resulting in less carryover as the magnetic beads travel down the length of the channel (Fig. 5.4b). In this experiment all conditions were kept consistent between the two channels except the applied voltage in order to study the movement of the negatively charged fluorescein dye.

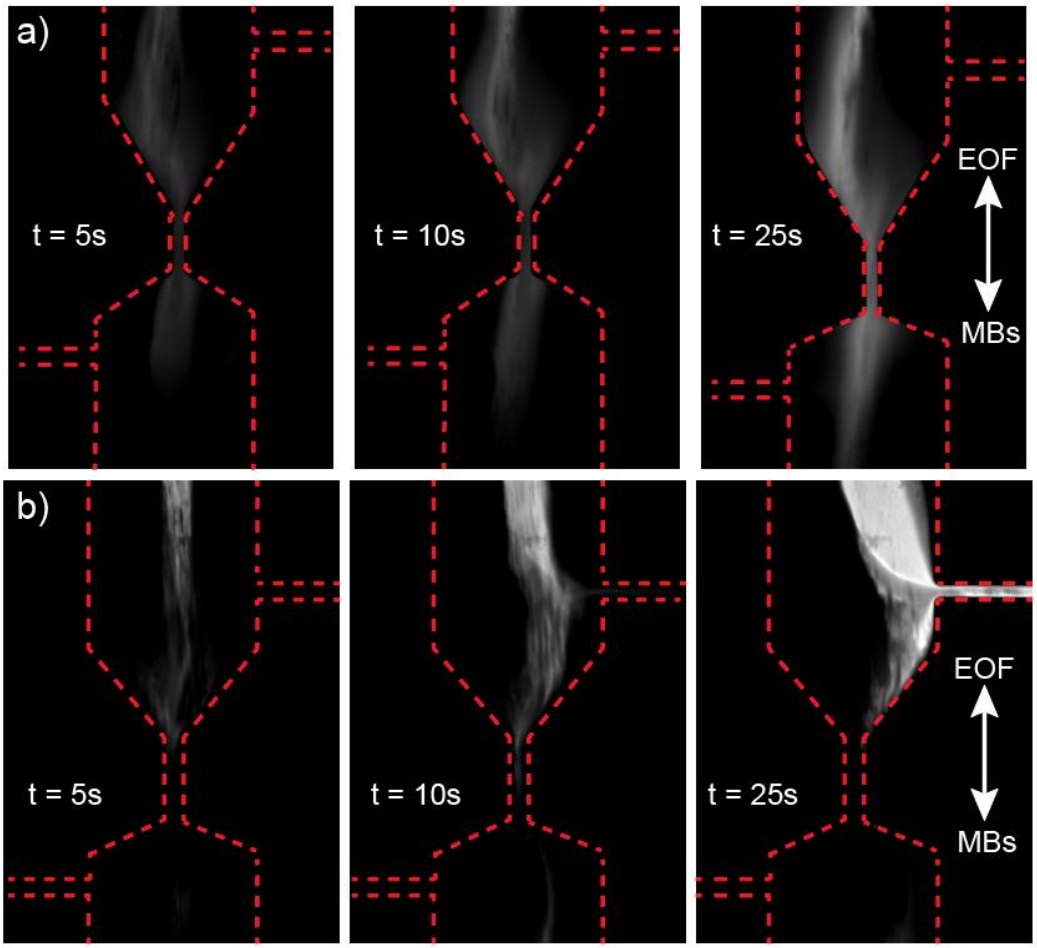

Figure 5.4: MSEP with fluorescein, microfluidic chip outlined in red, dashed lines and direction of EOF and magnetic beads (MBs) labeled. (a) No electric field applied. Fluorescein is carried with the magnetic beads as they are transported down the channel into well R (bottom, not visible). (b) 1000V applied between wells F and E. As fluorescein is pulled into the channel by magnetic bead motion, EOF sweeps it towards the cathode located in well F (right, not visible), preventing it from progressing through channel towards R.

MSEP was next applied toward the SPRI purification of pseudo-library and pseudo-adapter-dimer using a roughly [6 ng]: [1 ng], pseudo-library: pseudo-adapter dimer DNA solution to evaluate the purification capabilities with DNA before moving to a more complex sample. 10 µL of DNA solution was mixed with 8 µL Ampure XP (Beckman Coulter, Brea, CA, USA) SPRI bead mix to selectively bind pseudo-library and not pseudo-adapter-dimer. After a one-minute capture of the DNA on the beads, the bead mixture was either washed manually as in Fig. 5.1a or purified using MSEP as in Fig. 5.1b. Samples subjected to MSEP were processed with a range of applied voltages, including the no-voltage condition. The electrode leads were oriented so that the magnetic beads traveled in the direction of the potential gradient as they were

translocated from well S to R. Upon reaching well R, which contained 18 μL of resuspension buffer, the DNA could resuspend for two minutes. 16 μL of resuspension buffer was then aspirated and the pseudo-library and pseudo-adapter-dimer content was measured (Fig. 5.5).

The manual purification method recovered 5.8 ng/μL, or approximately 76% of the input pseudo-library amount. MSEP on average recovered 15% less than off-chip washing in total yield, with no significant difference among the electric fields tested. The percent of the total yield that consisted of pseudo-adapter-dimer (i.e., mol pseudo-adapter-dimer/ (mol pseudo-adapter-dimer + mol pseudo-library)) was assessed through qPCR analysis. It was found that while MSEP at zero applied voltage resulted in greater pseudo-adapter-dimer carryover than manual purification by a factor of 3.0, increasing the electric field brought the pseudo-adapter-dimer carryover down until no significant difference was observed between manual and MSEP purification.

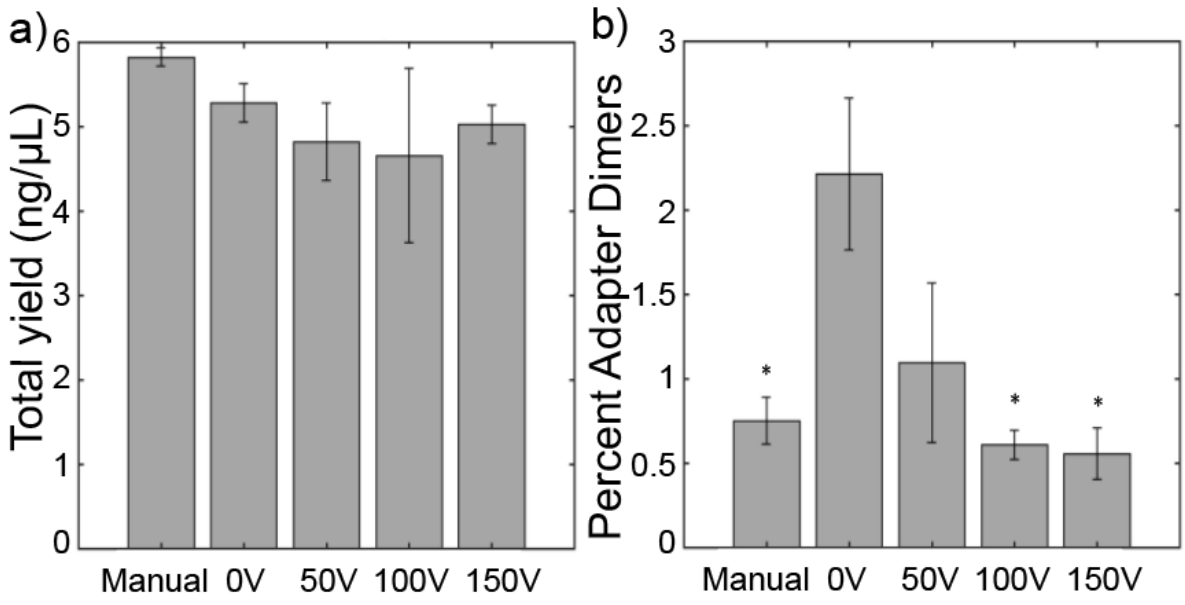

Figure 5.5: (a) Pseudo-library yield and (b) pseudo-adapter-dimer carryover comparing the manual SPRI purification method according to manufacturer's instructions to MSEP method on the microfluidic chip at different voltage conditions. * denotes $p < 0.05$ against 0V (two sample t-test)

These results indicate that higher voltages work better to remove adapter dimers and thus as the strength of the electroosmotic flow increase, so does the purification efficiency. In order to test the electroosmotic flow at voltages higher than 150V, COMSOL Multiphysics simulations were tested using a 2D Geometry of the

microfluidic chip design. The goal was to evaluate the effect of the electric field on the electroosmotic flow velocity in the field focusing channel located in the center of the microfluidic chip. Laminar flow physics were used with an Electroosmotic Velocity boundary condition. Isopropanol was used as the material for these simulations as it made up the majority of the separation buffer loaded into the microfluidic chip for the experiments. Various manufacturing sources were used to gather the properties necessary for this simulation such as the relative permittivity (17.9), density (785 kg m^{-3}), and dynamic viscosity (2.381 mPa S) of isopropanol. Other properties, such as electrical conductivity, were assumed when needed based on other reagent properties mixed in the separation buffer or SPRI bead mix which could influence the electroosmotic flow. The results of these simulations are presented in Figure 5.6a where at 0V the velocity is 0 μm/sec and at 1000V it is 0.18 μm/sec. Figure 5.6b illustrates the direction of the electroosmotic flow in these COMSOL simulations. Although the electroosmotic flow velocity can be increased by increasing the electric field, it is necessary to reduce the voltage in the microfluidic chip to avoid the detrimental effects of higher current, which may induce electrolysis and cause bubbles to form.

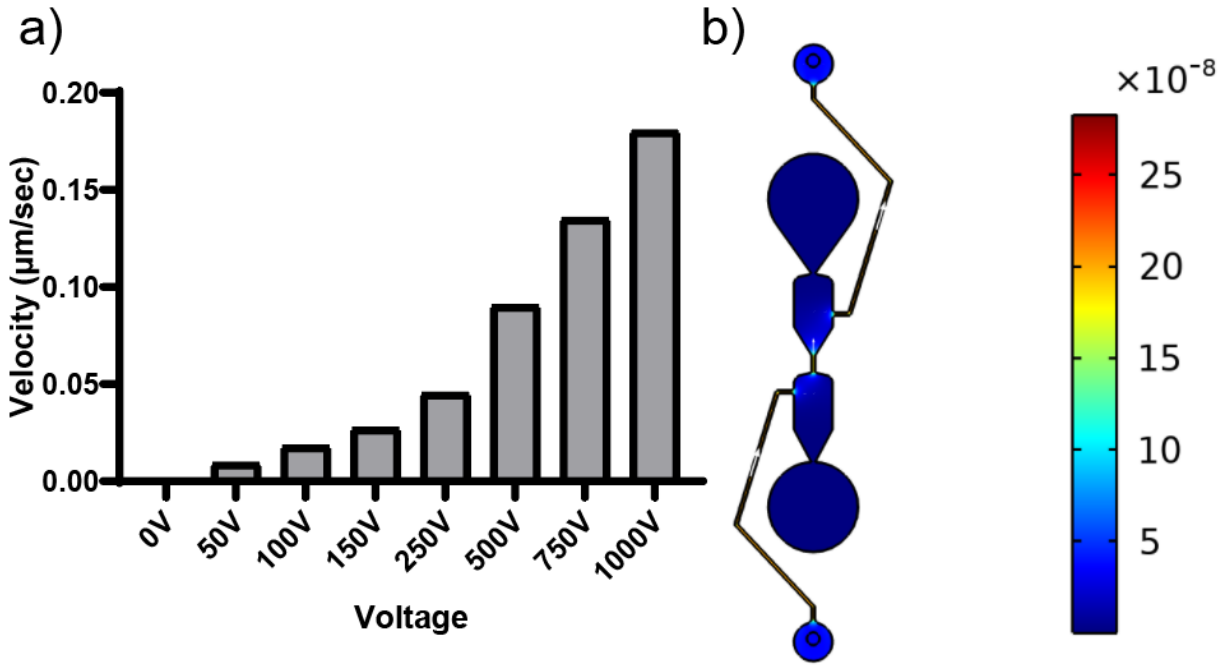

Figure 5.6: Numerical solutions of (a) electroosmotic flow velocity in field focusing channel of microfluidic chip at different voltages, and (b) velocity magnitude (m s-1) surface plot and current density arrows for electroosmotic flow.

5.4.5 E. coli library preparation and sequencing

Following the MSEP analysis using pseudo-library and pseudo-adapter-dimers, 100 ng of ultrasonically fragmented E. coli genomic DNA was prepared for Illumina whole genome sequencing using the NEXTFLEX Rapid DNA-Seq kit (Bioo Scientific, Austin, TX, USA), following the manufacturer's instructions except for magnetic bead purification. Two separate purification steps occur in the protocol: a post-ligation cleanup to remove adapter-dimers and a post-PCR amplification cleanup to remove residual primers. Four conditions were tested: 'Both' in which MSEP was employed for both cleanups; 'Lig' in which only the post-ligation cleanup was performed using MSEP; 'PCR' in which only the post-PCR cleanup was performed using MSEP, and 'None' in which MSEP was not used for either cleanup and purification was done manually using repeated washing and pipette mixing as in Fig. 5.1a. All other library preparation conditions were held identical across the four test cases. Libraries were assessed using the Agilent Bioanalyzer for quality control and sequenced on an Illumina MiSeq using 1x150 reads to a depth of 10x coverage.

The test conditions 'None' and 'PCR' produced libraries of similar yield and size distribution, resulting in an average library concentration of 15.5 ng/μL and an average fragment size of 571 bp (Fig. 5.7a). Meanwhile, 'Lig' and 'Both' libraries were more concentrated and larger in size, with an average library concentration of 26.4 ng/μL and an average fragment size of 631 bp (Fig. 5.7b). This discrepancy may be due to the manual post-ligation cleanup consisting of two consecutive SPRI purifications as opposed to only one purification which is done using MSEP. It is hypothesized that the manual cleanup may be less size-selective (i.e., allowing a greater proportion of smaller DNAs to bind to the magnetic beads), thus resulting in a smaller size distribution. Conversely, it is hypothesized when MSEP was employed for post-ligation purification only one, more size selective SPRI cleanup was used, thus shifting the library distribution toward larger DNAs. Further testing would need to be performed to evaluate the size selection capabilities of the MSEP platform more.

After sequencing, the percent of reads trimmed due to adapter-dimers was calculated (Fig. 5.7c). While all four purification cases exhibited low (< 1%) trim percentages, libraries with manually performed post-ligation cleanups had lower adapter-dimer content. This did not affect other QC metrics such as mapping quality, percent of genome covered, or GC% distribution, as no statistically significant differences were observed between samples purified with MSEP vs. manually. These specific metrics are provided in Table 5.1 and Figure 5.7d. The consistency between these results across sample groups indicates that the sequencing quality was not affected by the purification method used. This provides evidence that the MSEP method is able to purify the genomic library to the same standard for sequencing as conventional, manual purification. Lastly, given the larger library yield produced by MSEP samples, the adapter-dimer content could potentially be reduced by using a smaller volume of Ampure XP bead mix to further size select (bp) the captured DNA without detrimentally sacrificing library yield.

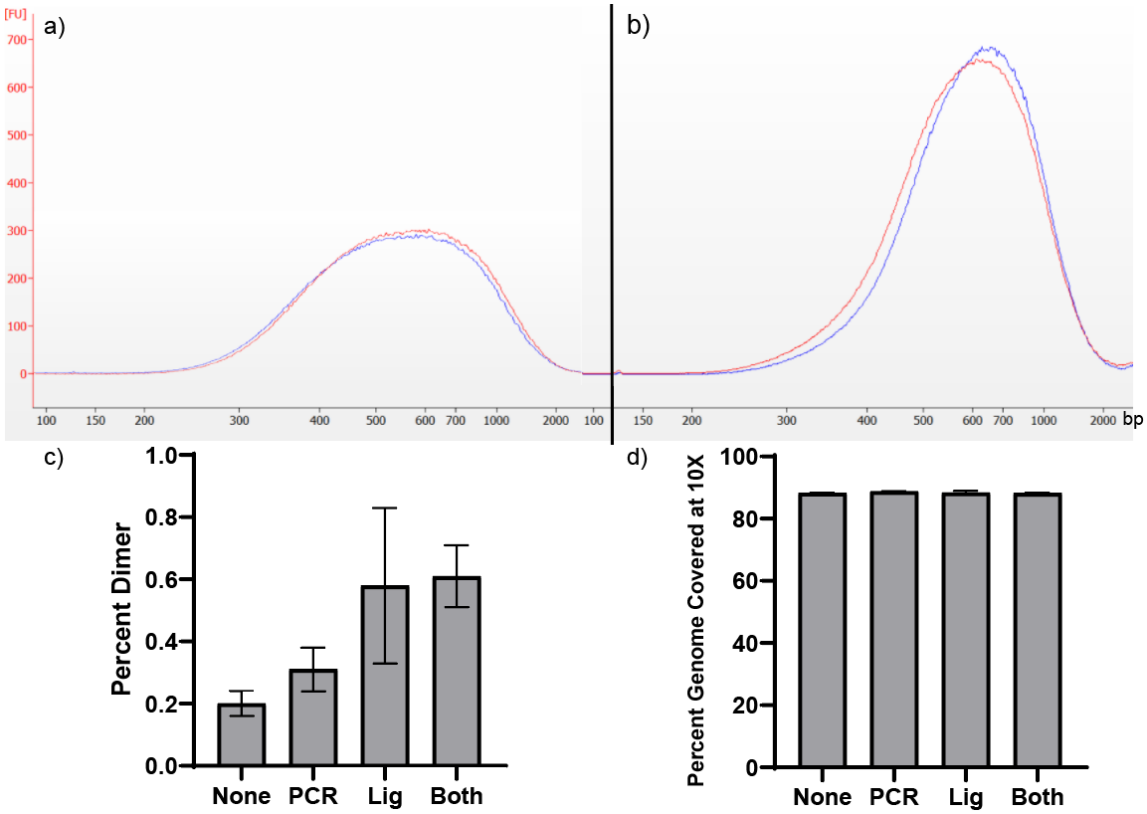

Figure 5.7: E. coli library preparation and sequencing results, plotting relative fluorescence vs DNA length. Electropherograms of (a) 'None' (red) and 'PCR' (blue) libraries; and (b) 'Both' (red) and 'Lig' (blue) libraries. Small adapter-dimer peaks located at 120 bp. (c) Adapter-dimer filter percent for all four samples; (d) Percent Genome Covered at 10X during sequencing.

Table 5.1: Sequencing Data Mapping Statistics. 'None' indicates manual cleanups were used for post-ligation and post-PCR purifications, 'PCR' indicates only the post-PCR cleanup was performed using MSEP, 'Lig' indicates only the post-ligation cleanup was done using MSEP, and 'Both' indicates MSEP was used for both post-ligation and post-PCR purifications.

Sample	Mean Coverage	Coverage Std	GC percentage	Mapping quality mean
1 – None	15.4627	5.0746	50.84	40.3576
2 – None	15.4614	5.0862	50.87	40.3736
3 – None	15.5143	5.0747	50.83	40.3789
4 – PCR	15.5998	5.1066	50.85	40.3698
5 – PCR	15.6411	5.1214	50.87	40.3738
6 – PCR	15.6127	5.0761	50.85	40.3788
7 – Lig	15.3398	5.0556	50.79	40.3574
8 – Lig	15.7163	5.1242	50.80	40.3346
9 – Lig	15.6359	5.1008	50.79	40.3785
10 – Both	15.4085	5.0445	50.84	40.3776
11 – Both	15.4067	5.0673	50.79	40.3822
12 – Both	15.6173	5.1096	50.91	40.3506

5.5 Discussion

The main advantage of using MSEP over manual washing is its time-saving capability. The manual SPRI procedure performed during the E. coli library preparation required approximately thirty minutes total to complete. On the other hand, the equivalent purification using MSEP requires only eleven minutes, representing a two thirds reduction in time, as well as decreasing the number of pipetting actions from fourteen to five. Reducing the number of steps requiring manual intervention will eventually lead to less human error and fewer wasted samples. This is achieved here by eliminating liquid handling steps. The permanent magnet motion, which circumvents the need to pipette by simply translocating the magnetic beads from one well to another, is automated and thus completely hands-off. Device setup is also simple,

as electrodes are the only connection needed to be made; no pressure lines or external pumps need to be connected.

Another potential benefit of this method is the possibility to achieve higher purity than with conventional washing for certain applications. The method described in this manuscript was tailored for SPRI purification; this particular chemistry relies on high salt and PEG concentrations to precipitate and capture DNA; therefore, the magnetic beads must be washed with alcohol solution to prevent the DNA from hydrating and resuspending. As mentioned previously, this decreases the effective charge of not only the DNA bound to the magnetic beads but the non-binding DNA contaminants as well. As a result, the electrophoretic mobility of these non-binding contaminants is low, and they must be swept away by EOF to achieve separation from the magnetic beads. If however the binding chemistry is different and the separation buffer is aqueous, the electrophoretic mobility can be significant—DNA, for example, has a free solution mobility of 3.75×10^{-4} to 4.5×10^{-4} $cm^2V^{-1}s^{-1}$ [156]. This could prove useful for applications such as exome and mRNA enrichment, which require sequence-specific hybridization followed by a magnetic bead pull-down. Another important consideration for the current design is that as the separation buffer and resuspension buffer are both loaded on the microfluidic chip at the same time, there is a potential for the two reagents to mix due to the solubility of the alcohol-based separation buffer in the water-based resuspension buffer. This mixing has the potential to inhibit PCR or other enzyme-involved reactions. Previously, it has been found that PCR is still 89% efficient even when 10% of the starting sample volume is isopropanol, which was the base of the separation buffer used in these experiments[157]. Additionally, when an alternative, alcohol-based wash buffer was added to qPCR samples, there was no statistically significant difference in the C_t values from the qPCR reactions when 20% of the reaction volume was the alcohol-based wash buffer vs. 0%[158]. Due to these previous examples, it is hypothesized that the separation buffer had a minimal effect on the enzymatic reactions following MSEP, but it is something to consider moving forward.

Additionally, when considering the potential for the MSEP platform more, it is hypothesized that an electrophoretically dominated transport, in which $|\mu_{EP}| > |\mu_{EOF}|$, would theoretically provide superior

depletion of charged contaminants from the surfaces of magnetic beads compared to hydrodynamic methods such as EOF or pressure-driven flow in this microfluidic chip. In the latter, the no-slip boundary condition at the solid-liquid interface prevents contaminants directly adjacent to the surface of a magnetic bead from advecting with respect to the magnetic bead. The Coulomb force, however, is not subject to the no-slip condition; thus, electrophoretic separation would likely succeed in effectively removing charged contaminants not only from the bulk of the flow but from the particle surfaces as well. To utilize this method of separation in this microfluidic chip the EOF must be reduced. This may be done by high ionic strength, low pH, and the addition of nonionic surfactants[159,160] or polyvinylpyrrolidone[161] as dynamic coatings. EOF may even be reversed through the surface coating of cationic surfactants such as CTAB[162], which would result in constructive rather than destructive interaction between EOF and electrophoresis. Alternatively, the cathodic EOF may be strengthened though the addition of SDS[155] or treatment with sodium hydroxide[163].

5.6 Conclusion

This research has introduced a novel magnetic bead-based purification method utilizing the translocation of analyte-adsorbed magnetic beads from a contaminated well to a well containing purified buffer. The passage of magnetic beads occurs through a microfluidic channel that connects the sample well and the resuspension well, in addition to two other wells in which electrodes are inserted and a voltage is applied. This results in an electroosmotic flow that washes the magnetic beads as they traverse the length of the channel, which effects the separation of the magnetic beads from any non-adsorbed but hydrodynamically interacting contaminants by advecting those contaminants in the opposite direction of the magnetic bead velocity. Fluorescent imaging qualitatively confirmed a cathodic EOF and electromigration of DNA, while qPCR analysis demonstrated the device's efficacy in removing small DNAs. This method benefits from automated magnetic bead transport, requiring fewer steps and much less time to complete. Though only NGS library preparation was performed, it is believed that this method could be adapted for any bead-based separation scheme, such as sequence-specific hybridization, micro solid phase extraction, and immunoprecipitation.

5.7 Acknowledgements

The authors wish to thank John Murphy for his help in assembling the linear magnetic stage. The authors would like to acknowledge financial support from Brown University and PerkinElmer.

5.8 Supplemental Information

5.8.1 MSEP device uniformity

Magnetic Separation and Electrokinetic Purification (MSEP) is performed on an 80 x 60 mm PDMS-glass microfluidic chip consisting of 16 identical separators, making it capable of purifying 16 individual samples (Supplemental Figure 5.1a). The separators and their constituent wells are spaced 9 mm apart to allow for loading and aspiration with a multichannel pipette. To ensure uniformity and desired shape, the wells of the device were formed by curing the PDMS in a sandwich mold composed of an SU-8 master mold to form the microfluidic features and a machined aluminum mold to form the outline and wells of the device (Supplemental Figure 5.1b). The two molds are aligned and held together with spring clamps, then rotated 90 degrees to stand upright. Uncured PDMS is then poured into the top opening. Once cured, the PDMS is released from both molds and the thin film of PDMS formed by the narrow gap between the well negatives and the SU-8 is punched out. The result shown in Supplemental Figure 5.1c is highly consistent wells with exact placement and sides that are square with the bonded glass (bar a one-degree draft angle to facilitate the mold release). This method circumvents deformation issues associated with conventional PDMS hole-punching (Supplemental Figure 5.1c) and is necessary when a precise liquid column height is needed to prevent unwanted hydrostatic pressure disparities between wells.

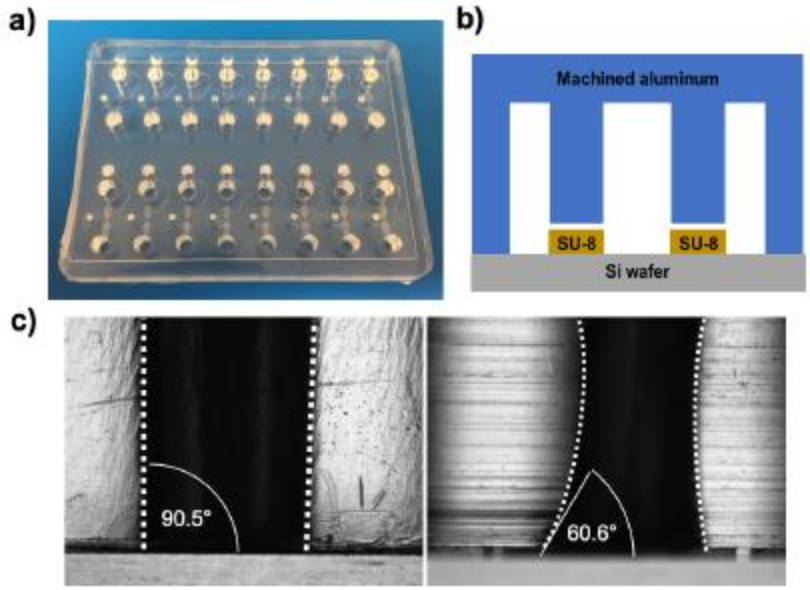

Figure SI 5.1: Fabrication of MSEP device. (a) Image of the device, which consists of 16 sets of highly uniform, precisely spaced wells. (b) Schematic of the soft-lithography process. A sandwich mold was created by mating a machined aluminum mold with the SU-8 master. Uncured PDMS was then poured into the cavity. (c) Wells generated by the sandwich mold (left) compared with those created by post-cure with an equivalent diameter punch (right).

CHAPTER 6

Integrated magneto-electrophoresis microfluidic chip purification on library preparation device for preimplantation genetic testing for aneuploidy detection

---

Chapter 6 has been published as an original research article.

Schneider, L., Fraser, M., Tripathi, A., *Integrated Magneto-Electrophoresis Microfluidic Chip Purification on Library Preparation Device for Preimplantation Genetic Testing for Aneuploidy Detection*, **RSC Advances**, 11, 14459-14474, 2021.

6.1 Abstract

Next generation sequencing (NGS) technology has revolutionized the field of personalized medicine through providing patient specific diagnostic information on a nucleic acid level. A key bottleneck in the NGS workflow is the preparation of nucleic acids for sequencing, or library preparation. One approach to overcoming this bottleneck on time and resources is through automating library preparation as much as possible from the stage of DNA extraction to a sequence-ready sample. Here, we have integrated microscale purification and macroscale PCR amplification to create an automated platform to replace manual DNA library preparation and magnetic bead-based cleanup steps. This microfluidic chip integrates magnetic bead transport and electrokinetic flow to remove unbound adapter dimers and other impurities from samples. We incorporate this method to develop an automated NGS DNA library preparation device that also includes macro- and microfluidic reagent movement and mixing and a thermoelectric cooler for controlled capillary heating and cooling. We greatly reduce the hands-on time, amount of pipetting required, and volumes of reagents needed as we test the feasibility of the platform on the clinically important diagnostic field of preimplantation genetic testing for aneuploidy (PGT-A). We prepared euploid and aneuploid five cell samples for sequencing and found our results were accurate for the cell samples with a sequencing quality equivalent to the standard of the DNA libraries prepared manually. Our device platform utilizes concepts such as: magneto-electrophoresis, integrated capillary PCR, and automated sample loading and unloading onto a microfluidic chip.

6.2 Introduction

Next generation sequencing (NGS) has contributed significantly to the field of personalized medicine since DNA sequencing can be used to answer questions about an individual's genetic makeup[164]. NGS is used routinely in cancer diagnostics[165], infectious disease detection[166], in vitro fertilization embryo testing[167], and more[164]. As NGS technologies continue to advance, there remains a consistent need for improvements in DNA library preparation workflows, meaning when the DNA is prepared for sequencing. Manual library preparation is often impacted by variations between samples since the protocol requires precise and accurate reagent handling and time management[55,137]. One strategy to combat this limitation is to automate the DNA library preparation where all biomolecular and chemical processes can be performed without any variability caused by user interactions (i.e. manual pipetting). This automation can provide more consistency between results by reducing the risk of cross-contamination of materials, pipetting errors, and other mistakes caused by manual reagent handling[168]. Automated library preparation can be performed by high throughput methods using robotic liquid handling machines such as the Sciclone G3 NGSx instrument[169] (PerkinElmer, Hopkinton, MA, USA) or NGS DreamPrep (Tecan Trading AG, Switzerland) as well as lower throughput technologies that utilize microfluidics[170,171], or other semi-automated techniques. Microfluidic based automated approaches are notably beneficial because they reduce analysis time, reagent consumption, and costs, while also increasing accuracy. Larger scale robotics and laboratory equipment may be less exact due to reagent volume constraints compared to what is achievable on a microfluidic scale device[172]. Current microfluidic devices for DNA library preparation for NGS incorporate droplet-based digital microfluidics with microfluidic mixing[170,171], automated multi-column chromatography[173], and more.

One key step that has limited previous automated microfluidic devices for NGS library preparation is DNA purification using solid-phase reversible immobilization (SPRI) magnetic beads. SPRI magnetic beads used for DNA purification are suspended in a buffer with high poly(ethylene glycol) (PEG) and salt concentrations that encourages DNA to bind to the surface of the carboxyl-coated magnetic beads[21]. The DNA coated beads are collected using a magnet followed by wash steps before the DNA is eluted from the beads in a resuspension buffer, creating a highly purified DNA suspension[21]. Wash steps are performed

using chaotropic compounds, such as ethanol, because nucleic acids precipitate in the presence of alcohols and will not desorb from the magnetic beads until the alcohol is removed and the beads are rehydrated[107]. The conventional SPRI protocol involves many pipetting steps that can negatively affect the bead mix if not performed precisely. The device described herein thus incorporates a unique microfluidic chip for DNA purification to reduce the pipette handling of the SPRI beads by the automated system. The motivation for using a microfluidic chip was to limit potential errors that could occur from unintentionally discarding liquid via multiple pipetting steps or vigorously mixing the SPRI beads. Furthermore, manual DNA library preparation is a time consuming and laborious process that has become one of the major bottlenecks for advancing NGS. An automated platform for DNA library preparation can significantly improve the workflow by precise liquid handling and time management to prevent human errors or sample variations. The proposed platform has the potential to offer NGS for smaller-scale laboratory studies, eventually replacing high throughput liquid handling robots without compromising the quality of the sequencing library.

Microfluidic chips have been used for successful molecular purification previously by incorporating interfaces such as oil[10] to aid in purification efficacy. To limit the number of additional reagents needed for this device, the microfluidic chip was designed to incorporate electrodes that could create an applied electric field within the chip. This chip is therefore able to combine the concepts of magnetophoresis and electrophoresis which we refer to as magneto-electrophoresis. Magnetophoresis is used to move the magnetic SPRI beads through a viscous medium using an external magnetic field[174] and electrophoresis is used to move the DNA not adsorbed to the SPRI beads away from the purified sample and thus improve the DNA purification process. There are indeed several studies (shown in Table 6.1) performed on DNA purification by selectively binding DNA onto magnetic beads and transporting them to a purified buffer on a microfluidic device. The techniques come under the purview of magnetophoresis. A majority of these studies pertain to the magnetic beads' motion under synergetic action of magnetic and pressure-driven flow fields. Here, no-slip boundary conditions ($\vec{v} \cdot \hat{n} = 0$) on the bead surface allows for unbound molecules near the beads to carry over with the beads. Hence, the magnetophoresis is often diffusion-limited as the

unbound molecules near the bead surface have to diffuse out into the large velocity field. In contrast, our innovation overcomes this limitation and utilizes magnetic bead transport through an electric field. Here, the unbound molecules, outside a very thin Debye length around the beads, experience a velocity ($\vec{v} = -\varepsilon\zeta\vec{E}/\eta$) proportional to the electric field. Hence, magneto-electrophoresis efficiently removes unbound molecules from the bead cluster. Through incorporating a microfluidic chip for the DNA purification into the automated device design, SPRI beads can still be used for the purification without the need for multiple wash buffer exchanges and potential pipetting errors. Capillary electrophoresis, such as in this design, has been used for nucleic acid sizing, genotyping, and DNA sequencing analysis[175]. DNA purification using microfluidics has also been done previously[176,177], but, as seen in Table 6.1, incorporating magnetophoresis with electrophoresis to assist in purification with SPRI beads has not been explored in this manner until now.

Table 6.1: Select microfluidic platforms used for separating and purifying nucleic acids.

Study	Mechanism of Separation	Application	Use of Electric Field to enhance separation
Our method	Electrophoresis and magnetophoresis where beads are moved through stationary fluid	DNA purification during NGS library preparation	Yes
Xu et al.[178]	Magnetophoresis and fluid flow	Nucleic acid purification from PCR mixture	No
Tan et al.[173]	Column chromatography with fluid flow in a "purification circuit"	DNA purification during NGS library preparation	No
Hale et al.[179]	Magnetophoresis and continuous fluid flow	DNA separation from blood	No
Azimi et al.[139]	Magnetic micromixer with buffer exchanges	DNA extraction from whole blood	No
Kim et al.[171]	Digital microfluidics with magnetic bead capture and buffer exchanges	DNA purification during NGS library preparation	No
Karle[180]	Magnetophoresis and fluid flow	DNA extraction from cell lysate	No
Vojtíšek[181]	Magnetophoresis where beads are moved through continuous fluid flow	DNA hybridization and isolation	No
Deraney et al.[182]	Magnetophoresis and electroosmotic flow	Nucleic acid extraction and purification from plasma	Yes

The scientific and technological rigor of this new device was tested for use in the diagnostic field of preimplantation genetic testing for aneuploidy (PGT-A). One in six couples of reproductive age are affected by infertility, thus in vitro fertilization (IVF) is an essential tool used to increase a couple's chances of a successful pregnancy[183]. PGT-A can be performed during IVF and involves performing an embryo biopsy of one to ten cells – known as a trophectoderm (TE) biopsy – followed by genetic analysis testing for Mendelian, chromosomal, and mitochondrial abnormalities[184,185]. PGT-A specifically determines when there are an abnormal number of chromosomes or sub-chromosomal deletions or duplications in the embryo[55]. NGS can be used to perform 24-chromosome aneuploidy screening and offers complete low pass genomic coverage, rapid results, the ability to detect more subtle abnormalities, and has a reasonably low cost per base[55,186]. During NGS the genomic sample that is removed from the TE biopsy is first amplified

using Whole Genome Amplification (WGA) before moving into the DNA library preparation workflow. PGT-A was chosen as the application for the development of this system because it is highly sensitive to the sample preparation workflow, outlined in Figure 6.1a and 6.1b, and will clearly indicate whether the system is performing optimally or not.

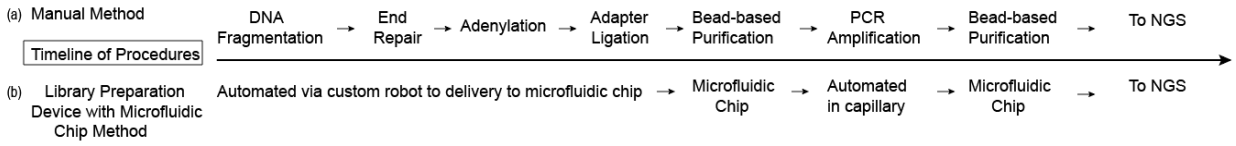

Figure 6.1: Protocol outlines for Manual and Library Preparation Device with Microfluidic Chip methods.

One major scientific innovation contributing to the success of this automated device is the microfluidic chip used for DNA purification during library preparation. This microfluidic chip is designed with two wells – one containing the SPRI beads with DNA adsorbed to them and the other a resuspension buffer – connected by a channel to move the sample through using automated magnet motion. Simultaneous magnetophoresis and electrophoresis are used to move the beads from one well to the next while also applying an electric field to the connecting channel to induce electrokinetically-driven migration of non-adsorbed DNA in the opposing direction of the magnetic bead transfer. The combination of these phenomenon results in the automated purification of the DNA library using magneto-electrophoresis. This automatic workflow has been coupled with automatic macro-and microfluidic reagent movement and mixing as well as a thermoelectric cooler for controlled capillary heating and cooling. Through scaling down the reagents used on this device and automating the library preparation process, this device can prepare DNA for sequencing while saving both time and money. Notably, the 2.5-hour library preparation process is reduced to less than 10 minutes of hands-on time from the start of the procedure and only ~1/3 by volume of the reagents are used compared to the manufacturer's instructions. We successfully apply the novel microfluidic chip workflow towards the purification procedures during NGS library preparation on the automated device and demonstrate its efficacy through both library preparation and sequencing for PGT-A.

6.3 Materials and Methods

6.3.1 Microfluidic chip fabrication

The microfluidic chip used during the DNA purification process was made from polydimethylsiloxane (PDMS). A Sylgard 184 elastomer base and curing agent were mixed in a 10:1 ratio for one min, then placed in a vacuum chamber for 40 min to dissolve any air bubbles in the mixture. A 2-part sandwich mold was used to make the microfluidic chip with one part made from SU-8 and the other made from aluminum. The SU-8 master mold contains the microfluidic design, and the aluminum mold contains a peg formation that mirrors the circular well design on the SU-8 mold. The 2-part sandwich mold helps to create more uniform wells for sample loading during testing compared to punching a hole through the PDMS to create a well after it solidifies. Following the vacuum chamber, the SU-8 and aluminum molds were clamped together with an opening where the PDMS could fill the molds. The fixture was then placed in a 70°C oven for 1.5 hours to allow the PDMS to solidify. Next, the two parts of the sandwich mold were taken apart and the PDMS was removed from the aluminum mold. Four reagent wells per DNA purification separator were formed during the PDMS curing process (Figure 6.2) and a hole punch was used to ensure all PDMS was cleared from the wells. The internal diameters of the hole punches used were 0.75 mm for the Negative Electrode Well, 1.2 mm for the Positive Electrode Well, and 3.5 mm for the Sample Input and Elution Wells. The PDMS and a 1 mm thick glass slide were then cleaned with isopropanol, dried with nitrogen gas, then treated with a plasma wand at high radiofrequency to irreversibly bond the two pieces together. The microfluidic chip was then returned to the 70°C oven for 30 minutes, then kept at room temperature for at least 24 hours before use to ensure uniform chip-to-chip zeta potential.

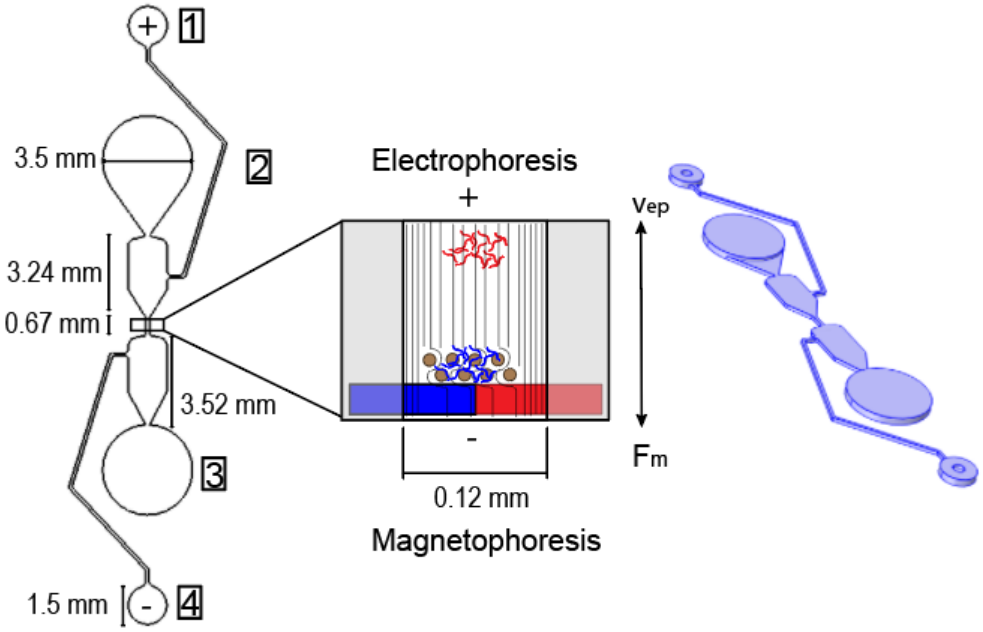

Figure 6.2: Microfluidic chip for DNA purification using magneto-electrophoresis design and dimensions 2D and 3D perspectives. Electrophoresis and magnetophoresis opposing forces are shown where the DNA library, in blue, is adsorbed to the Purification Beads moving toward the Elution Well through a stationary Separation Buffer using magnetophoresis, while the unwanted DNA primer and adapter dimers, in red, are moving toward the Sample Input Well via electrophoresis. Electric field lines are also pictured through the center channel and moving through the Purification Beads. Wells of the microfluidic chip are identified as: (1) Positive Electrode Well, (2) Sample Input Well, (3) Elution Well, (4) Negative Electrode Well.

6.3.2 Electrokinetic microfluidic chip modeling and measurements

Analysis of the reactions that take place during DNA library preparation was first performed to provide a breakdown of the chemical and molecular processes in the protocol and provide motivation for why DNA purification is performed and why electrophoresis aids in this purification. The microfluidic chip was designed to utilize electrophoretic mobility to attract any unwanted free DNA (i.e. primer dimers and adapter dimers) to a positive electrode, taking advantage of DNA's negative charge. This was used to enhance the DNA purification as the Positive Electrode Well was positioned nearest the Sample Input Well and away from the Elution Well. This electrophoretic mobility would oppose the magnetophoresis movement of the Purification (SPRI) Beads which are transferred from the Sample Input Well to Elution Well during DNA purification. These opposing forces are visualized in Figure 6.2 where the DNA library, shown in blue, is mixed with the Purification Beads and moved toward the Elution Well using magnetophoresis, while the unwanted DNA dimers, shown in red, move toward the Sample Input Well via

electrophoresis. Computational analysis was next performed to evaluate the electrokinetic phenomenon occurring in the microfluidic chip when the steady electric field was applied, including electrophoresis and electroosmosis. Analyzing these electrokinetic phenomena was important for the design of the Separation Buffer that filled the microfluidic chip to ensure it was conducive to electrophoresis as a purification method and not electroosmosis as the two electrokinetic phenomena opposed each other in this application. Additionally, COMSOL Multiphysics Modeling Software 5.4 was used to interpret the effect of the Electric Potential differential and electrophoresis within the microfluidic channel. A 2D CAD drawing of the microfluidic chip for one separator was imported into COMSOL and an oblate spheroid shape was added to the center channel to represent the SPRI bead cluster movement during purification. Next, Electric Currents and Transport of Diluted Species Physics were modeled to provide the Electric Potential and Concentration within the microfluidic chip in a Stationary Study. This study showed the dispersion of the electric field and the concentration gradient of the diluted DNA in the channel. Additionally, Laminar Flow Physics was incorporated into the COMSOL Stationary Study to investigate the effect the microfluidic chip wall conditions have on the electroosmotic flow in the channel. Furthermore, experimental testing was performed to quantitatively characterize the on-chip purification. DNA amplicons of 485 base pairs (bp) and 123-bp were used to represent the average DNA library and adapter dimer sizes (bp), respectively, to study the microfluidic chip purification for this application. A DNA amplicon mixture of 200 ng or 100 ng of both DNA sizes (bp) were tested using on-chip and off-chip (following Purification Bead manufacturer instructions) purification procedures to better compare the microfluidic chip purification to existing methods.

6.3.3 Device fabrication and system operation

This automated NGS library preparation device (Figure 6.3) consists of an x-stage for left-right motion and a z-stage for up-down motion. The stages are both linear screw-drive stages (IGUS, East Providence, RI, USA) with a stepper motor controlled by a script in the Si Programmer application (Applied Motion Products, Watsonville, CA, USA). The x-stage houses the microfluidic chip for DNA purification and the reagent plate containing all PG-Seq kit library preparation reagents (PerkinElmer Health Sciences

(Australia), Thebarton, SA, Australia) and additional reagents used for wash steps. The z-stage holds two cannulas that move together, perpendicular to x-stage motion. These metal cannulas have an airtight connection to PTFE (Teflon) tubing (inner diameter 1.02 mm) (Small Parts, Inc., Logansport, IN, USA) which is then connected to flexible polyethylene tubing (inner diameter 0.79 mm) held by electronic pinch valves (NPV Series, Clippard Instrument Laboratory Inc., White Oak, OH, USA). These pinch valves are used to select for one of two cannulas by pinching the undesired cannula to prevent air and liquid movement in that tubing. The tubing in the pinch valves has another airtight connection to more flexible polyethylene tubing (inner diameter 1.59 mm) which is held in the thermoelectric cooler device. This tubing ultimately attaches to a 500 μL Hamilton Gastight Syringe (Reno, NV, USA) which is controlled by a syringe pump (PHD 2000 Programmable, Harvard Apparatus, Holliston, MA, USA) for all liquid handling. The thermoelectric cooler (12711-5P31-15CQ Thermoelectric/Peltier Module, Custom Thermoelectric, Bishopville, MD, USA) used in this device is attached to a copper plate that has been milled to provide spaces for the flexible polyethylene tubing to fit. Around one-third of the tubing directly contacts the copper surface and is held in place by an insulated door that is screwed on to make a tight fit so that heat can be transferred efficiently between the thermoelectric cooler and copper plate to the reagents within the tubing. A LabVIEW VI was used to control the thermoelectric cooler based on real time feedback from a thermocouple (National Instruments, Austin, TX, USA) positioned in flexible polyethylene tubing filled with mineral oil adjacent to where the reagents are loaded. A neodymium bar magnet (K&J Magnetics, Pipersville, PA, USA) is used in conjunction with the microfluidic chip for SPRI bead movement during DNA purification and is mounted to and controlled by a small hobby servo motor which flips the magnet up and down as designated in the script. The x-stage moves in respect to the magnet to transfer Purification Beads through the microfluidic chip for DNA purification, details of this movement are explained in Figure 6.4. The overall device platform is controlled by script-based preprogrammed sequences or manual keystrokes through a master Python script loaded onto a Raspberry Pi with hand-shaking to the Harvard Apparatus syringe pump and Si Programmer (Applied Motion Products, Watsonville, CA, USA) scripts used to control the x- and z-stages. Analysis of the heating and cooling of the thermoelectric cooler during

capillary PCR and mixing on the reagent plate are major features of the device that were also analyzed by COMSOL Multiphysics Modeling Software 5.4 simulations and testing in this study. Dimensional analysis of the device was also performed to ensure the reagent volumes would be conducive to the device platform and the reagent plate was set up to avoid any cross contamination between reagents and this analysis is expanded upon in the Supplementary Material.

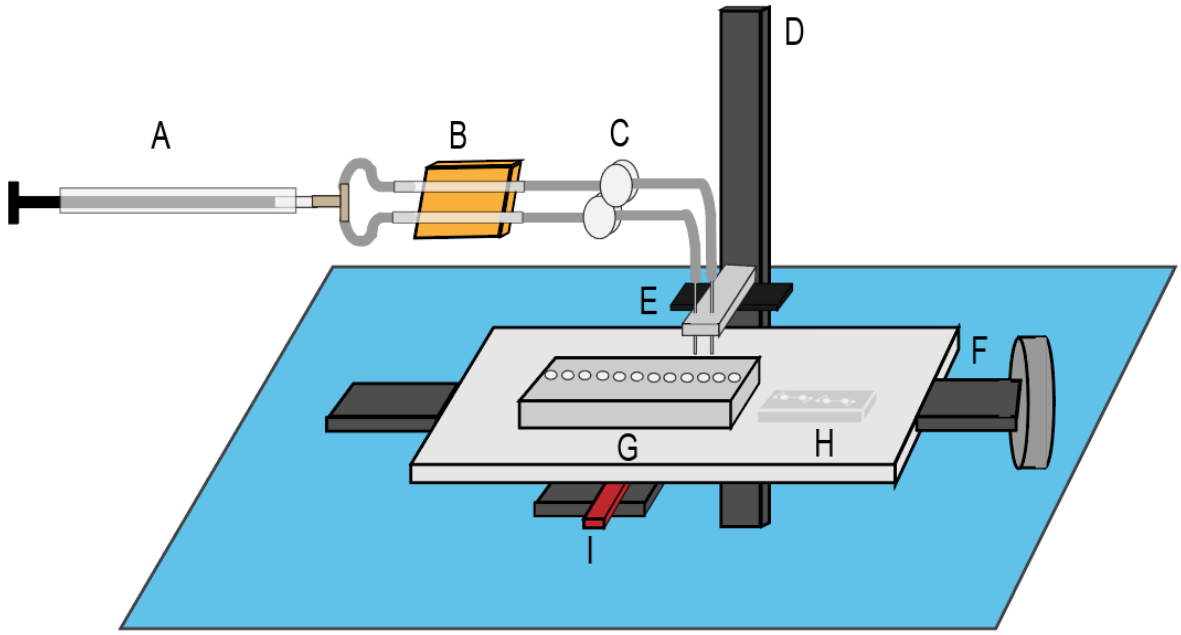

Figure 6.3: Device Fabrication Schematic: (A) Syringe pump, (B) Thermoelectric cooler, (C) Pinch valves to control Cannulas (D) Z-stage, (E) Cannula 1 and Cannula 2, (F) X-Stage. (G) Reagent plate, (H) Microfluidic chip for DNA purification, (I) Magnet for DNA purification.

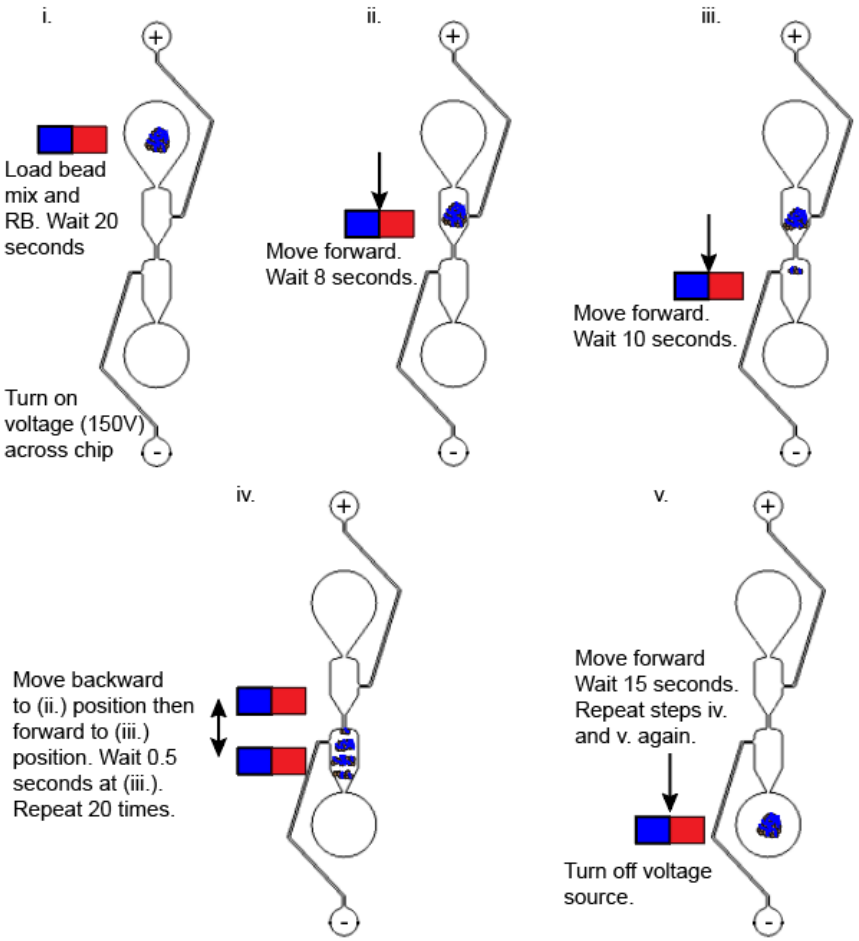

Figure 6.4: Schematic of the magnet movement used to move the Purification Beads with adsorbed DNA library (shown in blue) from the Sample Input Well to Elution Well during DNA purification steps.

6.3.4 Application of DNA samples for next generation sequencing library preparation

The NGS library preparation was performed using the PG-Seq kit 2.0 workflow (PerkinElmer Health Sciences (Australia), Thebarton, SA, Australia) which involves: combined fragmentation, end repair, and adenylation; barcoded adapter ligation; PCR amplification; and two Purification Bead cleanup steps, using SPRI beads, following the barcoded adapter ligation and PCR amplification steps (Figure 6.1). Initial assay testing of the microfluidic chip and device platform was performed using Lambda DNA (New England Biolabs, Ipswich, MA, USA) for library preparation. The DNA library preparation quantity and quality were evaluated by analyzing the DNA library concentration (ng/μL), yield (ng/μL), average size (bp) of the DNA library, and library purity (A_{260}/A_{280} ratio). This was done by running one microliter of DNA library sample on the Agilent Bioanalyzer 2100 machine with the Agilent DNA 1000 Kit and DNA Chip for On-

Chip-Electrophoresis (Agilent Technologies, Santa Clara, CA, USA). In order to have a sequencing-ready DNA sample, at least 4 ng/μL of library is needed in a 20 μL sample and since the library size (bp) is critical for cluster generation on the flow-cell using Illumina technology, an average DNA library size of 400 bp was set as the benchmark[137]. Library purity was improved by reducing the concentration of adapter and PCR primer dimers which are created when excess adapters or PCR primers bind to each other and then participate in the amplification process[187]. This dimerization drastically interferes with downstream DNA sequencing processes[137]. These conditions were compared between sample preparations on-device and manually both using seven PCR cycles, unless otherwise stated. For sequencing testing, two distinct human cell samples were tested: euploid cells (46, XX) from peripheral lymphocyte cells from a healthy female donor of proven fertility (PerkinElmer Health Sciences (Australia), Thebarton SA, Australia) and aneuploid cells (48, XXY, +21) from fibroblast cells (Coriell Institute, Camden, NJ, USA). Each of the cell samples were manually sorted into 5-cell aliquots, representing a TE biopsy, then whole genome amplified (WGA) according to standard PG-Seq kit 2.0 instructions to provide a starting DNA concentration of 40ng/μL for library preparation. The DOPlify procedure includes cell lysis followed by optimized DOP-PCR amplification. The DNA was purified manually using a Purification Bead (SPRI bead) cleanup at a 0.9× bead to DNA volume ratio prior to DNA library preparation. All research was carried out in accordance with Brown University's research guidelines and regulations. Additionally, an MTA (Assurance Form) was signed and approved by Coriell Institute (Camden, NJ, USA) to use the cell lines in this study and all materials were unidentified. Sequencing data was also gathered for samples to determine the accuracy of detecting the expected aneuploid vs euploid cell samples using the MiSeq sequencer (Illumina, San Diego, CA, USA). The sequencing results were read at 1x150 bp and normalized to 500,000 reads per sample. The reads were trimmed to 1x75 bp to match the standard PG-Seq kit 2.0 protocol and sequence analysis was performed using the PG-Find Software (PerkinElmer Health Sciences Australia, Adelaide, SA, Australia).

6.4 Results

6.4.1 Analysis of reaction kinetics for DNA library preparation steps

Along with DNA library purification, the effectiveness of this device ultimately depends on successful reaction kinetics for each process of this workflow. Equations 6.1-6.3 are used to breakdown the three major enzymatic steps in this assay to model the DNA that makes up the final prepared library, assuming 100% reaction efficiency. The first step in the procedure, fragmentation, is represented by Equation 6.1, where the initial genomic DNA (D_g) is enzymatically fragmented into n, number of DNA fragments. Each of these DNA fragments ($D_1,\ D_2, \ldots\ D_{n-1}, D_n$) represent a unique part of the genomic DNA. The number of DNA fragments produced in this reaction is controlled by a fragmentation reaction rate constant, k_f, which is a function of the reaction temperature and buffer conditions including enzyme concentrations, as well as, the initial concentration of the genomic DNA. As specified by the manufacturer, users can adjust the input genomic DNA concentration and the reaction time to produce different fragment sizes (bp) which will be normally distributed around the intended size. By controlling these factors, the number of fragments, n, can therefore be increased or decreased.

The next enzymatic process in the DNA library preparation is the barcoded adapter ligation. As represented by Equation 6.2, this step in the procedure will increase the size (bp) of each DNA fragment (D_n) by adding a barcoded adapter (D_a) to both ends of all fragments. This step does not increase the number of fragments in solution, thus D_L still represents one of n number of DNA fragments which is now ligated to two barcoded adapters. This reaction is controlled by a ligation reaction rate constant, indicated as k_L. This is a function of temperature, buffer conditions, enzyme concentrations, and concentration of barcoded adapters. The final enzymatic step in this procedure is the PCR amplification for the ligated DNA fragments. Equation 6.3 represents the theoretical yield of the number of DNA fragments in the final library (D_F). The exponential increase in the number of each ligated DNA fragment (D_L) during PCR is controlled by the number of PCR cycles (j) performed[188]. Since PCR amplifies each ligated DNA fragment individually, the final number of DNA fragments in the prepared library (D_F) must be multiplied by the number of fragments in the solution, n. This process is controlled by an amplification reaction rate constant (k_A), which is a function of the

temperature cycling, buffer conditions, and enzyme, primer, and nucleotide (dNTP) concentration in the buffer mixture.

One problem that may occur during PCR amplification is primer or adapter dimer formation and amplification, represented as an exponential increase (i) in the number of barcoded adapters (D_a) or PCR primers (D_p) (Figure 6.5a). Dimerization negatively affects the quality of prepared libraries and will disrupt downstream DNA sequencing by interfering with the DNA library binding to the flow cell[137]. Since these dimers are between 70bp - 130bp, it is more kinetically favorable for them to bind to the flow cell first, leaving longer fragments of DNA that contain important genetic information left with no place to bind. This can reduce the amount of reads per sample and reduce the sequence information or coverage, which will reduce the amount of useful data for that sample[137]. But, with effective DNA purification, these adapters can be eliminated from samples and the resulting library (D_F) will be ready for sequencing (Figure 6.5b).

$$D_g \xrightarrow{k_f} D_1 + D_2 + \cdots + D_{n-1} + D_n \qquad (6.1)$$

$$D_n + 2D_a \xrightarrow{k_L} D_L \qquad (6.2)$$

$$[D_L * 2^j] * n \xrightarrow{kA} D_F \qquad (6.3)$$

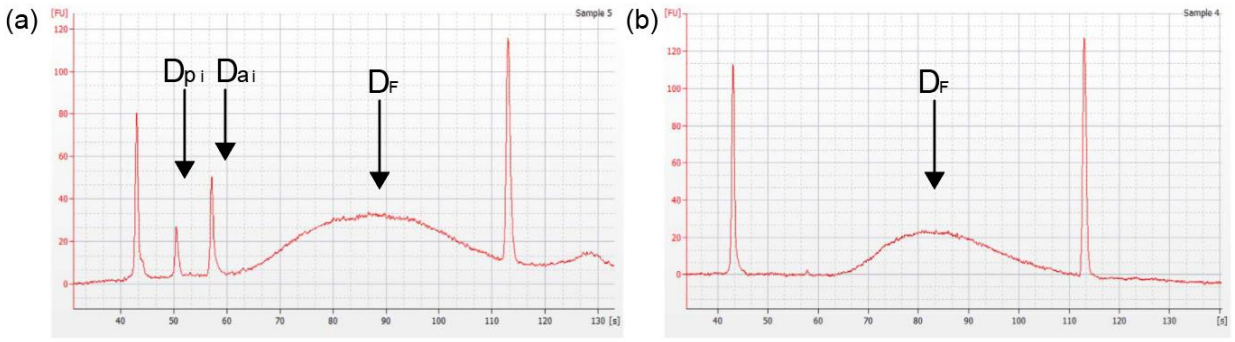

Figure 6.5: Agilent Bioanalyzer 2100 electropherogram analysis of prepared DNA libraries (a) An example of a low quality DNA library due to peaks in electropherogram at ~50 seconds and 57 seconds, corresponding to ~70 bp (D_{pi}, primer dimer) and ~130 bp (D_{ai}, adapter dimer). (**b**) An example of a high-quality DNA library with efficient DNA purification. Note removal of primer dimer (D_{pi}) and adapter dimer (D_{ai}) peaks showing an improvement in prepared DNA library quality.

6.4.2 Electrokinetic microfluidic chip modeling and measurements

The post-ligation and post-amplification DNA purifications were performed on a microfluidic chip to purify the DNA library and remove adapter and primer dimers using magneto-electrophoresis. The microfluidic chip (Figure 6.2) was positioned on the x-stage (Figure 6.3) of the automated library preparation device. When being used, the Separation Buffer was first loaded into the Positive Electrode well, filling the microfluidic chip. Following that, the positive and negative electrodes were placed in the respective wells and the neodymium bar magnet was engaged to be adjacent to the glass slide of the microfluidic chip. Next came the automatic loading of the Purification Bead mix with DNA library adsorbed to it in the Sample Input Well while Resuspension Buffer was loaded into the Elution Well simultaneously. The voltage source of 150V was then applied through the microfluidic chip while the x-stage began to move left to right above the stationary bar magnet, transferring the bead mix through the channel and into the Resuspension Buffer. The magneto-electrophoresis protocol is further illustrated in Figure 6.4 which explains the magnet motion necessary to move the Purification Bead mix from the Sample Input Well to the Elution Well. Once the bead mix was in the Elution Well, the magnet was disengaged to remove the magnetic field while the DNA de-adsorbed from the Purification Beads into the Resuspension Buffer for four minutes, resulting in a purified sample. The magnet was then reengaged to move the Purification Beads out of the Elution Well so that the purified DNA could be automatically removed from the Elution Well without transferring any Purification beads to the next reagents in the protocol.

One important design feature considered for this microfluidic chip was the Separation Buffer which was used to wash the Purification Beads. This buffer filled the microfluidic chip center channels and was designed to (1) contain enough chaotropic compounds so that the DNA remained adsorbed to the beads during the movement through the chip; (2) not evaporate from the channel before the cleanup could be performed; and (3) reduce the electroosmotic flow within the channel. Therefore, isopropanol contributed to the majority of the Separation Buffer as an alcohol with a larger molecular weight compared to ethanol which is conventionally used, so it will evaporate more slowly from the microfluidic chip. The last criteria for the Separation Buffer design was reducing the electroosmotic flow in the chip. Since DNA is negatively

charged, the microfluidic chip was designed to use electrophoresis to increase the cleanup efficiency of adapter and primer dimers. Electrophoresis works by separating samples, such as nucleic acids or proteins, using a high voltage differential based on the motion of the charged surface relative to a stationary liquid[175,189]. The electrophoretic velocity (v_{ep}) in the microfluidic chip (Equation 6.4)[190], is based on the electrophoretic mobility (μ_{ep}) and electric field (E). The solute's charge affects the electrophoretic mobility of the DNA in the buffer (Equation 6.5)[190] and therefore this electrophoretic velocity moves towards the positive electrode, based on the negative charge of DNA, where q is the solute's charge, η is the buffer viscosity, and r is the solute's radius.

Electroosmosis on the other hand is the electrokinetic motion of the ionized liquid in relation to the stationary charged surface by an applied electric field.[189] The electroosmotic flow velocity or the rate at which the buffer moves through the capillary is also a function of the mobility and electric field applied in the system (Equation 6.6)[190]. Conversely, electroosmotic mobility is based on the buffer dielectric constant (ε), zeta potential of the channel wall (ζ), and buffer viscosity (η), as seen in Equation 6.7[190]. The zeta potential is directly proportional to the charge on the capillary walls, which in this case is the negatively charged glass slide[190]. This then attracts positive ions to the negatively charged wall creating an electric double layer that, when a steady electric field is applied, will cause migration of the positive ions toward the negative electrode, which will create a bulk flow of liquid in the same direction[190]. Since the total velocity of the DNA in the applied electric field is controlled by the electrophoretic and electroosmotic velocities (Equation 6.8), it is essential for the Separation Buffer to be designed in a way so that the electroosmotic velocity is decreased enough to make electrophoresis the dominating electrokinetic velocity because these two phenomena work in opposite directions in the microfluidic chip.

$$v_{ep} = \mu_{ep} E \qquad (6.4)$$

$$\mu_{ep} = \frac{q}{6\pi\eta r} \qquad (6.5)$$

$$v_{eof} = \mu_{eof} E \qquad (6.6)$$

$$\mu_{eof} = \frac{\varepsilon\zeta}{4\pi\eta} \qquad (6.7)$$

$$v_{tot} = v_{ep} + v_{eof} \qquad (6.8)$$

Specific buffers added to isopropanol to the reduce the electroosmotic flow included LabChip Sipper Chip Coating Reagent 8 (PerkinElmer, Hopkinton, MA) which is a positively charged additive designed to be added to the separation buffer of an EZ Reader (PerkinElmer, Hopkinton, MA, USA). This reagent binds to silanol groups in glass channels to neutralize the negatively charged glass. TWEEN and PEG were also added into this separation buffer mix because they acted as surfactants to reduce electroosmotic flow velocity by adsorbing to the capillary wall[191,192]. These reagents accounted for ~40% of the total Separation Buffer volume, with isopropanol accounting for the remaining 60% to ensure the DNA would remain precipitated onto the Purification Beads during movement through the microfluidic chip.

COMSOL Multiphysics Modeling Software was utilized to show the direction of the DNA electrophoresis in the microfluidic chip. A 2D Stationary Study of one separator on the microfluidic chip was imported into COMSOL and the Positive Electrode Well was assigned an Electric Potential of 150V (Figure 6.2) to match the experimental testing. The anticipated transport direction of the free DNA (diluted species) not adsorbed to the Purification Beads was towards the Sample Input Well and away from the Elution Well. An Electric Potential of 0V was assigned to the Negative Electrode Well in the device. A DNA size of 130 bp was selected to model the migration of the free DNA because it represents the size of the adapter dimers that will be purified out of solution. The diffusion of the isolated linear DNA molecules was calculated to be 3.21 $\mu m^2/s$ based on an experimentally derived scaling law comparing the diffusion coefficient of linear DNA to the length of the linear DNA molecules[193]. The migration in the electric field is controlled by the electric potential and the Nernst-Einstein relation with a charge number of -260 based on the negative phosphate backbone in the 130-mer DNA. A concentration of 20 ng/μL (in a stepwise function in the y-direction) was assigned to each well to visualize the movement of any diluted species that may be in those wells. This model excludes the effect that the Purification Beads will be having in the channel although an oblate spheroid shape was added to the center of the channel to represent the bead cluster on the chip. Due

to the complexity of the Separation Buffer used to fill the microfluidic chip in these experiments along with the buffers in the Purification Bead mix carrying the DNA library for purification, the simulations were performed with isopropanol as a model material since it makes up ~60% of the Separation Buffer. The Electric Currents and Transport of Diluted Species Physics were modeled, and Figure 6.6 provides the Electric Potential (6a) and Concentration (6b) plots. It is clear the electric potentials are largest in the Electrode Wells and the concentration plot shows the direction that the concentration gradient is moving is towards the positive electrode as anticipated due to the applied electric field.

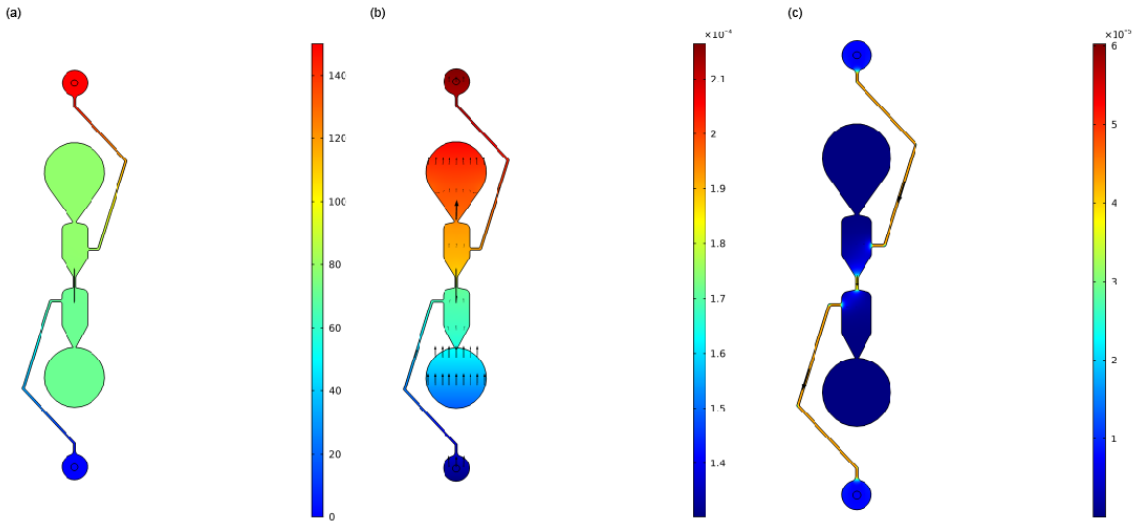

Figure 6.6: Electrophoresis in microfluidic chip analysis using COMSOL Multiphysics Modeling Software Stationary Study: (a) Electric Potential (V) surface plot. (b) Concentration (mol/m3) surface plot with Arrow Surface representing the Concentration Gradient. Concentration gradient is largest at the positive electrode, as expected for the negatively charged DNA being modeled. (**c**) Velocity magnitude (m/s) surface plot with Arrow Surface plot representing the Velocity field under electroosmotic flow conditions. The highest velocity is in the center channel.

COMSOL Modeling was also used to visualize any electroosmotic flow and its effect on the transport of DNA in the channel. Under the Laminar Flow Physics module, different Wall boundary conditions were tested to analyze the effect on the velocity in the center channel caused by the electroosmotic flow. A 'No Slip' Wall condition was first assigned to all channels within the microfluidic device to represent the neutralization of the electric double layer by the Separation Buffer. This simulation shows a velocity of 0 m/s in the channels, meaning that there is no electroosmotic flow under these conditions. Conversely, the

Wall Condition can be set to 'Electroosmotic velocity' based on the electric field induced electroosmotic flow. The mobility for this model is based on a glass zeta potential of -0.1V and a Relative permittivity of isopropanol (17.9). The result of this simulation shows that Velocity Magnitude concentrated in the center channel is $3.84x10^{-5} \pm 1.00\ x10^{-7}$ (m/s) moving in the direction of the negative electrode (Figure 6.6c). When Flow Coupling the Laminar Flow and Transport of Diluted Species Physics though, the negatively charged DNA diluted species still showed a concentration gradient with the largest amount of diluted species (DNA) at the positive electrode, indicating that the electrophoretic mobility was still controlling the free DNA movement.

To further characterize the microfluidic chip, the recovery efficiency of DNA purified on-chip was quantified. DNA amplicons of 485-bp and 123-bp were mixed with either 200 ng or 100 ng of each size to create the input DNA sample for purification. In both on-chip and off-chip testing the DNA was suspended in 36 μL of nuclease free water then combined with 36 μL of Purification Beads for four minutes, as is done on the device. Next, the on-chip tests followed the on-device purification procedure, explained previously, while the off-chip tests followed the Purification Bead manufacturer's instructions, followed by DNA elution in 20 μL of Resuspension Buffer. Figure 6.7 shows the Recovery Efficiency (%) of the two DNA sizes where the anticipated result was 100% Recovery Efficiency for the 485-bp amplicon, representing the full capture of the DNA library, and 0% Recovery Efficiency for the 123-bp amplicon, representing the removal of adapter dimers.

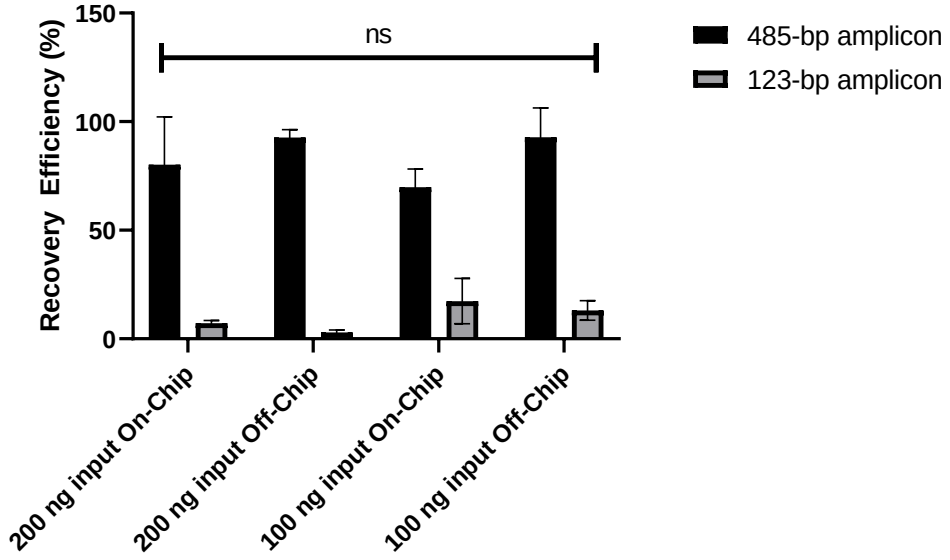

Figure 6.7: Recovery Efficiency (%) of various DNA purification testing conditions with different amounts of DNA purified on- and off-chip. Analysis of the testing resulted in no statistically significant difference in Recovery Efficiency Between the different groups using a 2-way ANOVA, P value = 0.3902 (n = 3).

6.4.3 Capillary PCR modeling and measurements

The custom thermoelectric cooler heating system was required to heat reagents from 98°C to 65°C to 72°C during PCR cycling. Thermoelectric cooler heat transfer modeling during PCR thermocycling was performed using COMSOL Multiphysics Modeling Software 5.4 to analyze the dispersion of the thermoelectric cooler heating to the reagents contained in the flexible polyethylene tubing. A 3D drawing was made of the copper plate, tubing, and reagents in the tubing to focus on the efficiency of the heat transfer from a heat source which represented the thermoelectric cooler (Figure 6.8). Heat Transfer in Solids and Fluids was used in a Time Dependent Study to model and analyze the rate of heating and cooling of reagents. This rate was then compared to experimentally determined rates gathered from the LabVIEW VI used to control the thermoelectric cooler via thermocouple real time feedback. In the model, water was used as an example liquid in the tubing to be heated and cooled. The thermoelectric cooler material for this modeling was Alumina (Al_2O_3) since the thermoelectric cooler being used is made of 127 couples between lapped ceramic (Al_2O_3) faces (Custom Thermoelectric, Bishopville, MD, USA). COMSOL Multiphysics Modeling heating and cooling rates were gathered for each step in PCR amplification in a Time Dependent

Study derived by Equations 6.9 and 6.10. Material properties were used to provide values for these equations where ρ is the density, C_p is the heat capacity at constant pressure, and k is the thermal conductivity.

$$\rho C_p \frac{\delta T2}{\delta t} + \rho C_p \mathbf{u} \cdot \nabla T2 + \nabla \cdot \mathbf{q} = Q \qquad (6.9)$$

$$\mathbf{q} = -k\nabla T2 \qquad (6.10)$$

$$Q_0 = \frac{P_0}{V} \qquad (6.11)$$

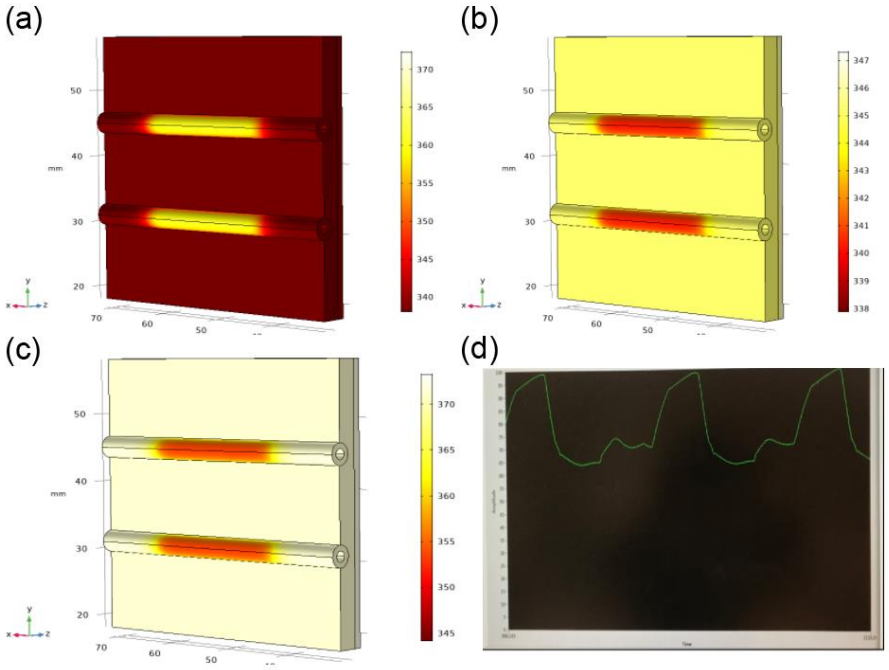

Figure 6.8: Thermoelectric cooler Heat Transfer in Solids and Fluids modeling using COMSOL Multiphysics Modeling Software Time Dependent Study (COMSOL label in kelvin) (a) 98°C to 65°C at 2 seconds. (b) 65°C to 72°C at 2 seconds. (c) 72°C to 98°C at 2 seconds. (d) Experimentally gathered LabVIEW VI plot (time vs temperature) of heating and cooling of reagents in flexible polyethylene tubing.

Table 6.2 shows a comparison of the experimentally derived heating and cooling rates, acquired from LabVIEW graphs (Figure 6.8d) vs. the modeling heating and cooling rates. The COMSOL Modeling Rates (Table 6.2) are based on the time it takes for the water to heat from the initial temperature ($T2$) to the next temperature in the PCR cycle ($T_0\ when\ T2 = T_0$) divided by the temperature change (°C). This is done using the thermoelectric cooler as a Heat Source domain and the Boundary of the thermoelectric cooler

adjacent to the copper plate as the next temperature (T_0). The heat rate (Q_0) was based on the maximum value provided by the thermoelectric cooler specifications (141.3 W) and calculated by Equation 6.11 in the COMSOL simulations. Figure 6.8a-c presents the different heating and cooling Time Dependent studies at 2 seconds. The Experimental and Modeling Rates were 0.07°C/sec and 0.04°C/sec different for the heating steps, while the cooling step from 98°C to 65°C was 0.5°C/sec slower in the Modeling Rate. It is hypothesized that the COMSOL Multiphysics Software Modeling was so different to the experimentally determined rate of cooling because the COMSOL Geometry does not include the aluminum fin heat sink. The heat sink was used on the device to regulate the thermal performance of the thermoelectric cooler, especially during cooling[194]. Therefore, this can account for the larger difference in the cooling rates as compared to the near consistency of the heating rates between the experiments and modeling.

Table 6.2: Comparison of the Experimental and Modeling Rates of Heating and Cooling of the thermoelectric cooler.

PCR Reaction Step	Experimental Rate	Modeling Rate
98°C to 65°C	2.45°C/sec (13.5 sec)	1.92°C/sec (17.2 sec)
65°C to 72°C	0.78°C/sec (9.0 sec)	0.85°C/sec (8.2 sec)
72°C to 98°C	1.69°C/sec (15.4 sec)	1.65°C/sec (15.8 sec)

One problem observed during the 98°C heating step of the capillary PCR reaction was evaporation of reagents within the tubing. To mitigate this evaporation and reduce any sample loss, a strategy was used to reduce the vapor pressure in the heated plug of liquid and therefore reduce the amount of evaporation based on the Clausius-Clapeyron equation (Equation 6.12) [195].

$$\mathrm{p(T) = p(T_0)exp\,[-\frac{\Delta H_{vap}}{R}\left(\frac{1}{T_0} - \frac{1}{T}\right)]} \qquad (6.12)$$

This equation shows that a change in the temperature (T) difference can affect the vapor pressure (p), but since the temperature changes are specific for the PCR amplification, another factor needed to be altered. The heat or enthalpy of vaporization (ΔH_{vap}) was then evaluated since it characterizes the amount of energy needed for molecules to escape from the liquid state into a gas. The enthalpy of vaporization is affected by the pressure in the system, since evaporation will happen faster if there is less force on the surface keeping the molecules from converting to a gas at a higher temperature. Therefore, external pressure was applied to

reduce the rate of evaporation by closing the pinch valve associated with whichever cannula the liquid was contained in and moving the syringe pump forward almost the entire volume of the 500µL Hamilton Gastight Syringe. This pressurization added between 5 and 7psi of pressure to the reagents in the tubing. This was critical to reducing evaporation, especially during heating, and to perform an efficient reaction with a large enough yield for sequencing.

6.4.4 Microfluidic liquid handling and mixing modeling and analysis

Efficient liquid movement and reagent mixing was considered to reduce any unwanted air bubbles that may interfere with reactions. This was done by modeling the liquid handling as seen in Figure 6.9a which shows three different heights the Cannulas would stop at for withdrawing or dispensing reagents. Fluid withdrawal occurred at height Z_0, while dispensing took place at height A (~2 mm from bottom of well) for certain reagents. A more complex dispensing pattern was used for larger volumes or more viscous reagents. In these steps a volume of liquid began dispensing at height A but the z-stage holding the Cannulas gradually moved to height B, just above the reagent plate (~9 mm) by the time all liquid was dispensed. The movement of the z-stage holding the cannulas vs. the pump dispensing the fluid is pictured graphically in Figure 6.9b, where a wait time was incorporated as the pumping began, then the z-stage moved up slowly, finishing dispensing before reaching height B. The wait time for the pump was used to account for the liquid movement delay, which occurs especially for more viscous reagents (i.e. Ligase Buffer Mix) because a larger pressure force in the tubing is needed to move the reagents. The wait time was also used to account for the rate of reagent dispensing so that the Cannula (z-stage) movement correlated with how much liquid was dispensed into the well; the more liquid in the well, the higher the cannula arm was which reduced the chance of making air bubbles when mixing. A faster z-stage movement rate was used to move the cannulas back into the reagent well after reaching height B, with the goal of agitating any air bubbles that may have been formed during the liquid dispensing. This patterned movement was performed eight times during reagent mixing steps and optimized to sufficiently mix all buffers and enzymes to ensure an efficient reaction.

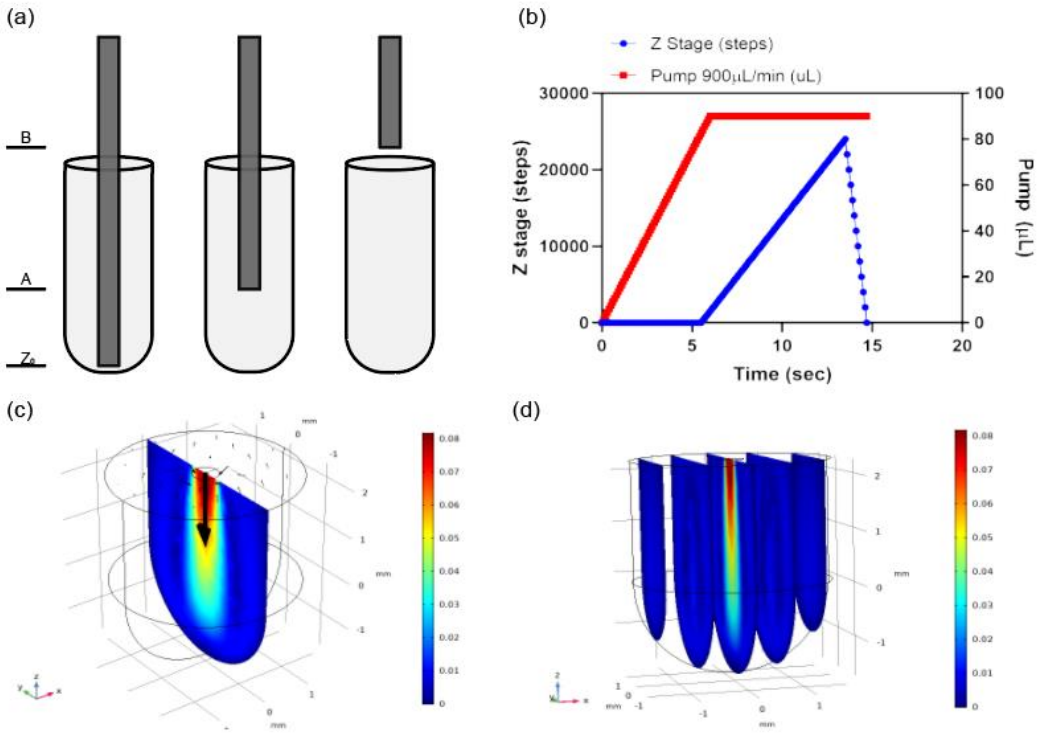

Figure 6.9: Liquid handling analysis: (a) Cannula heights for dispensing and sipping liquids. (b) Big add z-stage movement vs. pump timing. Modeling using COMSOL Multiphysics Modeling Software Stationary Study: (c) Mixing profile in reagent well, Slice: Velocity magnitude (m/s) Arrow Surface: Velocity field, (**d**) Mixing profile in reagent well, 5 slices, Slice: Velocity magnitude (m/s).

Reagent mixing was also investigated using COMSOL Multiphysics Modeling Software 5.4. A 4 mm tall-cylindrical geometry matching the wells of the reagent plate was built in 3D with a 0.25 mm-radius circle on the top of the cylinder, representing the inner diameter of a Cannula. This circle became the inlet boundary in the Laminar Flow Physics being simulated in both Stationary and Time Dependent Studies. The top of the cylinder surrounding the inlet circle was assigned as the outlet boundary to account for conversion of mass in the model. There was a no slip wall condition and an inlet velocity of the dispensing in the z-direction, V_z = Q/A = 0.0764m/s. The outlet pressure was zero. Results of these simulations are provided in Figure 6.9c where a center slice of the 3D well in the Stationary Study is provided. The Velocity magnitude (m/s) output plot show the mixing velocity was concentrated in the center of the well below the inlet and the Time Dependent Study showed the liquid reached its mixing profile by 0.25 seconds at this velocity. Additionally, Figure 6.9c shows the pattern of the mixing by the Arrow Surface plot, with the

mixing circling back up to the top of the reagent well in an elongated ring shape that is maintained over the 2 second Time Dependent Study conducted. The elongated ring mixing shape is represented in 2D but remains consistent in 3D, as seen in the 5-slice image of the simulation (Figure 6.9d). Proper mixing is vital for the success of the DNA library preparation and this modeling shows an efficient mixing profile.

6.4.5 On-device library preparations

Before the microfluidic chip was used on the device platform DNA libraries were prepared manually as a benchmark to compare on-chip and on-device testing to. The DNA library concentration (ng/μL), quality (A_{260}/A_{280} ratio), and yield prepared in these different tests is presented in Figure 6.10a-c and all DNA was resuspended in a 20 μL volume. DNA quality was evaluated using the A_{260}/A_{280} ratio of sample absorbance at 260 nm and 280 nm as this is used to assess the purity of DNA where a ratio of ~1.8 is considered pure. The Manual Prep Large Volumes results use 500 ng of input Lambda DNA (New England Biolabs, Ipswich, MA, USA) and five PCR cycles. All other tests use scaled down volumes more conducive to the dimensions of the device using 180 ng of the same input DNA and 5 PCR cycles for the Manual Prep Small Volumes and 7 PCR cycles for the other tests. Full dimensional analysis of the reagent volume scale down is presented in the Supplementary Material as well as the reagent plate layout design process using the two-cannula system. Table 6.3 and Table 6.4, respectively, show then end result of this analysis to set up the device for library preparation.

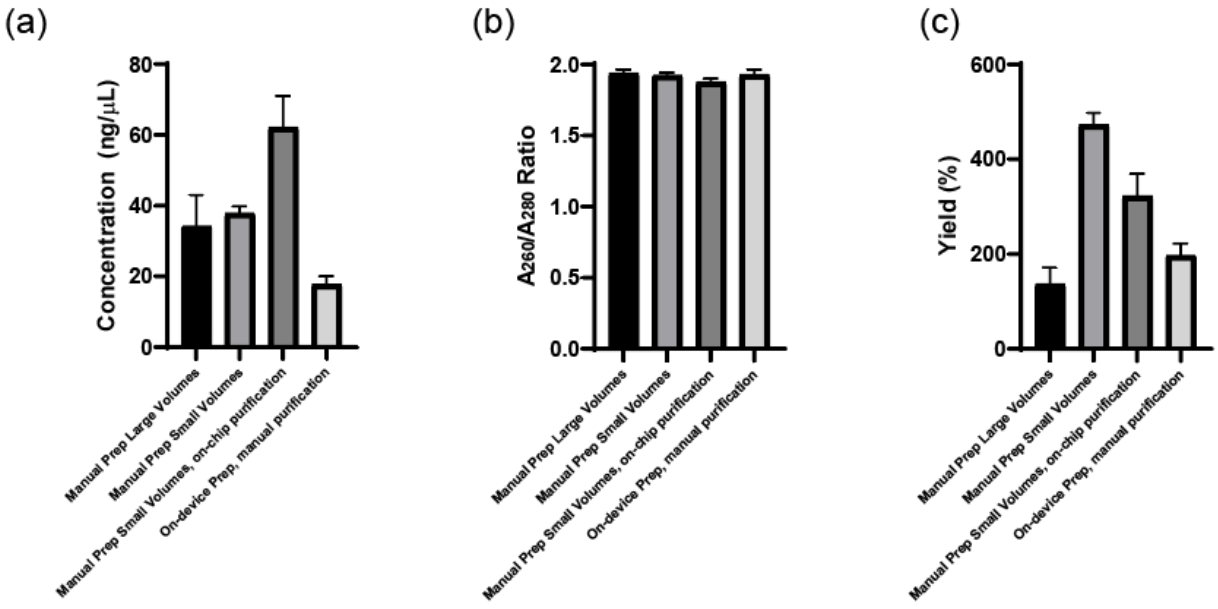

Figure 6.10: (a) Concentration (ng/μL) (b) quality (A260/A280 ratio), and (c) yield (%) of DNA libraries prepared using manual library preparation under various conditions.

Table 6.3: Reagent volumes used in the manual library preparation according to manufacturer's instructions and on the automated device. PL = post-ligation, PA = post-amplification

Reagent	Manual Preparation Volumes (μL)	On-Device Volumes (μL)
DNA	5 μL = 200 ng	5 μL = 200 ng
Fragmentase Buffer	5 μL	2 μL
Fragmentase Enzyme	11 μL	4 μL
Fragmentase Water	29 μL	7 μL
Ligase Buffer	44.5 μL	17 μL
Ligase Enzyme	3 μL	1 μL
Barcoded Adapters	2.5 μL	2 μL
Purification Beads (PL)	100 μL	36 μL
Resuspension Buffer (PL)	28 μL	25 μL
PCR Master Mix	25 μL	20 μL
PCR Primers	2 μL	2 μL
Purification Beads (PA)	45 μL	36 μL
Resuspension Buffer (PA)	33 μL	32 μL

Table 6.4: Reagent plate layout and identity of the cannula used on the automated device. PL = post-ligation, PA = post-amplification

Well	Reagents	Cannula
1	DNA/ Fragmentase Buffer/ Fragmentase Enzyme/ nuclease free water	1
2	Wash Buffer: 0.5 M EDTA	1
3	Wash Buffer: nuclease free water	1
4	Barcoded Adapters	1

5	PCR Master Mix	2
6	PCR Primers	2
7	Resuspension Buffer (PA)	2
8	Purification Beads (PA)	1
9	Purification Beads (PL)	1
10	Ligase Buffer/ Ligase Enzyme	1
11	Resuspension Buffer (PL)	2

Lastly, to test how this microfluidic chip and device perform in a sequencing application, two DNA samples were prepared for sequencing on the device (one euploid and one aneuploid) and two were prepared for sequencing manually (one euploid and one aneuploid) using the same two starting whole genome amplified samples. Although the sample number is limited, the following results indicate a successful first application of this chip and device design. Quality control results of these libraries obtained through Agilent Bioanalyzer analysis are provided in Figure 6.11a and 11b, showing the library concentration and size results, respectively. The samples prepared manually had an average DNA concentration of 57.57 ± 10.66 ng/μL in 20 μL of sample while the sampled prepared on-device had an average DNA concentration of 19.52 ± 0.76 ng/μL under the same conditions. Figure 6.11b shows that the average library size produced on-device was around 400 bp, which was the set benchmark for the experiment. Additionally, all four samples passed the purification standard for sequencing through observing the absence of adapter or primer dimers using electropherograms of the samples obtained from the Agilent Bioanalyzer (i.e. Figure 6.5b) and had a A_{260}/A_{280} value ~1.8 (Figure 6.11c). Lastly, the DNA library yields comparing the amount of input DNA to final amount of DNA library is presented in Figure 6.11d. Sample quality control results were also gathered during sequencing and are presented in Table 6.5. Overall, the most important information from the DNA sequencing was the diagnostic results from testing five cell aneuploid or euploid samples as this is imperative for the field of PGT-A. The PGT-A karyotype results in Figure 6.11e-h indicate this device was able to produce DNA libraries that could specifically identify an aneuploid cell sample vs. euploid cell sample.

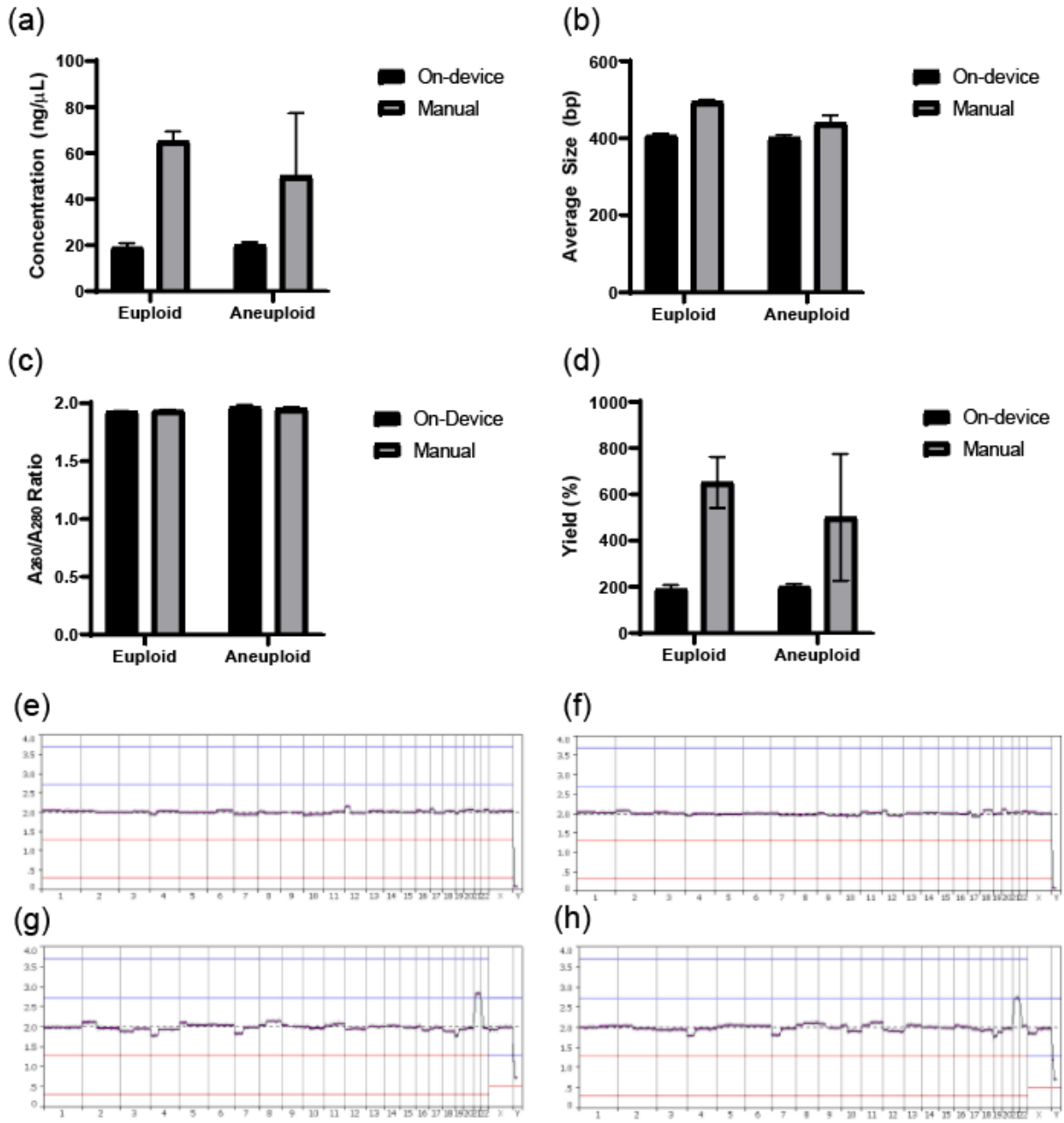

Figure 6.11: (a) Concentration (ng/μL) (b) average size (bp) (c) quality (A260/A280 ratio), and (d) yield (%) of prepared DNA libraries from euploid and aneuploid 5 Cell Samples. (e) PGT-A karyotype result for a Euploid 5 Cell Sample prepared on-device (f) PGT-A karyotype result for a Euploid 5 Cell Sample prepared manually. (**g**) PGT-A karyotype result for an Aneuploid 5 Cell Sample (48, XXY, +21) prepared on-device. (**h**) PGT-A karyotype result for an Aneuploid 5 Cell Sample (48, XXY, +21) prepared manually.

Table 6.5: Sample Quality Control Information from Illumina MiSeq sequencing analysis and PG-Find Software for DNA libraries prepared on the device and manually.

Trial	Total Reads	% Mapped Reads aligned to hg19	PG-Find Quality Score
Euploid Sample manual preparation	502553	98.81	0.0404
Euploid Sample on-device	503579	97.74	0.0402
Aneuploid Sample manual preparation	502397	98.56	0.0496
Aneuploid Sample on-device	503705	96.07	0.0497

6.5 Discussion

Overall, the microfluidic chip with magneto-electrophoresis used in this application was able to contribute to the purification of DNA library on an automated device platform and result in an accurate PGT-A diagnosis. In addition to that, the reagent scale down and device automation can save users time and money as only ~1/3 of the reagent volumes are used and the hands-on time of the procedure is reduced from 2.5 hours to less than 10 minutes. Additionally, with less user interaction this device can help to reduce human errors that may interfere with the success of the library preparation. When comparing the DNA libraries prepared on-device to those prepared manually it was important to note that to be conducive to downstream sequencing, there needs to be >4 ng/μL of DNA library produced. Thus, although a larger yield was produced using manual preparation and there was variation between the amount of DNA prepared between tests, incorporating additional PCR cycles on the device could be used to increase the quantity of DNA to the range produced manually. For the goal of comparing directly though, seven PCR cycles were used in the final protocols although this can always be adjusted. The smaller yield on the device was most likely due to reagent evaporation or sample loss within the tubing. Reagent evaporation would have occurred while reagents loaded onto the reagent plate at the beginning of the protocol were waiting to be used throughout the ~2.5-hour library preparation. Although sacrificial liquid was added to reagents to mitigate this concern, it is still a possibility. A more probable factor that could contribute to a decrease in DNA library yield on the device is sample loss within the device tubing throughout the protocol run. Future iterations of this device platform would benefit from decreasing the tubing length where possible and using fewer connecting pieces between tubing as this is where sample loss was often found if it occurred. This

was an essential learning from this first-generation device, while there was still enough DNA library prepared to be conducive to downstream sequencing, mitigating any sample loss within the protocol run is an essential task for further iterations. However, when comparing the library yield of this device to other platforms in the literature, yields as low as 60%[173] and as high as 236%[196] were reported when comparing the amount of DNA after PCR amplification to the initial DNA input. Therefore, our device platform is still performing as well or better than these existing technologies.

While DNA quantity differed between preparation methods, the quality of the DNA prepared on-device and cleaned by the microfluidic chip using magneto-electrophoresis remained relatively consistent between samples prepared on the device and manually. When characterizing the Recovery Efficiency (%) of the microfluidic chip DNA purification compared to the off-chip, manual purification, there was no statistically significant difference found between the groups (2-way ANOVA, n=3, P value = 0.3902). The goal of this testing was to fully capture and purify the 485-bp amplicon, representing the DNA library, while removing the 123-bp amplicon, representing adapter dimers. The microfluidic chip was chosen for this device to reduce the amount of pipette handling of the Purification Bead mix to limit the chances of unintentionally discarding or disturbing the bead mix on the automated platform. The microfluidic chip simply requires the loading of the bead mix with adsorbed DNA and the removal of the purified DNA without adding and removing wash buffers. Studying the Recovery Efficiency under various conditions showed that the microfluidic chip purification can perform as well as the conventional off-chip methods used in manual library preparation. The quality of the DNA purification is further evaluated by analyzing the accuracy of the sequencing data. The percent of mapped reads to the reference genome (hg19) is a useful measurement of the overall sequencing accuracy with a larger percentage showing more accuracy. Lower mapped reads can be caused by incomplete fragmentation, low yields, or remaining adapters in the final libraries. The percent of mapped reads also indicates if there is any contaminating non-human DNA. Although the percent of mapped reads was higher for the manually prepared samples, there was not a statistically significant difference in the percentages when comparing the two groups (unpaired t-test, n=2, P value = 0.1705). Additionally, the PG-Find Quality Scores were compared, which measure the bin to bin variance in reads

for each sample before smoothing, similar to the standard deviation where a lower score means more reliable data. A higher quality score can indicate low quality DNA or problems with WGA or library preparation. Since there is no statistically significant difference between the on-device and manually prepared sample quality scores and the same WGA sample was prepared using manual and automated methods (unpaired t-test, n=2, P value = 0.9947), this indicates the library preparation quality was equivalent.

One more advantage of this microfluidic chip that can be utilized in the future is the capacity to induce electroosmotic flow in the chip as opposed to electrophoresis. Through altering the Separation Buffer to change the boundary conditions in the microfluidic channel and switching the positive and negative electrode positions, the design can be optimized for electroosmotic flow. One advantage of electroosmotic flow is that it creates a bulk liquid flow where electrophoresis moves charged ions within a solution. This may be beneficial for purifying a sample of non-charged particles depending on the application. Electroosmotic flow and magnetic bead movement has been explored previously[182] but not for NGS library preparation to date. Overall, the preliminary data for this microfluidic chip and library preparation device presented in the current study has demonstrated that it can deliver high quality, reliable NGS library preparations and an accurate PGT-A result in an efficient amount of time with minimal user interaction.

6.6 Conclusions

As NGS continues to contribute and influence the field of personalized medicine it is essential that the engineered technologies for DNA library preparation are meeting the standard for accurate sequencing and diagnosis. This research presents a novel magnetic bead-based purification microfluidic chip that combines magnetic bead movement and electrokinetic purification, termed magneto-electrophoresis. We also demonstrate precise capillary PCR and reagent mixing through modeling and experimental data. Overall, DNA libraries prepared using this device met the same standard as those libraries prepared manually and PGT-A samples were accurately diagnosed following NGS analysis. This low-throughput method can be scaled up but is ideal for smaller laboratories where a high-throughput robotic liquid handler is not a feasible option for automating library preparation. This microfluidic chip and device have the capabilities to be

translated to other sample preparation procedures using extracted genomic DNA samples for different diagnostic applications and other methods that require a robust, simple magnetic bead-based purification method.

6.7 Acknowledgements

We would like to thank Francis Cui for his help in designing the microfluidic chip and device for this project. Additionally, we thank John Murphy for his work designing and building the device, Andrew Brodsky for helping put the device together and mechanical trouble shooting, Jacob Feder for working on electrical components of the device, Josh Kinman for sequencing the DNA samples, and Kimberly Warren for analyzing the sequencing data.

6.8 Supplemental Information

6.8.1 Methods for Optimizing the automated library preparation device

Reagent volume change analysis and organization

The automated device platform utilizes flexible polyethylene tubing for liquid movement and a custom reagent plate which limits the reagent volumes that can be used. Dimensional analysis of the tubing and reagent plate were performed to ensure that reagent volumes were conducive to this scaled down device while also considering evaporation of reagents that may occur on the reagent plate. Off-device DNA library preparations were initially performed based on the dimensional analysis to evaluate the effect of reducing reagent volumes on DNA library yield. One microliter of DNA library sample was run on the Agilent Bioanalyzer 2100 machine with the Agilent DNA 1000 Kit and DNA Chip for On-Chip-Electrophoresis (Agilent Technologies, Santa Clara, CA, USA). After the reduced volumes were optimized, the protocol was analyzed to determine the organization of the reagents in the reagent plate. Since this device utilizes a two-cannula system for all reagent handling, there are no pipette tip changes throughout the whole protocol. This means that the reagent plate organization needed to be set in a way so that a cannula would not interfere with any reagents prematurely that could contaminate the DNA library sample. Additionally, this organization also included determining which cannula should handle which reagents for a successful DNA library preparation.

6.8.2 Analysis and Results for Optimizing the automated library preparation device

Reagent volume change analysis and organization

The PG-Seq kit library preparation involves three main steps: (1) DNA fragmentation, end repair, and adenylation; (2) adapter ligation; and (3) PCR amplification. Steps (1) and (3) of this protocol require reagent heating for proper enzymatic reactions, therefore, these reactions take place on the thermoelectric cooler. It is important that the entire liquid volume fits in the tubing adjacent to the thermoelectric cooler so that it can be heated equally throughout the reactions. The flexible polyethylene tubing in the thermoelectric cooler setup has an inner diameter of 1/16" or 1.6 mm. Using the manufacturers dimensions plus or minus the specified tolerances, the maximum reagent volume that can fit on the 40 ± 0.25 mm wide thermoelectric cooler was calculated to be (80 ± 0.5) μL. Another dimensional constraint to the maximum volumes possible for this device platform was the size of the reagent wells on the custom reagent plate used. These wells were cylindrical in shape with the bottom of the well curved, representing one-half of a sphere. With a radius of 1.75 mm and total height of 8 mm and both dimensions having a tolerance of ± 0.25 mm, the maximum volume that can be contained on the reagent plate was calculated to be (71 ± 20) μL. Therefore, it was determined that the reagent plate well volume would control the maximum volumes used on the device.

One more important consideration used in the reagent volume design process was the amount of evaporation occurring while the reagent plate was open to the atmosphere during the protocol. Strategies to reduce the effects of evaporation include reducing time scales ($t_{reaction} << t_{evaporation}$), changing device geometries to reduce the ratio of exposed areas to volumes, or adding a higher boiling point component to reduce the vapor pressure in the reagent[195]. Another strategy, which was used in this application, is adding sacrificial water around the liquid of interest[195]. This latter strategy was adapted in this case by adding sacrificial nuclease free water to the reagents instead. Initially, 2 μL of sacrificial water was added to reagents to reduce the proportion of reagents that would be evaporated from each well. The amount of sacrificial water added was then adjusted based on the equation for evaporation rate and the thin-film model of mass transfer between the liquid and bulk vapor phases, which assumes that the liquid concentration changes slowly over

time[197]. The time dependent process of this transport is described by Supplemental Equation 6.1 where the number of moles of component i, N_i, changes over time, t, and this is in balance with the interfacial surface area, A, and molar flux, j_i, of i in moles per area per time. The rate of evaporation will be the flux at the interface.

$$\frac{dN_i}{dt} = -Aj_i \qquad \text{(Supplemental Equation 6.1)}$$

Therefore, it was determined that reagents being used later in the protocol would receive 3 µL or 4 µL of sacrificial water per reagent well since more evaporation would occur by the time that they are used in the protocol. Nuclease free water was used because it would not contaminate any reagents and as the nuclease free water evaporates it will minimize the proportion of the volume lost from each reagent[195].

The last consideration for determining the final volumes used in the complete automated device procedure was the two buffer exchanges that occur during the DNA purification steps on the microfluidic chip. There are two steps in this workflow where reagents are added together before the DNA library is purified from these reagents. The post-ligation cleanup includes reagents from DNA fragmentation, end repair, and adenylation; adapter ligation; and the first Purification Bead mix. The post-amplification cleanup includes reagents from PCR amplification and the second Purification Bead cleanup. Therefore, the total volume of these mixes plus the sacrificial water needed to fall within the reagent plate maximum allowance of (71 ± 20) µL, also taking into consideration the evaporation that will occur over time.

Table 6.3 in the main text outlines the final reagent volumes used in this procedure on-device vs. the standard off-device manual sample preparation volumes provided in the manufacturer's instructions. In the original manual protocol, 50 µL of total volume is used for the DNA fragmentation, end-repair, and adenylation step as well as for the adapter ligation step. For the on-device protocol, the 1:1 ratio of these reagents was maintained by using ~1/3 of the volume of each at 18 µL. The only difference in this ratio being that the barcoded adapters were included in the 50 µL ligation mix volume off-device but not on-device to avoid reducing the already small volume as much as possible. Additionally, off-device there was a 1:1 ratio of reagents to Purification Bead mix for the first wash at 100 µL:100 µL. This was nearly

maintained on-device at 38 µL:36 µL but adjusted slightly because the barcoded adapters were not included in the 18 µL reagent volume for the ligation mix. The total volume of these reagents when they were combined was 74 µL which falls within the range determined via dimensional and evaporation analysis. Following the first microfluidic chip purification step, the purified DNA library was eluted into the Resuspension Buffer and combined with PCR primers and PCR master mix for library amplification. The PCR master mix volume was reduced by 5 µL from the manufacturer's instructions to maintain the proportion of the mix to the Resuspension Buffer containing the DNA due to evaporation. The PCR primers were kept at 2 µL because reducing that volume could lead to less precise reagent plate loading. The Purification Bead mix was again 36 µL for this second cleanup because this agreed with the 0.9× bead to reagent volume ratio from the manufacturer's instructions off-device, again accounting for reagent evaporation. The total amount of reagents combine before the second microfluidic chip purification post-amplification was calculated to be 83 µL based on the input reagent volumes. This total amount was again within the desired range of (71± 20) µL.

Both standard and reduced reagent volumes (Table 6.3) were initially tested off-device through manual preparation before translation onto the automated platform. Results were analyzed using the Agilent Bioanalyzer 2100 and showed an average with standard deviation of 29.34 ± 2.17 ng/µL of library yield for the large volumes specified by the manufacturer and 38.65 ± 1.59 ng/µL of library yield for the small volumes adjusted to be used on the device. These libraries were prepared from 500 ng and 180 ng of Lambda DNA, respectively (New England Biolabs, Ipswich, MA, USA). In addition to these new volumes being better suited to the dimensions of this device, end users also benefit from cost savings for reagents since most reagent volumes have been reduced.

After the optimal volumes were established for the on-device automated platform, the reagent plate was designed so that the two-cannula system could handle all reagents without any contamination of the final DNA library. One cannula (Cannula 1) was selected to handle both Purification Bead mixes, while Cannula 2 manipulates all purified DNA. The goal was to separate any reagents that could negatively affect or contaminate the prepared sample through residual reagents remaining in the tubing or submerging in an

unwanted reagent in the reagent plate prematurely since the cannulas move in parallel. Table 6.4 in the main text provides the well number and associated reagent used for this assay as well as which cannula manipulated that reagent. The bead mix used in the post-ligation cleanup was optimized to account for the viscous Ligase Buffer Mix used. To ensure all Purification Beads were able to make it through the microfluidic chip, 65% of the mixture was 0.05% TWEEN to provide a surfactant to aid in bead movement. Additionally, 35% of the mixture was Purification Beads but at a doubled concentration to increase the magnetic field of the beads to help improve their movement by the magnet. This was done by taking 70 μL of Purification Beads, collecting them with a magnet, removing 35 μL of the buffer, and resuspending the now concentrated bead mix. No alterations needed to be made to the post-amplification Purification Bead mix. Lastly, wash steps for the tubing were considered to eliminate any unwanted enzymes that were carried over from previous reactions that would negatively affect upcoming reactions in the DNA library preparation process, to improve the quantity and quality. This included rinsing Cannula 1 tubing containing the Fragmentase Enzyme after the fragmentation step to reduce any cross-contamination. The wash buffers 0.5 M EDTA (Thermo Fisher Scientific, Waltham, MA, USA) then nuclease free water (IDTE, Coralville, IA, USA) were utilized as an alternative method for inactivating the Fragmentase Enzyme as opposed to heat. Agilent Bioanalyzer results were critical in performing quality control for the prepared DNA libraries prior to sequencing.

CHAPTER 7

Progress and challenges in laboratory-based diagnostic and screening approaches for aneuploidy detection during pregnancy

---

Chapter 7 has been published as a review article.

Schneider, L., Tripathi, A., *Progress and Challenges in Laboratory-Based Diagnostic and Screening Approaches for Aneuploidy Detection during Pregnancy*, **SLAS TECHNOLOGY: Translating Life Sciences Innovation**, 24726303211021787, 2021.

7.1 Abstract

Aneuploidy is caused by problems during cellular division and segregation errors during meiosis that lead to an abnormal number of chromosomes and initiate significant genetic abnormalities during pregnancy or the loss of a fetus due to miscarriage. Screening and diagnostic technologies have been developed to detect this genetic condition and provide parents with critical information about their unborn child. In this review, we highlight the complexities of aneuploidy as a disease as well as multiple technological advancements in testing that help to identify aneuploidy at various timepoints throughout pregnancy. We focus on aneuploidy diagnosis during preimplantation genetic testing which is performed during in vitro fertilization as well as prenatal screening and diagnosis during pregnancy. This review focuses on DNA-based analysis and laboratory techniques for aneuploidy detection through reviewing molecular- and engineering-based technical advancements. We also present key challenges in aneuploidy detection during pregnancy including sample collection, mosaic embryos, economic factors, and social implications of this testing. The goal of this review is to synthesize broad information about aneuploidy screening and diagnostic sample collection and analysis during pregnancy and discuss major challenges the field is still facing despite decades of advancements.

Keywords: aneuploidy; prenatal testing; preimplantation genetic testing for aneuploidy

7.2 Introduction

Aneuploidy is linked to a variety of diseases and conditions during tumor growth in cancer[198,199], the development of a fetus during pregnancy[200], and more. These conditions involve the presence of unbalanced genomes in cells due to copy number variations depending on lost or gained chromosomes, and can also lead to imbalances in protein stoichiometry[201,202]. Notably, aneuploidy is a result of errors during cell division including mitotic errors such as spindle-assembly checkpoint (SAC) pathway mutations, premature loss of chromatid cohesion, atypical kinetochore attachment, or extra centrosomes[201]. Segregation errors during meiosis can also cause aneuploidy cell formation; these errors include, missegregation of homologous chromosomes during meiosis I or of sister chromatids during meiosis II[201]. When gametes develop these errors and are then fertilized, this can lead to embryos with one or three copies of a specific chromosome, instead of the normal two copies. Aneuploidy occurs in around 0.4-0.6% of newborns and is responsible for more than 50% of spontaneous abortions or miscarriages[55,200,203]. Many of these chromosomally abnormal conceptions are associated with increased maternal age which has become a more relevant factor over time as it is becoming more common for women to be pregnant later in life. For example, the proportion of pregnancies in women 35-39 and 40-44 has increased 9% and 15%, respectively, from 2007 to 2016 in the United States alone[55,200,204].

While aneuploid embryos do lead to a disproportionate amount of miscarriages, there are a limited number of aneuploidies that are still compatible with human life[202]. The most common of those aneuploidies is trisomy 21, also known as Down Syndrome, accounting for more than 50% of aneuploidy cases, which include live births, fetal deaths, and pregnancy terminations[200]. Next is trisomy 18 (Edward's syndrome) at 15% and trisomy 13 (Patau's syndrome) at 5% of cases which generally result in only a few months of survival for the baby[200,202]. Lastly, sex chromosome aneuploidies (45, X and 47, XXX, XXY, and XYY) account for about 12% of these aneuploidy cases[200]. Trisomy 21 occurs once in every 750 live births and involves an extra copy of the more than 300 genes located on chromosome 21[205]. This genetic alteration can lead to a variety of phenotypic changes including learning difficulties, cardiac deficiencies, distinctive facial features, and leukemia among others[206]. One possible explanation as to why fetal development is still

possible for trisomy 13, 18, and 21 cases is that they have the fewest number of transcripts that they encode on their respective chromosomes, limiting the consequences that can occur from a lost or extra chromosome copy compared to others.

Ultimately, there is a need for proper detection of aneuploidy during embryo development to inform parents of the health of the developing baby. Aneuploidy detection can occur at various timepoints during pregnancy using prenatal testing or even before pregnancy during in vitro fertilization (IVF) if preimplantation genetic testing for aneuploidy (PGT-A) is performed. PGT-A is used for patients with recurrent pregnancy loss or implantation failures which may be caused by a woman's decline in fertility as a result of increased maternal age or a number of other factors[55]. PGT-A is used in conjunction with IVF to select the embryos with the best potential chance of survival and normal development[55]. A trophectoderm (TE) biopsy is used for sample collection during PGT-A which removes cells for genomic analysis that eventually become the placenta and ensures the developing embryo in the inner cell mass is not disturbed[207]. Genomic analysis is used to make an even more informed decision as to which embryos are the best to transplant, it also allows for more single embryo transfers which reduces the chance of twins or other sets of multiple babies[55]. This is beneficial because it can lead to fewer preterm births and low birthweight infants and provides a better chance that a healthy pregnancy will be achieved sooner[55]. PGT-A is highlighted as one aneuploidy diagnostic method in Table 7.1.

Table 7.1: Selected techniques for aneuploidy diagnosis testing during pregnancy.

Test	Timeframe of Testing	Overview of Sample Collection	Considerations for this form of testing
Preimplantation Genetic Testing for Aneuploidy (PGT-A)	Used in conjunction with IVF prior to embryo implantation[55].	Use TE biopsies at day 5-6 of embryo development [208]. TE biopsies remove around 5-10 cells during the blastocyst stage of development, removing cells that ultimately become the placenta during pregnancy[207,209-211].	Less than 5% false positive rate[212,213].
Amniocentesis	Second or third trimester of pregnancy[59,214].	Involves inserting a needle through a woman's abdomen into the uterus to retrieve a sample of amniotic fluid for testing[215].	Detection rate of greater than 99% and a 5% false positive rate[59,216].
Chorionic Villus Sampling (CVS)	First trimester of pregnancy[59].	Sample retrieval performed by using a needle that can be inserted	Detection rate of greater than 99% and

		through the abdomen or vaginally through the cervix to withdraw a sample of placental tissue for fetal karyotyping and other testing[59,215].	false positive rate of 3-5%[59,216].
Cordocentesis	Second trimester of pregnancy[217]	Fixed needle guided under transabdominal ultrasound for fetal blood sampling via the umbilical cord.[217]	Associated with higher fetal loss rate than amniocentesis.[217]

Another point in the pregnancy progression where aneuploidy detection occurs is in prenatal testing. This is done using a variety of different sample collection and analysis techniques. Since 2007, the American College of Obstetricians and Gynecologists (ACOG) has advised that all pregnant women are offered prenatal screening for fetal aneuploidy but at least 20% of women elect for no aneuploidy screening, even without financial barriers[200,218]. Some screening methods that have been or are currently available for aneuploidy detection are first trimester screening; quadruple marker screening; integrated, stepwise sequential, and contingent screening; and non-invasive prenatal testing (NIPT)[219,220]. Screening techniques cannot technically provide an aneuploidy diagnosis but are crucial in informing patients of the possibility of having an affected fetus and whether further diagnostic testing should be performed[221]. Table 7.2 features some key characteristics of each of these screening methods while DNA-based, laboratory methods will be discussed in greater detail in this work. In addition to screening options during prenatal testing there are diagnostic options that may be recommended when a pregnancy is at a higher risk for aneuploidies[220]. Chorionic villus sampling (CVS) and amniocentesis are both invasive diagnostic tools and were previously associated with a risk of miscarriage at a rate between 0-2%[59,215]. However, more recent studies have challenged that figure and concluded that neither CVS nor amniocentesis are associated with an increased risk of miscarriage or stillbirth, especially when compared to a control group of women with similar risk profiles[222,223]. Cordocentesis is one more, less common, prenatal diagnostic procedure that has been used when diagnostic information cannot be gathered by amniocentesis or CVS[217]. Table 7.1 shows more information about these diagnostic tests that can be used for aneuploidy detection during pregnancy.

Table 7.2: Selected techniques for aneuploidy screening testing during pregnancy.

Test	Timeframe of Testing	Overview of Sample Collection	Considerations for this form of testing
Non-invasive prenatal testing (NIPT) using cell free DNA (cfDNA)	First or second trimester of pregnancy [59,221].	Whole blood samples are taken from mothers and centrifuged to separate plasma, which contains the cell-free fetal DNA (cffDNA), from the rest of the blood components[59].	False positive rate around 0.1%[59,221].
First trimester screening	First trimester of pregnancy[214].	Ultrasound and maternal blood test used for analyzing fetal nuchal translucency (NT), free β-human chorionic gonadotrophin (β-hCG), and pregnancy-associated plasma protein-A (PAPP-A)[214,219].	Detection rate of 85-95% when also considering maternal age (maternal age alone detection rate is 30-50%) and false positive rate of 5%[219,220].
Quadruple Marker Screen (Quad Screen)	Second trimester of pregnancy[214].	Maternal blood is used for this serum screening testing which measures β-hCG, alpha-fetoprotein (AFP), unconjugated estriol (uE3), and dimeric inhibin-A (DIA)[214].	Detection rate of 81% and screen positive rate of 5%[214].
Integrated, Stepwise Sequential, and Contingent Screening	First and second trimesters of pregnancy[214].	Maternal blood is used as these tests are performed during first trimester screening and then quad screening[214].	Detection rate ranges between 88-96% and screen positive rate of 5%[214].

Overall, these techniques show many sample retrieval strategies for PGT-A and prenatal testing for aneuploidy diagnostics and screening. This review will aim to discuss multiple molecular- and engineering-based sample analysis approaches that have been used for this important detection technology with a major focus on DNA-based analysis. Additionally, this review will discuss specific challenges researchers, clinicians, and expecting parents face when using these different types of tests including sample collection, mosaic embryos, economic factors, and social implications of aneuploidy detection testing.

7.3 Molecular-based approaches for detecting and studying aneuploidy

Following sample collection there are a variety of techniques that can be used for detection and analysis of fetal aneuploidy on a genetic level in both PGT-A and prenatal testing. First, we will discuss molecular-based approaches that have been used and adapted for these forms of testing.

7.3.1 FISH, SNP arrays, and aCGH

One cell-based molecular technique of historic significance in the aneuploidy detection field to begin with is fluorescent in situ hybridization (FISH). FISH works by hybridizing highly specific probes to different chromosomes that can be used to identify the number of copies of a given chromosome in a nucleus[224]. This technique has been performed using cells from chorionic villus and amniotic fluid samples during prenatal testing and was once seen as a major step in the field because it could be performed more rapidly than other existing techniques such as cytogenetic analysis[224,225]. In 2013, Rosner et al. performed a retrospective study on 470 patients who had CVS and FISH detection within one day and had a 90% sensitivity and 99.4% specificity in their results[226]. FISH has also been performed on PGT-A samples and was extremely beneficial for patients of advanced maternal age with repetitive implantation failure[227]. In a prospective, randomized control trial study performed by Rubio et al. in 2012, they found a significant increase in live-birth rates per patient when FISH analysis was performed on chromosomes 13, 15, 16, 17, 18, 21, 22, X, and Y compared to patients with no PGT-A analysis[227]. While FISH has been a crucial technique used in aneuploidy detection, many DNA-based technologies continue to outperform this technique due to the low resolution, limits on how many chromosomes can be analyzed, and accuracy of the technique compared to others[228].

In addition to detection, this molecular technique can also be used to study diseases caused by aneuploidy, such as Down Syndrome. Korbel et al. used FISH as a technique to aid in creating a high-resolution genetic map of Down Syndrome phenotypes based on analyzing 30 subjects who carry rare segmental trisomies of different regions of chromosome 21[229]. This research group mapped segmental trisomies at exon-level resolution to find regions of the genome that cause 8 different phenotypes associated with Down Syndrome[229]. This study shows the advantages of using advanced genomics with a rare patient population to study copy-number variation and complex diseases that was not previously feasible.

In addition to FISH, there are array-based molecular-based technologies for aneuploidy detection. Array-based technological advancements in PGT-A chromosome testing have included array comparative genomic hybridization (aCGH) and single-nucleotide polymorphism arrays (SNP-arrays). These techniques

use whole genome amplification (WGA) of genomic DNA which has the potential to introduce small sample quality issues with potential defects in testing these samples[55]. Following WGA, aCGH works by loading the fluorescently labeled amplified DNA and reference DNA to a microarray where the DNA from the two sources then compete to hybridize to thousands of DNA probes associated with sequences on different chromosomes[55]. Following hybridization, the fluorescent signal is read, and a chromosomal copy number of the DNA is calculated based on the reference DNA[55]. In a study performed by Kan et al. of 220 amniotic fluid or chorionic villi samples, all but one triploidy case were concordant with conventional cytogenetic results and 7/220 samples also had copy number variants detected with aCGH that were not found in the cytogenetic results[230]. Large clinical cohort studies using microarray analysis have also been performed. Notable, studies by Shaffer et al. and Wapner et al. included 2858 and 4406 women, respectively[231,232]. In the report by Shaffer et al. it was found that microarray analysis was able to identify clinically significant genomic alterations in 6.5% of total cases with one or more abnormal ultrasound finding where most of these cases were less than the resolution of karyotyping[232]. Similarly, in the work by Wapner et al., additional, clinically significant cytogenetic information was also identified by chromosomal microarray analysis that was not present with karyotyping[231]. Large clinical studies, such as these, provide evidence for sub-stratification of specific anomalies that can be successfully detected by these forms of analysis.

aCGH has also been a widely used tool to analyze samples during PGT-A and many retrospective cohort studies have been performed comparing Next Generation Sequencing (NGS) and aCGH results during PGT-A since aCGH is a primary test performed while NGS continues to grow in its use in the field. One finding on a cohort study of 548 sample analyzed by NGS and 368 by aCGH was that there was a significantly higher implantation rate in the NGS group at 71.6% vs. 64.6% in the aCGH group[233]. Additionally the ongoing pregnancy/live birth rate for the NGS group was at 62% and again significantly higher than the aCGH group in this study at 54.4%[233].

SNP-arrays are another array-based analysis method for aneuploidy detection that use fluorescently labeled probes that bind to thousands of SNPs throughout the genome which is used to identify alleles which vary within a population – each person has 2 allele copies, one on each chromosome[55]. SNP-based testing has been utilized as a high-resolution genome scan during prenatal screening[234]. Parental DNA may also be used during SNP-array analysis to identify inherited DNA and help to recognize allele dropout where alleles do not amplify and are therefore undetected during analysis[235,236]. Faas et al. performed a study using a 250,000 SNP array and was able to identify microdeletions, inherited copy number variants, copy number variants with uncertain clinical relevance, and homozygous stretches through using this array-based method providing information beyond aneuploidy analysis[234]. Zimmermann et al. also performed targeted SNP-based analysis using cffDNA where five chromosomes in 145 samples that passed a DNA quality test were correctly called for a total of 725/725 correct calls.[237]. Additionally, Curnow et al. utilized targeted SNP-based analysis to identify triploid, unrecognized twin, and vanishing twin pregnancies[238]. The study included 30,795 clinical cases for NIPT for fetal whole-chromosome aneuploidies and successfully identified any previously unrecognized cases[238]. Another form of targeted chromosomal analysis is Digital Analysis of Selected Regions (DANSR™) assays. Juneau et al. used the DANSR™ targeted approach with microarrays and NGS and found that the microarray method provided faster and more accurate results for the cffDNA measurements[239]. Stokowski also performed targeted cfDNA analysis using DANSR™ with microarray quantitation and was able to identify 107/108 trisomy 21 cases, 29/30 trisomy 18 cases, and 12/12 trisomy 13 cases with a specificity of 100% for all chromosomes[240].

SNP-arrays are also used during PGT-A and have been found to be as accurate as metaphase karyotyping, which is the technical standard for chromosome analysis[241]. In a study performed analyzing 1,800 IVF cycles with 24-chromosome SNP-arrays, Simon et al. determined that SNP-based PGT-A could reduce the negative effects maternal age has on IVF outcomes[241]. They also found that through using their testing method, there was also no statistically significant difference in pregnancy outcomes between single embryo transfer and double-embryo transfer cycles[241].

7.3.2 Polymerase Chain Reaction-based technology

Polymerase chain reaction (PCR) has been the gold standard molecular-based test for many diagnostic fields from infectious diseases[242] to precision medicine[243]. It is an enzyme-driven process that can replicate a few copies of DNA molecules into large quantities because the amount of DNA in a starting sample is generally too low for accurate measurement[242]. Quantitative PCR (qPCR), quantitative fluorescence-PCR (QF-PCR), or real-time PCR, are all terms for different PCR-based tests for detection and quantification[243]. Table 7.3 provides pros and cons of PCR-based technologies that can be considered by researchers and clinicians. Researchers have used qPCR during PGT-A to provide a result within 4 hours and allow for the transfer of fresh embryos[55]. This has been done using multiplexed qPCR to amplify sequences on different chromosomes and calculate the chromosomal copy number efficiently with an error rate of 1%[55]. qPCR has been verified extensively for chromosomes with common aneuploidies including chromosomes 13, 18, 21, X, and Y. However, in one randomized control trial it was even shown that PGT-A using qPCR can be performed for all 24 chromosomes in a four-hour window with 41/42 samples consistent with karyotype diagnosis or 42/42 after a minimum threshold for concurrence is applied[244]. In another study by Scott et al. comparing IVF outcomes between groups who did or did not undergo PGT-A using qPCR, they found that the group with qPCR-based PGT-A had an implantation rate of 66.4% vs. 47.9% in the control group and delivery rates of 84.7% vs. 67.5% in the control group, showing a statistically significant difference[245].

Table 7.3: Pros and Cons Analysis of DNA-based Molecular Techniques.

Test	Pros	Cons
Polymerase Chain Reaction-based Technology	- Rapid testing option[55] - Can provide PGT-A results fast enough to allow for fresh embryo transfer[55]. - Digital PCR is a technically simple, relatively inexpensive, and easy to implement in diagnostic settings[246].	- PCR shows number of target DNA, not whole genome, which is biologically limiting[246]. - Not suitable for detecting segmental aneuploidies[247].
Sequencing-based Technology	- NGS has the highest genomic coverage for PGT-A and can even be used to identify partial aneuploidies and mosaic embryos[55].	- There can be a nonuniform distribution of sequencing reads aligned to a chromosome[249]. - Low genome coverage and high amplification bias as two

	- Can provide the power to statistically differentiate chromosome counts, even at lower fetal fractions[248].	problems associated with single cell genomics applicable to this testing[250].
Array-based Technology: aCGH and SNP arrays	- Whole-genome aCGH can even be performed and offers high resolution analysis of genomic alterations and copy number variations[230,251]. - SNP-based arrays can be used for triploidy and haploidy detection, embryo fingerprinting determination, and identification of the parental origin of the aneuploidy[241].	- Does not detect every genetic disease or syndrome[251]. - NGS has statistically significantly better implantation rates during PGT-A than aCGH[233].

QF-PCR has also been adapted for prenatal screening on large cohorts (7,720[252] and 9,080[253] prenatal samples) for trisomies 13, 18, and 21. Mann et al. reported that out of the 7,720 prenatal samples they tested, 97% of them received a report on the business day after the sample was received with no misdiagnosis for non-mosaic trisomies[252]. This shows how PCR-based technologies can provide answers quickly and accurately. QF-PCR has also been used for rapid prenatal testing by targeting segmental duplications in the genome, known as SD-QF-PCR[254,255]. This procedure co-amplifies sections of DNA duplicated within the genome on two different chromosomes using a single pair of fluorescent primers. The two chromosomes read as two different sizes when analyzed by capillary electrophoresis[254] or melt curve analysis[255] and result in a relative dosage to determine aneuploidy samples. Digital PCR (dPCR) is another form of PCR that can be used in prenatal testing for aneuploidies such as trisomy 21 using cffDNA[256]. dPCR utilizes multiplex PCR analysis on diluted nucleic acid samples whose positive amplification signal is read as single template molecules[256]. This is then used to determine the template concentration in the original samples while not relying on dose-response relationships like reporter dyes used in qPCR[256]. A study by Lo et al. showed that through using digital PCR on noninvasive trisomy 21 testing, they were able to accurately detect trisomy 21 in samples containing 25% fetal DNA in 2007, where current digital PCR technology can analyze samples at less than 4% fetal DNA[256,257]. In a study by Tan et al. they showed dPCR can be used for multiplex droplet dPCR during NIPT using universal locked nucleic acid probes to test for fetal

aneuploidy[258]. They were able to accurately diagnose 60/60 clinical maternal plasma samples using their accessible, cost effective method[258]. El Khattabi et al. also validated their dPCR methodology using multiplex PCR to show the correct function of their probes for technical optimization followed by validating clinical samples for trisomy 21 with fetal DNA fractions as low as 5%[246].

7.3.3 Sequencing-based technology

Following the completion of the Human Genome Project in 2003 sequencing has taken over many diagnostic fields including those related to aneuploidy. NGS is one form of sequencing that has drawn attention because of the amount of detailed information it provides about the genomic sample[259]. Table 7.3 also includes pros and cons of sequencing-based technology as it is considered for genomic analysis during aneuploidy detection testing. The procedure for NGS on Illumina platforms uses whole genome amplification (WGA), DNA fragmentation, then library preparation which involves adapter ligation and PCR amplification[55]. Examples of WGA techniques that are used to perform copy number variation detection on single or limited cell numbers, including aneuploidy detection, are PicoPLEX DNA-Seq, DOPlify, REPLI-g, and Ampi-1 WGA[260]. These methods, and others vary in amplification technique (i.e. multiple displacement amplification vs. PCR), genome coverage, representation bias, error rates, yield, and robustness[260]. Following DNA library preparation and sequencing, the data is analyzed by comparing the result to a reference genome where researchers are able to gather the chromosomal copy number information and aneuploidy diagnosis[55]. With the continued technological expansion of NGS, Fiorentino et al. were able to develop a method for 24-chromosome aneuploidy screening for use in PGT-A[261]. A retrospective study was performed to compare the NGS-based method to existing karyotyping of single cells or array comparative genomic hybridization (aCGH) data[261]. They found a NGS specificity for aneuploidy call or individual chromosome copy number reading of 99.98% and a sensitivity of 100% as well as a specificity and sensitivity of 100% for aneuploid embryo calls[261].

NGS has also been used in PGT-A with human embryonic blastocoel fluid (BF) or blastocyst culture conditioned medium (BCCM) as a starting sample instead of a TE biopsy[262]. BF is fluid found inside the embryo that can be aspirated out and is less invasive than a biopsy because no cells are removed while

BCCM is fluid found in the culture plate during IVF and can be easily collected for sample analysis[263]. The retrieval of BF and BCCM is less invasive and technically challenging than a TE biopsy making it easier and more cost effective to use for testing[262]. In one example, results of NGS with these starting samples from Kuznyetsov et al. show 47/47 of the samples amplified successfully and the concordance rate of whole chromosome copy number per sample between this method and using TE biopsies as a starting sample was 100% and 98.2% per single chromosome[262]. In another, more recent, study by Kuznyetsov et al. using cell-free embryonic DNA found in spent embryo culture medium (SCM) and BF, the concordance rate per sample for ploidy status compared to the TE biopsy was 97.8%[264]. These alternative starting samples for PGT are known as non-invasive PGT, or niPGT. In a recent review of the implications of this form of sample testing for PGT, it was found that BF or SCM can offer DNA suitable for genetic analysis but there are still mixed conclusions regarding whether it can consistently provide accurate clinical diagnostic information[265]. Li et al. found the results of their analysis with SCM differed from the TE biopsy samples[266] and Jiao et al. reported 90% and 86% clinical concordance between BCCM and TE biopsy, respectively, compared to the blastocyst-stage embryo[267]. Several other studies have also used BF or SCM for niPGT-A using NGS and found different levels of success with these alternative starting samples[263,266,268-272]. While there are many economic and practical reasons for testing from these samples, the reliability, concordance of genetic results with that of the embryo, and DNA quality all pose issues and support the need for further analysis of this starting sample[265]. Lastly, the sensitivity and specificity of NGS for PGT-A has also been helpful in detecting chromosomally mosaic embryos which have two or more cytogenetically distinct cell lines[273]. High resolution NGS is sensitive enough to detect mosaicism when 20% or more of the cells in the biopsy are aneuploidy – meaning 1 of 5 cells in a 5-cell biopsy[55].

NGS has also been used in prenatal screening to count or genotype different cffDNA fragments, even at lower fetal fractions[248]. The fetal fraction is the fraction of cell free DNA that originates from the fetus/placenta as opposed to the maternal cell free DNA that is always circulating[248]. More specifically, cffDNA comes from cytotrophoblastic cells in the placenta where apoptosis is a main mechanism controlling the release of fetal DNA[274]. Using NGS, cfDNA is aligned to each chromosome in order to

determine these important counts[249]. Researchers have noticed cases of nonuniform distribution of sequencing reads aligned to a chromosome which they hypothesize is related to the GC content of the cfDNA which affects PCR and bridge amplification on Illumina platforms[249]. Regardless of these problems, NGS-based technologies such as VeriSeq™ (Illumina, Inc., San Diego, CA) have been used to screen pregnant women for fetal aneuploidy of chromosomes 21, 18, 13, X, and Y at a minimum 10 weeks gestation with only 2-hours of hands-on time for a technician[61]. The MiSeq and NextSeq platforms from Illumina (San Diego, CA) have also been successfully used with cffDNA for aneuploidy detection with a 10.9% failure rate in 3,594 MiSeq cases and 8.7% failure rate in 1,000 NextSeq cases[275]. Targeted NGS has also been utilized to analyze selected genomic regions of interest for NIPT[276]. In a report by Koumbaris et al. a blind study showed 100% diagnostic sensitivity while being more cost-effective as an NGS-based method for NIPT[276]. Overall, NGS is a powerful tool that provides specific chromosomal copy number analysis and is only predicted to grow in its use for aneuploidy detection.

7.3.4 Bioinformatic methods to study aneuploidy

Aneuploidy diseases can also be studied using bioinformatic techniques, such as genome-wide association studies (GWAS), that depend on molecular-based technologies and are able to analyze genetic samples to learn more about diseases. In late 2019, Chernus et al. published the first GWAS to identify genes associated with maternal nondisjunction of chromosome 21 as a way to investigate predisposing factors to this aneuploidy causing error[277]. The study utilized genotyping of 749 live birth offspring with trisomy 21 and 1,437 parents to identify mothers with nondisjunction errors in their oocyte[277]. The GWAS analysis found many new potentially associated loci with nondisjunction errors and candidate gene analysis was also performed which found candidate genes that were strongly associated with maternal nondisjunction of chromosome 21[277]. This study goes beyond detecting aneuploidy and aims to learn more about what may cause aneuploidy embryos so that the knowledge on this genetic irregularity can continue to expand and help inform patients. Additionally, other studies have also used GWAS and candidate gene analysis to investigate different phenotypes associated with aneuploidy-related diseases such as Alzheimer's disease[278,279], congenital heart defect[280], and Down syndrome-associated atrioventricular septal defect

which is a heart abnormality people with Down syndrome have a 2000-fold higher risk of having[281]. More recently, Starostik et al. even used published single-cell RNA sequencing data of 74 human embryos to better understand aneuploidy during early human development[282]. This bioinformatic analysis uncovered mosaic aneuploidies in 59/74 samples and by reconstructing histories of chromosome segregation found 55 samples had mitotic aneuploidies and 23 had meiotic aneuploidies[282]. One more finding from this study was that aneuploidy cells up-regulated immune response genes and down-regulated proliferation, metabolism, and protein processing genes[282]. Studies such as these that dive deeper into the genetics of people or families with Down Syndrome or other aneuploidy diseases can lead to a lot of progress in the understanding of these fields and data collected during NGS.

7.4 Engineering-based approaches for detecting aneuploidy

In addition to molecular-based improvements to aneuploidy testing, there have been many advancements to the engineered technologies that have been used in conjunction with the molecular tests. Here, we present some of the advancements in fluidic, mechanical, and electrical engineering work that has contributed immensely to the field of aneuploidy detection.

7.4.1 Microfluidic-based approaches

Microfluidic technologies involve controlling and manipulating fluids and particles at the micrometer scale and have numerous benefits compared to working with larger volumes which are outlined in Table 7.4[283]. Microfluidics have been explored for scientific and technological advancements in aneuploidy detection for human assisted reproduction, and mammalian gamete and preimplantation embryo biology[284]. However, there is currently no microfluidic-based technique for TE biopsy genetic analysis during PGT-A[284]. Nevertheless, there are currently multiple non-invasive, microfluidic-based techniques that analyze biochemical signals to aid in embryo selection during IVF, as opposed to using genetic analysis[284]. One study by O'Donovan et al. used a microfluidic chip to monitor oxygen consumption of embryos to assess their metabolism and aid in embryo selection prior to implantation during IVF[285]. While this is not a genetic-based aneuploidy detection method, it is still used to assist in the embryo selection process to increase the chances of a successful pregnancy, just as aneuploidy testing does.

Table 7.4: Pros and Cons Analysis of Engineering Techniques.

Test	Pros	Cons
Microfluidic-based approaches	Smaller sample and reagent volumes, rapid sample processing, increased sensitivity, lower cost, enhanced portability, and the capability to be integrated and automated which can reduce human intervention and error[283].	Currently no microfluidic-based technique for TE biopsy genetic analysis during PGT-A.
Automated technology	Automatic sample preparation, reactions, and analysis save a lot on hands on labor time[286]	Limited use of automation in the field of automated sample preparation for PGT-A as no current technology is filling this need.

Meanwhile, microfluidic devices have been utilized in prenatal testing for fetal aneuploidy detection. For example, Fan et al. designed a microfluidic digital PCR system to be used for rapid, allele independent molecular detection of aneuploidy using amniocentesis and CVS starting samples[287]. Microfluidic digital PCR was able to accurately detect 40/40 fetal trisomy cases across chromosomes 21, 18, and 13 with each detection taking under six hours[287]. Conversely, Winter et al. used a slanted inertial microfluidic device to isolate circulating extravillous trophoblasts from maternal peripheral blood during prenatal testing[288]. With between 1 and 5 of these fetal cells per milliliter of blood, their microfluidic device was able to enrich for this rare cell type with 79% recovery and perform successful aneuploidy detection[288].

Additionally, Ho et al. created a microfluidic-based same-day prenatal diagnostic FISH assay chip[289]. Nanostructured titanium dioxide coated the chips to facilitate cell adhesion thus pretreatment and hybridization occurred in the microchannels of their device with on-chip detection showing results concordant with off-chip karyotypes within 3 hours of sampling using 20-fold less probes within the microfluidic FISH system[289]. One more microfluidic-based system for aneuploidy analysis utilizes silicon-based nanostructured microfluidics for capture of circulating fetal nucleated red blood cells (fnRBC) and extravillous cytotrophoblasts (EVT) for noninvasive prenatal testing[290]. Huang et al. used specific antibodies in conjunction with the microfluidic system for efficient capture of the targeted cells in maternal blood, 14-22 fnRBC/4 mL and 1-44 EVT/4 mL[290]. Samples then went through genetic analysis for diagnosis using a variety of techniques including FISH, aCGH, and NGS. Microfluidics have been used in the

development of rapid molecular prenatal diagnostics since microchips have the ability to save time and costs by reducing the amount of reagents used, protocol times because reagents are more concentrated in microchannels, and thus turnover times for results[289].

7.4.2 Automated technology

Automation has also provided important benefits to the progress of technological and engineering advancements in aneuploidy detection. Numerous research and commercial labs have been pursuing advancements related to automated sample analysis using techniques like NGS in prenatal screening and PGT-A during aneuploidy testing[291]. Other groups are still investigating alternative ways to automate sample preparation, detection, and analysis though. One alternative automated prenatal screening option has been contributed by Van Opstal et al. that uses multiplex ligation-dependent probe amplification (MLPA) with one PCR reaction for quick, easy, automated DNA isolation and multiplex analysis of amniotic fluid samples[286]. They found 100% sensitivity and specificity for common aneuploidies using this automated technique compared to FISH karyotypes[286]. Their method used automatic sample preparation, reactions, and analysis saving a lot on hands on labor time[286]. Automated microscopy has also been used in FISH analysis[292] and to analyze circulating fetal cells as a potential for chromosomal analysis[293]. Automated FISH analysis was implemented because the manual process is both expensive and labor intensive requiring a high skill level and subjective interpretation of signals[292]. Wauters et al. developed an automated FISH examination platform for amniotic fluid cells and was able to correctly diagnose 146/146 samples compared to karyotype results with three aneuploidy cases[292]. More recently, cfDNA has also been subjected to innovations in automated analysis using NGS during NIPT[294]. Crea et al. utilized the Ion Proton sequencing platform to screen for fetal trisomy 13, 18, and 21 with 100% sensitivity and specificity for 110 samples[294]. CfDNA has also been incorporated into an automated, digitally enabled assay for aneuploidy screening by Dahl et al. who used molecular probe technology to label target chromosomes then enriched for single molecules for imaging by passing them through a nanofilter[295]. They classified 30/30 trisomy 21 pregnancies correctly using their core Vanadis NIPT assay[295] and are affiliated with Vanadis Diagnostics,

a PerkinElmer company, showing the translation of this form of automated screening from research labs to larger biotechnology companies.

7.5 Challenges and considerations for the field of aneuploidy detection during pregnancy

7.5.1 Fetal Fraction during NIPT

The field of aneuploidy detection has had numerous advancements over the lifespan of this form of testing. With these advancements though have come many challenges which continue to push research in the field forward. One of the first challenges that may be faced in PGT-A and prenatal testing is retrieving a starting sample that is large and pure enough for accurate analysis. Although simple to retrieve, one of the more challenging starting samples to use for testing has been cffDNA during NIPT. This is because the average fetal fraction of cffDNA in maternal plasma can be less than 3% to up to 30%, with an average range of 10-15% between 10 and 20 gestational weeks[248]. Many studies have shown that accuracy in testing results increases as fetal fraction increases and that samples with fetal fractions of less than 3-4% are not suited for aneuploidy screening tests[248]. In order to detect a trisomy sample, the method must be able to distinguish a 50% increase in the amount of cffDNA from a specific chromosome which has placed many limitations on detection methods since it is challenging to identify this difference in the fetal DNA when the fetal fraction is such a small percentage. There are many biological influences on fetal fraction from both fetoplacental and maternal factors[63]. Fetoplacental influences on fetal fraction include gestational age, crown rump length, mosaicism, fetal aneuploidy, triploidy, and multiple pregnancy[63]. Maternal factors that affect fetal fraction consist of maternal weight, maternal autoimmune disease, low molecular weight heparin, assisted reproductive technology conception, maternal age, and more[63]. Many researchers have identified maternal weight as one of the most clinically significant influences on fetal fraction due to there being a fixed amount of fetal DNA in maternal plasma but an increased maternal weight increases the maternal circulatory volume thereby diluting the cffDNA in the system[63,248]. Vora et al. even reports that total cfDNA in maternal plasma at the time of the baby's birth is directly proportional to the mother's body mass index (BMI)[296]. This indicates that an increase in the total amount of cfDNA will also decrease the fraction of cfDNA that originates from the fetus (cffDNA) further complicating aneuploidy testing by

decreasing the starting sample[296]. Another factor that can alter the analysis of cffDNA is maternal malignancy which can affect the copy number variation profile in NIPT[297,298]. Cell-free tumor DNA can be detected in plasma just as cffDNA is during NIPT[298]. Tumor DNA can include duplications and deletions across the genome which can then alter the ratios between patient and reference DNA and provide test failures or unusual results[298]. A systematic review of literature reporting about false positive or false negative NIPT results showed that 15% of the explained false positive cases were due to maternal malignancy out of the 22 studies with 206 discordant cases analyzed[299]. This figure does not directly reflect true clinical frequency but identifies maternal malignancy as a potential reason for false positive NIPT[299].

7.5.2 Embryo Mosaicism

Another sample related factor that can impact aneuploidy detection during prenatal screening or PGT-A is the degree of mosaicism a sample has. Mosaicism occurs when there are both normal and aneuploidy cell lines in one embryo[208]. In NIPT, mosaicism will affect the sensitivity and specificity of screening, and in PGT-A mosaic embryos show decreased implantation rates and increased miscarriage rates compared to euploid or healthy embryos[55,63,248]. During PGT-A, the two cell types in one embryo can often cause aneuploidy misdiagnosis since a cell biopsy taken at an early stage may not accurately represent the ploidy status of the cells in the whole embryo[208]. According to previous studies on PGT-A, it was suggested that more than one cell should be biopsied for correct diagnosis[300], which is important since the prevalence of mosaicism has been reported to be as high as 20% of the embryo[301]. In a study by Gleicher et al. mathematical modeling was even employed to predict that a biopsy of at least 27 trophectoderm cells is needed to reach minimal diagnostic predictability[302]. The two models presented in the study assume that there is an even distribution of mosaicism in the trophectoderm, although mosaicism is usually clonal, and challenge the clinical utilization of current PGT-A sampling which generally use a six-cell biopsy[302].

Reciprocal errors are another biological challenge associated with mosaicism that must be overcome which involves one monosomy cell line for a chromosome and one trisomy cell line for that same chromosome in one embryo. In this case, when the sample is pooled together to be analyzed at once, these aneuploidies would go undetected by cancelling each other out and lead to a false-negative aneuploidy diagnosis[301].

There are also analytical challenges associated with mosaicism as statistical smoothing and copy number assignment algorithms are generally not updated to accurately call out mosaic chromosomes[301]. Additionally, there limitations regarding how to translate information about mosaicism to the clinic so that patients can understand the effects of particular chromosomal mosaicism on implantation, miscarriage, and having a healthy child[211,301]. Groups such as the Practice Committee of the *American Society for Reproductive Medicine (ASRM)*, *Genetic Counseling Professional Group (GCPG)*, *Preimplantation Genetic Diagnosis International Society (PGDIS)*, and *Society for Assisted Reproductive Technology (SART)* have all worked to provide statements or reports regarding the clinical management of mosaic and aneuploidy embryo transfer to address these limitations [303-305]. There have also been alternative statements presented in response, for example by the *International Do No Harm Group in IVF (IDNHG-IVF)* regarding concerns of increasing added procedures to IVF[306]. In addition to statements by groups or professional societies, continued research has been pursued regarding the safety of these embryo transfers by groups including Grati et al. who devised an evidence-based scoring system for prioritizing mosaic aneuploid embryos for transfer[307]. Overall, the attention to this topic further emphasizes the need for efficient, accurate diagnostic technology with targeted answers relevant to the clinic especially as more clinics are choosing to transfer mosaic embryos if patients do not have any euploid embryos they can transfer and they cannot undergo another cycle of IVF[55].

In prenatal diagnosis, chromosomal mosaicism presents a similar challenge during screening and often appear as full aneuploidies[308]. Depending on the prenatal testing performed, it is possible to find true fetal mosaicism (TFM) or confined placental mosaicism (CPM). Amniocentesis can be used to diagnose TFM while a test like NIPT could find TFM an CPM[308]. One problem with CPM is that in around 1% of cases, the CPM result would show an aneuploidy cell line based on reading cytotrophoblasts during cffDNA testing, while the fetus does not, causing in a false positive result[308]. Overall, mosaicism needs to be considered in both PGT-A and NIPT prenatal testing especially to make sure that patients are receiving accurate results.

7.5.3 Economic Considerations

In addition to challenges related to the samples being tested, another major challenge associated with aneuploidy detection and patients' access to testing is cost. Since the American College of Obstetricians and Gynecologists (ACOG) has advised that all pregnant women are offered prenatal screening for fetal aneuploidy, the majority of women do receive this testing, at least in the United States[218]. As there are a variety of prenatal tests that can be performed, test selection depends on factors such as a woman's prior risk, stage of pregnancy, access to healthcare services, cost, as well as patient preference[309]. The economic concerns related to offering specific types of testing has been investigated by many different groups since different tests incur different costs based on reagents and equipment needed as well as the amount of time the test takes. Gekas et al. investigated the cost-effectiveness and detection of Down Syndrome using rapid testing vs. karyotyping and found that rapid testing methods can detect common aneuploidies faster and are less expensive than karyotyping[310]. Through comparing the global costs of karyotyping and QF-PCR, the authors found on average karyotyping cost 0.97 million Canadian dollars more per year than QF-PCR over a variety of screening strategies[310]. Additionally, they found the cost-effective ratio – net cost divided by changes in health outcome – for QF-PCR was $24,084 per Down Syndrome detected, vs. $27,898 for karyotyping[310]. From this information, the authors even suggested that it may be appropriate to question the additional costs of karyotyping, which may be especially important in the United States where guidelines recommend karyotyping be performed as a follow up to a rapid aneuploidy diagnosis (RAD) when needed. Additionally, with prenatal testing Song et al. also studied the clinical and economic consequences of fetal trisomy 21 screening with NIPT using cfDNA in high-risk pregnancies[311]. When comparing NIPT to first trimester screening (FTS) and integrated screening (INT), which both look at serum markers, they found NIPT was more clinically effective at detecting trisomy 21 and less costly than the other two options even at a base price of $795[311]. Kaimal et al. also had a similar finding that for women 40 years or older, using cfDNA for primary screening is both optimal and cost-effective with a cost-effective ratio of $73,154 per quality-adjusted life-year[312]. Lastly, one more study done by Benn et al. corroborated the economic benefits to using NIPT for screening over other techniques[309]. They evaluated the economic value of replacing

conventional fetal aneuploidy screening with NIPT and found that it would reduce healthcare costs if it could be performed for $744 or less in the general pregnancy population[309].

Investigating costs and cost-benefit analysis is just as important when it comes to IVF and PGT-A. IVF treatment numbers have increased fourfold over the last 20 years to 160,000 treatment cycles annually as of 2018[313]. At an out-of-pocket cost ranging between $10,000 and $15,000 per treatment cycle, many states in the United States are turning to policy changes to mandate insurance coverage which would reduce prices to $2,000 to $3,000[313]. Unfortunately, with the large cost of IVF on its own, cost also remains a significant limiting factor to using PGT-A in every IVF patient[55]. Although these forms of testing can add an additional cost burden, Neal et al. found that it is actually more cost-effective over time for IVF patients with more than one embryo to perform PGT-A than it would be to use other non-genetic based tools to select an embryo for implantation[213]. With 8,998 patients from 74 IVF centers, the study found that using PGT-A could save $931 to $2,411, depending on the number of embryos screened[213]. Additionally, performing PGT-A reduced the treatment time by up to four months and these patients experienced fewer failed embryo transfers and clinical miscarriages[213]. Colins et al. also had a similar result from their decision analytic model for using PGT-A during IVF to increase live birth rates in women over 37[314]. They found that the cost of only IVF was $19,415 per cycle with a live birth rate of 13.4% and an incremental cost-effective ratio of $145,063[314]. This compared to when preimplantation genetic screening was also performed during IVF which increased live birth rates by 4.2% at an additional cost of $4,509, leading to an incremental cost-effective ratio of $105,489 per additional live birth[314]. Thus, although there is a cost associated with these additional techniques, it is important to consider the cost benefits patients will see over time, especially in reducing treatment times and improving results.

7.5.4 Social implications of testing

Another important consideration for challenges in the field of aneuploidy detection are the social implications associated with the testing. While ensuring safe and accurate tests is important, it is just as imperative to consider the affect this testing could have on people both physically and mentally. In 2019 Labonté et al. performed a scoping review of the evidence on psychological and social consequences to

performing NIPT[221]. Findings of this studied showed short term anxiety for women decreased with a negative NIPT test result and that regret associated with decisions made was generally low[221]. Conversely, Green et al. found that up to 30% of women with a positive aneuploidy result showed regret about performing a screening test[315]. One interesting note from Labonté et al. was that there remains to be a study on the long term effects of NIPT or on woman's partners' outcomes as the short term effects of the testing are currently the only metric being investigated[221]. This is a place where the field can continue to add value and important results for parents before they undergo these procedures.

Another social implication of this prenatal testing, specifically NIPT, is learning the sex of the baby which could expose societal issues where one sex is preferred over the other[316]. Farrell et al. utilized focus groups of pregnant women and women who had delivered in the past year to learn more about their opinion on this capability of NIPT among other factors[317]. They found that there were cases where women did not know they would learn the sex of the fetus from NIPT until they were asked if they wanted to know where others wanted NIPT specifically to learn the fetal sex[317]. One participant in the study cautioned that expecting mothers should be made aware of the purpose of the testing and the possibility of learning about genetic abnormalities from the testing[317].

This idea brings up an important point that as aneuploidy detection technology continues to advance, it is suggested by more doctors, and more patients are getting testing, it is also important that the level of education and counselling for this testing also grows. This counseling should specify the risks, benefits, and limitations of each kind of screening or diagnostic test so that pregnant women can make the best decision for their health and their baby's. As there may be a perceived pressure to undergo NIPT or other testing based on recommendations, this is even more of a reason why a realistic scope of the psychological and social consequences should be fully expressed before testing[221]. In addition to the educational value of this counseling, it also allows for reproductive autonomy. In a 2009 Research Highlight by Nature Review Genetics, the authors argue that prenatal testing is unique in that there is currently no cure to the genetic conditions being tested for and diagnosed; thus, they pose that the mother's only options are to "accept the child's impairment or to terminate the pregnancy"[318]. While testing for aneuploidy is an important tool, the

reproductive autonomy it provides also poses a third option for pregnant mothers which is to not perform the testing to begin with. With the use of informed consent, where women need to provide permission to perform this testing, this should always be an option, although it has been found that it often is not as these tests have become more routinized[318,319]. When given the option to undergo testing a cohort study published in 2016 shows that with more than 28,000 pregnancies screened with cfDNA, less than 40% of those women who screened positive chose to have invasive prenatal diagnosis as a follow up test[200]. In the Netherlands when a nationwide implementation study on NIPT, called TRIDENT-2, was offered as a first-tier test for all pregnant women in 2017, only 42% of women selected to undergo the testing[320]. These statistics, and many more show that a women's decision for testing during pregnancy cannot be assumed. It is the job of researchers, clinicians, and genetic counselors to provide a thorough analysis of benefits and risks for patients for different testing options so that they can best understand how this testing is meant to be helpful and informative regarding the health of their child if they choose to undergo testing[319]. Additionally, results of the testing must be managed since many gene variants with unclear or unknown significance (known as "variants of uncertain significance") during DNA sequencing of an unborn fetus can provide information to patients that is difficult to interpret[319]. As there is currently an insufficient number of experts in prenatal genetics to counsel all pregnant women pre- and post-testing this further emphasizes the need for more educational resources and informed consent[319].

In the case that a screening or diagnostic test does lead to a positive aneuploidy result, this testing can give women and families the opportunity to seek out support and references as soon as possible. Resources such as the National Down Syndrome Society (NDSS) is one example of a support network for disabilities caused by aneuploidy. NDSS provides access to Down Syndrome parent support groups with more than 375 affiliates as well as advice for parents when learning of a positive Down Syndrome diagnosis. Other resources such as Dads Appreciating Down Syndrome (D.A.D.S.) is specific to fathers of Down Syndrome children, Know Me First which has educational resources for parents when they receive and Down Syndrome diagnosis, and so many others are available. Knowledge of these resources can be just as important as knowledge of different forms of testing during pregnancy and can help mothers being tested

too. Overall, this testing has the ability to inform and empower expecting mothers by advising them regarding their child's health and tools and resources out there that they can look to for support, helping not only babies, but women.

7.6 Conclusion

This review paper analyzed a variety of different sample collection and analysis techniques for PGT-A and prenatal testing for aneuploidy, specifically focusing on laboratory-based technologies. While CVS and amniocentesis are extremely accurate diagnostic procedures, the invasive nature of these techniques and chance for miscarriage has pushed the field toward NIPT as a highly accurate screening tool. Although challenges have been exposed for NIPT such as low fetal fractions and mosaic embryos, economic considerations show that this test is more valuable over other screening options. Additionally, with the growth in analysis tools such as dPCR and NGS, NIPT sample analysis will consistently improve as a reliable and safe testing method. This review also aimed to explain that the progress in engineering can go along with molecular analysis progress to decrease human interaction during testing and increase accuracy of results. Lastly, social implications were discussed in tandem with the scientific analysis to explain how education and genetic counselling are necessary in this field of science and medicine.

7.7 Acknowledgements

We would like to acknowledge the support for this review paper from leading researchers in prenatal screening and PGT-A from Brown University and PerkinElmer. The authors acknowledge financial support from Brown University and PerkinElmer.

CHAPTER 8

A microfluidic platform for high-purity cell free DNA extraction from plasma for non-invasive prenatal testing

---

Chapter 8 has been submitted as an original research article.

Lindsay Schneider[1], Thomas Usherwood[1], and Anubhav Tripathi[1*]

[1]Center for Biomedical Engineering, Brown University, Providence, RI, 02912

8.1 Abstract

Increase the yield and purity of cell free DNA (cfDNA) extracted from plasma for non-invasive prenatal testing (NIPT) as inefficiencies in this extraction and purification can dramatically affect the sensitivity and specificity of the test. This work integrates cfDNA extraction from plasma with a microfluidic chip platform by combining magnetic bead-based extraction and electroosmotic flow on the microfluidic chip. Various wash buffers and voltage conditions were simulated using COMSOL Multiphysics Modeling and tested experimentally. When performing the first wash step of this assay on the microfluidic chip with 300 V applied across the channel there was a six-fold increase in the A_{260}/A_{230} ratio showing a significant improvement (p value 0.0005) in the purity of the extracted sample all while maintaining a yield of 68.19%. These values are critical as a high yield results in more sample to analyze and an increase in A_{260}/A_{230} ratio corresponds to a decrease in salt contaminants such as guanidinium thiocyanate which can interfere with downstream processes during DNA library preparation and potentially hinder the NIPT screening results. This technique has the potential to improve NIPT outcomes and other clinically relevant workflows that use cfDNA as an analyte such as cancer detection.

8.2 Introduction

Cell-free DNA (cfDNA) is fragmented genomic DNA free floating in the blood and was first identified in 1948 by Mandel and Metais[321]. More than 70 years later, cfDNA is used as a key diagnostic or screening tool for a variety of purposes, notably for cancer and non-invasive prenatal testing (NIPT)[322,323]. NIPT is utilized to detect cfDNA in maternal plasma that originates from villous trophoblasts in the placenta and is released due to apoptosis and analyzed since DNA from this region contains the fetal DNA sequence, which is useful in determining information regarding the pregnancy[274,324]. Specifically, NIPT has been adopted as a mainstream, primary method for aneuploidy screening, testing for chromosomal counts, as an abnormal number of chromosomes, or aneuploidy, is a major factor in causing miscarriages, as well as fetal growth and cognitive disabilities[325-328]. NIPT is advantageous in that it does not utilize an invasive procedure for sample collection such as amniocentesis or chorionic villus sampling which have a small (approximately 1%) risk of miscarriage[329,330]. As a screening technique NIPT can indicate the likelihood of an aneuploid pregnancy and inform the need for further testing, rather than work as a definitive, diagnostic test, where invasive testing may still be needed[331]. Using massively parallel sequencing or single nucleotide polymorphism–based analysis for NIPT has been shown to have a high sensitivity and specificity for identifying and comparing chromosome-specific sequences to determine if aneuploidies – typically trisomies 12, 18, and 21 – are present[323,329,332-334]. However, problems still remain with false positive results in the NIPT test, limiting its diagnostic potential[331,335]. One problem contributing to false positive results within this testing is the small amount of cfDNA sample that can be extracted from plasma for aneuploidy analysis. Table 8.1 identifies the total amount of cfDNA found in plasma among several sources ranging from 1.8 ng/mL to 22 ng/mL. However, the starting sample suitable for fetal aneuploidy testing is smaller than the concentrations outlined in Table 8.1 because the amount of DNA containing the fetal genomic information is only a percentage of the total cfDNA. This percentage, known as the fetal fraction, consists of cfDNA originating from the villous trophoblast cells, known as cell free fetal DNA (cffDNA), which is approximately 13.4% of the entire cfDNA sample[329]. The challenges created by this limited sample are amplified further by the fact that the amount of cffDNA in plasma is constantly increasing throughout

gestation; therefore, the amount of cffDNA available for the tests that occur earlier in pregnancy is even smaller, especially since NIPT can be offered as early as week 10 of the pregnancy[336,337]. Consequently, optimized extraction techniques are essential to gather a large, representative sample of cffDNA, and ensure that the testing result is concordant with the true chromosome counts[329].

Table 8.1: An outline of total amounts of cfDNA in plasma using various sources and patient types. Conversion of copies/mL to ng/mL is based on nuclear circulating DNA copy number calculation282 and table assumes 1 genome equivalent = 1 copy.

Paper	Total cfDNA in Plasma	Patient Type	cfDNA Extraction Method
Perkins et al.[338]	7.4 ng/mL	Healthy patients	QIAamp DNA Blood Midi Kit (spin column)
Chang et al.[339]	6 ng/mL 16 ng/mL	Healthy patients Patients with non-malignant diseases	QIAamp DNA Blood Kit (spin column)
Meddeb et al.[340]	1.69×10^3 copies/mL (5.6 ng/mL) 1.48×10^3 copies/mL (4.9 ng/mL)	Healthy males Healthy females	Qiagen Blood Mini kit (spin column)
Antonatos et al.[341]	6873 genome equivalents/mL (22.8 ng/mL) 4112 genome equivalents/mL (13.6 ng/mL)	Acute Myocardial Infarction Patients	QIAamp Blood Kit (spin column)
Kamm et al.[342]	14 ng/mL	Healthy subjects	N/A: used fluorescence readings to determine concentration
Dennin et al.[343]	6 ng/mL	Healthy subjects	N/A: used electron microscopy technique
Fournié et al.[344]	10 ng/mL	Healthy subjects	Precipitation using ethanol
Gautschi et al.[345]	1.8 ng/mL	Healthy subjects	QIAamp Blood Mini kit (spin column)
Herrera et al.[346]	11 ng/mL	Healthy subjects	Blood DNA Mini Kit (spin column)
Jahr et al.[347]	3.7 ng/mL	Healthy subjects	QIAamp Blood Kit (spin column)
Jung et al.[348]	20 ng/mL	Healthy subjects	NucleoSpin Blood Kit, QIAamp DNA Mini Kit, QIAamp Ultrasens Virus Kit, High Pure PCR Template Preparation Kit (spin columns)
Lui et al.[349]	8.3 ng/mL	Healthy volunteers	QIAamp Blood Kit (spin column)
Silva et al.[350]	15 ng/mL	Healthy subjects	QIAamp Blood Kit (spin column)
Stemmer[351]	3-22 ng/mL	Healthy subjects	KingFisher silicate magnetic beads and a KingFisher ML robotic magnetic particle processor (magnetic beads)

CfDNA isolation from plasma has been thoroughly commercialized with nucleic acid extraction kits available from many major biotechnology companies, many utilizing solid-phase extraction techniques. Solid-phase extraction procedures typically involve a silica or magnetic bead solid phase, to which cfDNA is adsorbed. This is achieved by using chaotropic agents, such as guanidinium thiocyanate (GTC) or guanidinium isothiocyanate, which disrupt the spheres of hydration around DNA molecules and allow for binding to the solid phase[352-354]. This effect has been shown to occur both with silica and magnetic bead solid phases, both of which are used in commercial technologies (Table 8.2)[353,355-358]. These commercial kits come in two major categories: spin columns and magnetic bead extraction kits[359]. Spin columns have the advantage of high percent yields of cfDNA, but are more difficult to automate[360]. On the other hand, magnetic bead-based approaches have significantly lower yields, but are significantly easier to automate[170]. Both bench-based techniques are labor intensive, time consuming, and often require technical machinery to operate (Table 8.2) and the efficiency of these techniques may influence the amount of cfDNA that can be extracted[360]. Moreover, chaotropic agents such as GTC used in solid-phase extraction are proven to inhibit enzymatic reactions like polymerase chain reaction (PCR) which is a critical step in preparing DNA for next generation sequencing (NGS), known as library preparation[361]. This is important as analysis of cfDNA for fetal aneuploidy detection has relied heavily on NGS so ensuring the accuracy of library preparation is essential for the overall success of the screening method, which motivates the need for high purity and yield cfDNA extraction techniques[240].

Table 8.2: Outline of commercially available cfDNA isolation kits from plasma, with essential protocol information.

Kit Name	Incubation Temperature (°C)	Time to complete (approx. min)	Type of Beads	Details
QIAamp Circulating Nucleic Acid Kit (QIAGEN Cat #55114)	60, on ice	<120 for 24 preps	Silica-based	Vacuum pump
Plasma/Serum Cell-Free Circulating DNA Purification Midi Kit (Norgen Biotek Cat #55600)	60	90	Column	Centrifugation
QIAamp MinElute ccfDNA Mini Kit (Qiagen Cat #55284)	56	45	Magnetic beads (unspecified)	Centrifugation
Maxwell® RSC ccfDNA Plasma Kit (Promega Cat #AS1480)	Not specified	70	Magnetic Beads (unspecified)	A Maxwell® Instrument

MagMAX™ Cell-Free DNA Isolation Kit (Applied Biosystems™ Cat #A29319)	4 (centrifugation), 60 (incubation)	35	Dynabeads™ MyOne™ SILANE technology	Centrifugation
NextPrep-Mag™ cfDNA Isolation Kit (Bioo Scientific Cat #NOVA-3825-01)	55 (binding, elution)	25	Magnetic Beads (unspecified)	None
chemagic cfDNA 2k kit H24 (PerkinElmer Cat #CMG-1302)	Not specified	Not specified	M-PVA Magnetic Beads	chemagic 360/MSM I Instrument
Apostle MiniMax™ High Efficiency Isolation Kit (Beckman Coulter Cat #C40604)	60 (binding)	60	Magnetic beads (unspecified)	Centrifugation, several vortexing steps
Mag-Bind® cfDNA Kit (Omega Bio-tek Cat # M3298-01)	60 (proteinase K treatment)	75	Mag-Bind® Particles CH	Compatible with automated platforms
Cell-Free DNA (cfDNA) Purification Kit (Active Motif Cat #25503)	60 (proteinase K treatment)	75	Magnetic beads (unspecified)	None
cfPure® Cell Free DNA Extraction Kit (BioChain Cat #K5011610)	60 (proteinase K treatment)	75	Silica-coated paramagnetic particles	None

In addition to commercial options, there are microfluidic-based cfDNA extraction techniques, but they often require complicated calibration and specialized equipment (Table 8.3)[362-365]. For example, Campos et al. made a microfluidic-based platform using many microscale vertical pillars to act as a solid phase to facilitate solid-phase extraction of cfDNA[363]. Despite several advantages, this technique has the disadvantage of requiring precision manufacturing for producing the mold for microfluidic chip fabrication[363]. Additionally, Perez-Toralla et al. also provides a microfluidic platform to isolate cfDNA using a magnetic bead solid phase[364]. However, this technique requires careful balancing of hydrodynamic and magnetic forces in a continuous-flow system to be effective[364]. To address these drawbacks and those of other researchers (Table 8.3), this study aims to fill a need in this research area for a simple, fast, and potentially high-throughput method for cfDNA extraction from maternal plasma. To do this, a solid-phase extraction-based approach is used to maximize the workflow's simplicity and potential for automation. Using a workflow based on the commercially available Bioo NextPrep cfDNA extraction kit's bench-based extraction protocol, a streamlined process was created using a polydimethylsiloxane (PDMS) microfluidic chip. The magnetic bead-based extraction assay is integrated onto the microfluidic chip platform which also incorporates an electric field to increase the purity of the extracted sample. While liquid phase isolation often relies on

electrophoresis or dielectrophoresis to force negatively charged DNA to migrate, this microfluidic chip utilizes electroosmotic flow (EOF) to force unwanted contaminants within the buffer to migrate away from the DNA captured on the magnetic beads as they are moved through the chip[15]. COMSOL Multiphysics® Modeling Software 5.6 (COMSOL Inc., Stockholm, Sweden) was used to study the applied electric field and EOF on the microfluidic chip, and validation and testing of the device was performed using AcroMetrix EDTA Plasma, where model cfDNA was added then re-extracted using the microfluidic system to evaluate DNA yield and purity. While this electrokinetic microfluidic device has a wide range of applicability outside prenatal testing in fields such as cancer detection from bodily fluids, this is the first time it has been used for NIPT.

Table 8.3: Select microfluidic platforms used for cfDNA isolation from plasma.

Authors	Advantages	Disadvantages
Perez-Toralla et al.[364]	• Performs sample preparation and detection on one device • Adaptable for different magnetic beads for different extraction procedures • Compatible with many DNA amplification techniques for analysis of DNA	• Requires sensitive balance of electric field with flow through microfluidic chip • Need to recirculate the magnetic particles to maximize the DNA capture • On-chip extraction is time consuming due to fluid flow at up to 1 μL/min
Campos et al.[363]	• High recovery of cfDNA-size DNA fragments • Fewer processing steps compared with commercial kits • Process can be scaled up	• Creating a mold for the microfluidic chip requires high precision manufacturing • Requires very low flow rates • Chip requires activation with UV/O_3
Gwak et al.[362]	• Requires a small volume of wash buffers • Reduction in sample losses compared with commercial kits	• Fairly long processing time • Requires a complex microfluidic chip system (with magnets and a continuous flow of buffers)
Yang et al.[365]	• Does not require syringe pump, just works on electric power • Quick extraction/detection time • Requires small sample volume	• Requires a complex microfluidic chip with multiple layers

8.3 Methods

8.3.1 Microfluidic chip design and fabrication

Soft lithography was used to fabricate the PDMS microfluidic chips used in this study. A Sylgard 184 elastomer base and curing agent (Ellsworth Adhesives, Wilmington, MA, USA) were mixed in a 10:1 ratio by mass and placed in a vacuum chamber to dissolve all air bubbles for 40 minutes. The PDMS-curing agent mixture was next poured onto an SU-8 mold pattern fabricated by photolithography. The design for the microfluidic chip, and thus the design on the SU-8 mold, was created using SOLIDWORKS (Dassault Systèmes, Vélizy-Villacoublay, France). The PDMS was set to cure for 1.5 to 2 hours at 70 °C, and after curing was complete, the PDMS was separated from the SU-8 mold. Four reagent wells were made per separator on the microfluidic chip using a hole punch to create each well (Figure 8.1). The internal diameters of the hole punches used were 2.5 mm, 1.2 mm, and 6 mm for the sample input well, electrode wells, and sample output wells, respectively. The larger well size for the output well was selected so that all the cfDNA-bound magnetic beads could be moved through the channel and easily collected since they are at a high concentration. The PDMS was then cleaned with isopropanol, dried with nitrogen gas, and bonded to a 1mm-thick glass slide using a plasma wand on both the PDMS and glass before pressing the two materials together. This bond was reinforced by placing the prepared microfluidic chip in the 70°C oven for at least 20 minutes before using it for subsequent testing.

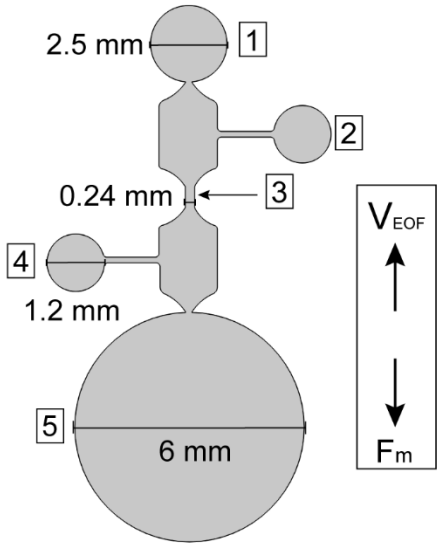

Figure 8.1: Design of one separator on microfluidic chip used for cfDNA extraction which utilizes opposing magnetic bead movement based on the force the external magnet exerts on the magnetic beads (Fm) and electroosmotic velocity (v_{EOF}) caused by the EOF-induced fluid movement of the wash buffer. Microfluidic chip labels: (1) Sample input well. (2) Negative electrode well. (3) Center channel where v_{EOF} is the highest. (4) Positive electrode well. (5) Sample output well.

8.3.2 DNA Sample for cfDNA extraction

Validation testing for the microfluidic platform for cfDNA extraction from plasma for NIPT was performed using a 149-base pair (bp) DNA amplicon as a model cfDNA sample. The model cfDNA was produced using One*Taq* 2X Master Mix with Standard Buffer and M13mp18 RF I DNA (New England Biolabs, Ipswich, MA, USA) with the forward primer sequence 5'- CGC CAG GGT TTT CCC AGT CAC GAC - 3' and the reverse primer sequence 5' – AGC GGA TAA CAA TTT CAC ACA GG - 3' (Integrated DNA Technologies, Coralville, IA, USA). The model cfDNA was added to AcroMetrix EDTA Plasma Dilution Matrix (ThermoFisher Scientific, Waltham, MA) at various amounts (ng) to create model human plasma samples for testing. The model human plasma samples were used as a starting point from which the model cfDNA was extracted using the extraction protocols of this study. This approach was particularly useful as the mass of DNA extracted could be compared with the mass of DNA added into the initial plasma to quantify the yield of the assay.

8.3.3 cfDNA extraction protocol

The protocol used for solid-phase cfDNA extraction from plasma for NIPT (Figure 8.2a) was adapted from the BIOO NextPrep-Mag cfDNA Isolation Kit (PerkinElmer, Austin, TX, USA). Manual refinement of the protocol was used to optimize the workflow that incorporated the microfluidic chip, or on-chip workflow. Each of the reagents listed here is part of the BIOO kit. To begin, the model human plasma samples were made using 1 mL of AcroMetrix EDTA Plasma Dilution Matrix (ThermoFisher Scientific, Waltham, MA) and various amounts of model cfDNA. This was combined with 1.25 mL of cfDNA Binding Solution, 24 µL of cfDNA Proteinase K, and 16 µL of cfDNA Magnetic Beads in a 5 mL tube with vortexing after each reagent was added. The sample was then incubated for 15 minutes at 55 °C. The magnetic beads were then resuspended by vortexing, the sample was placed on a magnetic stand, and the supernatant was removed. The magnetic beads were then washed on a magnetic stand once with 1.5 mL of cfDNA Wash 1 and twice

with 1.5 mL of cfDNA Wash 2. During each washing step the respective wash buffer was added to the tube, the tube was removed from the magnetic stand, the sample was vortexed, then returned to the stand for magnetic bead collection and wash buffer removal. Following all washing steps, the magnetic beads were then resuspended in at least 12 µL of cfDNA Elution Solution and heated at 55 °C for 5 minutes. The sample was then returned to the magnetic stand where the magnetic beads were collected, and the extracted sample was then removed and stored for future analysis.

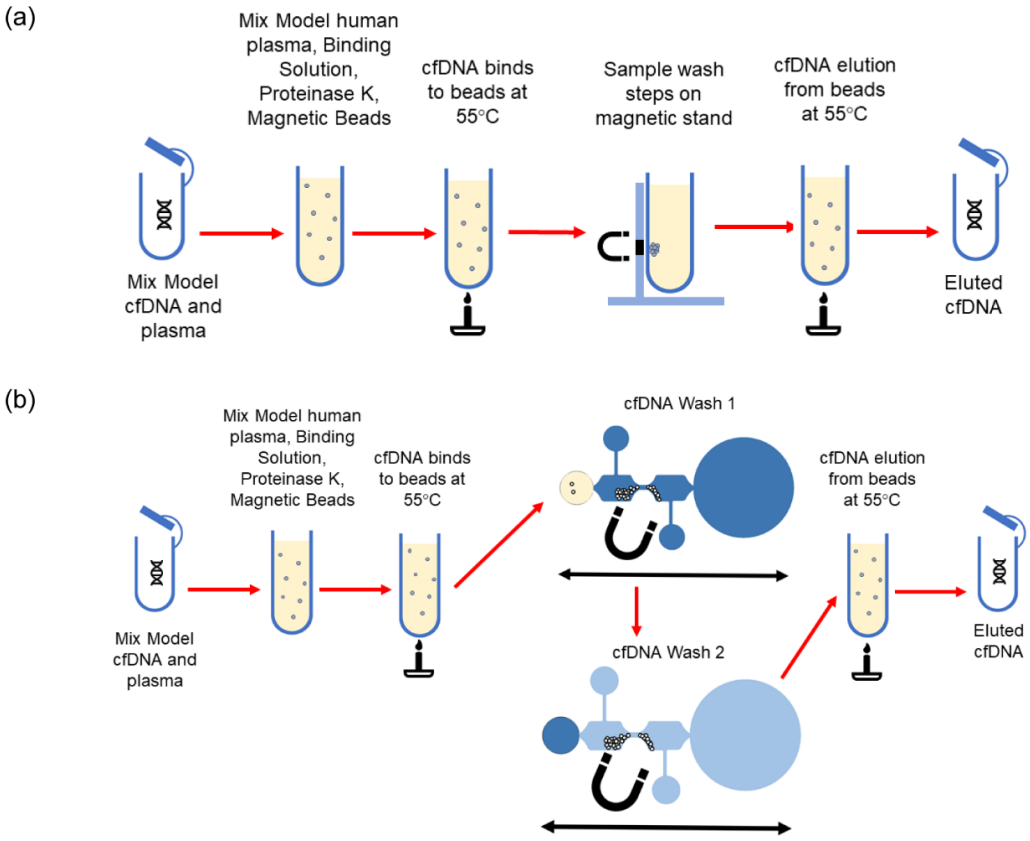

Figure 8.2: Cell free DNA extraction protocol for (a) manual and (b) on-chip purification methods.

8.3.4 CfDNA extraction protocol using separator on the microfluidic chip

The following protocol was used for when both wash steps were performed on the microfluidic chip, however, tests were also conducted where one wash step was performed on-chip and one test was performed manually (for instance, this first wash step might be performed on-chip while the second wash step might be performed manually). In these cases, the on-chip protocol was followed for the buffer being tested on-

chip, while the manual protocol was utilized for all other steps. The on-chip protocol (Figure 8.2b) starts by combining and vortexing AcroMetrix EDTA Plasma Dilution Matrix (ThermoFisher Scientific, Waltham, MA), model cfDNA, cfDNA Binding Solution, Proteinase K, and cfDNA Magnetic Beads, then incubating the sample at 55 °C for 15 minutes as in the manual protocol. The beads were then vortexed and collected with a magnet and the supernatant was removed. Next, the magnetic beads were resuspended in 25 μL of Wash 1 and were transferred to the input well of the separator on the microfluidic chip. Before loading the beads, the separator was filled through the electrode well with Wash 1 to fill the full channel and 100 μL of Wash 1 was added to the sample output well, details of this method are provided in Figure 8.3. Electrodes were placed in the two electrode wells and either 0 V, 50 V, 100 V, 200 V, or 300 V was applied across the channel. The beads were then added to the sample input well and transported through the separator to the sample output well using an external neodymium magnet (D86-N52, K&J Magnetics, Pipersville, PA, USA). The magnetic beads were extracted from the sample output well, collected in a new tube, and the voltage source was turned off. This tube was placed on a magnetic rack where Wash 1 could be fully removed, and the magnetic beads could be resuspended in 25 μL of Wash 2. Before the magnetic beads could be added to a new separator, it was filled with Wash 2 and 100 μL of Wash 2 was also added to the sample output well. The same transport procedure was conducted once the magnetic beads were added to the sample input well. The resulting bead-buffer solution was then collected in a tube, placed on a magnetic rack, and the remaining Wash 2 that the magnetic beads were suspended in was removed. Elution of the DNA proceeded this as in the manual procedure using at least 12 μL of the cfDNA Elution Solution.

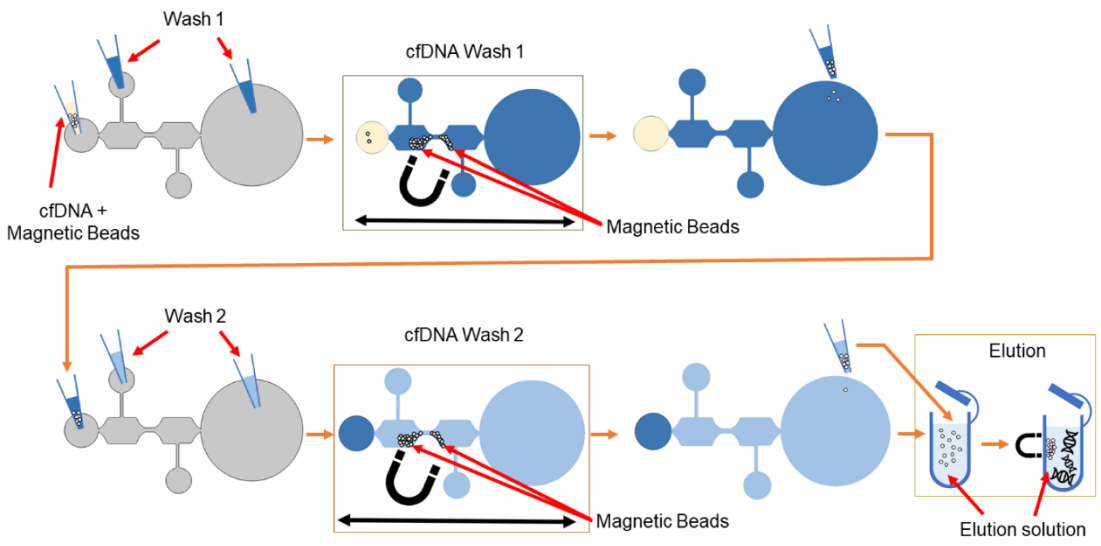

Figure 8.3: Mechanistic understanding of how to use separator on cfDNA extraction device.

8.3.5 Quantification and evaluation of extracted cfDNA

Analysis of cfDNA eluate sample yield was performed using the Agilent Bioanalyzer 2100 Machine (Agilent Technologies, Santa Clara, CA, USA). The Agilent DNA 1000 Kit and DNA Chip (Agilent Technologies, Santa Clara, CA, USA) were used for On-Chip Electrophoresis, and the resulting electropherogram traces were analyzed to identify the DNA concentration (ng/µL) of 149-bp cfDNA input sample and the eluate to calculate the cfDNA yield. Additionally, the NanoDrop 1000 UV-Vis Spectrophotometer (Thermo Scientific, Waltham, MA) was used to evaluate the purity of the extracted cfDNA, utilizing the A_{260}/A_{280} and A_{260}/A_{230} ratios which compare the sample's absorbance of ultraviolet light at 260 nm, 230 nm, and 280 nm.

8.3.6 Microfluidic chip modeling of one separator on microfluidic chip

Computational modelling using COMSOL Multiphysics® Modeling Software 5.6 was used to evaluate the applied electric field and EOF through the separator on the microfluidic chip. Simulations were performed for 50 V, 100 V, 200 V, and 300 V conditions across the separator for two fluids matching the fluid dynamic and electrical properties (density, dynamic viscosity, dielectric permittivity, and conductivity) of the Wash 1 and Wash 2 buffers. Density, dielectric permittivity, and conductivity were estimated based on existing values in the literature, while the dynamic viscosity of the buffers was measured using an Advanced

Rheometer (AR) 2000 (TA Instruments, New Castle, DE, USA). Using the Electric Currents, Laminar Flow, and Transport of Diluted Species Physics modules as well as the Potential Coupling Multiphysics module, the electric potential and flow velocity was plotted across the microfluidic chip separator's area. For each experimental treatment, ten points were chosen manually along the middle of the center channel of the separator (Figure 8.1) to characterize the center channel velocity, and these values were averaged to gain a metric for this velocity. This result was compared against variations in wash buffer and potential difference to investigate the microfluidic chip purification properties as an increase in electroosmotic velocity is predicted to correlate to a decrease in unwanted contaminants such as GTC and an increase in purity which is critical for downstream sequencing for NIPT analysis. In addition to varying the buffer and electric potential, the width of the center channel of the separator was also varied to evaluate its effect on the electroosmotic velocity in the separator. The center channel width used in this study was 0.24 mm, however 0.12 mm, 0.15 mm, 0.18 mm, and 0.21 mm channel widths were also modeled to provide insight into the effect that chip geometry has on the electroosmotic velocity.

8.3.7 Statistical analysis

Results in this study are presented as an average ± standard deviation using at least n = 3. Where appropriate, a two-tailed t-test or ordinary one-way analysis of variance (ANOVA) was used where* $p< 0.05$, ** $p<0.01$, *** $p<0.001$, and **** $p<0.0001$.

8.4 Results

Controls using the manual protocol according to manufactures instructions were first used as a metric for comparison for the yield and purity of the microfluidic-based purification assay. To begin, since a major concern with NIPT is extracting enough genetic material for downstream analysis representative of the fetal genome, it was critical to understand how the manual protocol performed under various amounts of starting sample. As outlined in Table 8.1, the amount of cfDNA that is found in patients can vary from at least 1.8 to 22 ng/mL. Therefore, this test evaluated different amounts of input DNA from 10 ng/mL to 60 ng/mL. The average yield for 1 mL of plasma with a starting concentration of 60 ng/mL was 61.90 ± 2.56%, 55 ng/mL was 51.79 ± 6.48%, 27 ng/mL was 53.88 ± 3.56%, and 10 ng/mL was 60.91 ± 6.52%. This yield is

equal to or more than four commercially available cfDNA extraction kits analyzed by Diefenbach et al. using 3 mL of plasma with 500 ng/mL of low molecular weight DNA ladder spiked in[359]. Additionally, the effect of vortexing throughout the protocol was evaluated to inform the design and protocol of the microfluidic chip. cfDNA samples in plasma were extracted using only manual pipetting of reagents while keeping all other variables constant. The result of this test is provided in Figure 8.4a and showed a statistically significant difference between the vortex and no vortex conditions with a yield of 34.84 ± 5.84% without vortexing, which is roughly half of the yield found when vortexing the reagents during the protocol. Furthermore, another condition that was tested before evaluating the procedure using the microfluidic chip was the effect the volume of magnetic beads used in this assay has on the overall yield of the extracted cfDNA. Since the magnetic beads for the BIOO NextPrep-Mag cfDNA Isolation Kit are at a high concentration around 12 x 10^9 beads/mL, it is likely they can get clumped together within the microfluidic chip and block the movement of all the beads and DNA through the separator. It was important to understand if there is a correlation between the volume of magnetic beads used in the assay and the cfDNA yield to see if it would be possible to use a smaller volume of magnetic beads and reduce the chances of blocking the separator. The result of this study showed there is a linear correlation ($r^2 = 0.9832$) between the volume of input magnetic beads (µL) and the yield (%) of extracted cfDNA from 2 µL to 16 µL (Figure 8.4b and 8.4c). Therefore, the on-chip protocol was performed with 16 µL of magnetic beads per the manufacturer's instructions, and the geometry of the microfluidic chip was adapted accordingly to ensure all cfDNA-bound magnetic beads could fit on-chip.

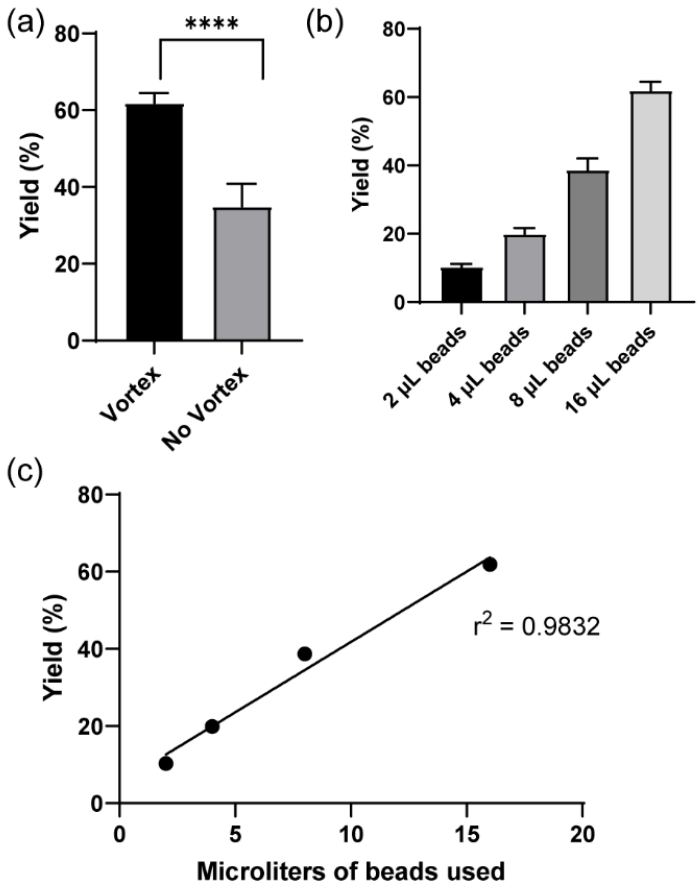

Figure 8.4: Manual protocol evaluation of BIOO NextPrep-Mag cfDNA Isolation Kit. Yield of DNA extracted using (a) vortexing vs no vortexing (two-tailed t-test p value = <0.0001). (b) & (c) different volumes of magnetic beads which showed a linear relationship (r^2 = 0.9832).

In addition to initial testing of the manual cfDNA extraction as specified in the BIOO kit, the mechanisms occurring on the microfluidic chip were examined further, especially the EOF used to increase the purity of the extracted cfDNA from plasma. In this assay, when the cfDNA-bound, magnetic beads are added to the chip they are dragged through the wash buffer-filled microfluidic channel, indicated in Figure 8.1, purifying the DNA as each magnetic bead is fully exposed to the wash buffer. To increase the purification of the cfDNA, EOF was used where the electroosmotic velocity (v_{EOF}) was a function of the electroosmotic mobility (μ_{EOF}) and electric field (E) which are based on the dielectric constant of the buffer (ε), zeta potential of the capillary surface (ζ), and the viscosity of the buffer (η) (Equation 8.1).

$$v_{EOF} = \mu_{EOF} E = -\frac{\varepsilon \zeta}{\eta} E \qquad (8.1)$$

The highest velocity () on the microfluidic chip was found within the center channel where all the beads move through during this procedure. Therefore, when the magnetic bead movement (F_m) opposes the direction of the , it is predicted this will increase the purity of the cfDNA as unwanted contaminants will migrate away from the sample output well where the beads are moving towards. COMSOL Multiphysics® Modeling 5.6 was utilized to study the EOF occurring in the microfluidic chip when an electric field was applied to the separator. Figure 8.5 presents the results of this EOF modeling where the electroosmotic velocity was evaluated within the center channel of the microfluidic chip under different voltage conditions for both Wash 1 and Wash 2. Due to differences in the properties of these buffers – Wash 1 contains guanidinium salts while Wash 2 is at least 75% ethanol based – a difference in the velocity (m/s) in the center channel of the separator was hypothesized. However, for both buffers a near-linear relationship between the voltage and velocity was observed. This linear increase in velocity as the voltage increases, indicates that that an increase in purity of the cfDNA sample should be expected at higher voltages due to the increase in electroosmotic velocity within the center channel.

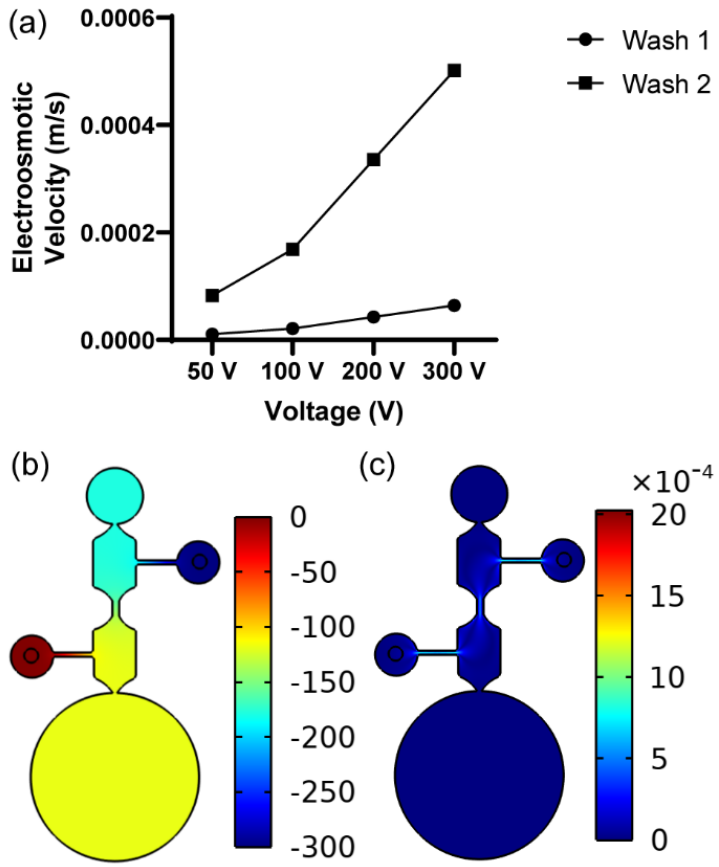

Figure 8.5: COMSOL Multiphysics Modeling results for (a) electroosmotic velocity in the center channel of the microfluidic chip as the voltage is varied for Wash 1 and Wash 2, (b) electric potential (V) surface plot, (c) velocity magnitude (m s^{-1}) surface plot using EOF boundary conditions. Both (b) and (c) are plotted using 300 V for Wash 2 as a representative sample.

When incorporating the magnetic bead purification steps onto the microfluidic chip, the results showed a statistically significant difference in the yield (%) of the extracted cfDNA between tests with only Wash 1 on-chip, only Wash 2 on-chip, both washes on-chip, and both washes performed manually (one-way ANOVA p value: 0.0024) (Figure 8.6a). The highest yield reported was 75.39% with both washes on-chip, possibly due to the reduced wash buffer volumes when performing the wash steps on the microfluidic chip. More significant than the change in yield between these conditions was the change in the A_{260}/A_{230} ratios (one-way ANOVA p value: 0.0003). When performing only Wash 1 on-chip the A_{260}/A_{230} ratio averaged at 0.25 ± 0.13 compared to 0.08 ± 0.07 for both washes performed manually which was a statistically significant difference (unpaired two-tail t-test, p value 0.0197). This is significant as it shows that the microfluidic chip purification was able to remove salt contamination better than the manual method. More

specifically, GTC contamination which makes up a proportion of the cfDNA Binding Solution and Wash 1 and absorbs at approximately 230 nm thus altering the A_{260}/A_{230} ratio. There was no statistically significant difference in the A_{260}/A_{280} ratios for the conditions tested which can indicate that the amount of DNA and proteins extracted remained consistent between these trials as DNA is absorbed at 260 nm and proteins are absorbed at 280 nm.

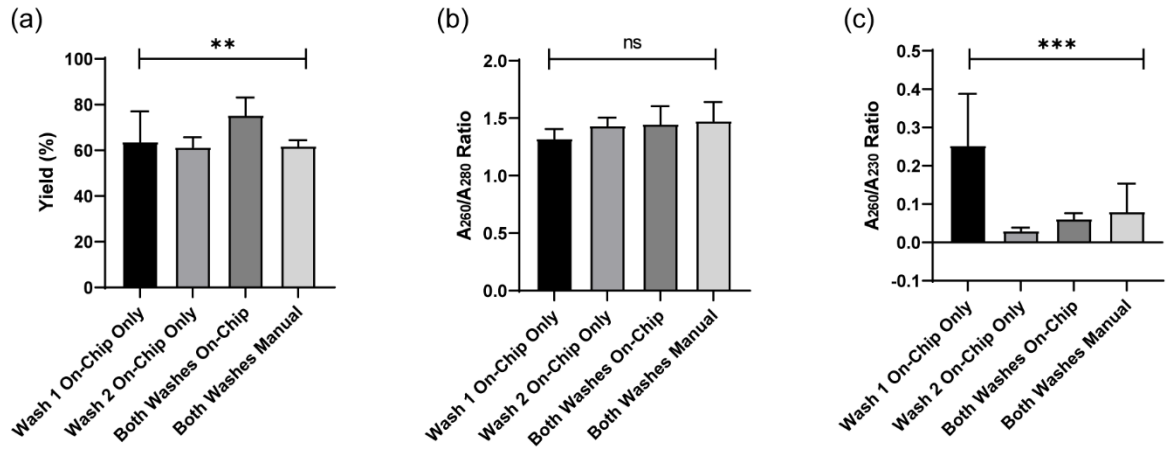

Figure 8.6: Yield and purity of extracted model cfDNA varying the washing steps performed on- and manually with no applied voltage (0 V). (a) yield (%) p value = 0.0024; (b) A_{260}/A_{280} Ratio p value = 0.1890; (c) A_{260}/A_{230} p value = 0.0003 (One-way ANOVA).

On-chip testing with the electric field applied to the separator was then performed and the results are presented in Figure 8.7. As explained in the COMSOL Multiphysics® Modeling, the purpose of the separator on the microfluidic chip was to induce EOF in the center channel to increase the purity of the extracted cfDNA. This effect was supported by the experimental results where an increase in A_{260}/A_{230} ratio between 0 V and 300 V was observed with the average ratios being 0.25 ± 0.13 and 0.46 ± 0.04, respectively, for only Wash 1 on-chip, indicating a statistically significant difference (unpaired two-tail t-test p value 0.0005). Additionally, the 300 V condition for only Wash 1 on-chip maintained a high yield of 68.19%, exceeding many commercial magnetic bead-based extraction assays. The A_{260}/A_{230} ratio (Figure 8.7c) for only Wash 2 on-chip was significantly less than for only Wash 1 on-chip across all voltage conditions; the p values were 0.0023 for the 0 V condition, then <0.0001 for 50 V, 100 V, 200 V, and 300 V conditions (unpaired two-tail t-test). Additionally, only Wash 1 on-chip consistently resulted in a higher

yield when comparing between voltage conditions while the A_{260}/A_{280} ratio remained relatively consistent among all conditions tested.

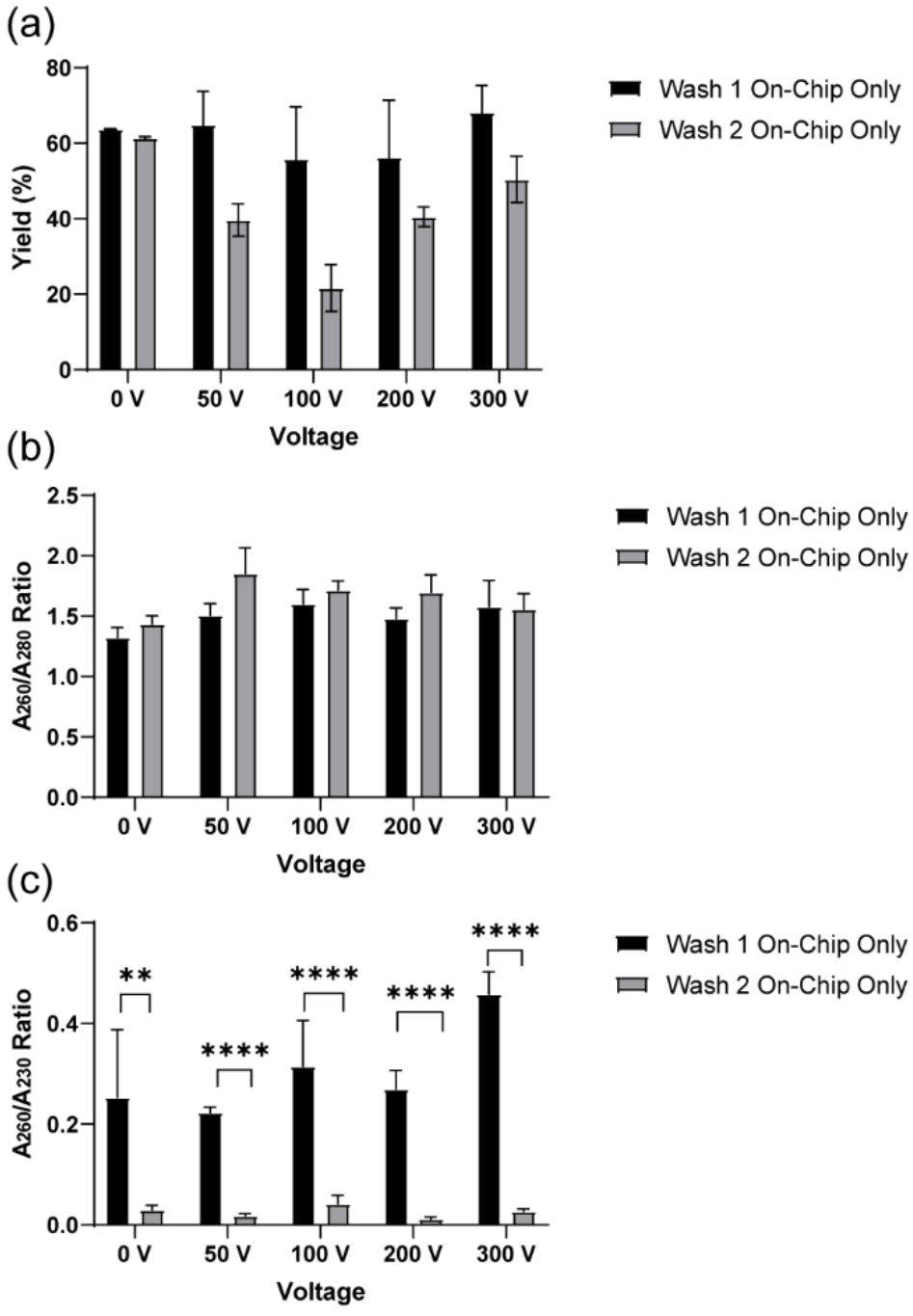

Figure 8.7: Analysis of extracted cfDNA using either Wash 1 on-chip only or Wash 2 on-chip only under different voltage conditions: (a) yield (%), (b) A_{260}/A_{280} Ratio, (c) A_{260}/A_{230} Ratio.

In addition to testing only Wash 1 or Wash 2 using the separator on the microfluidic chip, both washes together were also tested on-chip for the 300 V condition, as this voltage showed the highest purity cfDNA sample when only Wash 1 was performed on-chip. The results of this testing (Figure 8.8) compare both washes performed on-chip for the 0 V and 300 V conditions. Previous testing had showed that increasing the applied voltage also increased the A_{260}/A_{230} ratio, however, there was no statistically significant difference in this metric between the 0 V and 300 V conditions. The only statistically significant difference from this test was between the yield of extracted cfDNA where it was higher for the 0 V setting (unpaired two-tail t-test, p value 0.0015).

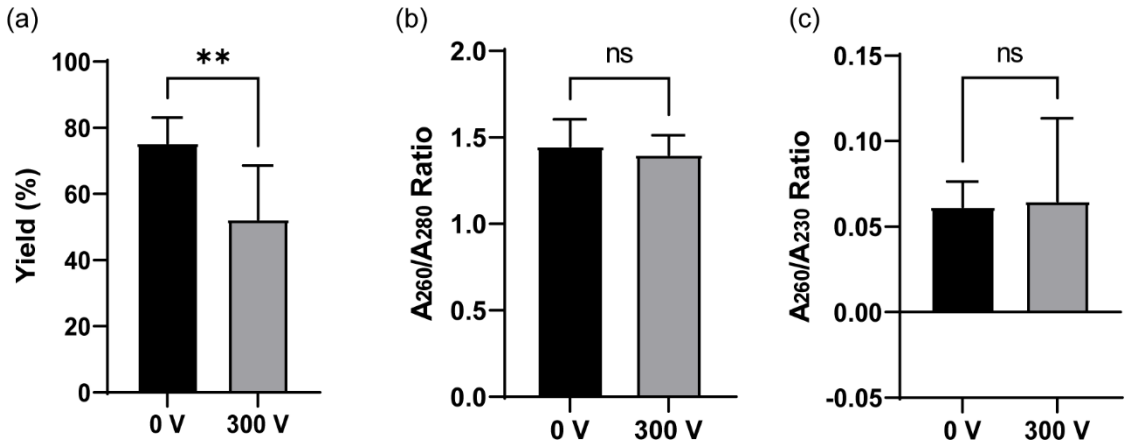

Figure 8.8: Analysis of extracted cfDNA with both wash steps performed using a separator on the microfluidic chip under 0 V and 300 V conditions: (a) yield (%), (b) A_{260}/A_{280} Ratio, (c) A_{260}/A_{230} Ratio.

8.5 Discussion

This work proposes the use of microfluidic chip-based purification in an existing cfDNA extraction protocol. The main benefit of incorporating the designed microfluidic separator into the manual cfDNA extraction assay is the significant increase in the purity of the extracted samples while not adding an additional, complex step. The increase in purity is critical because it can be correlated to the decrease in contaminating salts such as GTC. The main purity metric for this study, A_{260}/A_{230} ratio, showed a three-fold increase from an average of 0.08 ± 0.07 to 0.25 ± 0.13, when only Wash 1 was performed on-chip compared to the manual protocol. Additionally, when the EOF was incorporated into the microfluidic chip separator the A_{260}/A_{230} ratio further increased to an average of 0.46 ± 0.04 for only Wash 1 on-chip. This is

an almost six-fold change from the commercial method and supports the hypothesis that on-chip EOF can be used to increase the purification of the cfDNA extracted from the plasma sample. While these improvements are significant, it is important to note that an A_{260}/A_{230} ratio greater than 1.8 is generally considered purified by conventional standards, thus, the significant improvement seen using EOF is critical for reaching a purification standard closer to this metric. In addition to the use of EOF significantly improving the purity of the extracted cfDNA, it was noted that using the microfluidic separator also improved the purity even without the electric field. One explanation for this phenomenon is that when the magnetic beads move through the separator, they are thoroughly mixed with the wash buffer that is in the channel as they move in a two-dimensional streamline at the bottom of the microfluidic chip as each bead is attracted to the external magnet. Therefore, each magnetic particle is fully exposed to the wash buffer in the channel, similar to vortexing, but with less mechanical forces that could damage the magnetic beads or DNA. Compared with a brief, one-time vortexing steps as in the commercial procedure, the microfluidic chip allows the magnetic beads to be continuously mixed with the wash buffer in relative motion for an extended period, allowing for increased removal of impurities in the sample due to constant magnetic bead movement within the stationary wash buffer. One more result to note regarding the purity of the extracted samples was that when both washes were performed on-chip or only Wash 2 on-chip, regardless of the voltage condition, the A_{260}/A_{230} ratio was significantly lower than with only Wash 1 on-chip. One reason for this could be that the microfluidic chip system is more optimal for removing salt contaminants, such as GTC which are found in the cfDNA Binding Solution and Wash 1 and would need to be purified from the cfDNA-bound magnetic bead mix. Conversely, when Wash 2 is used on-chip there are less contaminants that can be purified from the bead mix and instead the prolonged mixing with the ethanol-based wash buffer does not increase the purity from the manual purification method. Thus, even though the COMSOL Multiphysics® Modeling resulted in a larger for Wash 2, the was more optimal for removing contaminants found in Wash 1.

In addition to the purity increasing significantly when performing Wash 1 on the microfluidic chip, the yield of the assay was also affected by using a separator for the washing steps. The setup that resulted in

the highest yield for this assay was both washes on-chip using the 0 V condition at 75.39 ± 7.75%. One reason on-chip purification results in an increase in cfDNA yield is because the reduced volumes used for the microfluidic chip purification will result in a reduced chance of cfDNA sample loss. In the manual method, 1.5 mL of Wash 1 is added and discarded when performing one or two washing steps, depending on the initial plasma volume. Additionally, 1.5 mL of Wash 2 is added and discarded for two washing steps with the buffer, resulting in up to 6 mL of these buffers added and discarded per sample of extracted cfDNA. Conversely, the microfluidic chip purification method instead adds and discards a maximum of 125 μL of each Wash 1 and Wash 2 when performing both reagent steps on-chip. This means that more concentrated samples are used, and less wash buffer is discarded, potentially reducing sample loss, for the on-chip method as the total volume of Wash 1 and Wash 2 combined is more than 40 times less than when performing the wash manually. Overall, the microfluidic chip-based purification is advantageous in significantly reducing wash buffer volumes and increasing the cfDNA yield. Additionally, in cases where 300 V was applied across the separator an explanation for the difference in cfDNA yield is that this voltage setting would occasionally produce bubbles in the microfluidic chip separator and obstruct the movement of the beads through the channel, therefore reducing the yield. These air bubbles are predicted to be caused by electrolysis since they predominantly originated at the negative electrode (cathode) where the water in the buffer could combine with electrons and cause water molecules to release hydrogen atoms which then form hydrogen bubbles. While these bubbles may have interfered with some trials, overall, they did not completely eliminate any sample from being extracted but were an important consideration in not testing any voltage conditions greater than 300 V. Overall, compared to other magnetic bead-based cfDNA extraction commercial kits, the average yield of 68.19% for Wash 1 only on-chip at 300 V was as good or better than that of other kits, and the purity at this condition is significantly higher than the commercial kit, making these settings the optimal conditions for this assay[359]. Additionally, these results indicate there can be some tunability of the procedure depending on the needs of the experiment. An electric field can be applied when decreasing the amount of GTC in the sample is the main priority, or it can be omitted if the experimental goal is to extract as much cfDNA as possible regardless of the purity.

While increasing the applied voltage in the microfluidic chip was not a feasible way to further increase EOF velocity and therefore the purity of the extracted cfDNA due to hydrolysis of the wash buffer at higher voltages, changing the dimensions of the center channel in the separator on the microfluidic chip was investigated as an alternative strategy. The effect the center channel width (mm) and applied electric field (V) has on the EOF velocity was studied using COMSOL Multiphysics® Modeling. Figure 8.9 shows the results of this analysis where microfluidic chip center channel widths of 0.12 mm, 0.15 mm, 0.18 mm, 0.21 mm, and 0.24 mm were simulated. The results show that the smallest center channel width (0.12 mm) at the highest voltage (300 V) resulted in the highest velocity (m/s) and could be used to increase the EOF and therefore the sample purity. However, the modeling also identifies that decreasing the channel width has a less significant effect on increasing the electroosmotic velocity than increasing the voltage for these simulations. For both Wash 1 (Figure 8.9a) and Wash 2 (Figure 8.9b), the heat maps show a smaller change in velocity between channel dimensions as compared to between voltage settings. In fact, the velocity in the 0.12 mm channel at 200 V was comparable to the velocity in the 0.24 mm channel at 300 V at 6.61 x 10^{-5} m/s and 6.41 x 10^{-5} m/s, respectively, for Wash 1 or 5.21 x 10^{-4} m/s and 5.02 x 10^{-4} m/s, respectively, for Wash 2. This indicates that using a wider center channel with higher voltage could still be the best option for this application since reducing the width of the channel by half may cause problems with bead movement and slow down the protocol rather than improve it.

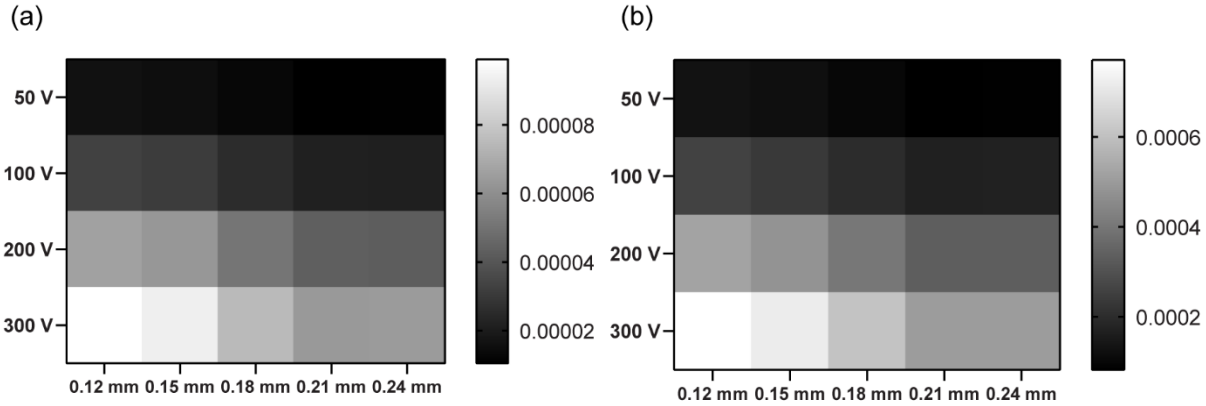

Figure 8.9: COMSOL Multiphysics® Modeling analysis of the electroosmotic velocity (m/s) in the center channel of the microfluidic chip separator at different dimensions and voltages for (a) Wash 1 and (b) Wash 2.

Along with the effect the microfluidic chip purification has on cfDNA yield and purity, an additional benefit includes the adaptability of the setup for different sample types. To begin, the microfluidic chip separator can be used with any volume of starting plasma sample since only the cfDNA-bound magnetic beads in 25 μL of the respective wash buffer is added to the microfluidic chip separator. Moreover, it is predicted that the reduced wash buffer volumes used on the microfluidic chip make it more advantageous for the extraction of lower amounts of cfDNA as the DNA will be more concentrated in the microliter scale volumes and be less likely to be discarded using the manual, larger buffer exchange method. During this study, the microfluidic setup was tested using a range of starting sample amounts to ensure that a clinically relevant sample of cfDNA could be extracted from the plasma. As small as 16.56 ng/mL and as large as 58.92 ng/mL was used for the input sample due to variations in the model cfDNA concentration as the same volume was added for each test. The success of this method at lower concentrations aligns with cfDNA amounts (ng/mL) measured by previous researchers and presented in Table 8.1 which indicates this method could be used with true patient samples. Furthermore, the yields calculated in this study even surpassed that of commercial cfDNA extraction products such as the automated MagMAX Cell-Free DNA Isolation kit (ThermoFisher Scientific) for less than 50 ng of input double stranded DNA, where the ThermoFisher Scientific system has a recovery rate below 40%. This work can be expanded further to investigate the extraction yield of cfDNA amounts less than 16 ng/mL using the microfluidic chip setup since manual protocol testing showed an extraction yield of 60.91 ± 6.52% for 10 ng of input DNA.

One last benefit to the simplicity of the microfluidic chip used in this protocol is the potential for automation. To use the microfluidic chip separator, either Wash 1 or Wash 2 simply fills the channel and wells, the electrodes are placed in the respective well, the power supply is turned on, and the cfDNA bead mix is moved through the separator into the sample output well (Figure 8.1) using an external magnet. Specifically, the external magnet moves repeatedly from the sample input well to the sample output well until all magnetic beads are through the channel. Thus, this two-dimensional, single-axis motion can easily be automated to drag the beads through the chip by moving it above a fixed external magnet. If this process is automated, it can further reduce the cost of the important extraction technique by using less reagents and

less hands-on time by the person performing this assay. There are existing automated platforms for cfDNA extraction such as the MagMAX cfDNA Isolation kit with KingFisher instrument (ThermoFisher Scientific), NucleoMag cfDNA kit (Takara), MagNA Pure 24 System (Roche), and more, but all require sophisticated devices or liquid handling machines as opposed to the simple, automated single-axis movement with fixed magnet needed for the automated purification using the microfluidic chip proposed in this study.

8.6 Conclusion

Overall, the accuracy of aneuploidy detection during NIPT is critical to understanding the health of the developing fetus. This microfluidic chip shows an increase the yield and purity of cfDNA extracted from plasma for NIPT which can improve the results of this testing. The optimal condition for extraction and purification using this microfluidic chip separator setup was found to be performing Wash 1 on-chip with 300 V applied across the microfluidic chip. This increased the A_{260}/A_{230} ratio six-fold indicating a significant increase in purity and salt removal from the sample. This method utilizes significantly smaller volumes of wash buffers while being an easily assembled microfluidic chip with the potential for simple automation. Overall, this study provides a novel technology for cfDNA extraction from plasma for clinically relevant diagnostic assays that use cfDNA as an analyte, specifically NIPT. It also present the theoretical underpinnings and simulations that explain the efficacy of the technique.

8.7 Acknowledgement

The authors would like to acknowledge technical support from PerkinElmer.

CHAPTER 9

Sequence to size-based separation using microfluidic electrophoresis for targeted cell-free DNA analysis

---

Chapter 9 has been submitted as an original research article.

Lindsay Schneider[1] and Anubhav Tripathi[1]*

[1]Center for Biomedical Engineering, School of Engineering, Brown University, Providence, RI, USA

9.1 Abstract

The aim of this research is to present a new method to identify and separate target DNA of the same size, in base pairs (bp), into different sizes based on the targeted sequences. This sequence-specific analysis can then be used to evaluate the presence of multiple targeted analytes in a sample without the need for fluorescence detection. This work displays the feasibility of this method using multiple different 150 bp target sequences separated via microfluidic electrophoresis into 230 bp to 330 bp peaks. Using a combination of denaturation, hybridization, ligation, purification, and universal amplification, this represents a simple, robust method for targeted analysis of short DNA sequences. This work shows a limit of detection of 3 pg (~ 1.825×10^7 copies) of input DNA using 20 PCR cycles and the ability for the method to be used for short DNA sequences extracted from a plasma sample, most importantly cell-free DNA. Overall, this method has the potential to be used for mutation detection and multiplexed analysis without the need for multiple fluorophores or significant optimization due to varying melting temperatures between PCR primers and can qualitatively evaluate the presence of specific target sequences in a variety of molecular diagnostic applications.

9.2 Introduction

Nucleic acid testing is a critical tool for the detection of sequence-specific molecules in a biological sample[27,366]. The sequence-specific analysis allows for the detection of diseases, mutations, infections, and more[366,367]. While a number of methods have been developed to address this need, there remains a fundamental challenge to increase the sensitivity and specificity of any detection assay as much as possible[367]. Through increasing these metrics, testing can become more robust and result in fewer false positive or false negative readouts for researchers, clinicians, and patients.

Major nucleic acid amplification techniques such as polymerase chain reaction (PCR) have become a gold standard in the field for sequence-specific analysis of a number of targets, including SARS-CoV-2, other infectious diseases, and more[5,368]. PCR benefits from being a simple, widespread tool with both qualitative and quantitative readouts but is limited in some respects due to the need for thermal cycling hardware[5]. Additional isothermal amplification techniques such as loop mediated isothermal amplification (LAMP)[41], rolling circle amplification (RCA)[47], and nucleic acid sequence-based amplification (NASBA)[69] have addressed this limitation by removing the need for thermal cycling and being performed at one reaction temperature. Overall, many of these nucleic acid amplification techniques can be run using single-plex or multiplexed setups for the detection of multiple targets at one time. However, multiplexing can be limited due to both reaction conditions and detection equipment[27,369]. Multiplexed reactions are affected by interactions between additional primer sets, amplification bias, and masking of low abundance targets by high abundance targets sequestering reaction components[27]. Additionally, multiplexed PCR equipment, for example, is limited to the detection of four to five fluorescent channels to detect fluorescent dyes at various wavelengths[369]. This is challenging as the amount of multiplexing possible is reliant on the number of detectors, and there is a need for discrimination in detectable wavelengths to prevent cross-talk[369].

For these reasons, many alternative methods have been explored to provide multiplexed analysis of target nucleic acids beyond conventional, multiplexed nucleic acid amplification techniques. Namely, researchers have expanded into more complex analysis tools of note to this research study which detects the presence or quantity of an amplified target based on the amplicon length (bp) as opposed to a sequence readout or

fluorophore. One example of these techniques is multiplex ligation-dependent probe amplification (MLPA). This method is a multiplexed assay used for the detection of copy number variations of genomic DNA[370,371]. In order to do this, two sequence-specific probes are hybridized to a target DNA sequence, ligated, then amplified by PCR with fluorescently labeled primers binding to the probe sequences[370]. The probes used during MLPA contain universal primer binding sites and stuffer sequences to vary the length of the DNA target based on the length of the stuffer sequence[370]. The amplified MPLA product is detected using capillary electrophoresis with fluorescence detection, and the area under the curve of each size peak is compared to a reference sample to determine the relative quantity of each amplicon, and therefore copy number[370]. MLPA has been used for a number of targeted gene applications, such as *BRCA1* and *BRCA2*, *DMD*, and *NF1* gene analysis, as well as methylation-specific analysis[371,372]. MLPA is advantageous for multiplexing of DNA targets using a universal primer set for PCR amplification to avoid biases or amplification efficiency limitations due to varying melting temperatures between PCR primer sets. However, one major limitation of MLPA to note is that the relative signal intensities found during capillary electrophoresis detection vary due to characteristics of the input DNA including age of the DNA, isolation method, solution, degradation, contamination, and more[371]. Lastly, the use of MLPA for cell-free DNA (cfDNA) sample analysis, which is important for this research, is challenging due to the presence of contaminants that may be used for plasma preparation, such as EDTA, heparin, or acid citrate dextrose (ACD)[373].

Another nucleic acid analysis method that detects the presence of a target based on the amplicon length (bp) is tetra-primer amplification refractory mutation system polymerase chain reaction (ARMS-PCR). This is a simple, economical detection method used to genotype single nucleotide polymorphisms (SNPs)[374,375]. In this method, four primers are used in a single PCR reaction then analyzed using gel or capillary electrophoresis[374,376]. The primers are designed in a way so that two non-allele-specific primers amplify a region contain a SNP of interest (outer primers)[374]. Next, this DNA is used as a template for the allele-specific primers (inner primers) which create allele-specific fragment sizes[374]. Applications for tetra-primer ARMS-PCR have been found in SNP genotyping for cancer[376,377], and it has even been combined with

lateral flow assays for rapid, simple detection[378]. One limitation of this method is that the optimization process for eliminating false-positives and false-negatives can be very laborious and time-consuming which may limit the adaptability of this method to many applications efficiently[374]. Moreover, ARMS-PCR has been limited in its use for cfDNA mutation detection due to its insufficient specificity[379].

While these methods have many benefits, there are limitations in the need for substantial optimization or probe design. Thus, in this work, we present a unique qualitative nucleic acid test method that captures sequence-specific targets and enzymatically increases the target length before universal amplification and microfluidic electrophoresis detection. This method has been tested for multiplexed analysis of up to six target sequences and analyzed for sensitivity and specificity. Additionally, this method was tested for the application of cfDNA screening because this DNA is naturally fragmented into pieces of <200 bp long, ideal for this method[380]. CfDNA screening is used for a variety of applications, namely, non-invasive prenatal testing for fetal chromosomal aneuploidy or fetal genotyping during pregnancy and cancer screening[380,381]. In order to perform cfDNA analysis, the analyte must be extracted from a plasma sample[381]; therefore, this method was tested with DNA extracted from plasma to evaluate whether it would work with this sample type. Overall, with the continuous need for efficient, robust nucleic acid testing techniques, this method provides a unique capture and detection protocol that has the potential to be used for SNP genotyping analysis, point mutation detection, and qualitative assessment for the presence of a specific nucleic acid target.

9.3 Materials and Methods

9.3.1 Sequence specific probe and size-based tag design method

Target DNA of 150 bp, representing DNA sizes relevant to cfDNA analysis, was used for method development and optimization for this assay (Figure 1a). Sequence-specific probes (Figure 1b) were designed for each target DNA as a complementary strand that can hybridize to one strand of the target sequence. Additionally, two size-based tags (Figure 1b) were designed as single stranded DNA sequences complementary to the sequence-specific probe adjacent to the target DNA region. Both probes and tags were ordered from Integrated DNA Technologies, (Coralville, IA, USA) and the size-based tags were

extended or shortened depending on the target DNA so that each target DNA or group of target DNA sequences could be identified by the size of the final product during analysis. Size-based tags were 5' phosphorylated if the 5' end of the tag was designed to be adjacent to the 3' end of the target DNA to ensure proper ligation. Lastly, every size-based tag was designed to include either a PCR primer recognition sequence or the complementary sequence so the DNA could be universally amplified using one set of PCR primers for easier detection (Figure 1d and 1e). The PCR primer recognition sites were not included in the sequence-specific probes so to avoid non-specific amplification when there was no target DNA in the sample. Overall, this sequence-specific probe and size-based tag design was critical to ensure all 150 bp target DNA could be identified during the size-based analysis.

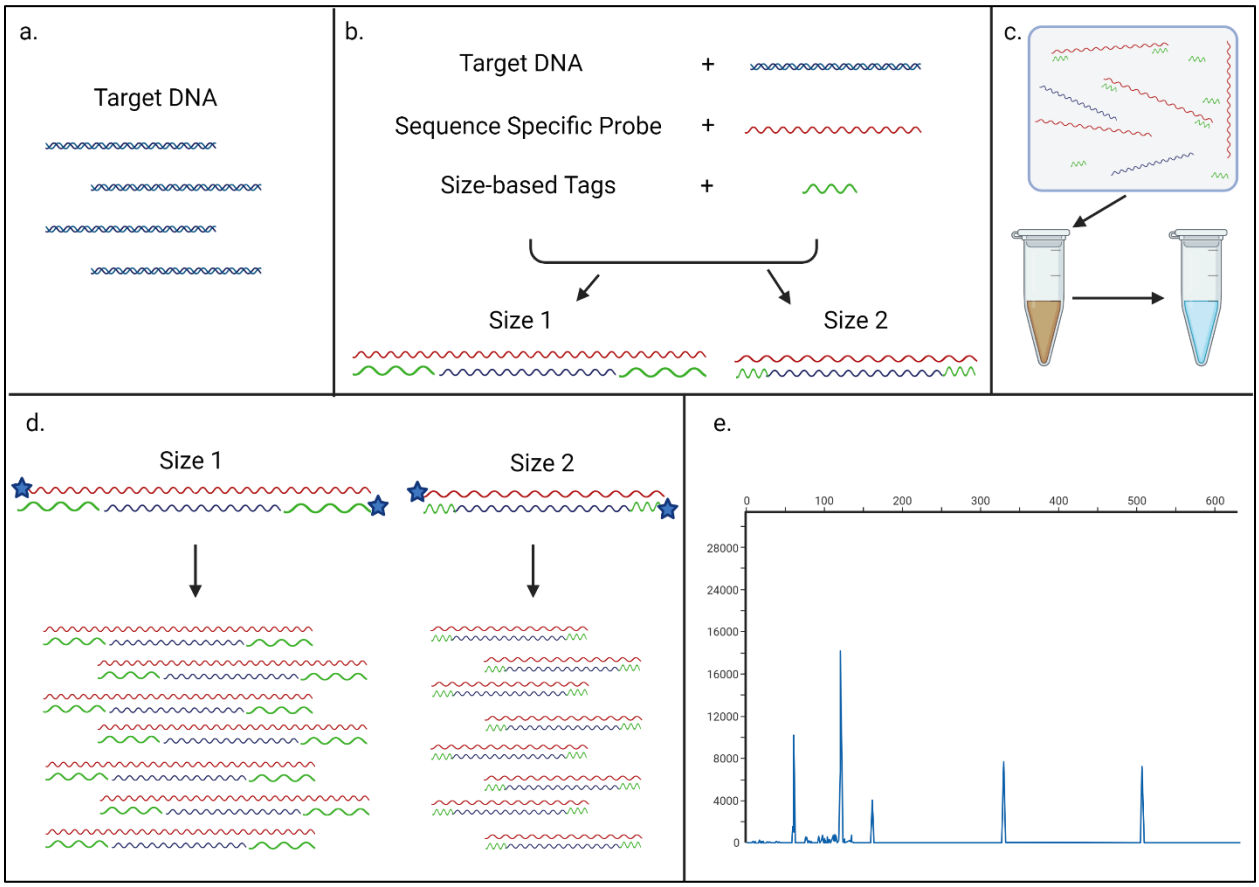

Figure 9.1: Methods diagram. (a) Target DNA of 150 bp. (b) Denaturation of double stranded DNA; hybridization of sequence specific probes and size-based tags; ligation of single stranded DNA; (c) DNA purification to remove excess sequence specific probes, size-based tags, and hybridized DNA without target sequence. (d) DNA amplification using PCR with universal primers. (e) Sample product analysis via microfluidic electrophoresis. Created with BioRender.com

9.3.2 Detailed size-based tagging and separation method

Targeted DNA amplicons were designed for M13mp18 RF plasmid DNA (New England Biolabs (NEB), Ipswich, MA, USA) and PCR amplification was utilized to create the starting sample for this method using One *Taq* 2x Master Mix with Standard Buffer (NEB, Ipswich, MA, USA). PCR protocol details and primers are provided in Supplemental Tables 1 and 2, respectively. Following amplicon preparation, the DNA is purified using a 1.8X solid-phase reversible immobilization (SPRI) bead-based cleanup (AMPure XP, Beckman Coulter, Brea, CA, USA) and quantified via Agilent Bioanalyzer (Santa Clara, CA, USA). The target DNA is then treated with T4 polynucleotide kinase for 5'-phosphorylation before subsequent ligation (NEB, Ipswich, MA, USA). This reaction follows the manufactures instructions using 25 μL of purified target DNA, 5 μL T4 PNK reaction buffer, 5 μL ATP (10mM), 1 μL (10 units) of T4 PNK, and nuclease free water up to the 50 μL reaction volume. The DNA is heated to 37°C for 30 minutes, then the enzyme is heat-inactivated at 65°C for 20 minutes.

Following DNA preparation, the size-based tagging and separation method is performed (Figure 1b). A DNA mixture of target DNA, sequence-specific probes, and size-based tags is mixed in a 1:1 ratio with annealing buffer (10 mM Tris, pH 7.5 – 8.0; 50 mM NaCl; 1mM EDTA). This mixture is then heated to 95°C for 5 min and cooled at a ramp rate of 0.1°C/sec stopping ever 10°C for 5 min until the reaction reaches 25°C for 5 min. During this time, sequence-specific probes are hybridized to target DNA and made double stranded using size-based tags that are also hybridized to the probe, adjacent to the target sequence. Next, the size-based tags and target DNA are ligated using 2 μL (80 units) *Taq* DNA Ligase, 5 μL *Taq* DNA Ligase Reaction Buffer, annealed target DNA, and nuclease free water up to the 50 μL reaction volume. This mixture is then heated to 45°C for 15 min to create a new single stranded DNA template that can be used for further size-based analysis.

Following these steps, the ligated target DNA is purified using AMPure XP SPRI paramagnetic beads at a 0.6X ratio according to manufacturer's instructions and resuspended in 50 μL of nuclease free water (Beckman Coulter, Brea, CA, USA). Figure 1c shows this step with the removal of excess sequence-specific probes, size-based tags, and hybridized DNA without the target sequence. Lastly, the purified product is

amplified (Figure 1d) using One *Taq* 2X Master Mix with Standard Buffer (NEB, Ipswich, MA, USA) for 20 PCR cycles also according to manufacturer's instructions (PCR Reaction Conditions, Supplemental Table 1). Universal primers are used for PCR amplification using the forward primer sequence 5'- CGGCTGCTTTGTTCATGGCT and reverse primer sequence 5'- CCGCATACCAGGAAGGGCGC (Integrated DNA Technologies, Coralville, IA, USA). Following PCR amplification, the samples are analyzed using the 2100 Bioanalyzer Instrument and Agilent DNA 1000 Kit for microfluidic electrophoresis (Figure 1e) (Agilent Technologies, Santa Clara, CA, USA). To run this analysis, 1 μL of PCR product was used and the sizes (bp) of the peaks on the resulting electropherogram are analyzed. Each sequence-specific probe and size-based tag results in a predicted size (bp) and the method is considered successful when the observed size (bp) matches the predicted size (bp) within the sizing resolution of the Agilent DNA 1000 Kit Guide. This sizing resolution is 5% between 100 and 500 bp.

9.3.3 Multiplex detection and analysis of DNA of same starting size (bp)

Following method development, the assay was tested using 50 bp tags and 90 bp tags, the sequence-specific probes and size-based tags are provided in Tables 1 and 2. Originally two target DNA were designed for each set of tags, referred to as target 1 and target 2 for both the 50 bp and 90 bp tags. The method was characterized by testing the target DNA individually and in a multiplexed system where four target DNA sequences were used to create two size outputs, two target DNA per size. Following initial characterization, additional target DNA, sequence-specific probes, and size-based tags were designed for 30 bp tags, 40 bp tags, 60 bp tags, 70 bp tags, and 80 bp tags to increase the multiplexing of the test, the sequence-specific probes and size-based tags are also provided in Tables 1 and 2, with one target per size.

Table 9.1: Sequence specific probes used for target DNA analysis.

Sample	Sequence (5' – 3')
30 bp target probe	GTCAGGTAAGGTATAATGAGCCAGTTCTTAAAATCGCATAAGGTAATTCACAATGATTAAAGTTGAAA TTAAACCATCTCAAGCCCAATTTACTACTCGTTCTGGTGTTTCTCGTCAGGGCAAGCCTTATTCACTG AATGAGCAGCTTTGTTACGTTGATGGTCCAGCTG
40 bp target probe	CCGATTTCGGTAAGGTAAACTGCGTGGGCGATGGTTGTTGTCATTGTCGGCGCAACTATCGGTATC AAGCTGTTTAAGAAATTCACCTCGAAAGCAAGCTGATAAACCGATACAATTAAAGGCTCCTTTTGGA GCCTTTTTTTTGGAGATTTTCAACGTGAAAAAATTATGTGAAGCGGTTATAAATCTG
50 bp target 1 probe	TGGGAAACACTGCCCTTTCAGCGGGCCATCAGCGGATAACAATTTCACACAGGAAACAGCTATGACCA TGATTACGAATTCGAGCTCGGTACCCGGGGATCCTCTAGAGTCGACCTGCAGGCATGCAAGCTTGGC ACTGGCCGTCGTTTTACAACGTCGTGACTGGGAAAACCCTGGCGTTGTTGATTTCCTGAAACGGGATA TCATCAA

50 bp target 2 probe	TGGGAAACACTGCCCTTTCAGCGGGCCATCTTGCTTCTGACTATAATAGTCAGGGTAAAGACCTGATTT TTGATTTATGGTCATTCTCGTTTTCTGAACTGTTTAAAGCATTTGAGGGGGATTCAATGAATATTTATGA CGATTCCGCAGTATTGGACGCTATCCAGTCTAAACATTTTATGTTGATTTCCTGAAACGGGATATCATCAA
60 bp target probe	GGGCTGCATCCACACTTTCACTCGGTGGGTTCCACGACCGTTGGTTTCTACATGCTCGTAAATTAGGAT GGGATATTATTTTTCTTGTTCAGGACTTATCTATTGTTGATAAACAGGCGCGTTCTGCATTAGCTGAACA TGTTGTTTATTGTCGTCGTCTGGACAGAATTACTTTACCTTTTGTCGGTACTTGGCGGCATAGCCGTTAT TGCGTACCAGATCGTCTGCGC
70 bp target probe	GTGCATGGCCACACCTTCCCGAATCATCATGGTAAACGTGCGTTTTCGCTAGCGTCTTAATCTAAGCT ATCGCTATGTTTTCAAGGATTCTAAGGGAAAATTAATTAATAGCGACGATTTACAGAAGCAAGGTTATT CACTCACATATATTGATTTATGTACTGTTTCCATTAAAAAAGGTAATTCAAATGAAATTGTTAACTGTGT CCGGAAAAGCCGCGACGAACTGGTATCCCAGGTGGCCTGAACG
80 bp target probe	GGATGCGACGAATTTTCGCCGCCCCATAAAGTACGCCCACGACTCGTTCGCACTGGCCCGCTAACGAG GAAAGCACGTTATACGTGCTCGTCAAAGCAACCATAGTACGCGCCCTGTAGCGGCGCATTAAGCGCGG CGGGTGTGGTGGTTACGCGCAGCGTGACCGCTACACTTGCCAGCGCCCTAGCGCCCGCTCCTTTCGCT TTCTTCAAGGTAACGTCACCACGCGGCGAACGATGGCCTCTTCCAGCCAGCACAGAAACATCTGGC
90 bp target 1 probe	ATCCGCCAGCAGGAGCTGGACTTTACTGATGCCCGTTATATCTGCGAAAAGACCGGGATCTGGACCCG TGCCTCTGACTTTGTTCAGGGTGTTCAGTTAATTCTCCCGTCTAATGCGCTTCCCTGTTTTTATGTTATTC TCTCTGTAAAGGCTGCTATTTTCATTTTTGACGTTAAACAAAAAATCGTTTCTTATTTGGATTGGGATAAAT AATATGGCTCAAAAAACTACCGTGAAAAGTCGGTGGATGTGGCGGGTTATGATGAACTTGCTGCTTTTGA TGATGATAT
90 bp target 2 probe	ATCCGCCAGCAGGAGCTGGACTTTACTGATGCCCGTTATATCTGCGAAAAGACCGGGATCTGGACCCG TGGCTCTAATCTATTAGTTGTTAGTGCTCCTAAAGATATTTTAGATAACCTTCCTCAATTCCTTTCAACTG TTGATTTGCCAACTGACCAGATATTGATTGAGGGTTTGATATTTGAGGTTCAGCAAGGTGATGCTTTAGA TTTTTCATTTGCAAAAAACTACCGTGAAAAGTCGGTGGATGTGGCGGGTTATGATGAACTTGCTGCTTT TGATGATGATAT

Table 9.2: Size-based tags used for target DNA analysis.

Sample	Sequence (5’ – 3’)
30 bp target tag 1	CTTACCTGACGCGCCCTTCCTGGTATGCGG
30 bp target tag 2	CGGCTGCTTTGTTCATGGCTCAGCTGGACC
40 bp target tag 1	GTTTACCTTACCGAAATCGGGCGCCCTTCCTGGTATGCGG
40 bp target tag 2	CGGCTGCTTTGTTCATGGCTCAGATTTATAACCGCTTCAC
50 bp target 1 and 2 tag 1	GATGGCCCGCTGAAAGGGCAGTGTTTCCCAGCGCCCTTCCTGGTATGCGG
50 bp target 1 and 2 tag 2	CGGCTGCTTTGTTCATGGCTTTGATGATATCCCGTTTCAGGAAATCAACA
60 bp target tag 1	CGGTCGTGGAACCCACCGAGTGAAAGTGTGGATGCAGCCCGCGCCCTTCCTGGTATGCGG
60 bp target tag 2	CGGCTGCTTTGTTCATGGCTGCGCAGACGATCTGGTACGCAATAACGGCTATGCCGCCAA
70 bp target tag 1	AGCGAAAACGCACGTTTACCATGATGATTCGGGAAGGTGTGGCCATGCACGCGCCCTTCC TGGTATGCGG
70 bp target tag 2	CGGCTGCTTTGTTCATGGCTCGTTCAGGCCACCTGGGATACCAGTTCGTCGCGGCTTTTCC GGACACAGT
80 bp target tag 1	CGGGCCAGTGCGAACGAGTCGTGGGCGTACTTTATGGGGCGGCGAAAATTCGTCGCATC CGCGCCCTTCCTGGTATGCGG
80 bp target tag 2	CGGCTGCTTTGTTCATGGCTGCCAGATGTTTCTGTGCTGGCTGGAAGAGGCCATCGTTC GCCGCGTGGTGACGTTACCTT
90 bp target 1 and 2 tag 1	CACGGGTCCAGATCCCGGTCTTTTCGCAGATATAACGGGCATCAGTAAAGTCCAGCTCCT GCTGGCGGATGCGCCCTTCCTGGTATGCGG
90 bp target 1 and 2 tag 2	CGGCTGCTTTGTTCATGGCTATATCATCATCAAAAGCAGCAAGTTCATCATAACCCGCCACA TCCACCGACTTTTCACGGTAGTTTTTTG

9.3.4 Specific and sensitive nucleic acid detection and analysis of target sequences

In addition to testing the method using purified DNA at various starting concentrations, the robustness of the assay was evaluated. This robustness testing was necessary to better understand the translatability of the method to more real-life applications. The sensitivity of the assay was tested by evaluating the limit of

detection for two target DNA sequences, 50 bp target 1 and 90 bp target 1. This testing began with 30 ng of input DNA for each target (60 ng total) which was serially diluted 10:1, 100:1, 1,000:1, and 10,000:1 using nuclease free water (Integrated DNA Technologies, Coralville, IA, USA) to 0.003 ng of each target. Following microfluidic electrophoresis, the resulting electropherograms were evaluated for the presence of a peak at the predicted size to determine if the target DNA could be identified at lower input concentrations. In addition to testing the sensitivity of the assay in a dilute sample, the method was characterized further to evaluate whether it would work when the target DNA was diluted in a more complex DNA sample. For this testing 4 ng of target DNA for the 40 bp tags, 60 bp tags, and 70 bp tags (12 ng total of target DNA) was combined with either Human Female Genomic DNA (Promega, Madison, WI, USA) or 149 bp purified amplicons of M13mp18 DNA (NEB, Ipswich, MA, USA). Roughly 500 ng of Human Female Genomic DNA was used to dilute the target DNA in the starting sample or 10 ng of M13mp18 DNA amplicon. The genomic DNA was selected for this testing because it is a longer length and more complex sample, while the amplicon was selected because it is from the same starting sample as the target DNA, just a different sequence. The method was performed with these complex samples and the electropherograms were evaluated for the presence of the predicted peak sizes.

9.3.5 Method using targeted DNA amplicon extracted from plasma

One potential application for this DNA analysis method is cfDNA variant detection as the length of this target DNA is conducive to this method. One important step in utilizing this method for cfDNA analysis is target DNA extraction from plasma. This was done using the BIOO NextPrep-Mag cfDNA Isolation Kit (PerkinElmer, Austin, TX, USA) for solid-phase extraction. In this test, 8 ng of target DNA corresponding to the 40 bp tags, 60 bp tags, and 70 bp tags (24 ng total target DNA) was spiked into 1 mL of AcroMetrix EDTA Plasma Dilution Matrix (ThermoFisher Scientific, Waltham, MA, USA) and the manufactures instructions were followed for the extraction of the target DNA. Following the extraction, the method proceeded according to Figure 1, outlined previously. The goal of this test was to evaluate the method in a more complex system and evaluate the sensitivity when the target DNA does not start in a purified buffer.

9.4 Results

In order to demonstrate the capabilities of this method, two size tags were originally used with two target DNA sequences for each size. The purpose of this work was to observe the sequence-specific tagging method of the individual target DNA, multiplex analysis, as well as the ability to group target DNA into the same output size. Figure 2a visualizes the size (bp) of the target DNA prior to the method, while Figure 2b shows the shift in size following this method. In this case the 50 bp target 1 and target 2 were used, as well as 90 bp target 1 and 2. The predicted sizes for these target DNA was 250 bp and 330 bp, respectively. The peak sizes in Figure 2b are 3.86 ng/μL for 50 bp target 1 (Sample 1), 13.25 ng/μL for 50 bp target 2 (Sample 2), 3.80 ng/μL for 90 bp target 1 (Sample 3), and 0.24 ng/μL for 90 bp target 2 (Sample 4). This testing also demonstrated that even when an equal amount of target DNA for each target is inputted into the method, the output DNA concentrations vary, in this case between 0.24 ng/μL and 13.25 ng/μL. In addition to running this method with individual DNA targets, the multiplexing capabilities for this method were tested. Figure 2c shows the electropherogram graph for the simultaneous detection of 50 bp target 1 and 90 bp target 1, resulting in relatively consistent concentrations at 3.44 ng/μL and 2.06 ng/μL, respectively, and the output peak sizes matching the predicted peak sizes, within the tolerances for the Bioanalyzer kit being used. Additionally, Figure 2d shows the result of all four target DNA sequences (50 bp target 1 and target 2, 90 bp target 1 and 2) in the sample. These peak sizes again fell within the range of the size predicted based on the sequence-specific probes and size-based tags.

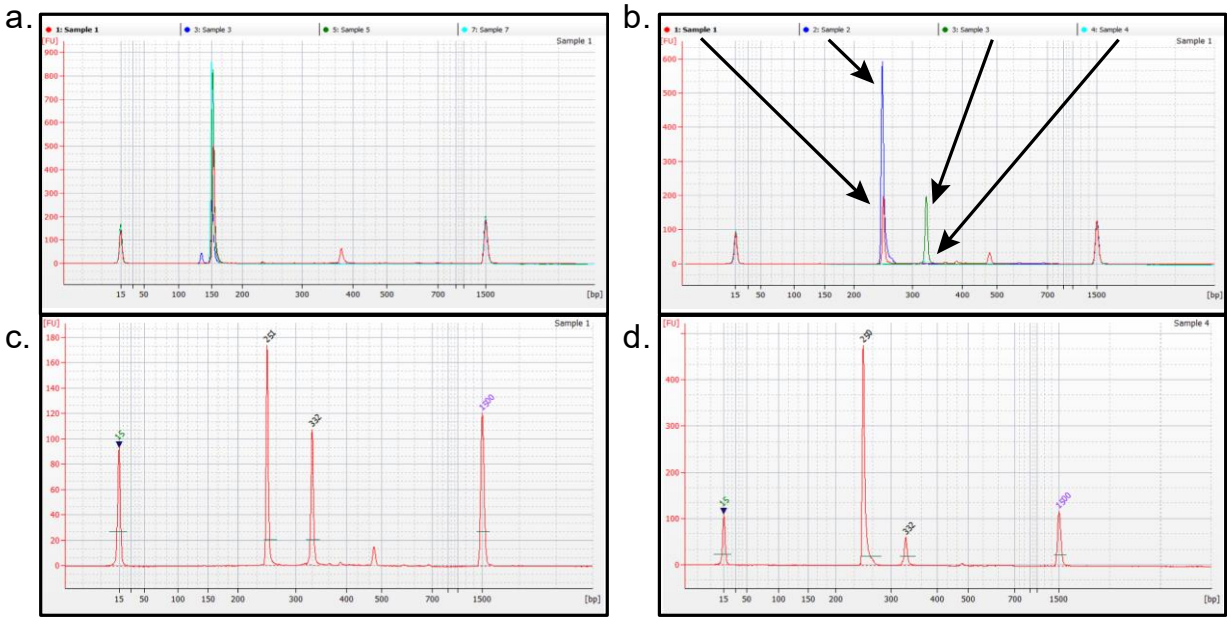

Figure 9.2: Multiplex method controls. (a). Starting target DNA for four sequences, all with peaks at 150 bp. (b) Individual method analysis with each target DNA, two sequences tagged with 50 bp tags (250 bp total size) and two sequences tagged with 90 bp tags (330 bp total size). (c) Multiplexed method analysis of two target DNA in one reaction, one of each size. (d) Multiplexed method analysis of four target DNA in one reaction, two of each size.

Following testing with two different size tags, sequence-specific probes and size-based tags were designed for additional sizes. Five new target DNA were prepared, and sequence-specific probes were designed with 30 bp tags, 40 bp tags, 60 bp tags, 70 bp tags, and 80 bp tags. Each of these target DNA were analyzed using the Agilent Bioanalyzer following PCR amplification and SPRI bead-based purification. The average target DNA size (bp) is provided in Table 3 as well as the predicted product size (bp) following this method. This predicted size is based on the target DNA size plus the additional length of the two size-based tags added, this size-based tag length is specified in each sample name. Additionally, the sizing resolution of the Bioanalyzer kit being used is 5%, therefore, each predicted size includes this specification as well. The average output size for each sample is shown in Table 3 where the 30 bp target showed no peak detection on the electropherogram while the other four sizes resulted in 100% correlation between the predicted size and the output size.

Table 9.3: Individual sample analysis using different sequence specific probes and size-based tags.

Sample Name	Target DNA Size (bp)	Predicted Size ± sizing resolution for Bioanalyzer (bp)	Average Output Size (bp) (n = 4)
30 bp target	152 bp	212 ± 10 bp	No detection
40 bp target	150 bp	230 ± 11 bp	235 bp
60 bp target	156 bp	276 ± 13 bp	278 bp
70 bp target	156 bp	296 ± 14 bp	293 bp
80 bp target	165 bp	325 ± 16 bp	332 bp

Following the individual size-based analysis, the method was tested in a multiplexed system where all five DNA targets were mixed together as well as 50 bp target 1 and 90 bp target 1, resulting in a simple multiplexed assay with 7 individual target DNA sequences. Figure 3 shows a representative electropherogram output of this test with peaks at 236 bp, 251 bp, 279 bp, and 294 bp, corresponding to the 40 bp target, 50 bp target, 60 bp target, and 70 bp target, respectively. The last peak at 333 bp is considered inconclusive in this study because both the 80 bp target and 90 bp target showed a peak at this size range when tested individually, this will be a key consideration for future applications of this method as to avoid conflicting results during multiplexing analysis. Lastly, when investigating the electropherogram further a small peak (0.09 ng/µL) can be identified at 212 bp which is hypothesized to correspond to the 30 bp target. However, this peak is below the fluorescence height threshold used to analyze the other peak sizes, therefore, it cannot be concluded that the method works with 30 bp size-based tags.

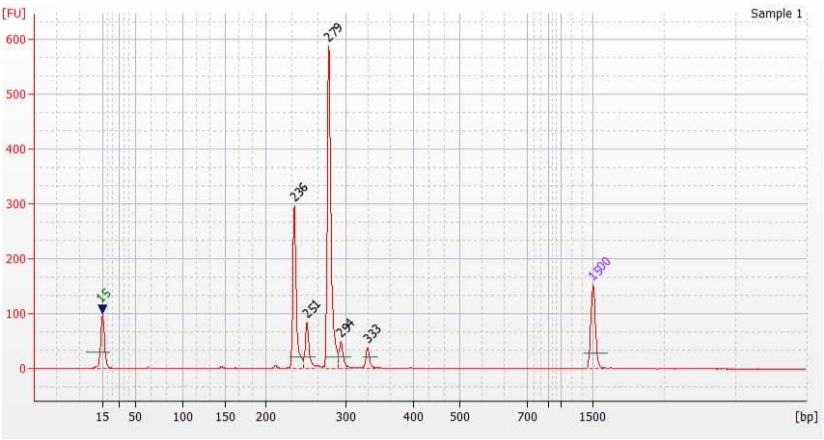

Figure 9.3: Multiplex detection and analysis target DNA of same starting size using sequence specific probes and size-based tags of 30 bp, 40 bp, 50 bp, 60 bp, 70 bp, 80 bp, and 90 bp.

Along with the multiplexing results for this method, sample sensitivity and specificity was investigated to better test the robustness of the method. As it was important to investigate the translatability of this approach to cfDNA analysis and other applications, testing how much input DNA was needed to detect a peak on the electropherogram was crucial for determining what applications this method could be applied to. Figure 4 represents the results of this test where 30 ng of 50 bp target 1 and 30 ng of 90 bp target 1 were serially diluted and tested using this method and 20 PCR cycles. Figure 4a shows the average concentration (ng/µL) of each peak for each input DNA amount where the 250 bp peak corresponded to the 50 bp size-based tags and the 330 bp peak corresponded to the 90 bp size-based tags. The 330 bp peak had a limit of detection of 0.3 ng while the 250 bp peak was 0.003 ng. While a small peak (0.14 ± 0.04 ng/µL) was detected at 250 bp in the no template control (NTC) due to non-specific amplification, there was a statistically significant difference between that concentration and the concentration for 0.003 ng input DNA for the 250 bp peak (* 0.0157, unpaired t-test). While it was still a minimal amount of DNA (0.20 ± 0.05) found at this input sample amount, this result shows the potential for target DNA sequences to be detected at low picogram input concentrations.

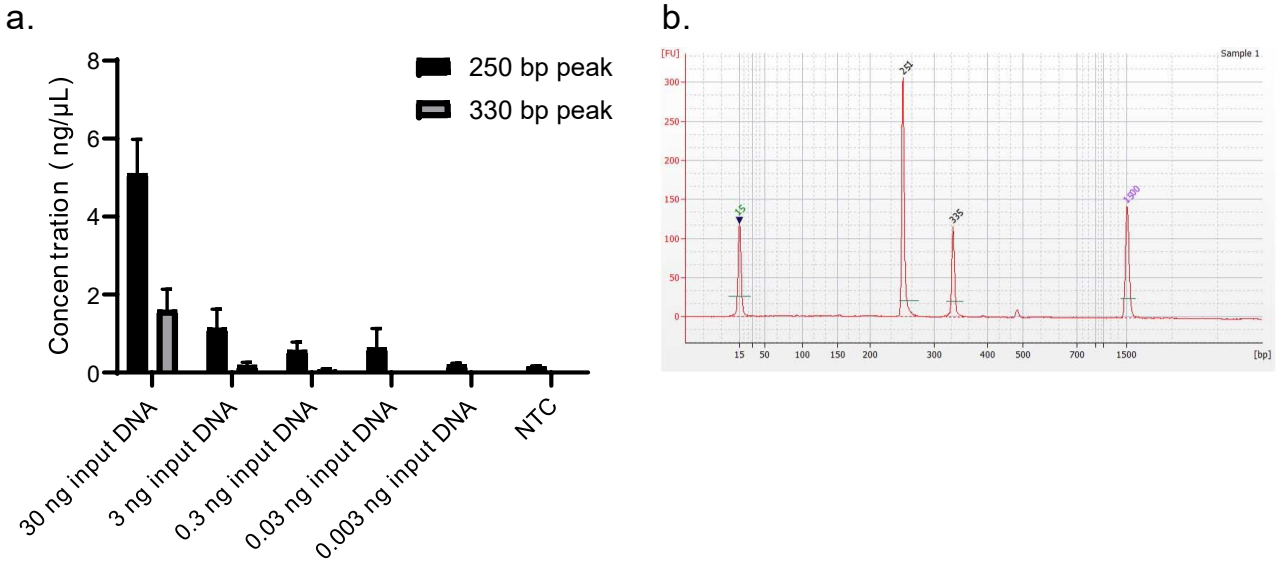

Figure 9.4: Limit of detection analysis. a. Concentration (ng/µL) analysis of various amounts of input DNA. b. Representative electropherogram of 30 ng input DNA per target. Note there is an additional peak around 500 bp, this is from the 50 bp target 1 input sample.

Sample complexity was also tested to analyze the specificity and robustness of this method. To do this target DNA was diluted in either human genomic DNA or fragmented M13mp18 DNA. The predicted peak sizes for this testing, based on the tags used for the target DNA, are 230 ± 11 bp, 276 ± 13 bp, and 296 ± 14 bp. Figure 5 shows the results of both tests with representative electropherograms while Table 4 provides the average size (bp) and concentrations (ng/μL) of the peaks. The results show that for both sample types there was 100% agreement between the predicted size and the output size, even in the more complex samples where the target DNA, sequence-specific probes, and size-based tags may have been less thermodynamically likely to hybridize due to the concentration of non-targeted DNA sequences.

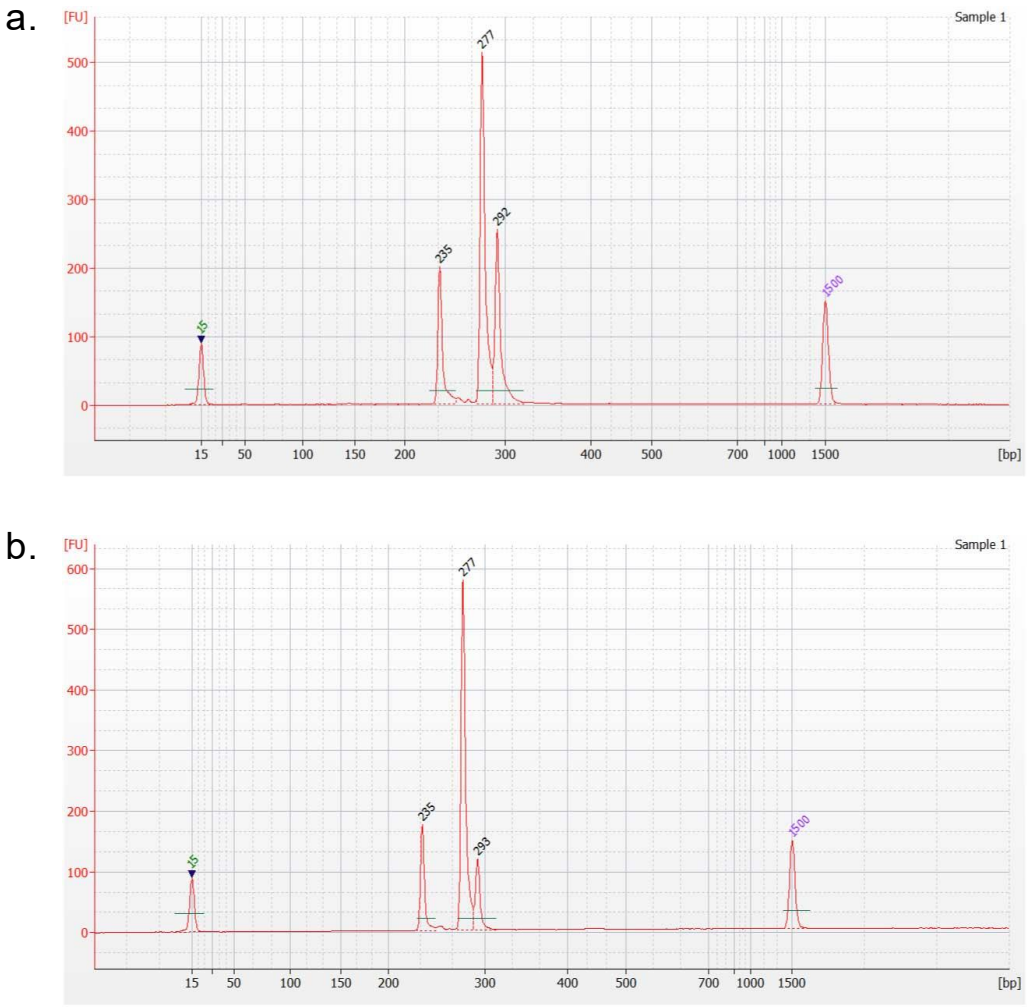

Figure 9.5: Specificity testing of target DNA, 40 bp target, 60 bp target, and 70 bp target, diluted in (a) 500 ng human gDNA or (b) 10 ng M13mp18 149-bp DNA.

Table 9.4: Specificity testing of target DNA, 40 bp target, 60 bp target, and 70 bp target, diluted in 500 ng human gDNA or 10 ng M13mp18 149-bp DNA.

Sample Name	Predicted Size ± sizing resolution for Bioanalyzer (bp)	Average Output Size (bp)	Average Concentration (ng/μL)
40 bp target in gDNA	230 ± 11 bp	231.8 ± 1.9 bp	4.24 ± 0.6 ng/μL
60 bp target in gDNA	276 ± 13 bp	273.4 ± 2 bp	10.17 ± 0.5 ng/μL
70 bp target in gDNA	296 ± 14 bp	288.5 ± 2.4 bp	4.76 ± 0.6 ng/μL
40 bp target in M13mp18	230 ± 11 bp	231.7 ± 1.9 bp	2.78 ± 0.5 ng/μL
60 bp target in M13mp18	276 ± 13 bp	272.7 ± 2.4 bp	9.92 ± 1 ng/μL
70 bp target in M13mp18	296 ± 14 bp	288.1 ± 2.6 bp	1.90 ± 0.3 ng/μL

The last test of sample sensitivity and transferability to the future application of cfDNA analysis was performed with target DNA extracted from 1 mL of AcroMetrix EDTA Plasma Dilution Matrix using the BIOO NextPrep-Mag cfDNA Isolation Kit. With 24 ng of total target DNA added into the 1 mL of plasma before extraction, the concentration and purity of the extracted DNA was evaluated to better understand the input sample for this DNA analysis method. The concentration of the 150 bp target DNA was measured using the Agilent Bioanalyzer and was found to be 0.535 ng/μL, 0.44 ng/μL, and 0.455 ng/μL for the three plasma samples tested. Additionally, the purity of these samples were tested using the NanoDrop 1000 UV-Vis Spectrophotometer (Thermo Scientific, Waltham, MA, USA), by means of the A_{260}/A_{280} and A_{260}/A_{230} ratios which compare the sample's absorbance of ultraviolet light at 260 nm, 230 nm, and 280 nm. This was important because the cfDNA isolation kit contains PCR inhibitors in the form of chaotropic salts, namely guanidinium thiocyanate (GTC), in multiple buffers which may affect downstream amplification efficiency results. GTC and other chaotropic salts are absorbed at 230 nm, therefore, the A_{260}/A_{230} ratio is an important metric in understanding the presence of this inhibitor in the sample[382]. Where the target DNA added to the plasma averaged at 2.26 for the A_{260}/A_{230} ratio, the extracted target DNA averaged at 0.09 indicating a larger amount of GTC which has the potential to reduce the PCR efficiency in this method. Table 5 presents the results of this method with the average output size (bp) and concentration (ng/μL) of the three plasma samples tested. While the concentrations of each of the different peaks were reduced for these samples, 100% of the peak sizes fell within the range of the predicted sizes.

Table 9.5: Method results for target DNA extracted from plasma. *Indicates one of the two tests per sample did not amplify for this target size.

Sample Name	Target Name	Predicted Size ± sizing resolution for Bioanalyzer (bp)	Average Output Size (bp)	Average Concentration (ng/μL)
Plasma Sample 1	40 bp target	230 ± 11 bp	233.0 ± 1.6 bp	2.12 ± 0.1 ng/μL
	60 bp target	276 ± 13 bp	275.2 ± 1.8 bp	7.89 ± 0.7 ng/μL
	70 bp target	296 ± 14 bp	290.0 ± 1.5 bp	0.41 ± 0.1 ng/μL
Plasma Sample 2	40 bp target	230 ± 11 bp	231.6 ± 1.3 bp	1.05 ± 0.5 ng/μL
	60 bp target	276 ± 13 bp	272.4 ± 2 bp	5.04 ± 1.8 ng/μL
	70 bp target	296 ± 14 bp	286.5 ± 0.7 bp*	0.53 ± 0.01 ng/μL*
Plasma Sample 3	40 bp target	230 ± 11 bp	232.8 ± 2.6 bp	2.61 ± 0.2 ng/μL
	60 bp target	276 ± 13 bp	274.8 ± 4 bp	9.51 ± 0.3 ng/μL
	70 bp target	296 ± 14 bp	290.0 ± 3.8 bp	0.70 ± 0.1 ng/μL

9.5 Discussion

A major outcome of this method development was that the sequence-specific probes and size-based tags consistently changed the overall DNA size as seen in the electropherogram analysis. Additionally, the final DNA sizes matched the predicted sizes based on the designed sequence-specific probe and size-based tag lengths accounting for the sizing resolution outlined by the Agilent DNA 1000 Kit Guide. Whether in single-plex or multiplexed assays, this method was specific for targeted nucleic acid analysis while avoiding the need for complex probe designs or PCR optimization. It was also noted that when the target DNA was diluted in nuclease free water, additional DNA, or extracted from a plasma sample, it did not decrease in specificity.

While the size (bp) of the final DNA structures were consistently predicted, the relative concentration (ng/μL) of the final products varied depending on the target sequence and run. Although universal PCR primers were used in this work to avoid amplification biases due to primer sequences, DNA peak sizes on the electropherogram consistently resulted in different concentrations (ng/μL) depending on the target DNA. The kinetics of the single stranded DNA hybridization and ligation are hypothesized to have played a role in these concentration differences, as well as the purification step in the assay may also contribute since the SPRI beads being used have size selection capabilities. The SPRI bead size selection occurs when different volumetric ratios of DNA and beads are used. In this method, a ratio of 0.6X beads to DNA is

utilized, however, as the beads settle to the bottom of the solution between uses, it is possible they were not evenly resuspended before being used for some trials. Therefore, the volumetric ratio could be changed and affect the DNA sizes captured during purification prior to amplification. Additionally, it is predicted that repeated freeze-thaw cycling of single stranded DNA probes and tags as well as double stranded target DNA may have caused nucleic acid degradation over time and affected the final concentration of the size-based product.

One challenge that arose during this method development was non-specific amplification of sequence-specific probes and size-based tags without target DNA. An important strategy to combat this was to remove the PCR primer sequence or complementary sequence from the sequence-specific probes so that the only way a size could amplify was if ligation had occurred and the tag-target-tag sequence was present. Additionally, adding the purification step was critical for removing any hybridized sequence-specific probe and size-based tag products without target DNA so that they could not be amplified. As mentioned previously, the SPRI beads used have size selection capabilities which means they will capture larger DNA sequences first and remove smaller DNA sequences. Thus, it is hypothesized that excess sequence-specific probes, size-based tags, and the hybridized product of these single stranded DNA will all have smaller masses than the double stranded DNA containing the target. They will therefore be removed using the SPRI method, while the double stranded DNA product will be captured and purified to be used during PCR amplification.

Due to the robustness testing in this study, this method shows the potential for applications using cfDNA extracted from plasma. One potential application that uses cfDNA is prenatal gene sequence screening during non-invasive prenatal screening (NIPT). NIPT uses a maternal blood draw to extract cfDNA originating from the mother and fetus, referred to as cell-free fetal DNA (cffDNA)[323]. The cffDNA has been used for aneuploidy analysis, such as trisomy 21 or Down Syndrome[323]. However, this analyte can also be utilized for mutation screening[383]. Therefore, this method can be designed to identify target mutations that can lead to significant medical problems by analyzing gene-specific sequences. Sequence-specific probes can be created for a target mutation and be assigned to one length. Since this method uses Taq Ligase, the

single stranded DNA target and tags needs to be hybridized with no gap to the complementary sequence-specific probe. This is beneficial as it allows for the resolution of single nucleotide variants because the sequences need to be lined up exactly in order for proper ligation and amplification to occur. To ensure the sequence-specific probe will match the exact DNA target containing the mutation, a restriction enzyme digestion or PCR amplification step could be used around the targeted mutation to guarantee the exact sequence matching the sequence-specific probe is present.

Overall, this multiplexed nucleic acid analysis method is ideal for smaller starting size DNA for simple, robust detection. This assay also shows the potential for grouping target sequences by size (bp) if needed while still multiplexing. Through the use of universal PCR primers, this protocol can be performed at one annealing temperature without the needed for primer optimization for every target which may be necessary with a method like ARMS-PCR. Lastly, this method only requires one sequence-specific probe to hybridize to the target DNA, compared to two in MLPA. This is advantageous as the target DNA can be captured through one hybridization reaction and the size-based tags, which also hybridize to the probes, can be added at a higher ratio to ensure they are hybridized without the potential for non-specific amplification that can interfere with the method results. If sequence-specific probes needed to be added in excess this could lead to a potential peak on the electropherogram in the predicted size range and interfere with the accuracy of the results.

9.6 Conclusion

In summary, this research presents the development of a method for sequence-specific nucleic acid analysis using a DNA capture approach. Through the combination of sequence-specific probes and size-based tags, target DNA sequences of similar lengths can hybridize to complementary probes and be separated by size (bp) using microfluidic electrophoresis. The sensitivity of this assay was tested for an input sample down to 3 pg while the specificity was analyzed by diluting target DNA into genomic or fragmented DNA and the outcome sizes matched the predicted sizes 100% of the time. Lastly, the method was tested for the application of cfDNA extracted from plasma and maintained the same specificity as found in purified

starting samples. The next steps for this work will be to apply the method design to specific cfDNA analysis or additional applications and further test the robustness of this simple, accurate nucleic acid test.

9.7 Acknowledgements

This work was in part supported by Perkin Elmer's research grant to Brown University. Additionally, the authors would like to acknowledge Amar Kamath and others from PerkinElmer for their guidance and material supplies.

9.8 Supplemental Information

Table SI 9.1: PCR Reaction Conditions for Target Preparation and Protocol Amplification

PCR Reaction	Target Preparation	Protocol Amplification
Initial Denaturation	94°C for 30 sec	94°C for 30 sec
Cycling	40 cycles - 94°C for 30 sec - Target specific annealing temp for 45 sec - 68°C for 60 sec	20 cycles - 94°C for 30 sec - 58° for 45 sec - 68°C for 60 sec
Final Extension	68°C for 5 min	68°C for 5 min
Hold	10°C	10°C

Table SI 9.2: Forward and reverse primer sequences for preparing target DNA and annealing temperature used during PCR amplification.

Target	Forward Primer (5' – 3')	Reverse Primer (5' – 3')	Annealing Temp for PCR
30 bp tag DNA target	ATCAACGTAACAAAGCTGCT	GTATAATGAGCCAGTTCTTA	43°C
40 bp tag DNA target	ATAATTTTTTCACGTTGAAA	TGCGTGGGCGATGGTTGTTG	39°C
50 bp tag DNA target 1	ACGCCAGGGTTTTCCCAGTC	AGCGGATAACAATTTCACACAGG	60°C
50 bp tag DNA target 2	TAAAATGTTTAGACTGGATA	TTGCTTCTGACTATAATAGT	49°C
60 bp tag DNA target	GTACCGACAAAAGGTAAAGT	TTGGTTTCTACATGCTCGTA	47°C
70 bp tag DNA target	TAACAATTTCATTTGAATTA	AGCGTCTTAATCTAAGCTAT	35°C
80 bp tag DNA target	GAAGAAAGCGAAAGGAGCGG	CTAACGAGGAAAGCACGTTA	49°C
90 bp tag DNA target 1	AGCCATATTATTTATCCCAA	CCTCTGACTTTGTTCAGGGT	51°C
90 bp tag DNA target 2	CAAATGAAAAATCTAAAGCA	GCTCTAATCTATTAGTTGTT	49°C

CHAPTER 10

Conclusions

10.1 Summary

This thesis focuses on fundamental approaches to developing and improving molecular diagnostic technologies, specifically through the use of microfluidic methods. This work ranges from the investigation into molecular transport for nucleic acid extraction and purification to exploring reaction kinetics for amplification and detection. The three main approaches guiding this thesis towards these method developments and improvements were (1) reducing false positive testing errors; (2) increasing sample purity for efficient downstream processes such as amplification; and (3) reducing human error that may be affected by precise and accurate reagent handling and time management. Based on these themes, we can draw the following conclusions and suggestions for future work.

10.2 Conclusions

10.2.1 Reducing false positive testing errors

While this is a critical theme for the development of any molecular diagnostic test, Chapters 2 and 9 specifically address the reduction of false positive testing errors. To begin, Chapter 2 presents the development of a mathematical model to predict the structure sizes (bp) of DNA concatemers created using LAMP, an isothermal amplification technique for nucleic acids. Due to the different structure sizes produced, they will appear as a banding pattern on a gel electrophoresis plot, thus, this model is able to predict the specific banding pattern of different sized LAMP structures based on the input target DNA and primer sequences. Through the use of capillary electrophoresis this was tested for robustness and translatability to a number of applications found in the literature. Overall, the ability to predict a true positive vs false positive result prior to running any experiments was a major outcome of this study.

This work has the potential to be expanded upon further as LAMP continues to grow as a nucleic acid amplification technique for a variety of applications. Not only can the mathematical model be used for LAMP assay optimization, the data collected from these experiments provides more insight into how this

amplification technique works. While the size (bp) of the LAMP structures was the focus of this work, the concentration (ng/μL) of the LAMP products at each size can be investigated further to draw more conclusions regarding the total copy number of the target DNA sequences in the sample as well as the proportion of different structure sizes produced during a reaction.

Next, Chapter 9 also address this theme of reducing false positive testing errors through the development of a robust, simple, multiplexed nucleic acid test. This method combines target DNA, sequence specific probes, and size-based tags to transform DNA of similar sizes (bp) into different sizes for separation using capillary electrophoresis. With a 100% correlation between predicted sizes and outcome sizes, this method can qualitatively assess the presence of multiple target DNA sequences in a sample due to the specificity incorporated into the method design.

One future direction for this work is to translate the method to be used for quantitative studies as well as qualitative studies. While the size (bp) of the target DNA sequences is robustly consistent with the predicted size, it would be advantageous to understand the kinetics of the hybridization, ligation, purification, and amplification reactions more in order to predict and understand different concentrations for final products.

10.2.2 Increasing sample purity

As nucleic acid extraction and purification make up two of the five main steps in the molecular diagnostics workflow, developing methods to improve these processes was a major focus of this thesis work. Overall, Chapters 4, 5, 6, and 8 are related directly to this major theme. More specifically, Chapters 4, 5, and 8 all utilize a combination of magnetic bead transport coupled with EOF on a microfluidic chip for increasing the purity of the target DNA sample used in that study. Chapter 4 explores investigating these phenomena for reducing carryover contamination, Chapter 5 focuses on the application of NGS library preparation and removing primer and adapter dimers, and lastly, Chapter 8 investigates cfDNA extraction and purification for the application of NIPT. In all cases, the microfluidic chip setup was able to show an increase in sample purity for each applicable application.

Chapter 6 also focuses on increasing sample purity using a microfluidic chip but with magnetic bead transport coupled with electrophoresis as an alternative electrokinetic phenomenon. This chapter is again

working towards the application of NGS library preparation, but for the application of diagnosing aneuploidy during PGT-A. In this chapter, an automated library preparation device was constructed that combines precise liquid handling, mixing, and thermoelectric cooler-based heating and cooling along with the automated loading and transport of DNA-bound magnetic beads in a microfluidic chip for sample purification.

Future work for these microfluidic chip designs could be to test alternative starting sample types, such as blood and saliva, to understand how this combination of magnetic bead transport and EOF or electrophoresis can help to purify nucleic acids. Additionally, it would be advantageous to further characterize and quantify EOF vs electrophoresis within the microfluidic channel to better understand the fundamental phenomenon as they are applied to the application of nucleic acid extraction and purification.

10.2.3 Reducing human error

This last major theme is important because it focuses on simplifying and automating molecular diagnostic technologies to reduce the chances and impact of human errors. This theme is addressed in Chapter 3 as well as Chapter 6. In Chapter 3, the method of reducing the number of reagents and the time needed for sample preparation is tested for a COVID-19 detection test. In this work, dry and wet nasal swabs are tested using the procedure and the wet swab conditions include samples where RNA extraction is performed (treated sample) as well as using the universal transport medium the wet swab is stored in as the starting sample for the assay (untreated sample). For the dry and untreated sample types the RNA extraction procedure is excluded as the DirectDetect method is optimized for PCR analysis without extraction which uses fewer reagents and protocol steps that can be negatively impacted by human error. This work shows that the dry and untreated sample types performed as well or better than the treated sample type which required RNA extraction, showing how reducing the complexity of an assay does not reduce the accuracy. The work in Chapter 6 is again explored for this theme as it involves using automation for the nucleic acid sample preparation process for NGS. This work shows a new automated method which requires little user operation which reduces the potential for human errors.

These two chapters highlight the potential for reducing human errors in molecular diagnostics tests by requiring less hands-on time. Future work for this theme could be to apply these principles to even more diagnostic applications. One benefit of the device created in Chapter 6 was its simplicity. Instead of utilizing an expensive liquid handler, a two-cannula system was used for liquid movement with a microfluidic chip for purification, and a thermoelectric cooler for PCR. In theory, any assay that required liquid handling, purification, and heating can be performed with this device, thus, increasing the throughput and accuracy will be critical for adapting more procedures to this setup.

10.3 Future research directions

While a lot of work was accomplished in this thesis, there are numerous directions and ideas that can be expanded upon further.

10.3.1 Translate methods to real patient samples

One major limitation of the work presented in this thesis is the lack of transferability of the developed methods to real patient samples. Out of the eight research chapters presented, only one utilized real patient samples. Thus, to further test and validate this work, this is an important future direction. One consideration for this future direction is the limited availability of specific sample types which were investigated in this thesis, such as for the applications of PGT-A and NIPT. Therefore, increasing collaborations with clinical labs could ensure that technologies, such as those presented in this thesis, can be tested for transferability to the true clinical samples they are designed for.

10.3.2 Increase understanding of cfDNA sample used for aneuploidy detection

As aneuploidy detection was the main application explored in this thesis, one future direction can be dedicated to investigating sequences of aneuploidy cfDNA samples to design more targeted extraction methods for aneuploidy screening during NIPT. Through increasing the fundamental research into determining fetal fraction, to analyzing patterns in DNA sequences present in an aneuploidy sample, this insight can help to improve the development of screening methods for NIPT. Next steps in this field of research can involve computational analysis of existing data for NIPT as well as targeted assessment of patient samples. The goal would be to analyze if specific DNA sequences are more statistically likely to be

found in an NIPT sample which screens positive for aneuploidy. If so, that information can be used to created more targeted DNA extraction methods for those specific sequences when extracting cfDNA from maternal plasma, instead of aiming to extract as much sample as possible.

10.3.3 Expanding the use of electrokinetics on microfluidic devices

While this thesis explored the use of EOF and electrophoresis on a microfluidic device for nucleic acid extraction and purification, it was limited in that additional electrokinetic phenomenon can also be studied. Specifically, for this thesis research, a constant voltage and current supply was applied to the microfluidic chip for all applications. However, using more intricate pulsating, variable, or alternating currents could also be used to further explore the effect on nucleic acid purification. While the focus of the research was to migrate contaminants away from the DNA-bound magnetic beads, changing the type of current applied to the microchannel may lead to further discoveries surrounding how the magnetic beads interact with the electric field as well as free contaminants. Additionally, dielectrophoresis is another method used for liquid phase extraction, thus, future research could also focus on incorporating this method into a microfluidic chip designed for nucleic acid extraction and purification coupled with magnetic bead-based solid phase extraction. Lastly, another future direction can be to use electrokinetics on microfluidic devices for the extraction of multiplexed target molecules (i.e., nucleic acids and proteins) from biological samples, this thesis only explores nucleic acid technologies so investigating other biological molecules can also be advantageous.

10.3.4 Incorporating CRISPR/Cas nucleic acid detection into method designs

While technologies such as PCR and LAMP, which have been around for a number of years, were the basis of this thesis work, these techniques are limited in some capacity by their sensitivity and specificity. Therefore, one newer nucleic acid detection method that can be explored further to develop more sensitive and specific molecular diagnostic technologies is Cluster Regularly Interspaced Short Palindromic Repeats (CRISPR)-associated nuclease (Cas)-based sensing[384]. What makes this technique unique for diagnostic applications is that a target nucleic acid sequence can be hybridized to which induces enzymatic cleavage of both the target sequence and untargeted collateral cleavage of all single stranded RNA[384]. Thus, if the

untargeted RNA contains quenched fluorescent nucleotides, this enzymatic cleavage cascade will lead to the unquenching of fluorophore and an efficient increase in signal amplification up to 10,000 times the original target sequence concentration[384]. This highly selective and sensitive method could be used for future research in aneuploidy detection, mutation analysis, cfDNA screening methods, and more.

10.4 Contributions of this thesis

10.4.1 Contributions to the field

The following list summarizes the contributions of this thesis to the field:

- Created molecular diagnostic tools that are translatable to any application
    - LAMP model to predict false-positive diagnostic tests can be used for any LAMP assay.
    - Electrokinetic microfluidic chip design can be used for any nucleic acid extraction and purification application and be optimized for different starting samples including plasma for cfDNA extraction, NGS library preparation, and more.
- Contributed knowledge on the DNA product sizes and geometries produced during LAMP.
- Investigated fundamental molecular biology and biochemistry principles in NGS library preparation to enable translatability onto an automated platform.
    - Including reaction components and kinetics needed for DNA fragmentation, ligation, purification, and amplification.
- Tested and analyzed a diagnostic test for COVID-19, which reduced the amount of time and reagents needed, during the worldwide pandemic to contribute to the extensive diagnostic testing needs during this time.
- Designed a method for targeted, multiplexed DNA analysis without the need for multiple fluorophores which can be used for applications such as cfDNA analysis.
- Reviewed progress and challenges in laboratory-based diagnostic and screening approaches for aneuploidy detection during pregnancy.

10.4.2 Contributions to the scientific community

The following list summarizes the contributions of this thesis work to the scientific community at Brown University and beyond:

- Mentored undergraduate and master's students for research, innovation, and communication skills.
- Presented work at numerous conferences and symposiums through oral and poster presentations.
- Focused on advancements in prenatal testing to empower patients with critical information about their unborn child.
- Developed methods with universal applications for detection using LAMP, NGS library preparation for any DNA sequencing, and targeted DNA analysis.
- Established automated technology that incorporated controlled heating and cooling, liquid motion and mixing, and microfluidic purification which is adaptable and scalable to different procedures.
- Used tools to investigate and model microfluidic devices translatable to numerous device designs.
- Utilized fundamental molecular biology and physics tools to solve problems and approach research questions.

REFERENCES

1 Ohno, M. & Caughey, A. The role of noninvasive prenatal testing as a diagnostic versus a screening tool–a cost-effectiveness analysis. *Prenatal diagnosis* **33**, 630-635 (2013).

2 Zhang, S. *et al.* Nucleic acid testing for coronavirus disease 2019: demand, research progression, and perspective. *Critical Reviews in Analytical Chemistry*, 1-12 (2020).

3 Devonshire, A. S. *et al.* Towards standardisation of cell-free DNA measurement in plasma: controls for extraction efficiency, fragment size bias and quantification. *Analytical and bioanalytical chemistry* **406**, 6499-6512 (2014).

4 Clausen, F. B., Krog, G. R., Rieneck, K. & Dziegiel, M. H. Improvement in fetal DNA extraction from maternal plasma. Evaluation of the NucliSens Magnetic Extraction system and the QIAamp DSP Virus Kit in comparison with the QIAamp DNA Blood Mini Kit. *Prenatal Diagnosis: Published in Affiliation With the International Society for Prenatal Diagnosis* **27**, 6-10 (2007).

5 Park, S., Zhang, Y., Lin, S., Wang, T.-H. & Yang, S. Advances in microfluidic PCR for point-of-care infectious disease diagnostics. *Biotechnology advances* **29**, 830-839 (2011).

6 Nasseri, B. *et al.* Point-of-care microfluidic devices for pathogen detection. *Biosensors and Bioelectronics* **117**, 112-128 (2018).

7 Cui, F., Rhee, M., Singh, A. & Tripathi, A. Microfluidic sample preparation for medical diagnostics. *Annual review of biomedical engineering* **17**, 267-286 (2015).

8 Mach, A. J., Adeyiga, O. B. & Di Carlo, D. Microfluidic sample preparation for diagnostic cytopathology. *Lab on a Chip* **13**, 1011-1026 (2013).

9 Siegrist, J. *et al.* Validation of a centrifugal microfluidic sample lysis and homogenization platform for nucleic acid extraction with clinical samples. *Lab on a Chip* **10**, 363-371 (2010).

10 Cui, F. R., Wang, J., Opal, S. M. & Tripathi, A. Isolating Influenza RNA from Clinical Samples Using Microfluidic Oil-Water Interfaces. *PLoS ONE* **11**, e0149522, doi:10.1371/journal.pone.0149522 (2016).

11 Troiano, D., Deraney, R. N. & Tripathi, A. Effect of surfactants on carryover liquid volume in immiscible phase magnetic bead separation. *Colloids and Surfaces A: Physicochemical and Engineering Aspects* **513**, 188-195 (2017).

12 Zhu, Z. *et al.* Single-molecule emulsion PCR in microfluidic droplets. *Analytical and bioanalytical chemistry* **403**, 2127-2143 (2012).

13 Segato, T. P. *et al.* Microfab-less microfluidic capillary electrophoresis devices. *Analytical Methods* **5**, 1652-1657 (2013).

14 Le Roux, D. *et al.* An integrated sample-in-answer-out microfluidic chip for rapid human identification by STR analysis. *Lab on a Chip* **14**, 4415-4425 (2014).

15 Xu, Z., Qiao, Y. & Tu, J. Microfluidic Technologies for cfDNA Isolation and Analysis. *Micromachines* **10**, 672, doi:10.3390/mi10100672 (2019).

16 Jing, M. & Bowser, M. T. Isolation of DNA aptamers using micro free flow electrophoresis. *Lab on a Chip* **11**, 3703-3709 (2011).

17 Turgeon, R. T. & Bowser, M. T. Micro free-flow electrophoresis: theory and applications. *Analytical and bioanalytical chemistry* **394**, 187-198 (2009).

18 D'Amico, L., Ajami, N., Adachi, J., Gascoyne, P. & Petrosino, J. Isolation and concentration of bacteria from blood using microfluidic membraneless dialysis and dielectrophoresis. *Lab on a Chip* **17**, 1340-1348 (2017).

19 Abd Rahman, N., Ibrahim, F. & Yafouz, B. Dielectrophoresis for biomedical sciences applications: A review. *Sensors* **17**, 449 (2017).

20 Li, P., Li, M., Yue, D. & Chen, H. Solid-phase extraction methods for nucleic acid separation. A review. *Journal of Separation Science* (2021).

21 Xu, Y. *et al.* Solid-phase reversible immobilization in microfluidic chips for the purification of dye-labeled DNA sequencing fragments. *Analytical chemistry* **75**, 2975-2984 (2003).
22 Kim, J. *et al.* Nucleic acid isolation and enrichment on a microchip. *Sensors and Actuators A: Physical* **195**, 183-190 (2013).
23 Baldessari, F. & Santiago, J. G. Electrophoresis in nanochannels: brief review and speculation. *Journal of Nanobiotechnology* **4**, 1-6 (2006).
24 Dutta, P. & Beskok, A. Analytical solution of combined electroosmotic/pressure driven flows in two-dimensional straight channels: finite Debye layer effects. *Analytical chemistry* **73**, 1979-1986 (2001).
25 Kim, S. M., Burns, M. A. & Hasselbrink, E. F. Electrokinetic protein preconcentration using a simple glass/poly (dimethylsiloxane) microfluidic chip. *Analytical Chemistry* **78**, 4779-4785 (2006).
26 Chang, C.-M. *et al.* Nucleic acid amplification using microfluidic systems. *Lab on a Chip* **13**, 1225-1242 (2013).
27 Craw, P. & Balachandran, W. Isothermal nucleic acid amplification technologies for point-of-care diagnostics: a critical review. *Lab on a Chip* **12**, 2469-2486 (2012).
28 Freeman, W. M., Walker, S. J. & Vrana, K. E. Quantitative RT-PCR: pitfalls and potential. *Biotechniques* **26**, 112-125 (1999).
29 Hindson, B. J. *et al.* High-throughput droplet digital PCR system for absolute quantitation of DNA copy number. *Analytical chemistry* **83**, 8604-8610 (2011).
30 VanGuilder, H. D., Vrana, K. E. & Freeman, W. M. Twenty-five years of quantitative PCR for gene expression analysis. *Biotechniques* **44**, 619-626 (2008).
31 Lan, L. *et al.* Positive RT-PCR test results in patients recovered from COVID-19. *Jama* **323**, 1502-1503 (2020).
32 Vasudevan, H. N. *et al.* Digital droplet PCR accurately quantifies SARS-CoV-2 viral load from crude lysate without nucleic acid purification. *Scientific reports* **11**, 1-9 (2021).
33 Ward, D. G. *et al.* Multiplex PCR and next generation sequencing for the non-invasive detection of bladder cancer. *PloS one* **11**, e0149756 (2016).
34 Moltzahn, F. *et al.* Microfluidic-based multiplex qRT-PCR identifies diagnostic and prognostic microRNA signatures in the sera of prostate cancer patients. *Cancer research* **71**, 550-560 (2011).
35 Li, N. *et al.* Digital PCR quantification of miRNAs in sputum for diagnosis of lung cancer. *Journal of cancer research and clinical oncology* **140**, 145-150 (2014).
36 Yang, C. *et al.* Integrative analysis of microRNA and mRNA expression profiles in non-small-cell lung cancer. *Cancer gene therapy* **23**, 90-97 (2016).
37 Staines, K. *et al.* A versatile panel of reference gene assays for the measurement of chicken mRNA by quantitative PCR. *PloS one* **11**, e0160173 (2016).
38 Karamitros, T. & Magiorkinis, G. A novel method for the multiplexed target enrichment of MinION next generation sequencing libraries using PCR-generated baits. *Nucleic acids research* **43**, e152-e152 (2015).
39 Kou, R. *et al.* Benefits and challenges with applying unique molecular identifiers in next generation sequencing to detect low frequency mutations. *PloS one* **11**, e0146638 (2016).
40 Chang, C.-C. *et al.* Diagnostic devices for isothermal nucleic acid amplification. *Sensors* **12**, 8319-8337 (2012).
41 Notomi, T. *et al.* Loop-mediated isothermal amplification of DNA. *Nucleic Acids Research* **28**, e63-e63 (2000).
42 Ahn, S. J. *et al.* Rapid and simple colorimetric detection of multiple influenza viruses infecting humans using a reverse transcriptional loop-mediated isothermal amplification (RT-LAMP) diagnostic platform. *BMC infectious diseases* **19**, 1-12 (2019).
43 Roy, S., Mohd-Naim, N. F., Safavieh, M. & Ahmed, M. U. Colorimetric nucleic acid detection on paper microchip using loop mediated isothermal amplification and crystal violet dye. *ACS sensors* **2**, 1713-1720 (2017).

44 Lin, Q. *et al.* Graphene oxide-based suppression of nonspecificity in loop-mediated isothermal amplification enabling the sensitive detection of cyclooxygenase-2 mRNA in colorectal cancer. *Analytical chemistry* **91**, 15694-15702 (2019).
45 Jang, W. S. *et al.* Development of a multiplex Loop-Mediated Isothermal Amplification (LAMP) assay for on-site diagnosis of SARS CoV-2. *PloS one* **16**, e0248042 (2021).
46 Park, G.-S. *et al.* Development of reverse transcription loop-mediated isothermal amplification assays targeting severe acute respiratory syndrome coronavirus 2 (SARS-CoV-2). *The Journal of Molecular Diagnostics* **22**, 729-735 (2020).
47 Ali, M. M. *et al.* Rolling circle amplification: a versatile tool for chemical biology, materials science and medicine. *Chemical Society Reviews* **43**, 3324-3341 (2014).
48 Zhao, H. *et al.* Analysis of CpG island methylation using rolling circle amplification (RCA) product microarray. *Journal of biomedical nanotechnology* **7**, 292-299 (2011).
49 Cheng, Y., Li, Z., Du, B. & Zhang, X. Homogeneous and label-free bioluminescence detection of single nucleotide polymorphism with rolling circle amplification. *Analyst* **133**, 750-752 (2008).
50 Cho, E. J., Yang, L., Levy, M. & Ellington, A. D. Using a deoxyribozyme ligase and rolling circle amplification to detect a non-nucleic acid analyte, ATP. *Journal of the American Chemical Society* **127**, 2022-2023 (2005).
51 Mullenix, M. C., Wiltshire, S., Shao, W., Kitos, G. & Schweitzer, B. Allergen-specific IgE detection on microarrays using rolling circle amplification: correlation with in vitro assays for serum IgE. *Clinical Chemistry* **47**, 1926-1930 (2001).
52 Coelho, B. J. *et al.* A digital microfluidics platform for loop-mediated isothermal amplification detection. *Sensors* **17**, 2616 (2017).
53 Hamidi, S. V., Ghourchian, H. & Tavoosidana, G. Real-time detection of H 5 N 1 influenza virus through hyperbranched rolling circle amplification. *Analyst* **140**, 1502-1509 (2015).
54 Lucchi, N. W. *et al.* Real-time fluorescence loop mediated isothermal amplification for the diagnosis of malaria. *PloS one* **5**, e13733 (2010).
55 Maxwell, S. M. & Grifo, J. A. Should every embryo undergo preimplantation genetic testing for aneuploidy?: A review of the modern approach to in vitro fertilization. *Best Practice & Research Clinical Obstetrics & Gynaecology* (2018).
56 Bianco, K., Caughey, A. B., Shaffer, B. L., Davis, R. & Norton, M. E. History of miscarriage and increased incidence of fetal aneuploidy in subsequent pregnancy. *Obstetrics & Gynecology* **107**, 1098-1102 (2006).
57 Homer, H. A. Preimplantation genetic testing for aneuploidy (PGT-A): The biology, the technology and the clinical outcomes. *Australian and New Zealand Journal of Obstetrics and Gynaecology* **59**, 317-324 (2019).
58 Gadsbøll, K. *et al.* Current use of noninvasive prenatal testing in Europe, Australia and the USA: A graphical presentation. *Acta obstetricia et gynecologica Scandinavica* **99**, 722-730 (2020).
59 Nicolaides, K. H., Syngelaki, A., Ashoor, G., Birdir, C. & Touzet, G. Noninvasive prenatal testing for fetal trisomies in a routinely screened first-trimester population. *American Journal of Obstetrics and Gynecology* **207**, 374.e371-374.e376, doi:https://doi.org/10.1016/j.ajog.2012.08.033 (2012).
60 Iwarsson, E. *et al.* Analysis of cell-free fetal DNA in maternal blood for detection of trisomy 21, 18 and 13 in a general pregnant population and in a high risk population–a systematic review and meta-analysis. *Acta obstetricia et gynecologica Scandinavica* **96**, 7-18 (2017).
61 Curnow, K. J., Sanderson, R. K. & Beruti, S. in *Prenatal Diagnosis* 325-345 (Springer, 2019).
62 La Verde, M. *et al.* Performance of cell-free DNA sequencing-based non-invasive prenatal testing: experience on 36,456 singleton and multiple pregnancies. *BMC medical genomics* **14**, 1-11 (2021).
63 Hui, L. & Bianchi, D. W. Fetal fraction and noninvasive prenatal testing: what clinicians need to know. *Prenatal diagnosis* **40**, 155-163 (2020).

64 Afzal, A. Molecular diagnostic technologies for COVID-19: Limitations and challenges. *Journal of advanced research* (2020).
65 Liu, G. & Rusling, J. F. COVID-19 antibody tests and their limitations. *ACS sensors* **6**, 593-612 (2021).
66 Mullis, K. B. & Faloona, F. A. in *Recombinant DNA Methodology* 189-204 (Elsevier, 1989).
67 Zanoli, L. M. & Spoto, G. Isothermal amplification methods for the detection of nucleic acids in microfluidic devices. *Biosensors* **3**, 18-43 (2012).
68 Lizardi, P. M. *et al.* Mutation detection and single-molecule counting using isothermal rolling-circle amplification. *Nature genetics* **19**, 225 (1998).
69 Deiman, B., van Aarle, P. & Sillekens, P. Characteristics and applications of nucleic acid sequence-based amplification (NASBA). *Molecular biotechnology* **20**, 163-179 (2002).
70 Adedeji, A., Abdu, P., Luka, P., Owoade, A. & Joannis, T. Application of loop-mediated isothermal amplification assay in the detection of herpesvirus of turkey (FC 126 strain) from chicken samples in Nigeria. *Veterinary World* **10**, 1383 (2017).
71 Iwamoto, T., Sonobe, T. & Hayashi, K. Loop-mediated isothermal amplification for direct detection of Mycobacterium tuberculosis complex, M. avium, and M. intracellulare in sputum samples. *Journal of clinical microbiology* **41**, 2616-2622 (2003).
72 Parida, M., Sannarangaiah, S., Dash, P. K., Rao, P. & Morita, K. Loop mediated isothermal amplification (LAMP): a new generation of innovative gene amplification technique; perspectives in clinical diagnosis of infectious diseases. *Reviews in medical virology* **18**, 407-421 (2008).
73 Poon, L. L. M. *et al.* Detection of human influenza A viruses by loop-mediated isothermal amplification. *Journal of clinical microbiology* **43**, 427-430, doi:10.1128/JCM.43.1.427-430.2005 (2005).
74 Subramanian, S. & Gomez, R. D. An empirical approach for quantifying loop-mediated isothermal amplification (LAMP) using Escherichia coli as a Model System. *PloS one* **9**, e100596 (2014).
75 Bakthavathsalam, P., Longatte, G., Jensen, S. O., Manefield, M. & Gooding, J. J. Locked nucleic acid molecular beacon for multiplex detection of loop mediated isothermal amplification. *Sensors and Actuators B: Chemical* **268**, 255-263, doi:https://doi.org/10.1016/j.snb.2018.04.081 (2018).
76 Suleman, E., Mtshali, M. S. & Lane, E. Investigation of false positives associated with loop-mediated isothermal amplification assays for detection of Toxoplasma gondii in archived tissue samples of captive felids. *Journal of Veterinary Diagnostic Investigation* **28**, 536-542, doi:10.1177/1040638716659864 (2016).
77 Abbasi, I., Kirstein, O. D., Hailu, A. & Warburg, A. Optimization of loop-mediated isothermal amplification (LAMP) assays for the detection of Leishmania DNA in human blood samples. *Acta Tropica* **162**, 20-26, doi:https://doi.org/10.1016/j.actatropica.2016.06.009 (2016).
78 Liu, W. *et al.* Establishment of an accurate and fast detection method using molecular beacons in loop-mediated isothermal amplification assay. *Scientific Reports* **7**, 40125, doi:10.1038/srep40125

https://www.nature.com/articles/srep40125#supplementary-information (2017).
79 Lorenz, T. C. Polymerase chain reaction: basic protocol plus troubleshooting and optimization strategies. *Journal of visualized experiments: JoVE* (2012).
80 Thai, H. T. C. *et al.* Development and evaluation of a novel loop-mediated isothermal amplification method for rapid detection of severe acute respiratory syndrome coronavirus. *Journal of Clinical microbiology* **42**, 1956-1961 (2004).
81 Dukes, J., King, D. & Alexandersen, S. Novel reverse transcription loop-mediated isothermal amplification for rapid detection of foot-and-mouth disease virus. *Archives of virology* **151**, 1093-1106 (2006).

82 Han, E.-T. *et al.* Detection of four Plasmodium species by genus-and species-specific loop-mediated isothermal amplification for clinical diagnosis. *Journal of clinical microbiology* **45**, 2521-2528 (2007).
83 Zuker, M. Mfold web server for nucleic acid folding and hybridization prediction. *Nucleic acids research* **31**, 3406-3415 (2003).
84 Nelson, D. & Cox, M. 495-532 (Freeman, New York, 2008).
85 Fauci, A. S., Lane, H. C. & Redfield, R. R. Covid-19—navigating the uncharted. *The New England Journal of Medicine* **382**, 1268-1269 (2020).
86 Li, Q. *et al.* Early transmission dynamics in Wuhan, China, of novel coronavirus–infected pneumonia. *The New England Journal of Medicine* **382**, 1199-1207 (2020).
87 Yu, C.-J. *et al.* Assessment of basic reproductive number for COVID-19 at global level: A meta-analysis. *Medicine* **100** (2021).
88 Nishiura, H. *et al.* Estimation of the asymptomatic ratio of novel coronavirus infections (COVID-19). *International journal of infectious diseases* **94**, 154 (2020).
89 Zou, L. *et al.* SARS-CoV-2 viral load in upper respiratory specimens of infected patients. *The New England Journal of Medicine* **382**, 1177-1179 (2020).
90 Tang, Y.-W., Schmitz, J. E., Persing, D. H. & Stratton, C. W. Laboratory diagnosis of COVID-19: current issues and challenges. *Journal of clinical microbiology* **58** (2020).
91 Yu, L. *et al.* Rapid detection of COVID-19 coronavirus using a reverse transcriptional loop-mediated isothermal amplification (RT-LAMP) diagnostic platform. *Clinical chemistry* **66**, 975-977 (2020).
92 Grant, B. D. *et al.* SARS-CoV-2 coronavirus nucleocapsid antigen-detecting half-strip lateral flow assay toward the development of point of care tests using commercially available reagents. *Analytical chemistry* **92**, 11305-11309 (2020).
93 Huang, C., Wen, T., Shi, F.-J., Zeng, X.-Y. & Jiao, Y.-J. Rapid detection of IgM antibodies against the SARS-CoV-2 virus via colloidal gold nanoparticle-based lateral-flow assay. *ACS omega* **5**, 12550-12556 (2020).
94 Mostafa, H. H. *et al.* Metagenomic next-generation sequencing of nasopharyngeal specimens collected from confirmed and suspect covid-19 patients. *Mbio* **11** (2020).
95 Bhoyar, R. C. *et al.* High throughput detection and genetic epidemiology of SARS-CoV-2 using COVIDSeq next-generation sequencing. *PloS one* **16**, e0247115 (2021).
96 Sheikhzadeh, E., Eissa, S., Ismail, A. & Zourob, M. Diagnostic techniques for COVID-19 and new developments. *Talanta*, 121392 (2020).
97 Lescure, F.-X. *et al.* Clinical and virological data of the first cases of COVID-19 in Europe: a case series. *The Lancet Infectious Diseases* **20**, 697-706 (2020).
98 Wozniak, A. *et al.* A simple RNA preparation method for SARS-CoV-2 detection by RT-qPCR. *Scientific Reports* **10**, 1-8 (2020).
99 Chu, D. K. *et al.* Molecular diagnosis of a novel coronavirus (2019-nCoV) causing an outbreak of pneumonia. *Clinical chemistry* **66**, 549-555 (2020).
100 Lauring, A. S. & Hodcroft, E. B. Genetic Variants of SARS-CoV-2—What Do They Mean? *JAMA* **325**, 529-531 (2021).
101 Andersson, D., Svec, D., Pedersen, C., Henriksen, J. R. & Ståhlberg, A. Preamplification with dUTP and Cod UNG Enables Elimination of Contaminating Amplicons. *Int J Mol Sci* **19**, 3185, doi:10.3390/ijms19103185 (2018).
102 Wölfel, R. *et al.* Virological assessment of hospitalized patients with COVID-2019. *Nature* **581**, 465-469 (2020).
103 Higgins, T. S., Wu, A. W. & Ting, J. Y. SARS-CoV-2 Nasopharyngeal Swab Testing—False-Negative Results From a Pervasive Anatomical Misconception. *JAMA Otolaryngology–Head & Neck Surgery* **146**, 993-994 (2020).
104 Shuren, J. & Stenzel, T. Covid-19 molecular diagnostic testing—lessons learned. *New England Journal of Medicine* **383**, e97 (2020).

105 *SARS-CoV-2 Reference Panel Comparative Data*, <https://www.fda.gov/medical-devices/coronavirus-covid-19-and-medical-devices/sars-cov-2-reference-panel-comparative-data> (2020).
106 Corporation, Q. *Lyra® Direct SARS-CoV-2 Assay Instructions for Use*, <https://www.fda.gov/media/138178/download> (2021).
107 Thatcher, S. A. DNA/RNA preparation for molecular detection. *Clinical chemistry* **61**, 89-99 (2015).
108 Chakravorty, S., Helb, D., Burday, M., Connell, N. & Alland, D. A detailed analysis of 16S ribosomal RNA gene segments for the diagnosis of pathogenic bacteria. *Journal of microbiological methods* **69**, 330-339 (2007).
109 Deraney, R. N. *et al.* Vortex-and Centrifugation-Free Extraction of HIV-1 RNA. *Molecular diagnosis & therapy* **23**, 419-427 (2019).
110 Tetala, K. K. & Vijayalakshmi, M. A review on recent developments for biomolecule separation at analytical scale using microfluidic devices. *Analytica chimica acta* **906**, 7-21 (2016).
111 Ali, N., Rampazzo, R. d. C. P., Costa, A. D. T. & Krieger, M. A. Current nucleic acid extraction methods and their implications to point-of-care diagnostics. *BioMed research international* **2017** (2017).
112 Berensmeier, S. Magnetic particles for the separation and purification of nucleic acids. *Applied microbiology and biotechnology* **73**, 495-504 (2006).
113 Reinholt, S. J. & Baeumner, A. J. Microfluidic isolation of nucleic acids. *Angewandte Chemie International Edition* **53**, 13988-14001 (2014).
114 Melzak, K. A., Sherwood, C. S., Turner, R. F. & Haynes, C. A. Driving forces for DNA adsorption to silica in perchlorate solutions. *Journal of colloid and interface science* **181**, 635-644 (1996).
115 Bakewell, D. J. & Morgan, H. Dielectrophoresis of DNA: time-and frequency-dependent collections on microelectrodes. *IEEE transactions on nanobioscience* **5**, 1-8 (2006).
116 Kalyanasundaram, D. *et al.* Electric field-induced concentration and capture of DNA onto microtips. *Microfluidics and nanofluidics* **13**, 217-225 (2012).
117 Yeo, W.-H., Chung, J.-H., Liu, Y. & Lee, K.-H. Size-specific concentration of DNA to a nanostructured tip using dielectrophoresis and capillary action. *The Journal of Physical Chemistry B* **113**, 10849-10858 (2009).
118 Ying, L. *et al.* Frequency and voltage dependence of the dielectrophoretic trapping of short lengths of DNA and dCTP in a nanopipette. *Biophysical journal* **86**, 1018-1027 (2004).
119 Liu, S. & Guttman, A. Electrophoresis microchips for DNA analysis. *TrAC Trends in Analytical Chemistry* **23**, 422-431 (2004).
120 Garcia-Schwarz, G., Rogacs, A., Bahga, S. S. & Santiago, J. G. On-chip isotachophoresis for separation of ions and purification of nucleic acids. *JoVE (Journal of Visualized Experiments)*, e3890 (2012).
121 Sze, A., Erickson, D., Ren, L. & Li, D. Zeta-potential measurement using the Smoluchowski equation and the slope of the current–time relationship in electroosmotic flow. *Journal of colloid and interface science* **261**, 402-410 (2003).
122 Horiuchi, K. & Dutta, P. Electrokinetic flow control in microfluidic chips using a field-effect transistor. *Lab on a Chip* **6**, 714-723 (2006).
123 Stone, H. A., Stroock, A. D. & Ajdari, A. Engineering flows in small devices: microfluidics toward a lab-on-a-chip. *Annu. Rev. Fluid Mech.* **36**, 381-411 (2004).
124 Polson, N. A. & Hayes, M. A. Microfluidics: controlling fluids in small places. *Analytical chemistry* **73**, 312A-319A (2001).
125 Sur, K. *et al.* Immiscible phase nucleic acid purification eliminates PCR inhibitors with a single pass of paramagnetic particles through a hydrophobic liquid. *The Journal of Molecular Diagnostics* **12**, 620-628 (2010).

126 Craven, T. J., Rees, J. M. & Zimmerman, W. B. On slip velocity boundary conditions for electroosmotic flow near sharp corners. *Physics of Fluids* **20**, 043603 (2008).
127 Schrader, C., Schielke, A., Ellerbroek, L. & Johne, R. PCR inhibitors–occurrence, properties and removal. *Journal of applied microbiology* **113**, 1014-1026 (2012).
128 Hayward, J. & Chitty, L. S. in *Seminars in Fetal and Neonatal Medicine.* 94-101 (Elsevier).
129 Lee, H. *et al.* Clinical exome sequencing for genetic identification of rare Mendelian disorders. *Jama* **312**, 1880-1887 (2014).
130 Meyerson, M., Gabriel, S. & Getz, G. Advances in understanding cancer genomes through second-generation sequencing. *Nature Reviews Genetics* **11**, 685-696 (2010).
131 Bentley, D. R. *et al.* Accurate whole human genome sequencing using reversible terminator chemistry. *nature* **456**, 53-59 (2008).
132 Consortium, I. Finishing the euchromatic sequence of the human genome. *Nature* **431**, 931-945 (2004).
133 Wetterstrand, K. A. DNA sequencing costs 2017: Data from the Nhgri Genome Sequencing Program (GSP). *National Human Genome Research Institute* (2018).
134 Kim, S. *et al.* High-throughput automated microfluidic sample preparation for accurate microbial genomics. *Nature communications* **8**, 1-10 (2017).
135 Coupland, P. Microfluidics for the upstream pipeline of DNA sequencing–a worthy application? *Lab on a Chip* **10**, 544-547 (2010).
136 Knierim, E., Lucke, B., Schwarz, J. M., Schuelke, M. & Seelow, D. Systematic comparison of three methods for fragmentation of long-range PCR products for next generation sequencing. *PloS one* **6**, e28240 (2011).
137 Head, S. R. *et al.* Library construction for next-generation sequencing: overviews and challenges. *BioTechniques* **56**, 61-passim, doi:10.2144/000114133 (2014).
138 Hawkins, T. L., O'Connor-Morin, T., Roy, A. & Santillan, C. DNA purification and isolation using a solid-phase. *Nucleic acids research* **22**, 4543 (1994).
139 Azimi, S. M., Nixon, G., Ahern, J. & Balachandran, W. A magnetic bead-based DNA extraction and purification microfluidic device. *Microfluidics and nanofluidics* **11**, 157-165 (2011).
140 Murphy, T. W., Hsieh, Y.-P., Zhu, B., Naler, L. B. & Lu, C. Microfluidic Platform for Next-Generation Sequencing Library Preparation with Low-Input Samples. *Analytical chemistry* **92**, 2519-2526 (2020).
141 Verbruggen, B., Leirs, K., Puers, R. & Lammertyn, J. Selective DNA extraction with microparticles in segmented flow. *Microfluidics and Nanofluidics* **18**, 293-303 (2015).
142 Hess, J. F. *et al.* Automation of Amplicon-Based Library Preparation for Next-Generation Sequencing by Centrifugal Microfluidics. *Analytical Chemistry* **92**, 12833-12841 (2020).
143 Liu, C.-J. *et al.* Magnetic-bead-based microfluidic system for ribonucleic acid extraction and reverse transcription processes. *Biomedical microdevices* **11**, 339-350 (2009).
144 Wang, J. *et al.* Subtyping clinical specimens of influenza A virus by use of a simple method to amplify RNA targets. *Journal of clinical microbiology* **51**, 3324-3330 (2013).
145 Wang, J., Morabito, K., Erkers, T. & Tripathi, A. Capture and separation of biomolecules using magnetic beads in a simple microfluidic channel without an external flow device. *Analyst* **138**, 6573-6581 (2013).
146 Wang, J., Morabito, K., Tang, J. X. & Tripathi, A. Microfluidic platform for isolating nucleic acid targets using sequence specific hybridization. *Biomicrofluidics* **7**, 044107 (2013).
147 Morabito, K., Kantor, R., Tai, W., Schreier, L. & Tripathi, A. Detection of HIV-1 minority variants containing the K103N drug-resistance mutation using a simple method to amplify RNA targets (SMART). *The Journal of Molecular Diagnostics* **15**, 401-412 (2013).
148 Zhang, L., Deraney, R. N. & Tripathi, A. Adsorption and isolation of nucleic acids on cellulose magnetic beads using a three-dimensional printed microfluidic chip. *Biomicrofluidics* **9**, 064118 (2015).

149 Snider, A., Nilsson, M., Dupal, M., Toloue, M. & Tripathi, A. A microfluidics workflow for sample preparation for next-generation DNA sequencing. *SLAS TECHNOLOGY: Translating Life Sciences Innovation* **24**, 196-208 (2019).
150 Berry, S. M., Alarid, E. T. & Beebe, D. J. One-step purification of nucleic acid for gene expression analysis via Immiscible Filtration Assisted by Surface Tension (IFAST). *Lab on a Chip* **11**, 1747-1753 (2011).
151 Spehar, A. M. *et al.* Electrokinetic characterization of poly (dimethylsiloxane) microchannels. *Electrophoresis* **24**, 3674-3678 (2003).
152 Manning, G. S. The molecular theory of polyelectrolyte solutions with applications to the electrostatic properties of polynucleotides. *Quarterly reviews of biophysics* **11**, 179-246 (1978).
153 Lukacs, G. L. *et al.* Size-dependent DNA mobility in cytoplasm and nucleus. *Journal of biological chemistry* **275**, 1625-1629 (2000).
154 Park, J.-G. *et al.* Interfacial and electrokinetic characterization of IPA solutions related to semiconductor wafer drying and cleaning. *Journal of the Electrochemical society* **153**, G811 (2006).
155 García, C. D., Dressen, B. M., Henderson, A. & Henry, C. S. Comparison of surfactants for dynamic surface modification of poly (dimethylsiloxane) microchips. *Electrophoresis* **26**, 703-709 (2005).
156 Stellwagen, N. C., Gelfi, C. & Righetti, P. G. The free solution mobility of DNA. *Biopolymers: Original Research on Biomolecules* **42**, 687-703 (1997).
157 Deraney, R. N., Schneider, L. & Tripathi, A. Synergistic Use of Electroosmotic Flow and Magnetic forces for Nucleic Acid Extraction. *Analyst* (2020).
158 Lee, K. & Tripathi, A. Parallel DNA Extraction From Whole Blood for Rapid Sample Generation in Genetic Epidemiological Studies. *Frontiers in genetics* **11**, 374 (2020).
159 Guan, Q., Noblitt, S. D. & Henry, C. S. Electrophoretic separations in poly (dimethylsiloxane) microchips using mixtures of ionic, nonionic and zwitterionic surfactants. *Electrophoresis* **33**, 2875-2883 (2012).
160 Badal, M. Y., Wong, M., Chiem, N., Salimi-Moosavi, H. & Harrison, D. J. Protein separation and surfactant control of electroosmotic flow in poly (dimethylsiloxane)-coated capillaries and microchips. *Journal of chromatography A* **947**, 277-286 (2002).
161 Milanova, D., Chambers, R. D., Bahga, S. S. & Santiago, J. G. Effect of PVP on the electroosmotic mobility of wet-etched glass microchannels. *Electrophoresis* **33**, 3259-3262 (2012).
162 Choi, H. *et al.* Surface modification of poly (dimethylsiloxane) microchip by using cetyltrimethylammonium bromide (CTAB). *Bulletin of the Korean Chemical Society* **25**, 560-562 (2004).
163 Hoek, I., Tho, F. & Arnold, W. M. Sodium hydroxide treatment of PDMS based microfluidic devices. *Lab on a Chip* **10**, 2283-2285 (2010).
164 Metzker, M. L. Sequencing technologies — the next generation. *Nature Reviews Genetics* **11**, 31, doi:10.1038/nrg2626 (2009).
165 Wakai, T. *et al.* Next-generation sequencing-based clinical sequencing: toward precision medicine in solid tumors. *International Journal of Clinical Oncology* **24**, 115-122, doi:10.1007/s10147-018-1375-3 (2019).
166 Gwinn, M., MacCannell, D. & Armstrong, G. L. Next-Generation Sequencing of Infectious PathogensNext-Generation Sequencing of Infectious PathogensNext-Generation Sequencing of Infectious Pathogens. *JAMA* **321**, 893-894, doi:10.1001/jama.2018.21669 (2019).
167 Palmerola, K. L., Vitez, S. F., Amrane, S., Fischer, C. P. & Forman, E. J. Minimizing mosaicism: assessing the impact of fertilization method on rate of mosaicism after next-generation sequencing (NGS) preimplantation genetic testing for aneuploidy (PGT-A). *J Assist Reprod Genet* **36**, 153-157, doi:10.1007/s10815-018-1347-6 (2019).

168 Buchan, B. W. & Ledeboer, N. A. Emerging Technologies for the Clinical Microbiology Laboratory. *Clinical Microbiology Reviews* **27**, 783-822, doi:10.1128/cmr.00003-14 (2014).
169 Durin, G., Gerwe, B., Duffy, S. & Lopez, A. Automating FFPE Samples from Extraction to NGS Library Preparation.
170 Kim, H. *et al.* A microfluidic DNA library preparation platform for next-generation sequencing. *PLoS One* **8**, e68988 (2013).
171 Kim, H. *et al.* Automated digital microfluidic sample preparation for next-generation DNA sequencing. *JALA: Journal of the Association for Laboratory Automation* **16**, 405-414 (2011).
172 Paegel, B. M., Blazej, R. G. & Mathies, R. A. Microfluidic devices for DNA sequencing: sample preparation and electrophoretic analysis. *Current Opinion in Biotechnology* **14**, 42-50, doi:https://doi.org/10.1016/S0958-1669(02)00004-6 (2003).
173 Tan, S. J. *et al.* A microfluidic device for preparing next generation DNA sequencing libraries and for automating other laboratory protocols that require one or more column chromatography steps. *PloS one* **8**, e64084 (2013).
174 Zborowski, M. & Chalmers, J. J. Magnetophoresis: Fundamentals and applications. *Wiley Encyclopedia of Electrical and Electronics Engineering*, 1-23 (1999).
175 Dolník, V., Liu, S. & Jovanovich, S. Capillary electrophoresis on microchip. *ELECTROPHORESIS: An International Journal* **21**, 41-54 (2000).
176 Tian, Q. *et al.* An integrated microfluidic system for bovine DNA purification and digital PCR detection. *Analytical Biochemistry* **491**, 55-57, doi:https://doi.org/10.1016/j.ab.2015.08.030 (2015).
177 Fujii, T. PDMS-based microfluidic devices for biomedical applications. *Microelectronic Engineering* **61**, 907-914 (2002).
178 Xu, Y. *et al.* Continuous Microfluidic Purification of DNA Using Magnetophoresis. *Micromachines* **11**, 187 (2020).
179 Hale, C. & Darabi, J. Magnetophoretic-based microfluidic device for DNA isolation. *Biomicrofluidics* **8**, 044118 (2014).
180 Karle, M. *et al.* Continuous microfluidic DNA extraction using phase-transfer magnetophoresis. *Lab on a Chip* **10**, 3284-3290 (2010).
181 Vojtíšek, M., Iles, A. & Pamme, N. Rapid, multistep on-chip DNA hybridisation in continuous flow on magnetic particles. *Biosensors and Bioelectronics* **25**, 2172-2176 (2010).
182 Deraney, R. N., Schneider, L. & Tripathi, A. Synergistic use of electroosmotic flow and magnetic forces for nucleic acid extraction. *Analyst* **145**, 2412-2419 (2020).
183 Treff, N. R. & Zimmerman, R. S. Advances in Preimplantation Genetic Testing for Monogenic Disease and Aneuploidy. *Annual Review of Genomics and Human Genetics* **18**, 189-200, doi:10.1146/annurev-genom-091416-035508 (2017).
184 Geraedts, J. & De Wert, G. Preimplantation genetic diagnosis. *Clinical genetics* **76**, 315-325 (2009).
185 Handyside, A. H. & Delhanty, J. D. A. Preimplantation genetic diagnosis: strategies and surprises. *Trends in Genetics* **13**, 270-275, doi:https://doi.org/10.1016/S0168-9525(97)01166-9 (1997).
186 Fragouli, E. Next generation sequencing for preimplantation genetic testing for aneuploidy: friend or foe? *Fertility and sterility* **109**, 606-607 (2018).
187 Das, S., Mohapatra, S. C. & Hsu, J. T. Studies on primer-dimer formation in polymerase chain reaction (PCR). *Biotechnology Techniques* **13**, 643-646 (1999).
188 Booth, C. S. *et al.* Efficiency of the polymerase chain reaction. *Chemical engineering science* **65**, 4996-5006 (2010).
189 DUTTA, P., WARBURTON, T. C. & Beskok, A. Analysis of Electroosmotically Driven Micro-Channel Flows. *J. Fluid Mechanic* (2000).

190 Tagliaro, F., Manetto, G., Crivellente, F. & Smith, F. P. A brief introduction to capillary electrophoresis. *Forensic Science International* **92**, 75-88, doi:https://doi.org/10.1016/S0379-0738(98)00010-3 (1998).
191 Schure, M. R. & Murphy, R. E. Viscous effects in capillary electrophoresis: theory and experiment. *Electrophoresis* **16**, 2074-2085 (1995).
192 Das, D., Al-Rjoub, M. F., Heineman, W. R. & Banerjee, R. K. Efficient capture of magnetic microbeads by sequentially switched electroosmotic flow—an experimental study. *Journal of Micromechanics and Microengineering* **26**, 055013 (2016).
193 Robertson, R. M., Laib, S. & Smith, D. E. Diffusion of isolated DNA molecules: Dependence on length and topology. *Proceedings of the National Academy of Sciences* **103**, 7310-7314, doi:10.1073/pnas.0601903103 (2006).
194 Shah, A., Sammakia, B. G., Srihari, H. & Ramakrishna, K. A numerical study of the thermal performance of an impingement heat sink-fin shape optimization. *IEEE Transactions on Components and Packaging Technologies* **27**, 710-717, doi:10.1109/TCAPT.2004.838879 (2004).
195 Berthier, E., Warrick, J., Yu, H. & Beebe, D. J. Managing evaporation for more robust microscale assays Part 1. Volume loss in high throughput assays. *Lab on a Chip* **8**, 852-859 (2008).
196 Aigrain, L., Gu, Y. & Quail, M. A. Quantitation of next generation sequencing library preparation protocol efficiencies using droplet digital PCR assays-a systematic comparison of DNA library preparation kits for Illumina sequencing. *BMC genomics* **17**, 458 (2016).
197 Smith, R. L. Predicting evaporation rates and times for spills of chemical mixtures. *The Annals of occupational hygiene* **45**, 437-445 (2001).
198 Gordon, D. J., Resio, B. & Pellman, D. Causes and consequences of aneuploidy in cancer. *Nature Reviews Genetics* **13**, 189-203 (2012).
199 Ben-David, U. & Amon, A. Context is everything: aneuploidy in cancer. *Nature Reviews Genetics*, 1-19 (2019).
200 Dashe, J. S. Aneuploidy Screening in Pregnancy. *Obstetrics and gynecology* **128**, 181-194, doi:10.1097/aog.0000000000001385 (2016).
201 Siegel, J. J. & Amon, A. New insights into the troubles of aneuploidy. *Annual review of cell and developmental biology* **28**, 189-214 (2012).
202 Torres, E. M., Williams, B. R. & Amon, A. Aneuploidy: cells losing their balance. *Genetics* **179**, 737-746 (2008).
203 Morton, C. & Lee, C. *Yen & Jaffe's Reproductive Endocrinology (Sixth Edition): Physiology, Pathophysiology, and Clinical Management*. 777-799 (2009).
204 Martin, J. A., Hamilton, B. E. & Osterman, M. J. Births in the United States, 2015. *NCHS data brief*, 1-8 (2016).
205 Roper, R. J. & Reeves, R. H. Understanding the basis for Down syndrome phenotypes. *PLoS genetics* **2** (2006).
206 Lana-Elola, E., Watson-Scales, S. D., Fisher, E. M. C. & Tybulewicz, V. L. J. Down syndrome: searching for the genetic culprits. *Disease models & mechanisms* **4**, 586-595, doi:10.1242/dmm.008078 (2011).
207 Esfandiari, N., Bunnell, M. E. & Casper, R. F. Human embryo mosaicism: did we drop the ball on chromosomal testing? *Journal of assisted reproduction and genetics* **33**, 1439-1444, doi:10.1007/s10815-016-0797-y (2016).
208 Brezina, P. R., Anchan, R. & Kearns, W. G. Preimplantation genetic testing for aneuploidy: what technology should you use and what are the differences? *Journal of assisted reproduction and genetics* **33**, 823-832, doi:10.1007/s10815-016-0740-2 (2016).
209 Zhang, S. *et al.* Number of biopsied trophectoderm cells is likely to affect the implantation potential of blastocysts with poor trophectoderm quality. *Fertility and sterility* **105**, 1222-1227. e1224 (2016).

210 McArthur, S. J. *et al.* Blastocyst trophectoderm biopsy and preimplantation genetic diagnosis for familial monogenic disorders and chromosomal translocations. *Prenat Diagn* **28**, 434-442, doi:10.1002/pd.1924 (2008).
211 Munné, S., Grifo, J. & Wells, D. Mosaicism: "survival of the fittest" versus "no embryo left behind". *Fertility and Sterility* **105**, 1146-1149, doi:https://doi.org/10.1016/j.fertnstert.2016.01.016 (2016).
212 Somigliana, E. *et al.* Cost-effectiveness of preimplantation genetic testing for aneuploidies. *Fertility and Sterility* **111**, 1169-1176, doi:https://doi.org/10.1016/j.fertnstert.2019.01.025 (2019).
213 Neal, S. A. *et al.* Preimplantation genetic testing for aneuploidy is cost-effective, shortens treatment time, and reduces the risk of failed embryo transfer and clinical miscarriage. *Fertility and sterility* **110**, 896-904 (2018).
214 Carlson, L. M. & Vora, N. L. Prenatal Diagnosis: Screening and Diagnostic Tools. *Obstet Gynecol Clin North Am* **44**, 245-256, doi:10.1016/j.ogc.2017.02.004 (2017).
215 Alfirevic, Z., Navaratnam, K. & Mujezinovic, F. Amniocentesis and chorionic villus sampling for prenatal diagnosis. *Cochrane Database of Systematic Reviews* (2017).
216 Wilson, K. *et al.* NSGC practice guideline: prenatal screening and diagnostic testing options for chromosome aneuploidy. *Journal of genetic counseling* **22**, 4-15 (2013).
217 Liao, C. *et al.* Efficacy and safety of cordocentesis for prenatal diagnosis. *International journal of gynecology & obstetrics* **93**, 13-17 (2006).
218 Garfield, S. S. & Armstrong, S. O. Clinical and Cost Consequences of Incorporating a Novel Non-Invasive Prenatal Test into the Diagnostic Pathway for Fetal Trisomies. *Journal of Managed Care Medicine* **15** (2012).
219 Dey, M., Sharma, S. & Aggarwal, S. Prenatal screening methods for aneuploidies. *N Am J Med Sci* **5**, 182-190, doi:10.4103/1947-2714.109180 (2013).
220 Nicolaides, K. H. Screening for fetal aneuploidies at 11 to 13 weeks. *Prenatal diagnosis* **31**, 7-15 (2011).
221 Labonté, V., Alsaid, D., Lang, B. & Meerpohl, J. J. Psychological and social consequences of non-invasive prenatal testing (NIPT): a scoping review. *BMC Pregnancy Childbirth* **19**, 385-385, doi:10.1186/s12884-019-2518-x (2019).
222 Wulff, C. *et al.* Risk of fetal loss associated with invasive testing following combined first-trimester screening for Down syndrome: a national cohort of 147 987 singleton pregnancies. *Ultrasound in Obstetrics & Gynecology* **47**, 38-44 (2016).
223 Salomon, L., Sotiriadis, A., Wulff, C., Odibo, A. & Akolekar, R. Risk of miscarriage following amniocentesis or chorionic villus sampling: systematic review of literature and updated meta-analysis. *Ultrasound in Obstetrics & Gynecology* **54**, 442-451 (2019).
224 Klinger, K. *et al.* Rapid detection of chromosome aneuploidies in uncultured amniocytes by using fluorescence in situ hybridization (FISH). *American journal of human genetics* **51**, 55 (1992).
225 Jobanputra, V., Roy, K. K. & Kucheria, K. Prenatal detection of aneuploidies using fluorescence in situ hybridization: a preliminary experience in an Indian set up. *Journal of biosciences* **27**, 155-163, doi:10.1007/bf02703772 (2002).
226 Rosner, M. *et al.* Detection of genetic abnormalities by using CVS and FISH prior to fetal reduction in sonographically normal appearing fetuses. *Prenatal diagnosis* **33**, 940-944 (2013).
227 Rubio, C. *et al.* Preimplantation genetic screening using fluorescence in situ hybridization in patients with repetitive implantation failure and advanced maternal age: two randomized trials. *Fertility and Sterility* **99**, 1400-1407, doi:https://doi.org/10.1016/j.fertnstert.2012.11.041 (2013).
228 Lall, M. *et al.* FISH is not Suitable as a Standalone Test for Detecting Fetal Chromosomal Abnormalities. *Journal of Fetal Medicine* **2**, 53-59, doi:10.1007/s40556-015-0043-1 (2015).
229 Korbel, J. O. *et al.* The genetic architecture of Down syndrome phenotypes revealed by high-resolution analysis of human segmental trisomies. *Proceedings of the National Academy of Sciences of the United States of America* **106**, 12031-12036, doi:10.1073/pnas.0813248106 (2009).

230 Kan, A. S. *et al.* Whole-genome array CGH evaluation for replacing prenatal karyotyping in Hong Kong. *PloS one* **9** (2014).
231 Wapner, R. J. *et al.* Chromosomal microarray versus karyotyping for prenatal diagnosis. *New England Journal of Medicine* **367**, 2175-2184 (2012).
232 Shaffer, L. G. *et al.* Detection rates of clinically significant genomic alterations by microarray analysis for specific anomalies detected by ultrasound. *Prenatal diagnosis* **32**, 986-995 (2012).
233 Friedenthal, J. *et al.* Next generation sequencing for preimplantation genetic screening improves pregnancy outcomes compared with array comparative genomic hybridization in single thawed euploid embryo transfer cycles. *Fertility and Sterility* **109**, 627-632, doi:https://doi.org/10.1016/j.fertnstert.2017.12.017 (2018).
234 Faas, B. H. *et al.* Non-targeted whole genome 250K SNP array analysis as replacement for karyotyping in fetuses with structural ultrasound anomalies: evaluation of a one-year experience. *Prenatal diagnosis* **32**, 362-370 (2012).
235 Srebniak, M. *et al.* Application of SNP array for rapid prenatal diagnosis: implementation, genetic counselling and diagnostic flow. *European Journal of Human Genetics* **19**, 1230-1237 (2011).
236 Landsverk, M. L. *et al.* Diagnostic approaches to apparent homozygosity. *Genetics in medicine* **14**, 877-882 (2012).
237 Zimmermann, B. *et al.* Noninvasive prenatal aneuploidy testing of chromosomes 13, 18, 21, X, and Y, using targeted sequencing of polymorphic loci. *Prenatal diagnosis* **32**, 1233-1241, doi:10.1002/pd.3993 (2012).
238 Curnow, K. J. *et al.* Detection of triploid, molar, and vanishing twin pregnancies by a single-nucleotide polymorphism–based noninvasive prenatal test. *American journal of obstetrics and gynecology* **212**, 79. e71-79. e79 (2015).
239 Juneau, K. *et al.* Microarray-based cell-free DNA analysis improves noninvasive prenatal testing. *Fetal diagnosis and therapy* **36**, 282-286 (2014).
240 Stokowski, R. *et al.* Clinical performance of non-invasive prenatal testing (NIPT) using targeted cell-free DNA analysis in maternal plasma with microarrays or next generation sequencing (NGS) is consistent across multiple controlled clinical studies. *Prenatal diagnosis* **35**, 1243-1246 (2015).
241 Simon, A. L. *et al.* Pregnancy outcomes from more than 1,800 in vitro fertilization cycles with the use of 24-chromosome single-nucleotide polymorphism–based preimplantation genetic testing for aneuploidy. *Fertility and sterility* **110**, 113-121 (2018).
242 Fredricks, D. N. & Relman, D. A. Application of polymerase chain reaction to the diagnosis of infectious diseases. *Clinical infectious diseases*, 475-486 (1999).
243 Ramirez, J. L. & Kratz, J. R. in *Companion Diagnostics (CDx) in Precision Medicine* 55-71 (Jenny Stanford Publishing, 2019).
244 Treff, N. R. *et al.* Development and validation of an accurate quantitative real-time polymerase chain reaction–based assay for human blastocyst comprehensive chromosomal aneuploidy screening. *Fertility and Sterility* **97**, 819-824.e812, doi:https://doi.org/10.1016/j.fertnstert.2012.01.115 (2012).
245 Scott, R. T., Jr. *et al.* Blastocyst biopsy with comprehensive chromosome screening and fresh embryo transfer significantly increases in vitro fertilization implantation and delivery rates: a randomized controlled trial. *Fertil Steril* **100**, 697-703, doi:10.1016/j.fertnstert.2013.04.035 (2013).
246 El Khattabi, L. A. *et al.* Could digital PCR be an alternative as a non-invasive prenatal test for trisomy 21: a proof of concept study. *PloS one* **11**, e0155009 (2016).
247 Poli, M. *et al.* Past, present, and future strategies for enhanced assessment of embryo's genome and reproductive competence in women of advanced reproductive age. *Frontiers in endocrinology* **10**, 154 (2019).

248 Canick, J. A., Palomaki, G. E., Kloza, E. M., Lambert-Messerlian, G. M. & Haddow, J. E. The impact of maternal plasma DNA fetal fraction on next generation sequencing tests for common fetal aneuploidies. *Prenatal diagnosis* **33**, 667-674 (2013).
249 Voelkerding, K. V. & Lyon, E. (Oxford University Press, 2010).
250 Ning, L. *et al.* Current challenges in the bioinformatics of single cell genomics. *Frontiers in oncology* **4**, 7 (2014).
251 Dugoff, L., Norton, M. E., Kuller, J. A. & Medicine, S. f. M.-F. The use of chromosomal microarray for prenatal diagnosis. *American journal of obstetrics and gynecology* **215**, B2-B9 (2016).
252 Mann, K., Donaghue, C., Fox, S. P., Docherty, Z. & Ogilvie, C. M. Strategies for the rapid prenatal diagnosis of chromosome aneuploidy. *European Journal of Human Genetics* **12**, 907-915 (2004).
253 Ogilvie, C. M., Donaghue, C., Fox, S. P., Docherty, Z. & Mann, K. Rapid prenatal diagnosis of aneuploidy using quantitative fluorescence-PCR (QF-PCR). *Journal of Histochemistry & Cytochemistry* **53**, 285-288 (2005).
254 Kong, X. *et al.* Rapid diagnosis of aneuploidy using segmental duplication quantitative fluorescent PCR. *PloS one* **9**, e88932-e88932, doi:10.1371/journal.pone.0088932 (2014).
255 Lou, J. *et al.* Rapid and simultaneous detection of common aneuploidies by quadruplex real-time polymerase chain reaction combined with melting curve analysis. *PloS one* **12**, e0171886-e0171886, doi:10.1371/journal.pone.0171886 (2017).
256 Lo, Y. M. D. *et al.* Digital PCR for the molecular detection of fetal chromosomal aneuploidy. *Proceedings of the National Academy of Sciences* **104**, 13116-13121, doi:10.1073/pnas.0705765104 (2007).
257 Camunas-Soler, J. *et al.* Noninvasive prenatal diagnosis of single-gene disorders by use of droplet digital PCR. *Clinical chemistry* **64**, 336-345 (2018).
258 Tan, C. *et al.* A multiplex droplet digital PCR assay for non-invasive prenatal testing of fetal aneuploidies. *Analyst* **144**, 2239-2247 (2019).
259 Goodrich, D. *et al.* A randomized and blinded comparison of qPCR and NGS-based detection of aneuploidy in a cell line mixture model of blastocyst biopsy mosaicism. *Journal of assisted reproduction and genetics* **33**, 1473-1480 (2016).
260 Deleye, L. *et al.* Performance of four modern whole genome amplification methods for copy number variant detection in single cells. *Scientific Reports* **7**, 3422, doi:10.1038/s41598-017-03711-y (2017).
261 Fiorentino, F. *et al.* Development and validation of a next-generation sequencing–based protocol for 24-chromosome aneuploidy screening of embryos. *Fertility and Sterility* **101**, 1375-1382.e1372, doi:https://doi.org/10.1016/j.fertnstert.2014.01.051 (2014).
262 Kuznyetsov, V. *et al.* Evaluation of a novel non-invasive preimplantation genetic screening approach. *PLoS One* **13** (2018).
263 Capalbo, A. *et al.* Diagnostic efficacy of blastocoel fluid and spent media as sources of DNA for preimplantation genetic testing in standard clinical conditions. *Fertility and Sterility* **110**, 870-879.e875, doi:10.1016/j.fertnstert.2018.05.031 (2018).
264 Kuznyetsov, V. *et al.* Minimally invasive cell-free human embryo aneuploidy testing (miPGT-A) utilizing combined spent embryo culture medium and blastocoel fluid–towards development of a clinical assay. *Scientific reports* **10**, 1-12 (2020).
265 Leaver, M. & Wells, D. Non-invasive preimplantation genetic testing (niPGT): the next revolution in reproductive genetics? *Human reproduction update* **26**, 16-42 (2020).
266 Li, P. *et al.* Preimplantation genetic screening with spent culture medium/blastocoel fluid for in vitro fertilization. *Scientific reports* **8**, 1-10 (2018).
267 Jiao, J. *et al.* Minimally invasive preimplantation genetic testing using blastocyst culture medium. *Human Reproduction* **34**, 1369-1379 (2019).

268 Tšuiko, O. *et al.* Karyotype of the blastocoel fluid demonstrates low concordance with both trophectoderm and inner cell mass. *Fertility and sterility* **109**, 1127-1134. e1121 (2018).
269 Xu, J. *et al.* Noninvasive chromosome screening of human embryos by genome sequencing of embryo culture medium for in vitro fertilization. *Proceedings of the National Academy of Sciences* **113**, 11907-11912 (2016).
270 Ho, J. R. *et al.* Pushing the limits of detection: investigation of cell-free DNA for aneuploidy screening in embryos. *Fertility and sterility* **110**, 467-475. e462 (2018).
271 Yeung, Q. S. *et al.* A prospective study of non-invasive preimplantation genetic testing for aneuploidies (NiPGT-A) using next-generation sequencing (NGS) on spent culture media (SCM). *Journal of assisted reproduction and genetics* **36**, 1609-1621 (2019).
272 Zhang, J. *et al.* Less-invasive chromosome screening of embryos and embryo assessment by genetic studies of DNA in embryo culture medium. *Journal of assisted reproduction and genetics* **36**, 2505-2513 (2019).
273 Munné, S. & Wells, D. Detection of mosaicism at blastocyst stage with the use of high-resolution next-generation sequencing. *Fertility and sterility* **107**, 1085-1091 (2017).
274 Taglauer, E. S., Wilkins-Haug, L. & Bianchi, D. W. Review: cell-free fetal DNA in the maternal circulation as an indication of placental health and disease. *Placenta* **35 Suppl**, S64-S68, doi:10.1016/j.placenta.2013.11.014 (2014).
275 Koc, A. *et al.* Targeted fetal cell-free DNA screening for aneuploidies in 4,594 pregnancies: Single center study. *Mol Genet Genomic Med* **7**, e00678-e00678, doi:10.1002/mgg3.678 (2019).
276 Koumbaris, G. *et al.* Cell-free DNA analysis of targeted genomic regions in maternal plasma for non-invasive prenatal testing of trisomy 21, trisomy 18, trisomy 13, and fetal sex. *Clinical chemistry* **62**, 848-855 (2016).
277 Chernus, J. M. *et al.* A candidate gene analysis and GWAS for genes associated with maternal nondisjunction of chromosome 21. *PLoS Genetics* **15** (2019).
278 Jones, E. L. *et al.* Evidence that PICALM affects age at onset of Alzheimer's dementia in Down syndrome. *Neurobiology of aging* **34**, 2441. e2441-2441. e2445 (2013).
279 Lee, J. H. *et al.* Candidate gene analysis for Alzheimer's disease in adults with Down syndrome. *Neurobiology of aging* **56**, 150-158 (2017).
280 Sailani, M. R. *et al.* The complex SNP and CNV genetic architecture of the increased risk of congenital heart defects in Down syndrome. *Genome research* **23**, 1410-1421 (2013).
281 Ramachandran, D. *et al.* Genome-wide association study of Down syndrome-associated atrioventricular septal defects. *G3: Genes, Genomes, Genetics* **5**, 1961-1971 (2015).
282 Starostik, M. R., Sosina, O. A. & McCoy, R. C. Single-cell analysis of human embryos reveals diverse patterns of aneuploidy and mosaicism. *Genome research* **30**, 814-825 (2020).
283 Zhang, J. *et al.* Fundamentals and applications of inertial microfluidics: a review. *Lab on a Chip* **16**, 10-34 (2016).
284 Smith, G. D. & Takayama, S. Application of microfluidic technologies to human assisted reproduction. *MHR: Basic science of reproductive medicine* **23**, 257-268 (2017).
285 O'Donovan, C., Twomey, E., Alderman, J., Moore, T. & Papkovsky, D. Development of a respirometric biochip for embryo assessment. *Lab on a Chip* **6**, 1438-1444 (2006).
286 Van Opstal, D. *et al.* Rapid aneuploidy detection with multiplex ligation-dependent probe amplification: a prospective study of 4000 amniotic fluid samples. *European Journal of Human Genetics* **17**, 112-121 (2009).
287 Fan, H. C., Blumenfeld, Y. J., El-Sayed, Y. Y., Chueh, J. & Quake, S. R. Microfluidic digital PCR enables rapid prenatal diagnosis of fetal aneuploidy. *American journal of obstetrics and gynecology* **200**, 543. e541-543. e547 (2009).
288 Winter, M. *et al.* Isolation of Circulating Fetal Trophoblasts Using Inertial Microfluidics for Noninvasive Prenatal Testing. *Advanced Materials Technologies*, 1800066 (2018).
289 Ho, S. S. *et al.* Same-day prenatal diagnosis of common chromosomal aneuploidies using microfluidics-fluorescence in situ hybridization. *Prenatal diagnosis* **32**, 321-328 (2012).

290 Huang, C.-E. *et al.* Noninvasive prenatal diagnosis of fetal aneuploidy by circulating fetal nucleated red blood cells and extravillous trophoblasts using silicon-based nanostructured microfluidics. *Molecular cytogenetics* **10**, 44 (2017).
291 Fiorentino, F. *et al.* Application of next-generation sequencing technology for comprehensive aneuploidy screening of blastocysts in clinical preimplantation genetic screening cycles. *Human Reproduction* **29**, 2802-2813 (2014).
292 Wauters, J. *et al.* Fully automated FISH examination of amniotic fluid cells. *Prenatal Diagnosis: Published in Affiliation With the International Society for Prenatal Diagnosis* **27**, 951-955 (2007).
293 Seppo, A. *et al.* Detection of circulating fetal cells utilizing automated microscopy: potential for noninvasive prenatal diagnosis of chromosomal aneuploidies. *Prenatal Diagnosis: Published in Affiliation With the International Society for Prenatal Diagnosis* **28**, 815-821 (2008).
294 Crea, F. *et al.* The IONA® test: development of an automated cell-free DNA-based screening test for fetal trisomies 13, 18, and 21 that employs the ion proton semiconductor sequencing platform. *Fetal diagnosis and therapy* **42**, 218-224 (2017).
295 Dahl, F. *et al.* Imaging single DNA molecules for high precision NIPT. *Scientific reports* **8**, 4549 (2018).
296 Vora, N. L. *et al.* A multifactorial relationship exists between total circulating cell-free DNA levels and maternal BMI. *Prenatal diagnosis* **32**, 912-914, doi:10.1002/pd.3919 (2012).
297 Ji, X. *et al.* Copy number variation profile in noninvasive prenatal testing (NIPT) can identify co-existing maternal malignancies: Case reports and a literature review. *Taiwanese Journal of Obstetrics and Gynecology* **57**, 871-877 (2018).
298 Benn, P., Plon, S. E. & Bianchi, D. W. Current Controversies in Prenatal Diagnosis 2: NIPT results suggesting maternal cancer should always be disclosed. *Prenatal diagnosis* **39**, 339 (2019).
299 Hartwig, T. S., Ambye, L., Sørensen, S. & Jørgensen, F. S. Discordant non-invasive prenatal testing (NIPT)–a systematic review. *Prenatal diagnosis* **37**, 527-539 (2017).
300 Munné, S., Weier, H., Grifo, J. & Cohen, J. Chromosome mosaicism in human embryos. *Biology of Reproduction* **51**, 373-379 (1994).
301 Scott, R. T. & Galliano, D. The challenge of embryonic mosaicism in preimplantation genetic screening. *Fertility and Sterility* **105**, 1150-1152, doi:https://doi.org/10.1016/j.fertnstert.2016.01.007 (2016).
302 Gleicher, N. *et al.* A single trophectoderm biopsy at blastocyst stage is mathematically unable to determine embryo ploidy accurately enough for clinical use. *Reproductive Biology and Endocrinology* **15**, 1-8 (2017).
303 Committee, P. Clinical management of mosaic results from preimplantation genetic testing for aneuploidy (PGT-A) of blastocysts: a committee opinion. *Fertility and Sterility* **114**, 246-254 (2020).
304 Cram, D. *et al.* PGDIS position statement on the transfer of mosaic embryos 2019. *Reproductive biomedicine online* **39**, e1-e4 (2019).
305 McGowan, R., Pilipenko, V., Smolarek, T. A., West, E. & Tolusso, L. K. Aneuploid embryo transfer: clinical policies and provider opinions at United States fertility clinics. *Fertility and Sterility* **114**, 110-117 (2020).
306 Gleicher, N. *et al.* The 2019 PGDIS position statement on transfer of mosaic embryos within a context of new information on PGT-A. *Reproductive Biology and Endocrinology* **18**, 1-8 (2020).
307 Grati, F. R. *et al.* An evidence-based scoring system for prioritizing mosaic aneuploid embryos following preimplantation genetic screening. *Reproductive biomedicine online* **36**, 442-449 (2018).
308 Grati, F. Implications of fetoplacental mosaicism on cell-free DNA testing: a review of a common biological phenomenon. *Ultrasound in Obstetrics & Gynecology* **48**, 415-423 (2016).

309 Benn, P. *et al.* An economic analysis of cell-free DNA non-invasive prenatal testing in the US general pregnancy population. *PloS one* **10** (2015).
310 Gekas, J. *et al.* Rapid testing versus karyotyping in Down's syndrome screening: cost-effectiveness and detection of clinically significant chromosome abnormalities. *European Journal of Human Genetics* **19**, 3-9 (2011).
311 Song, K., Musci, T. J. & Caughey, A. B. Clinical utility and cost of non-invasive prenatal testing with cfDNA analysis in high-risk women based on a US population. *The journal of maternal-fetal & neonatal medicine* **26**, 1180-1185 (2013).
312 Kaimal, A. J., Norton, M. E. & Kuppermann, M. Prenatal testing in the genomic age: clinical outcomes, quality of life, and costs. *Obstetrics & Gynecology* **126**, 737-746 (2015).
313 Hamilton, B. H., Jungheim, E., McManus, B. & Pantano, J. Health care access, costs, and treatment dynamics: Evidence from in vitro fertilization. *American Economic Review* **108**, 3725-3777 (2018).
314 Collins, S. C., Xu, X. & Mak, W. Cost-effectiveness of preimplantation genetic screening for women older than 37 undergoing in vitro fertilization. *Journal of assisted reproduction and genetics* **34**, 1515-1522 (2017).
315 Green, J. M., Hewison, J., Bekker, H. L., Bryant, L. D. & Cuckle, H. S. Psychosocial aspects of genetic screening of pregnant women and newborns: a systematic review. *Health technology assessment (Winchester, England)* **8**, iii, ix-x, 1-109, doi:10.3310/hta8330 (2004).
316 Cernat, A., De Freitas, C., Majid, U., Higgins, C. & Vanstone, M. Facilitating informed choice about non-invasive prenatal testing (NIPT): a systematic review and qualitative meta-synthesis of women's experiences. *BMC Pregnancy Childbirth* **19**, 1-15 (2019).
317 Farrell, R. M., Mercer, M. B., Agatisa, P. K., Smith, M. B. & Philipson, E. It's more than a blood test: patients' perspectives on noninvasive prenatal testing. *Journal of clinical medicine* **3**, 614-631 (2014).
318 Schmitz, D., Netzer, C. & Henn, W. An offer you can't refuse? Ethical implications of non-invasive prenatal diagnosis. *Nature Reviews Genetics* **10**, 515-515 (2009).
319 Johnston, J., Farrell, R. & Parens, E. Supporting women's autonomy in prenatal testing. *The New England journal of medicine* **377**, 505 (2017).
320 van der Meij, K. R. *et al.* TRIDENT-2: national implementation of genome-wide non-invasive prenatal testing as a first-tier screening test in the Netherlands. *The American Journal of Human Genetics* **105**, 1091-1101 (2019).
321 Sausen, M., Parpart, S. & Diaz, L. A., Jr. Circulating tumor DNA moves further into the spotlight. *Genome Med* **6**, 35-35, doi:10.1186/gm552 (2014).
322 Volik, S., Alcaide, M., Morin, R. D. & Collins, C. Cell-free DNA (cfDNA): clinical significance and utility in cancer shaped by emerging technologies. *Molecular Cancer Research* **14**, 898-908 (2016).
323 Brady, P. *et al.* Clinical implementation of NIPT–technical and biological challenges. *Clinical Genetics* **89**, 523-530 (2016).
324 Alberry, M. *et al.* Free fetal DNA in maternal plasma in anembryonic pregnancies: confirmation that the origin is the trophoblast. *Prenatal Diagnosis: Published in Affiliation With the International Society for Prenatal Diagnosis* **27**, 415-418 (2007).
325 Jia, C.-W. *et al.* Aneuploidy in early miscarriage and its related factors. *Chinese medical journal* **128**, 2772 (2015).
326 Carey, J. C. Perspectives on the care and management of infants with trisomy 18 and trisomy 13: striving for balance. *Current opinion in pediatrics* **24**, 672-678 (2012).
327 Cereda, A. & Carey, J. C. The trisomy 18 syndrome. *Orphanet journal of rare diseases* **7**, 1-14 (2012).
328 Goc, B. *et al.* Trisomy 18 in neonates: prenatal diagnosis, clinical features, therapeutic dilemmas and outcome. *Journal of applied genetics* **47**, 165-170 (2006).

329 Chiu, R. W. *et al.* Non-invasive prenatal assessment of trisomy 21 by multiplexed maternal plasma DNA sequencing: large scale validity study. *Bmj* **342** (2011).
330 Tabor, A. *et al.* Randomised controlled trial of genetic amniocentesis in 4606 low-risk women. *The Lancet* **327**, 1287-1293 (1986).
331 Reiss, R. E. & Cherry, A. M. Still a screening test: more attention needed to noninvasive prenatal test false-positive rates. *American Journal of Obstetrics & Gynecology* **209**, 160-161 (2013).
332 Sehnert, A. J. *et al.* Optimal detection of fetal chromosomal abnormalities by massively parallel DNA sequencing of cell-free fetal DNA from maternal blood. *Clinical chemistry* **57**, 1042-1049 (2011).
333 Palomaki, G. E. *et al.* DNA sequencing of maternal plasma to detect Down syndrome: an international clinical validation study. *Genetics in medicine* **13**, 913-920 (2011).
334 Taylor-Phillips, S. *et al.* Accuracy of non-invasive prenatal testing using cell-free DNA for detection of Down, Edwards and Patau syndromes: a systematic review and meta-analysis. *BMJ open* **6**, e010002 (2016).
335 Dugo, N. *et al.* Six consecutive false positive cases from cell-free fetal DNA testing in a single referring centre. *Journal of prenatal medicine* **8**, 31 (2014).
336 Minear, M. A., Lewis, C., Pradhan, S. & Chandrasekharan, S. Global perspectives on clinical adoption of NIPT. *Prenatal diagnosis* **35**, 959-967 (2015).
337 Bischoff, F. Z., Lewis, D. E. & Simpson, J. L. Cell-free fetal DNA in maternal blood: kinetics, source and structure. *Human reproduction update* **11**, 59-67 (2005).
338 Perkins, G. *et al.* Multi-purpose utility of circulating plasma DNA testing in patients with advanced cancers. *PloS one* **7**, e47020 (2012).
339 Chang, H.-W. *et al.* Assessment of plasma DNA levels, allelic imbalance, and CA 125 as diagnostic tests for cancer. *Journal of the National Cancer Institute* **94**, 1697-1703 (2002).
340 Meddeb, R. *et al.* Quantifying circulating cell-free DNA in humans. *Scientific reports* **9**, 1-16 (2019).
341 Antonatos, D., Patsilinakos, S., Spanodimos, S., Korkonikitas, P. & Tsigas, D. Cell-free DNA levels as a prognostic marker in acute myocardial infarction. *Annals of the New York Academy of Sciences* **1075**, 278-281 (2006).
342 Kamm, R. C. & Smith, A. G. Nucleic acid concentrations in normal human plasma. *Clinical chemistry* **18**, 519-522 (1972).
343 Dennin, R. DNA of free and complexed origin in human plasma: concentration and length distribution. *Klinische Wochenschrift* **57**, 451-456 (1979).
344 Fournié, G. J. *et al.* Plasma DNA as a marker of cancerous cell death. Investigations in patients suffering from lung cancer and in nude mice bearing human tumours. *Cancer letters* **91**, 221-227 (1995).
345 Gautschi, O. *et al.* Circulating deoxyribonucleic acid as prognostic marker in non–small-cell lung cancer patients undergoing chemotherapy. *Journal of Clinical Oncology* **22**, 4157-4164 (2004).
346 Herrera, L. J. *et al.* Quantitative analysis of circulating plasma DNA as a tumor marker in thoracic malignancies. *Clinical chemistry* **51**, 113-118 (2005).
347 Jahr, S. *et al.* DNA fragments in the blood plasma of cancer patients: quantitations and evidence for their origin from apoptotic and necrotic cells. *Cancer research* **61**, 1659-1665 (2001).
348 Jung, K. *et al.* Increased cell-free DNA in plasma of patients with metastatic spread in prostate cancer. *Cancer letters* **205**, 173-180 (2004).
349 Lui, Y. Y. *et al.* Predominant Hematopoietic Origin of Cell-free DNA in Plasma and Serum after Sex-mismatched Bone Marrow Transplantation. *Clinical Chemistry* **48**, 421-427, doi:10.1093/clinchem/48.3.421 (2002).
350 Silva, J. M. *et al.* Tumor DNA in Plasma at Diagnosis of Breast Cancer Patients Is a Valuable Predictor of Disease-free Survival. *Clinical Cancer Research* **8**, 3761-3766 (2002).

351 Stemmer, C. *et al.* Use of Magnetic Beads for Plasma Cell-free DNA Extraction: Toward Automation of Plasma DNA Analysis for Molecular Diagnostics. *Clinical Chemistry* **49**, 1953-1955, doi:10.1373/clinchem.2003.020750 (2003).
352 Vogelstein, B. & Gillespie, D. Preparative and analytical purification of DNA from agarose. *Proceedings of the National Academy of Sciences* **76**, 615-619 (1979).
353 Sun, N. *et al.* Optimization of influencing factors of nucleic acid adsorption onto silica-coated magnetic particles: application to viral nucleic acid extraction from serum. *Journal of Chromatography A* **1325**, 31-39 (2014).
354 Marko, M., Chipperfield, R. & Birnboim, H. A procedure for the large-scale isolation of highly purified plasmid DNA using alkaline extraction and binding to glass powder. *Analytical biochemistry* **121**, 382-387 (1982).
355 Yoza, B., Arakaki, A., Maruyama, K., Takeyama, H. & Matsunaga, T. Fully automated DNA extraction from blood using magnetic particles modified with a hyperbranched polyamidoamine dendrimer. *Journal of bioscience and bioengineering* **95**, 21-26 (2003).
356 Ribeiro-Silva, A., Zhang, H. & Jeffrey, S. S. RNA extraction from ten year old formalin-fixed paraffin-embedded breast cancer samples: a comparison of column purification and magnetic bead-based technologies. *BMC molecular biology* **8**, 1-10 (2007).
357 Boom, R. *et al.* Rapid and simple method for purification of nucleic acids. *Journal of clinical microbiology* **28**, 495-503 (1990).
358 Tian, H., Hühmer, A. F. & Landers, J. P. Evaluation of silica resins for direct and efficient extraction of DNA from complex biological matrices in a miniaturized format. *Analytical biochemistry* **283**, 175-191 (2000).
359 Diefenbach, R. J., Lee, J. H., Kefford, R. F. & Rizos, H. Evaluation of commercial kits for purification of circulating free DNA. *Cancer genetics* **228**, 21-27 (2018).
360 Lee, H., Na, W., Park, C., Park, K. H. & Shin, S. Centrifugation-free extraction of circulating nucleic acids using immiscible liquid under vacuum pressure. *Scientific reports* **8**, 1-11 (2018).
361 Thompson, R. E., Duncan, G. & McCord, B. R. An investigation of PCR inhibition using Plexor®-Based quantitative PCR and short tandem repeat amplification. *Journal of forensic sciences* **59**, 1517-1529 (2014).
362 Gwak, H. *et al.* On-chip isolation and enrichment of circulating cell-free DNA using microfluidic device. *Biomicrofluidics* **13**, 024113 (2019).
363 Campos, C. D. *et al.* Microfluidic-based solid phase extraction of cell free DNA. *Lab on a Chip* **18**, 3459-3470 (2018).
364 Perez-Toralla, K. *et al.* Microfluidic extraction and digital quantification of circulating cell-free DNA from serum. *Sensors and Actuators B: Chemical* **286**, 533-539 (2019).
365 Yang, J. *et al.* A microfluidic device for rapid quantification of cell-free DNA in patients with severe sepsis. *Lab on a Chip* **15**, 3925-3933 (2015).
366 Niemz, A., Ferguson, T. M. & Boyle, D. S. Point-of-care nucleic acid testing for infectious diseases. *Trends in biotechnology* **29**, 240-250 (2011).
367 Khodakov, D., Wang, C. & Zhang, D. Y. Diagnostics based on nucleic acid sequence variant profiling: PCR, hybridization, and NGS approaches. *Advanced drug delivery reviews* **105**, 3-19 (2016).
368 van Kasteren, P. B. *et al.* Comparison of seven commercial RT-PCR diagnostic kits for COVID-19. *Journal of Clinical Virology* **128**, 104412 (2020).
369 Gray, J. & Coupland, L. The increasing application of multiplex nucleic acid detection tests to the diagnosis of syndromic infections. *Epidemiology & Infection* **142**, 1-11 (2014).
370 Troxler, H., Kleinert, P., Schmugge, M. & Speer, O. Advances in hemoglobinopathy detection and identification. *Advances in clinical chemistry* **57**, 2 (2012).
371 Kozlowski, P., Jasinska, A. J. & Kwiatkowski, D. J. New applications and developments in the use of multiplex ligation-dependent probe amplification. *Electrophoresis* **29**, 4627-4636 (2008).

372 Serizawa, R. R. *et al.* Custom-designed MLPA using multiple short synthetic probes: application to methylation analysis of five promoter CpG islands in tumor and urine specimens from patients with bladder cancer. *The Journal of Molecular Diagnostics* **12**, 402-408 (2010).
373 Soave, A. *et al.* Copy number variations of circulating, cell-free DNA in urothelial carcinoma of the bladder patients treated with radical cystectomy: a prospective study. *Oncotarget* **8**, 56398 (2017).
374 Medrano, R. F. V. & de Oliveira, C. A. Guidelines for the tetra-primer ARMS–PCR technique development. *Molecular biotechnology* **56**, 599-608 (2014).
375 Mesrian Tanha, H., Mojtabavi Naeini, M., Rahgozar, S., Rasa, S. M. M. & Vallian, S. Modified tetra-primer ARMS PCR as a single-nucleotide polymorphism genotyping tool. *Genetic testing and molecular biomarkers* **19**, 156-161 (2015).
376 Zhang, C. *et al.* A novel multiplex tetra-primer ARMS-PCR for the simultaneous genotyping of six single nucleotide polymorphisms associated with female cancers. *PloS one* **8**, e62126 (2013).
377 Piccioli, P. *et al.* Multiplex Tetra-Primer Amplification Refractory Mutation System PCR to Detect 6 Common Germline Mutations of the MUTYH Gene Associated with Polyposis and Colorectal Cancer. *Clinical Chemistry* **52**, 739-743, doi:10.1373/clinchem.2005.060137 (2006).
378 Zhang, S. *et al.* Tetra-primer ARMS-PCR combined with GoldMag lateral flow assay for genotyping: simultaneous visual detection of both alleles. *Nanoscale* **12**, 10098-10105 (2020).
379 Xiang, Z. *et al.* Highly sensitive and specific real-time PCR by employing serial invasive reaction as a sequence identifier for quantifying EGFR mutation abundance in cfDNA. *Analytical and bioanalytical chemistry* **410**, 6751-6759 (2018).
380 Chiu, E. K. L., Hui, W. W. I. & Chiu, R. W. K. cfDNA screening and diagnosis of monogenic disorders–where are we heading? *Prenatal diagnosis* **38**, 52-58 (2018).
381 Mauger, F. *et al.* Comparison of commercially available whole-genome sequencing kits for variant detection in circulating cell-free DNA. *Scientific reports* **10**, 1-11 (2020).
382 Pereira, J. C., Chaves, R., Bastos, E., Leitão, A. & Guedes-Pinto, H. An efficient method for genomic DNA extraction from different molluscs species. *Int J Mol Sci* **12**, 8086-8095 (2011).
383 Chang, M. Y. *et al.* One-step noninvasive prenatal testing (NIPT) for autosomal recessive homozygous point mutations using digital PCR. *Scientific reports* **8**, 1-8 (2018).
384 van Dongen, J. E. *et al.* Point-of-care CRISPR/Cas nucleic acid detection: Recent advances, challenges and opportunities. *Biosensors and Bioelectronics* **166**, 112445 (2020).